

**Biochemical, functional, and evolutionary
aspects of flavonoid and benzoxazinoid
O-methylation in grasses**

Dissertation

in Partial Fulfilment of the Requirements for the Degree of
“doctor rerum naturalium” (Dr. rer. nat.)

**Submitted to the Council of the Faculty of Biological Sciences
of Friedrich Schiller University Jena**

**by Christiane Förster (Master of Science)
born on May 13, 1988 in Seligenstadt**

Reviewers:

1. Prof. Dr. Günter Theißen

Friedrich Schiller University Jena, Matthias Schleiden Institute,
Department of Genetics

2. Prof. Dr. Jonathan Gershenzon

Max Planck Institute for Chemical Ecology, Jena,
Department of Biochemistry

3. PD Dr. Thomas Vogt

Leibniz Institute of Plant Biochemistry, Halle (Saale),
Department of Cell and Metabolic Biology

Date of public defense: **June 3, 2022**

Table of Contents

1. Introduction	1
1.1 Specialized plant metabolism.....	1
1.2 Plant chemical defense repertoire and defense signaling	2
1.3 Grasses (Poaceae) and their chemical defenses	5
1.4 BX hydroxamic acids: Chemical properties and biological activity.....	8
1.5 The biosynthesis of BX hydroxamic acids in grasses	11
1.6 Flavonoids: widely distributed multifunctional plant metabolites	12
1.7 The biosynthesis of flavonoids	15
1.8 Plant O-methyltransferases	17
2. Manuscripts overview	19
2.1 Manuscript I	20
2.2 Manuscript II	21
2.3 Manuscript III	22
3. Manuscripts	23
3.1 Manuscript I	25
3.2 Manuscript II	41
3.3 Manuscript III	67
4. Discussion	89
4.1 Evolution of OMTs in the grasses.....	89
4.2 O-methylation of flavonoids: The position makes the difference.....	93
4.3 The flavonoid/O-methylflavonoid antifungal mode of action: direct inhibition versus signaling	96
4.4 Conclusion and future perspectives.....	100
5. Summary	101
6. Zusammenfassung	103
7. References.....	106
8. Acknowledgements	117
9. Eigenständigkeitserklärung	119
10. Curriculum Vitae.....	120

11. Supplemental Material.....123

11.1 Manuscript I.....124

11.2 Manuscript II.....140

11.3 Manuscript III.....198

11.4 Detailed author contributions to Manuscript I.....214

11.5 Detailed author contributions to Manuscript II.....216

11.6 Detailed author contributions to Manuscript III.....218

11.7 Supplemental Figures and Tables219

11.8 Supplemental Methods.....227

1. Introduction

Plants are under constant pressure from pests and pathogens posing a substantial challenge for agricultural food production. Global yield losses associated with agricultural pathogens and pests for five major food crops (maize, wheat, rice, potato and soybean) are estimated to be in the range of 17-30% (Savary et al., 2019). With an annual use of about 2 million tons and rising, pesticides are the most preferred measure for disease and pest management worldwide (Sharma et al., 2019). However, despite their benefits for crop protection and the associated increase in yield, excessive pesticide use can pose enormous threats to living organisms and entire ecosystems, which is why their use is highly controversial. Many pesticides are highly persistent, accumulating for instance in soil and water and finally entering the food chain, and so pose health hazards to animals and humans. Additionally, pesticides can be harmful to non-target insects including enemies of pests or beneficial soil microorganisms (Aktar et al., 2009; Sharma et al., 2019). On top of that, pesticide application also harbors the risk that pests will develop resistance to pesticides (Sharma et al., 2019). Therefore, it is of great importance to achieve sustainable disease and pest management methods that meet both economic and ecological criteria. Understanding natural plant defense mechanisms and their evolution is crucial for further developments in this field.

1.1 Specialized plant metabolism

Plants have evolved different mechanisms to protect themselves from detrimental organisms. These include physical barriers such as waxy cuticles, trichomes, thick cell walls or bark, and proteinaceous defenses such as proteinase inhibitors and hydrolases. However, chemical defense through the production of specialized metabolites, also known as secondary metabolites or plant natural products, is considered most important (Mithöfer and Boland, 2012; Zhan et al., 2014). Most specialized compounds fall into three major classes: terpenes, phenolics and nitrogen-containing compounds. These are synthesized mainly by the isoprenoid, phenylpropanoid, fatty acid/polyketide and alkaloid pathways, which use primary metabolites such as the central precursor acetyl-CoA or amino acids formed from the shikimic acid pathway (Dixon, 2001). In contrast to primary metabolites that are universal constituents of all plants and are indispensable for normal growth, development and reproduction, specialized metabolites are only required under certain

environmental conditions and show a huge diversity within the plant kingdom (Cluzet et al., 2020). Collectively, plant species synthesize more than 200,000 low-molecular-mass specialized metabolites (Dixon and Strack, 2003). This great diversity is thought to be mainly driven by interactions of plants with enemies and competitors, such as herbivores, pathogens, or other plants in their environment, which exert selection pressure resulting in an ongoing evolutionary process of adaptations and counter-adaptations in the plant and its enemies and competitors, respectively, also termed as evolutionary arms race or coevolution (Dawkins and Krebs, 1979; Ramawat and Goyal, 2020). However, apart from natural selection, it should not be forgotten that modern crop plants in particular have also undergone artificial selection by humans to increase yield, food quality characteristics such as taste and nutritional value, and suitability for cultivation. This domestication process has often reduced the resistance of modern versus wild cultivars; an observation that can probably be partly explained by an altered composition of specialized metabolites (Chen et al., 2015). Besides their role in defense, plant specialized metabolites are known to fulfill other important functions such as protection against abiotic stresses or attraction of pollinators and seed dispersers (Dixon and Paiva, 1995; Ramawat and Goyal, 2020). Therefore, each plant lineage produces its own set of specialized metabolites depending on its specific ecological niche (Pichersky and Lewinsohn, 2011). Some classes of specialized metabolites have a restricted taxonomical distribution, such as glucosinolates or isoflavonoids, which occur mainly in the Brassicales and Fabaceae, respectively (Fahey et al., 2001; Al-Maharik, 2019), while others such as flavonoids or terpenes are widely distributed across the plant kingdom (Mithöfer and Boland, 2012).

1.2 Plant chemical defense repertoire and defense signaling

Plant defense strategies fall into several categories depending on when they occur, the type of attacker they target, and how direct the defense response is. Defenses may act either directly or indirectly against the attacker. In direct defense, specialized metabolites may be toxic, growth inhibitory, repellent, or antinutritive to plant pathogens and/or herbivores (Mithöfer and Boland, 2012; Pedras and Yaya, 2015). Indirect chemical defenses, on the other hand, attract enemies of herbivores, for example, by volatile emission, or might work as internal defense signals. Benzoxazinoids and glucosinolates, for instance, not only act as direct defense compounds, but also trigger the deposition of callose as barrier against invaders (Maag et al., 2015).

Direct and indirect chemical defenses can be present independently of an attacking organism as preformed or constitutive defenses, or they can be synthesized upon pathogen or herbivore attack as induced defense (Mithöfer and Boland, 2012). In case of pathogen-related compounds, constitutive and induced defense metabolites are also termed phytoanticipins and phytoalexins, respectively (VanEtten et al., 1994). Both are defined as low molecular weight antimicrobial compounds, but in contrast to phytoanticipins, which are “present in plants prior to microbial infection or are produced from preformed constituents during infection” (VanEtten et al., 1994), phytoalexins are produced *de novo* after pathogen infection or abiotic stress (Paxton, 1980; Hammerschmidt, 1999). Therefore, *de novo* phytoalexin biosynthesis usually requires multiple enzymatic reactions, while phytoanticipins often result from simple hydrolytic cleavage, for instance, of glycosidic linkages (Pedras and Yaya, 2015). Importantly, Paxton’s definition does not specify whether or not phytoalexins are important for disease resistance (Paxton, 1980; VanEtten et al., 1994); however, several examples are known that provide good evidence for the role of phytoalexins in pathogen defense (Hammerschmidt, 1999) (for example compounds, see also chapter 1.3 below).

Typically, plants possess both constitutive and induced defenses to prevent further spread of a disease with the constitutive defenses designed to prevent pathogen entry, for example, and inducible defenses induced internally in case pathogens are successful in gaining entry (Zhan et al., 2014). Furthermore, some specialized metabolites serve as both constitutive and induced defenses in different plant species or even within the same species (VanEtten et al., 1994; Pedras and Yaya, 2015). While inducible anti-herbivore defenses usually accumulate both locally at the site of attack as well as systemically in the whole plant (Mithöfer and Boland, 2012), phytoalexin accumulation upon pathogen infection is restricted to the infection site (Nicholson and Hammerschmidt, 1992). Since many defensive metabolites are also toxic to the plant itself, constitutively produced compounds are often stored as inactive precursors (e.g. sugar conjugates) in specialized cells or certain cellular compartments (e.g. the vacuole). Upon tissue damage, for example, by herbivore feeding, they come into contact with hydrolyzing enzymes present in other cells or cell compartments that catalyze conversion to bioactive compounds. This type of defense is also known as two-component plant chemical defense; prominent examples include glucosinolates, cyanogenic glycosides, and benzoxazinoids (Pentzold et al., 2014). Induced defense compounds are considered to be more advantageous than constitutive defenses because

they minimize the risks of autotoxicity, do not incur costs in the absence of attackers, and can be tailored to combat specific invading organisms (Pappas et al., 2020).

To recognize and defend against different attackers with a high degree of specificity, plants possess a system of receptors and complex intracellular signaling networks that lead to downstream transcriptional reprogramming and establishment of plant defense responses, including the production of plant secondary metabolites. The first line of induced plant defense, known as pattern-triggered immunity (PTI), relies on the perception of chemical cues (elicitors) that either originate from the attacker itself (exogenous signal) or are released by the plant during the interaction with the attacking organism (endogenous signal) (Cluzet et al., 2020; Pappas et al., 2020). Depending on the organism responsible for its release, elicitors are termed pathogen-, microbe-, damage-, or herbivore-associated molecular patterns (PAMPs, MAMPs, DAMPs, or HAMPs, respectively) and comprise a diverse array of molecules. Well-known examples are structural components of pathogens (e.g. fungal chitin or bacterial flagellin), plant cell wall fragments or cytosolic constituents released upon tissue damage (e.g. by herbivore feeding), and components of the secretions (e.g. saliva) of herbivores (Maffei et al., 2012). All these molecular patterns are recognized by specific transmembrane receptors called pattern recognition receptors (PRRs) localized at the plant plasma membrane. Upon recognition, PRRs trigger downstream signaling events, such as the rapid elevation of cytosolic Ca^{2+} or generation of reactive oxygen species (ROS) and nitric oxide (NO), that in turn activate calcium-dependent protein kinase (CDPK) and mitogen-activated protein kinase (MAPK) cascades, resulting in the biosynthesis of phytohormones such as jasmonic acid (JA), salicylic acid (SA), and abscisic acid (ABA). These phytohormones form signaling networks that regulate the expression of defense-related genes (Seybold et al., 2014; Pappas et al., 2020). In case enemies overcome this first defensive layer, the plant immune system still has a second layer, the so-called effector-triggered immunity (ETI). ETI is activated when adapted pathogens or herbivores release effector proteins into the plant cell that suppress components of PTI and these effectors are in turn recognized by specific plant NB-LRR (nucleotide-binding leucine-rich repeats) proteins, thereby accelerating and amplifying the basal PTI response. In addition, ETI is often associated with a hypersensitive response (HR), a type of programmed cell death, at the site of pathogen infection (Noman et al., 2019).

1.3 Grasses (Poaceae) and their chemical defenses

The grass family (Poaceae) is a large plant family consisting of roughly 11,500 species in 768 grass genera (Soreng et al., 2017) and is by far the most economically important plant group (Hodkinson, 2018). It includes major staple food crops such as maize (*Zea mays*), wheat (*Triticum spp.*), rice (*Oryza spp.*), barley (*Hordeum vulgare*), rye (*Secale cereale*), sorghum (*Sorghum spp.*), and oat (*Avena sativa*); sugar crops such as sugarcane (*Saccharum spp.*); and also crops used for building material (bamboo; e.g. *Bambusa spp.* and *Phyllostachys spp.*) or biofuel production such as switchgrass (*Panicum virgatum*), giant miscanthus (*Miscanthus x giganteus*), and giant reed (*Arundo donax*) (Hodkinson, 2018; Scordia and Cosentino, 2019). Phylogenetic studies have divided the Poaceae in 12 subfamilies (Figure 1), with three small subfamilies (Anomochlooideae, Pharoideae, and Puelioideae) being the most early-diverged lineages and hence sister to all other grasses, while the majority of grasses are placed in two main clades, termed BOP and PACMAD based on the first initials of the included subfamilies (Soreng et al., 2017). The BOP and PACMAD lineages have been suggested to have diverged 55-70 million years ago between the late Cretaceous and early Eocene (Hodkinson, 2018).

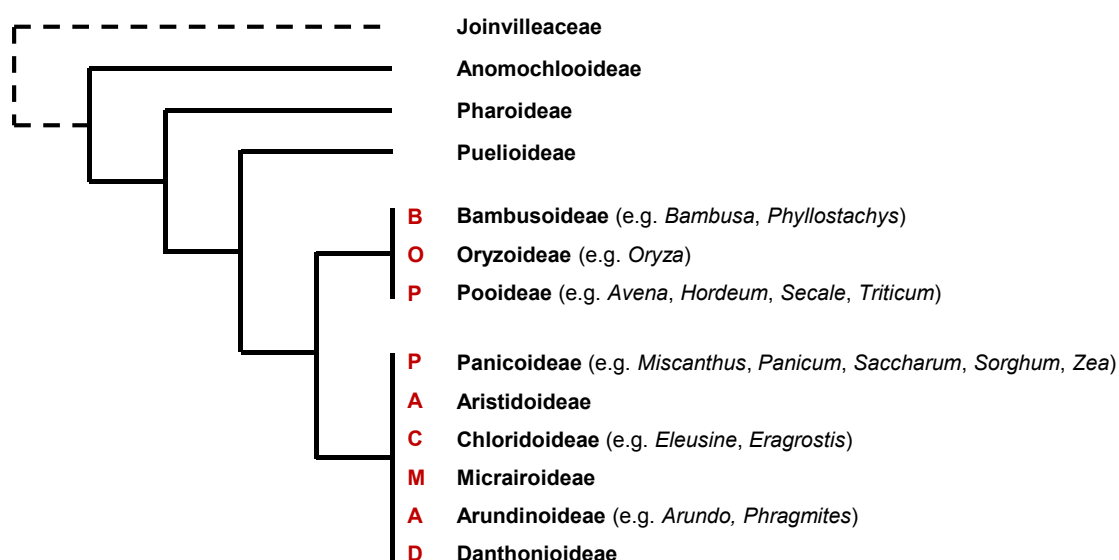


Figure 1. Simplified phylogeny of the grass family (Poaceae). Shown are the 12 subfamilies and Joinvilleaceae as outgroup. Some important example genera are given in brackets. Modified after Hodkinson (2018).

During the past decades, many different classes of defense compounds have been reported from the grass family (Degenhardt, 2009; Niemeyer, 2009; Ejike et al., 2013). Amongst these, benzoxazinoids (BXs), especially BX hydroxamic acids (Figure 2), belong to the most comprehensively studied secondary metabolites in this plant family (Niculaes et al., 2018). They occur mainly in grass species belonging to the two main clades PACMAD and BOP (e.g. maize, wheat, and rye; Figure 1), but are also found in a few dicotyledons (Frey et al., 2009; Kokubo et al., 2017). However, the vast majority of BX-related research, including the elucidation of their biosynthetic pathway and their biological activity (see chapters 1.4 and 1.5), has been conducted on the model plant maize, representing a huge genetic resource. BXs are stored as inactive glycosides in the vacuole. Upon tissue disruption and contact to specific β -glucosidases initially present in the plastids, BXs are hydrolyzed to reactive aglucones that can subsequently undergo rapid breakdown into benzoxazolinones (Figure 2 and 3, see also next chapter) (Niemeyer, 2009). The functional repertoire of BXs is diverse and includes defenses against chewing herbivores, piercing-sucking insects, microbes, and competing plants (allelopathy), as well as interactions besides defense such as iron acquisition and signaling (Niculaes et al., 2018). In general, BXs can be considered as both constitutive and induced defense compounds. However, in maize, high BX content (up to a few mg/g fresh weight) is usually only found constitutively in seedlings, but can also be rapidly induced in both young and old plants upon insect infestation or fungal infection (Ahmad et al., 2011; Huffaker et al., 2011a; Köhler et al., 2015; Maag et al., 2016).

Besides BXs, non-volatile, species-specific terpenoid phytoalexins are another group of well-known defensive specialized metabolites in the Poaceae (Figure 2). While maize produces acidic sesquiterpenoids termed zealexins and diterpenoids termed kauralexins and dolabralalexins (Huffaker et al., 2011b; Schmelz et al., 2011; Mafu et al., 2018), rice is known for synthesizing a no less extensive assortment of diterpenoids namely oryzalexins, phytocassanes, and momilactones (Wang et al., 2018). As typical for phytoalexins, these compounds accumulate in the plant after pathogen infection. In addition, many of these terpenoids exhibit antifungal activity *in vitro* and were shown to contribute to plant resistance against fungal pathogens *in vivo* (Wang et al., 2018; Ding et al., 2019; Ding et al., 2020). Kauralexins were also induced by stem herbivory of the European corn borer (*Ostrinia nubilalis*) and had a deterrent effect on this insect in choice assays (Schmelz et al., 2011). More recently, diterpene synthase families have been also reported from other monocot crops, including wheat, barley, sorghum and switchgrass (Murphy and Zerbe, 2020), indicating a broader distribution within the grass family.

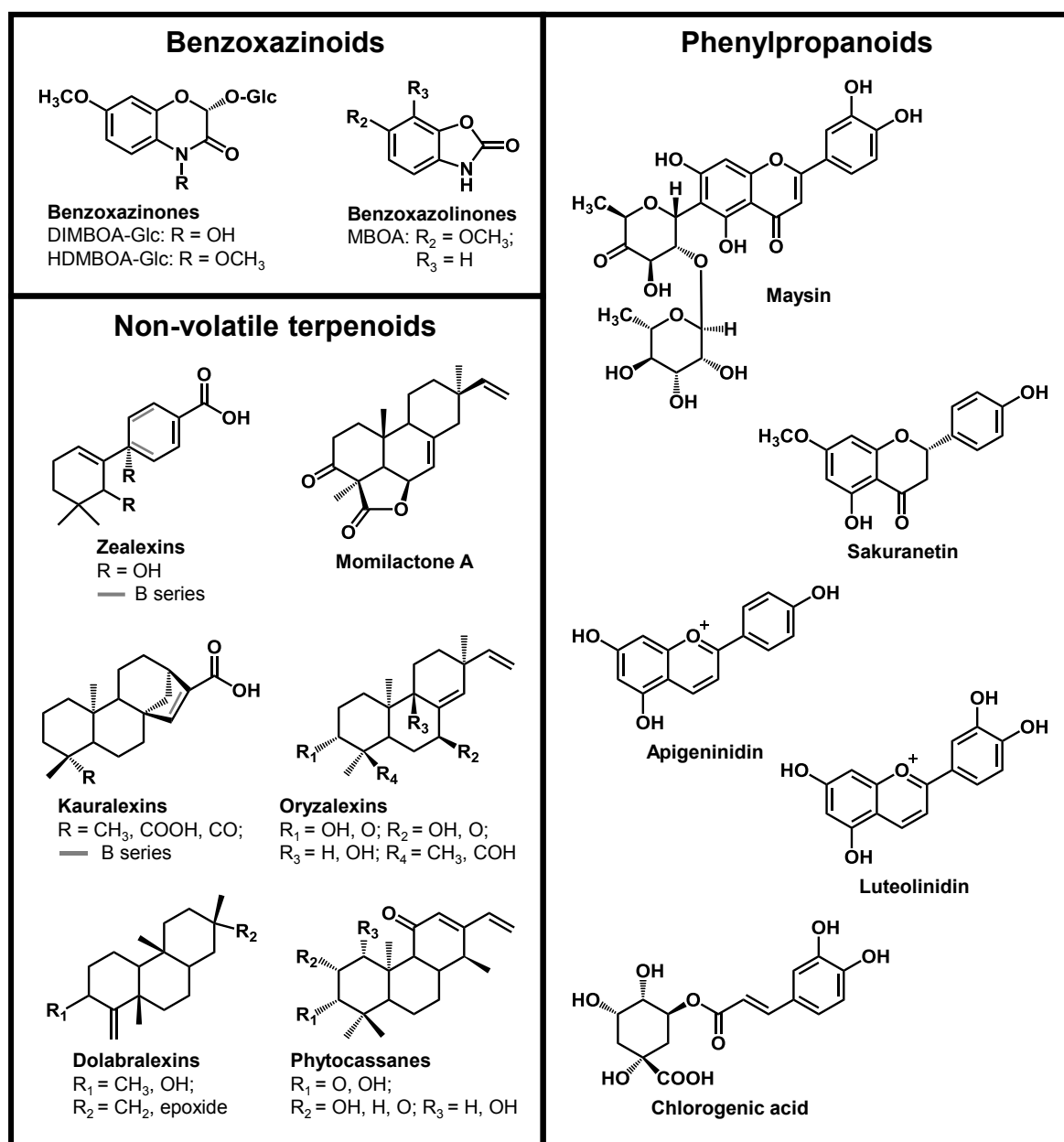


Figure 2. Common defense compounds in the Poaceae.

Non-volatile terpenoids: modified after Mafu et al. (2018) and Wang et al. (2018).

Some members of the Poaceae also produce phenylpropanoids upon insect or pathogen attack. Well-known examples are sakuranetin from rice, apigeninidin and luteolinidin from sorghum, maysin from maize, as well as chlorogenic acid (3-caffeoyl-quinic acid) (Figure 2). Sakuranetin is an *O*-methylated flavonoid phytoalexin that accumulates in rice leaves in response to infection with the rice blast fungus *Magnaporthe oryzae* or abiotic stress and shows *in vitro* antifungal activity to this and other fungal pathogens (Kodama et al., 1992;

Rakwal et al., 1996; Murata et al., 2020). In addition, this phytoalexin was also shown to inhibit the growth of *M. oryzae in planta* (Hasegawa et al., 2014). Similarly, apigeninidin and luteolinidin are also flavonoid phytoalexins. These red- to- orange colored 3-deoxyanthocyanidins have been shown to accumulate in inclusion bodies in the cytoplasm of epidermal cells infected with the anthracnose fungus *Colletotrichum graminicola*. They exhibit fungitoxic activity *in vitro*, and have been identified as resistance factors *in vivo* (Nicholson et al., 1987; Snyder and Nicholson, 1990; Lo et al., 1999). Maysin is another flavonoid derivative, more specifically a C-glycoside of the flavone luteolin. It accumulates in maize silks and is thought to be related to natural resistance against the herbivore corn earworm (*Helicoverpa zea*) (Waiss et al., 1979; Wiseman et al., 1992). Moreover, a derivative of the C-glycosylflavone isovitexin, namely Isovitexin-2'-O- β -[6-O-E-*p*-coumaroylglucopyranoside], found in UV-B irradiated rice leaves, reduced the fertility of the cotton bollworm (*Helicoverpa armigera*) (Caasi-Lit et al., 2007). Chlorogenic acid, a conjugate of caffeic acid and quinic acid, is a widely distributed plant natural product. In maize, it is induced in leaves, roots, silks, and kernels after insect herbivory or pathogen infection. It has been shown to reduce the growth of lepidopteran herbivores such as *H. zea* and fungal pathogens such as *C. graminicola in vitro* (Isman and Duffey, 1982; Bushman et al., 2002; Atanasova-Penichon et al., 2012; Balmer et al., 2013).

Several other classes of defense compounds occur in grasses, such as induced volatile mono- and sesquiterpenes, which act either directly or indirectly against attacking organisms (Degenhardt, 2009; Wang et al., 2018). Two classes of secondary metabolites, BXs and flavonoids, and an important enzyme class involved in the formation of these metabolites, namely O-methyltransferases, were of particular importance for my studies and are described in more detail in the following sections.

1.4 BX hydroxamic acids: Chemical properties and biological activity

BXs comprise benzoxazinones that share the basic 2-hydroxy-2*H*-1,4-benzoxazin-3(4*H*)-one (HBOA) skeleton (e.g. 2,4-dihydroxy-1,4-benzoxazin-3-one (DIBOA) or 2,4-dihydroxy-7-methoxy-1,4-benzoxazin-3-one (DIMBOA)) and their degradation products, known as benzoxazolinones (e.g. 6-methoxy-2-benzoxazolinone (MBOA)) (Figure 3). Depending on the substitution pattern on the heterocyclic nitrogen atom, benzoxazinones are further divided into lactams (N-H), hydroxamic acids (N-OH), and N-O-methylated derivatives (N-OCH₃) (Niemeyer, 2009).

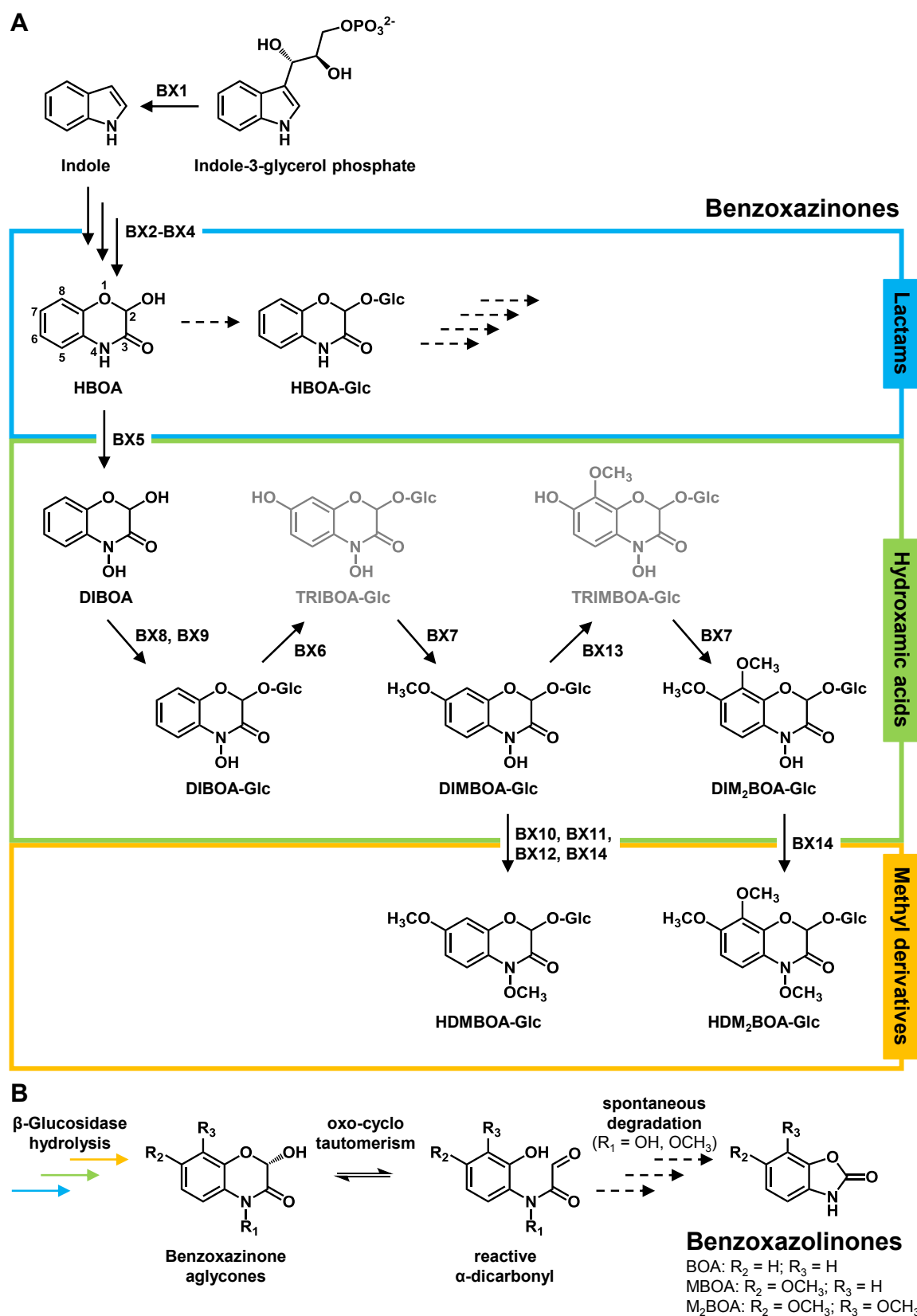


Figure 3. Biosynthesis of BXs in maize (A) and their transformation into reactive intermediates upon cell damage (B). Biosynthetic intermediates that do not usually accumulate are shown in grey. Dashed arrows indicate further steps. Modified after de Bruijn et al. (2018) and Wouters et al. (2016).

BX breakdown is initiated by enzymatic hydrolysis of the glycosidic bond, and the stability and reactivity of intermediates of this breakdown depends largely on the nature of the nitrogen function and additional functional groups on the benzoxazinone backbone (e.g. hydroxy and methoxy groups at positions 7 and 8). BX hydroxamic acids are the most abundant and active BX derivatives produced in plants. This is attributed mainly to the cyclic hemiacetal unit of their aglucones, which undergoes fast and reversible ring opening by oxo-cyclo-tautomerism, thereby generating highly reactive α -oxo-aldehyde intermediates (Figure 3B). Furthermore, upon heterolytic cleavage of the N-O bond, a reactive nitrenium (N^+) ion is formed. Both, the α -dicarbonyl moiety in the open ring form and the nitrenium ion are potent electrophilic sites that have been suggested to react with nucleophiles in proteins (e.g. amino and thiol groups) and nucleic acids, thus forming the basis for the deterrent and/or toxic effects of BXs to insect herbivores and pathogens (Niemeyer, 2009; Wouters et al., 2016). DIMBOA, for instance, was shown to inhibit proteases such as α -chymotrypsin and papain and so likely also be active against the digestive enzymes of insect herbivores (Perez and Niemeyer, 1989; Cuevas et al., 1990). This BX also inhibits aphid cholinesterases (Cuevas and Niemeyer, 1993), and interferes with detoxification enzymes of aphids such as glutathione S-transferases and catalases (Loayza-Muro et al., 2000; Mukanganyama et al., 2003). The ability of BX hydroxamic acids to chelate metal cations may also play a role in enzyme inhibition (Tipton and Buell, 1970; Marmion et al., 2013).

The reactivity and hence biological activity of BXs is enhanced by O-methylation, e.g. on the hydroxyl group at C-7 (as in DIMBOA and HDMBOA) or on the N-OH group (as in HDMBOA). For C-7 O-methylation, increased reactivity is probably due to the electron donating properties of the 7-methoxy group, which facilitates the cleavage of the N-O bond, while methylation on the N-OH group increases reactivity by the formation of a better leaving group at the nitrogen atom (Wouters et al., 2016). Indeed, HDMBOA degrades much more rapidly than DIMBOA, forming reactive intermediates (e.g. *o*-imidoquinone). This compound is considered one of the most active BXs and has been associated with increased resistance against chewing herbivores (Maresh et al., 2006; Glauser et al., 2011). Moreover, a correlation between the presence of 7-methoxy BXs and resistance to *Fusarium* pathogens was observed in wheat varieties (Søltoft et al., 2008). As a final result of ring opening of BX hydroxamic acid aglucones and subsequent spontaneous degradation, benzoxazolinones are formed, which themselves possess toxic properties to some organisms (Wouters et al., 2016). MBOA, for instance, inhibited the germination of

conidia and the growth of germ tubes of different fungal pathogens more effectively than its precursors (Oikawa et al., 2004).

1.5 The biosynthesis of BX hydroxamic acids in grasses

Studies on the biosynthesis of BX hydroxamic acids in maize (Figure 3A) started in the 1960s (Reimann and Byerrum, 1964), continued with the isolation and characterization of the core pathway genes in the 1990s and 2000s (Frey et al., 2009), and concluded recently with the full elucidation of the remaining steps (Meihls et al., 2013; Handrick et al., 2016). The first step of the pathway is the conversion of the shikimate pathway-derived indole-3-glycerol phosphate to indole by benzoxazinless 1 (BX1) in the chloroplast (Frey et al., 1997). BX1 is an indole-3-glycerolphosphate lyase and homologue of the alpha subunit of tryptophan synthase, but unlike the latter, it is active as a monomer (Frey et al., 2000). Subsequently, free indole undergoes four consecutive oxidation reactions catalyzed by the specific oxygen- and NADPH-dependent cytochrome P450 monooxygenases (CYPs) BX2, BX3, BX4, and BX5 in the endoplasmatic reticulum membrane, leading to the simplest BX hydroxamic acid DIBOA (Frey et al., 1997). Two cytosolic UDP-glucosyl-transferases, BX8 and BX9, then convert DIBOA to the stable glucoside (Glc) DIBOA-Glc (von Rad et al., 2001). In the cytosol, DIBOA-Glc is then further oxidized at C-7 by the Fe^{2+} /2-oxoglutarat-dependent dioxygenase (2-ODD) BX6 and subsequently O-methylated by the O-methyltransferase BX7 to DIMBOA-Glc (Frey et al., 2003; Jonczyk et al., 2008), which represents the most abundant BX in undamaged maize plants (Niemeyer, 1988; Cambier et al., 1999; Köhler et al., 2015).

However, upon induction by insect herbivory, fungal infection, or elicitor treatment (e.g. JA or CuCl_2), additional BXs are produced in maize and can become the predominant species. These include 2-hydroxy-4,7-dimethoxy-1,4-benzoxazin-3-one glucoside (HDMBOA-Glc), 2,4-dihydroxy-7,8-dimethoxy-1,4-benzoxazin-3-one glucoside ($\text{DIM}_2\text{BOA-Glc}$), and 2-hydroxy-4,7,8-trimethoxy-1,4-benzoxazin-3-one glucoside ($\text{HDM}_2\text{BOA-Glc}$) (Oikawa et al., 2001; Oikawa et al., 2004; Glauser et al., 2011; Marti et al., 2013; Handrick et al., 2016). The conversion of DIMBOA-Glc to its N-O-methyl derivative HDMBOA-Glc is catalyzed by three homologous O-methyltransferases, termed BX10, BX11, and BX12 (Meihls et al., 2013). HDMBOA-Glc was shown to be effective in deterring and reducing the growth of chewing herbivores (Glauser et al., 2011; Maag et al., 2016), and reducing aphid survival and reproduction *in vitro* (Cambier et al., 2001; Meihls et al., 2013). Its precursor DIMBOA-Glc, on the other hand, has been demonstrated to function as a defense signal that triggers

callose deposition, thus providing a resistance factor against phloem-feeding aphids (Ahmad et al., 2011; Meihls et al., 2013; Betsiashvili et al., 2015). Thus, caterpillar-induced depletion of DIMBOA-Glc in favor of HDMBOA-Glc represents a trade-off between aphid and caterpillar resistance in maize (Meihls et al., 2013; Tzin et al., 2015).

The final steps of the maize BX biosynthetic pathway were recently elucidated by Handrick et al. (2016) and involve the successive formation of C-8-O-methylated DIM₂BOA-Glc and HDM₂BOA-Glc from DIMBOA-Glc by the 2-ODD BX13 (homologous to BX6) and the O-methyltransferase BX14 (homologous to BX10-12), with BX7 being recruited to the pathway a second time. Accumulation of DIM₂BOA-Glc and HDM₂BOA-Glc were suggested to be associated with aphid resistance, but in contrast to DIMBOA-Glc due to direct toxicity rather than triggering callose deposition (Handrick et al., 2016; Song et al., 2017).

Besides maize, the core BX pathway leading to DIBOA-Glc and/or DIMBOA-Glc is also present in other cereals such as wheat and rye and is likely of monophyletic origin within the grass family (Frey et al., 2009; Makowska et al., 2015; Tanwir et al., 2017). Moreover, the accumulation of HDMBOA-Glc with a concomitant decline in DIMBOA-Glc was also observed in wheat after JA treatment (Oikawa et al., 2002). Although the DIMBOA-Glc 4-O-methyltransferase responsible for this reaction has been partially purified from JA-treated leaves (Oikawa et al., 2002), so far the corresponding gene remained to be unknown. The identification and characterization of the respective *BX10*-like gene in wheat and its evolution was one of the objectives of this work. Furthermore, I wanted to identify the ancestral enzymatic activity from which the DIMBOA-Glc O-methyltransferases evolved in grasses.

1.6 Flavonoids: widely distributed multifunctional plant metabolites

With an estimated number of more than 9,000 compounds and ubiquitous distribution throughout the plant kingdom, flavonoids are among the largest and most widespread groups of plant natural products (Williams and Grayer, 2004; Yonekura-Sakakibara et al., 2019). Research interest in this class of compounds has always been high, mainly driven by the fact that they have numerous health benefits for humans. For example, flavonoids are associated with anti-inflammatory, anti-cancer, cardio- and neuroprotective, antidiabetic, antibacterial, antifungal, and antiviral properties (Dias et al., 2021).

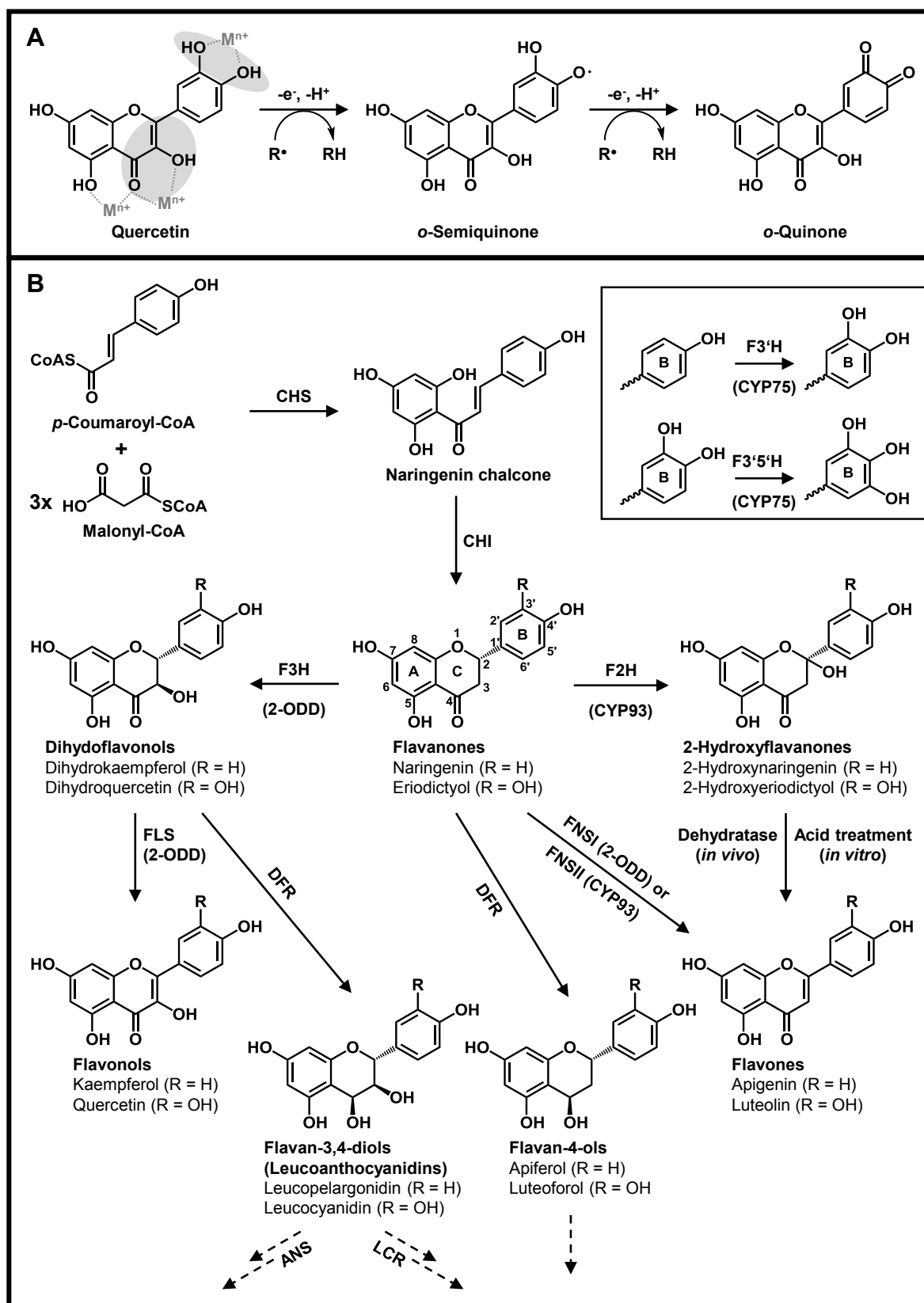
Flavonoids are derived from the phenylpropanoid and polyketide (or acetate) pathways and share a 15-carbon core structure (C6-C3-C6), consisting of two aromatic rings (A and B)

connected by a heterocyclic pyran ring (C) (Figure 4) (Tohge et al., 2017; de Souza et al., 2020). Based on variation in this heterocyclic ring system (e.g. hydroxylation, double bond formation, position of attachment of the B-ring), flavonoids are subdivided into several major subclasses such as flavanones, flavones, dihydroflavonols, flavonols, flavanols, anthocyanidins, and isoflavones (Marais et al., 2006). Within these classes, the substitution pattern of the A and B rings differs between individual compounds (Kumar and Pandey, 2013). Common modifications of the flavonoid backbone such as hydroxylation, glycosylation, O-methylation, and acylation further increase the structural diversity of flavonoids and alter their stability, solubility, and reactivity (Stobiecki and Kachlicki, 2006).

Given their enormous structural variety, it is not surprising that flavonoids serve as multifunctional molecules in diverse abiotic and biotic plant-environment interactions. Some of the well-known biological functions of flavonoids in plants include protection against oxidative stress and UV radiation due to their antioxidative and absorbing properties, attraction of pollinators and seed dispersers due to their colors, as well as defense against insect herbivores and pathogens likely based on various mechanisms (Mierziak et al., 2014). Some flavonoid derivatives such as the flavone C-glycoside maysin (see chapter 1.3) or isoflavonoid derivatives such as judaicin and maackianin found in chickpea (*Cicer arietinum*) have been shown to be deterrent or toxic to herbivores (Wiseman et al., 1992; Simmonds and Stevenson, 2001). However, the responses of insect herbivores to flavonoids can vary substantially, and several flavonoid glycosides even appear to act as feeding stimulants (Simmonds, 2003). Other flavonoids, such as the 3-deoxyanthocyanidins of sorghum (see chapter 1.3) or the flavan-3-ols of poplar, on the other hand, accumulate in the plant after pathogen infection and have been demonstrated to play a role in resistance to pathogens (Lo et al., 1999; Ullah et al., 2017). Simple flavonoid aglucones such as luteolin and apigenin may also be phytoalexins with antifungal activity (Du et al., 2010b).

Figure 4. Flavonoid antioxidant activity and biosynthesis. (A) Oxidation of quercetin upon scavenging of ROS (R^{\bullet}). Structural features and metal (M^{n+}) binding sites important for antioxidant activity are highlighted in grey. Modified after Kumar and Pandey (2013). **(B)** Core flavonoid biosynthetic pathways. Dashed arrows indicate further steps. Enzyme abbreviations: CHS, chalcone synthase; CHI, chalcone isomerase; F2H, flavanone 2-hydroxylase; F3H, flavanone 3-hydroxylase; F3'H/F3'5'H, flavonoid 3'/3',5'-hydroxylase; FNS, flavone synthase; FLS, flavonol synthase; DFR, dihydroflavonol 4-reductase; ANS, anthocyanidin synthase; LCR, leucoanthocyanidin reductase.





Although the exact mode of action of flavonoids is mostly unknown, activity is often associated with their antioxidant properties (Mierziak et al., 2014). Antioxidant activity relies mainly on the configuration and total number of free hydroxyl groups. Of particular importance are the hydroxylation pattern of the flavonoid B-ring (e.g. 3'4'-catechol structure), the presence of a 3-OH group, and a double bond between C-2 and C-3 in conjugation with a 4-oxo function. These features are essential for scavenging of ROS and metal ion chelation, two important mechanisms of antioxidant activity (Figure 4A). Modifications such as glycosylation or O-methylation usually reduce the antioxidant activity of flavonoids (Heim et al., 2002). The hydroxyl groups of the B-ring (catechol moiety) donate hydrogen and an electron to free radicals such as superoxide, hydroxyl, and peroxy radicals, thereby stabilizing them. In this process, the flavonoid is oxidized to a relatively stable *o*-semiquinone radical. Since free transition metal ions such as ferrous iron (Fe^{2+}) can enhance the production of ROS in the Fenton reaction, the ability of flavonoids to chelate these metal ions also contributes to their function as antioxidants. (Heim et al., 2002). In addition, flavonoids have been shown to inhibit enzymes involved in ROS generation such as animal xanthine oxidase and NADH oxidase (Hodnick et al., 1994; Cos et al., 1998). Since ROS are induced by various stresses, including pathogen infections, antioxidant flavonoids may be indirectly involved in plant resistance to necrotrophic pathogens through suppression of oxidative stress (Zhang et al., 2015). However, apart from their antioxidant activity, flavonoids have been shown to interact with lipids, nucleic acids, and proteins, suggesting additional mechanisms of action in relation to plant defense (Jiang et al., 2016).

1.7 The biosynthesis of flavonoids

Many efforts have been made to elucidate flavonoid biosynthetic pathways, leading to a detailed characterization of the pathways in several plant species (Tohge et al., 2017). The core pathway (Figure 4B) is well conserved across plants and starts with the phenylpropanoid pathway derivative, 4-coumaroyl-CoA, which is condensed with three malonyl-CoA subunits by the polyketide synthase chalcone synthase (CHS). Subsequently, the naringenin chalcone produced is cyclized by chalcone isomerase (CHI) to a flavanone (e.g. naringenin, eriodictyol), the central precursor and first branch point of the flavonoid biosynthetic pathway. The other central flavonoid subclasses are formed successively by the hydroxylating or desaturating activity of either membrane-bound CYPs or soluble 2-ODDs. Flavonoid 3'-hydroxylases (F3'Hs; CYPs) and flavonoid 3'5'-hydroxylases

(F3'5'Hs; CYPs) introduce a hydroxyl group on the flavonoid B-rings of various substrates belonging to different flavonoid subclasses. Dihydroflavonols (e.g. dihydrokaempferol, taxifolin) are synthesized from flavanones by flavanone 3-hydroxylases (F3Hs; 2-ODDs) and can be further converted to flavonols (e.g. kaempferol, quercetin) by flavonol synthases (FLSs; 2-ODDs).

Two distinct types of flavone synthases (FNS) desaturate the C-ring of flavanones and convert them directly to flavones (e.g. apigenin, luteolin) via different mechanisms (Martens and Mithöfer, 2005; Jiang et al., 2016). While FNSs of type I (FNSI) belong to the 2-ODDs and catalyze two sequential elimination reactions, FNSs of type II (FNSII) are CYPs that are proposed to generate the double bond via a reaction, where initial hydrogen abstraction from C-2 is followed by hydroxylation at this position and finally dehydration between C-2 and C-3 (Sawada and Ayabe, 2005; Cheng et al., 2014). Interestingly, several FNSII enzymes have been reported that seem to have lost their dehydratase activity resulting in the production of 2-hydroxyflavanones and hence are rather flavanone 2-hydroxylases (F2Hs), often involved in the biosynthesis of flavone C-glycosides in cereals (Akashi et al., 1998; Du et al., 2010a; Du et al., 2010b; Morohashi et al., 2012).

Additional enzymes such as dihydroflavonol 4-reductases (DFRs), anthocyanidin synthases (ANSs), and leucoanthocyanidin reductases (LARs) are involved in further steps leading to different flavanols and anthocyanidins. Finally, modifications such as glycosylation and O-methylation are catalyzed by specific flavonoid C- and O-glycosyltransferases and flavonoid O-methyltransferases (FOMTs), respectively (Winkel, 2006).

In many cases, these O-methylated flavonoids have been shown to be potent antimicrobial phytoalexins, often exhibiting higher antifungal activity than their non-O-methylated precursors. These include O-methylflavonoids found in the Poaceae family such as sakuranetin (7-methoxynaringenin; see chapter 1.3) (Kodama et al., 1992), the 3'5'-dimethoxylated flavone triclin from rice and other cereal crops (Kong et al., 2010; Zhou and Ibrahim, 2010), genkwanin (7-methoxyapigenin) found in maize (Balmer et al., 2013), polymethoxychalcones from barley (Ube et al., 2021), and 5-methoxyluteolinidin from sorghum (Lo et al., 1996). However, despite initial evidence that genkwanin accumulates in maize after infection with the fungal pathogen *C. graminicola* (Balmer et al., 2013), nothing was previously known about flavonoid phytoalexin biosynthesis in maize. Therefore, the main goal of this thesis was to investigate fungus-induced flavonoid metabolism in maize, identify and characterize O-methyltransferases as key players in the formation of O-methylated flavonoid phytoalexins, and investigate their role in pathogen defense.

1.8 Plant O-methyltransferases

As already mentioned in the preceding chapters, O-methylation of specialized plant metabolites is an important and ubiquitously distributed tailoring reaction that helps plants cope with different biotic and abiotic stresses. O-methylation is catalyzed by S-adenosyl-L-methionine (SAM)-dependent O-methyltransferases (OMTs), which transfer the methyl group of the co-substrate SAM to a hydroxyl moiety of various acceptor molecules. This produces S-adenosyl-L-homocysteine (SAH) and the corresponding methyl ether derivative, which exhibits reduced reactivity of hydroxyl groups and altered solubility. Methoxylated flavonoids also have altered biological activity, stability, intracellular localization, and metabolic fate compared to their hydroxylated progenitors (Ibrahim et al., 1987; Ibrahim et al., 1998).

Plant OMTs have been classified into three major groups, based on phylogenetic analysis, conserved amino acid sequence features, protein structures, and their substrate specificities: the caffeic acid OMTs (COMTs), caffeoyl-CoA OMTs (CCoAOMTs), and carboxylic acid OMTs (Joshi and Chiang, 1998; Noel et al., 2003; Lam et al., 2007). The latter belong to the SABATH methyltransferase family, share only marginal sequence similarities with the other classes of OMTs and are involved, for instance, in the methylation of phytohormones such as salicylic acid, jasmonic acid, and indole-3-acetic acid (Qu et al., 2010). CCoAOMTs are bivalent cation-dependent enzymes that have high sequence similarity with each other and specifically methylate the coenzyme A (CoA) esters of phenylpropanoids, mainly caffeoyl-CoA, an important step in the biosynthesis of monolignols (Noel et al., 2003). A distinct subtype of CCoAOMTs, named CCoAOMT-like enzymes, was shown to accept not only caffeoyl-CoA but also flavonoids as substrates (Ibdah et al., 2003; Lee et al., 2008). All remaining plant OMTs belong to the large COMT class, which accepts a variety of different substrates, including phenylpropanoids, flavonoids, alkaloids, and coumarins. COMTs are larger (40-43 kDa) than CCoAOMTs (26-30 kDa) and do not require bivalent cations for activity (Lam et al., 2007; Kim et al., 2010).

The majority of plant OMTs show remarkable substrate specificity as well as regiospecificity for certain hydroxyl groups (Ibrahim et al., 1998). However, multifunctional OMTs that are able to utilize structurally related compounds such as flavonoids and phenylpropanoids (Gauthier et al., 1998; Frick and Kutchan, 1999) or exhibit non-selective positional activity (Deavours et al., 2006; Itoh et al., 2016; Liu et al., 2020) have also been described. In some cases, different substrate specificities or regiospecificities have been associated with single

amino acid changes (Gang et al., 2002; Zhou et al., 2010). Therefore, amino acid sequence similarity alone is not sufficient for a correct prediction of substrate specificity (Schröder et al., 2002). Nevertheless, in general there is a good agreement between phylogenetic clustering of COMTs in distinct subclasses and the structural similarity of their preferred substrates (Joshi and Chiang, 1998; Lam et al., 2007). While some COMT genes appear to be evolutionary conserved across species, there are several examples that support divergent and convergent evolution within the COMT class. This means that structurally similar enzymes have diverged from a common ancestor to act on different substrates, or that structurally distinct enzymes that do not share a common ancestor have evolved independently (convergently) in different species to act on similar substrates (Lam et al., 2007).

The elucidation of crystal structures of isoflavone OMTs (IOMTs) from legumes by X-ray crystallography has revealed the structural basis of COMT-type OMT activity (Zubieta et al., 2001; Zubieta et al., 2002; Liu et al., 2006). In contrast to non-plant OMTs that are usually monomeric, all plant OMTs appear to be active as homodimers (Noel et al., 2003). COMTs additionally have an N-terminal domain that is involved in dimerization, with the dimer interface forming the back wall of the active site and therefore concurrently contributing to substrate binding. All other residues involved in substrate binding, SAM binding and catalysis are located in the C-terminal domain. A hydrophobic methionine-rich active site pocket is typical to ensure binding of the hydrophobic substrates (Zubieta et al., 2001). The methylation reaction follows a S_N2 -like mechanism, involving a conserved His base for deprotonation of the target hydroxyl group and negatively charged residues such as Glu or Asp for stabilization. Initial deprotonation is followed by nucleophilic attack of the generated phenolate anion of the substrate on the reactive methyl group of SAM (Zubieta et al., 2001; Zhou et al., 2010). In Manuscript III, I used the knowledge about IOMT structure-activity relationships to explore the determinants of substrate specificity of DIMBOA-Glc OMTs and their ancestors in grasses.

2. Manuscripts overview

2.1 Manuscript I

Convergent evolution of a metabolic switch between aphid and caterpillar resistance in cereals

Beibei Li, Christiane Förster, Christelle A. M. Robert, Tobias Züst, Lingfei Hu, Ricardo A. R. Machado, Jean-Daniel Berset, Vinzenz Handrick, Torsten Knauer, Götz Hensel, Wanxin Chen, Jochen Kumlehn, Ping Yang, Beat Keller, Jonathan Gershenzon, Georg Jander, Tobias G. Köllner, and Matthias Erb

Published in Science Advances (2018), 4, doi:10.1126/sciadv.aat6797

Summary:

The benzoxazinoid (BX) DIMBOA-Glc is converted to the N-O-methyl derivative HDMBOA-Glc upon induction by herbivory in both maize and wheat. Using a transcriptome-based approach, the herbivore-induced wheat gene encoding the DIMBOA-Glc 4-O-methyltransferase (OMT) *TaBX10* that catalyzes this reaction was identified. *TaBX10* was shown to be only distantly related to the previously characterized maize DIMBOA-Glc 4-OMT genes (*ZmBX10-ZmBX12*, and *ZmBX14*), suggesting independent evolution of these OMTs in wheat and maize. However, the function of these BXs in defense and defense regulation was shown to be the same in both species; the precursor DIMBOA-Glc is linked to callose-mediated aphid resistance and the product HDMBOA-Glc is linked to caterpillar resistance.

2.2 Manuscript II

Biosynthesis and antifungal activity of fungus-induced O-methylated flavonoids in maize

Christiane Förster, Vinzenz Handrick, Yezhang Ding, Yoko Nakamura, Christian Paetz, Bernd Schneider, Gabriel Castro-Falcón, Chambers C. Hughes, Katrin Luck, Sowmya Poosapati, Grit Kunert, Alisa Huffaker, Jonathan Gershenzon, Eric A. Schmelz, and Tobias. G. Köllner

Published in Plant Physiology (2021), doi:10.1093/plphys/kiab496

Summary:

In this study, the metabolism of flavonoids, particularly the formation of O-methylated flavonoids, after fungal infection was comprehensively investigated in maize. Three *OMT* genes (*ZmFOMT2*, *ZmFOMT4*, and *ZmFOMT5*) and a gene encoding a cytochrome P450 monooxygenase (CYP) of the CYP93G subfamily (F2H2) were identified and shown to be up-regulated upon fungal infection. The encoded enzymes exhibited distinct regiospecificity and were able to produce major constituents of the induced maize flavonoid blend *in vitro*, including a novel tautomeric di-O-methylated flavonoid derivative termed xilonenin. Xilonenin and other abundant O-methylflavonoids and non-O-methyl flavonoids showed varying antifungal activities in *in vitro* bioassays. The role of complex flavonoid mixtures in maize pathogen defense is discussed.

2.3 Manuscript III

Evolution of DIMBOA-Glc O-methyltransferases from flavonoid O-methyltransferases in the grasses

Christiane Förster, Jonathan Gershenzon, and Tobias G. Köllner

Submitted for publication to Molecules (MDPI)

Summary:

Two flavonoid 5-OMTs, ZmFOMT2 and ZmFOMT3, associated with flavonoid phytoalexin biosynthesis in maize are closely related to the DIMBOA-Glc 4-OMTs ZmBX10, ZmBX11, ZmBX12 and ZmBX14 (Manuscript II). Phylogenetic analyses and biochemical characterization revealed homologous enzymes in several other Poaceae species and suggested that DIMBOA-Glc 4-OMTs evolved from flavonoid OMTs in the PACMAD clade of the grasses. The enzymatic requirements for flavonoid and benzoxazinoid substrate specificity were studied by homology modeling and *in vitro* mutagenesis and indicated that complex amino acid changes are likely required for the activity switch.

3. Manuscripts

3.1 Manuscript I

Manuscript title: Convergent evolution of a metabolic switch between aphid and caterpillar resistance in cereals

Authors: Beibei Li, Christiane Förster, Christelle A. M. Robert, Tobias Züst, Lingfei Hu, Ricardo A. R. Machado, Jean-Daniel Berset, Vinzenz Handrick, Torsten Knauer, Götz Hensel, Wanxin Chen, Jochen Kumlehn, Ping Yang, Beat Keller, Jonathan Gershenzon, Georg Jander, Tobias G. Köllner, and Matthias Erb

Bibliographic information: Li, B., Förster, C., Robert, C.A.M., Züst, T., Hu, L., Machado, R.A.R., Berset, J.-D., Handrick, V., Knauer, T., Hensel, G., Chen, W., Kumlehn, J., Yang, P., Keller, B., Gershenzon, J., Jander, G., Köllner, T.G., and Erb, M. (2018). Convergent evolution of a metabolic switch between aphid and caterpillar resistance in cereals. *Sci Adv* 4, eaat6797.

The candidate is

☐ First author, ☐ Co-first author, ☐ Corresponding author, ☒ Co-author.

Status: published December 5 (2018) in Science Advances

Authors' contributions (in %) to the publication (indicated from 20%)

Author	Conceptual	Data analysis	Experimental	Writing the manuscript	Supply of material
Christiane Förster	/	25	25	/	/
Beibei Li	/	50	50	/	/
Jonathan Gershenzon	5	/	/	/	50
Tobias G. Köllner	40	5	5	40	/
Matthias Erb	50	/	/	60	50

PLANT SCIENCES

Convergent evolution of a metabolic switch between aphid and caterpillar resistance in cereals

B. Li¹, C. Förster², C. A. M. Robert¹, T. Züst¹, L. Hu¹, R. A. R. Machado¹, J.-D. Berset¹, V. Handrick^{2*}, T. Knauer², G. Hensel³, W. Chen³, J. Kumlehn³, P. Yang^{4†}, B. Keller⁴, J. Gershenzon², G. Jander⁵, T. G. Köllner^{2‡}, M. Erb^{1‡}

Tailoring defense responses to different attackers is important for plant performance. Plants can use secondary metabolites with dual functions in resistance and defense signaling to mount herbivore-specific responses. To date, the specificity and evolution of this mechanism are unclear. Here, we studied the functional architecture, specificity, and genetic basis of defense regulation by benzoxazinoids in cereals. We document that DIMBOA-Glc induces callose as an aphid resistance factor in wheat. O-methylation of DIMBOA-Glc to HDMBOA-Glc increases plant resistance to caterpillars but reduces callose inducibility and resistance to aphids. DIMBOA-Glc induces callose in wheat and maize, but not in *Arabidopsis*, while the glucosinolate 4MO-I3M does the opposite. We identify a wheat O-methyltransferase (TaBX10) that is induced by caterpillar feeding and converts DIMBOA-Glc to HDMBOA-Glc in vitro. While the core pathway of benzoxazinoid biosynthesis is conserved between wheat and maize, the wheat genome does not contain close homologs of the maize DIMBOA-Glc O-methyltransferase genes, and *TaBX10* is only distantly related. Thus, the functional architecture of herbivore-specific defense regulation is similar in maize and wheat, but the regulating biosynthetic genes likely evolved separately. This study shows how two different cereal species independently achieved herbivore-specific defense activation by regulating secondary metabolite production.

INTRODUCTION

The capacity to resist a large diversity of herbivores is essential for plant fitness in nature and yield in agriculture. Plant resistance strategies are complicated by the fact that herbivores with different lifestyles are susceptible to different types of defenses. Chewing herbivores, for instance, ingest entire leaf parts and are therefore susceptible to plant toxins that accumulate throughout the leaf (1, 2). By contrast, piercing-sucking herbivores, such as aphids, often feed directly from the phloem and are therefore most susceptible to phloem-specific defenses (3, 4). The resulting selection pressure for herbivore-specific deployment of defenses has important consequences for the evolution, physiology, and ecology of plant immunity against herbivores (5–7).

To mount herbivore-specific defense responses, plants have evolved several regulatory mechanisms. Phytohormonal signaling and cross-talk, for instance, allow plants to finely regulate their induced responses (8). In this context, jasmonate (JA) signaling is often associated with induced resistance to chewing herbivores, while salicylate (SA) signaling is associated with resistance to piercing-sucking insects (9). However, the picture is likely more complex, as plants use a variety of hormones to form signaling networks that allow for targeted responses against chewing and piercing-sucking herbivores (8, 10).

Apart from hormonal cross-talk, plants can also use secondary metabolites as defensive switches. In maize, the benzoxazinoid 2,4-dihydroxy-7-methoxy-1,4-benzoxazin-3-one- β -D-glucopyranose (DIMBOA-Glc) and its aglucone DIMBOA are positive regula-

tors of callose induction and are associated with increased aphid resistance (11), while the DIMBOA-Glc O-methylation product 2-(2-hydroxy-4,7-dimethoxy-1,4-benzoxazin-3-one)- β -D-glucopyranose (HDMBOA-Glc) acts as a feeding deterrent against both aphids and chewing herbivores in vitro (12, 13). Upon caterpillar attack, maize plants transform DIMBOA-Glc into HDMBOA-Glc by up-regulating the transcription of three closely related O-methyltransferases (OMTs) (ZmBX10–ZmBX12) (13, 14). By contrast, upon aphid attack, the aglucone DIMBOA is secreted into the apoplastic space, and DIMBOA-Glc levels remain high (11). Maize DIMBOA-Glc OMTs may therefore act as metabolic switches between caterpillar and aphid resistance. However, the relative contributions of DIMBOA-Glc and HDMBOA-Glc to in planta caterpillar resistance remain to be determined.

Similar to benzoxazinoids in grasses, glucosinolates can regulate callose deposition in *Arabidopsis* (*Arabidopsis thaliana*). 4-Hydroxyindol-3-yl-methyl glucosinolate (4MO-I3M) is necessary and sufficient to induce callose in response to microbe-associated molecular patterns such as the flagellin peptide flg22 (15). Callose deposition depends on the myrosinase PENETRATION 2 (PEN2) and may therefore be elicited by 4MO-I3M breakdown products (15). Callose deposition upon infection with fungal and oomycete pathogens is still intact in PEN2- and 4MO-I3M-deficient mutants, suggesting that 4MO-I3M is not strictly required for induced callose deposition in *Arabidopsis* (16). Despite their differences, 4MO-I3M and DIMBOA share some structural and biosynthetic similarities, including an aromatic ring bearing an O-methoxy group, a glucose moiety and indole as a precursor. Whether the capacity of benzoxazinoids and glucosinolates to regulate callose is conserved across mono- and dicotyledons is unclear (17).

A common feature of regulation of herbivore-specific defenses is that these defenses can result in signaling trade-offs. The induction of SA-mediated defenses by piercing-sucking insects, for instance, suppresses JA-dependent volatile defenses against other herbivores (18). Furthermore, many early signaling elements, which are required for induced defenses against chewing herbivores, result in

Copyright © 2018
The Authors, some
rights reserved;
exclusive licensee
American Association
for the Advancement
of Science. No claim to
original U.S. Government
Works. Distributed
under a Creative
Commons Attribution
License 4.0 (CC BY).

¹Institute of Plant Sciences, University of Bern, Bern, Switzerland. ²Max Planck Institute for Chemical Ecology, Jena, Germany. ³Leibniz Institute of Plant Genetics and Crop Plant Research, Gatersleben, Germany. ⁴Department of Plant and Microbial Biology, University of Zürich, Zürich, Switzerland. ⁵Boyce Thompson Institute, Ithaca, NY, USA.

*Present address: John Innes Centre, Norwich, UK.

†Present address: Institute of Crop Science, Chinese Academy of Agricultural Science, Beijing, China.

‡Corresponding author. Email: matthias.erb@ips.unibe.ch (M.E.); koellner@ice.mpg.de (T.G.K.)

SCIENCE ADVANCES | RESEARCH ARTICLE

susceptibility against piercing-sucking insects (19–21). Whether secondary metabolite switches also result in similar trade-offs is less understood. In maize, caterpillar feeding increases aphid reproduction in some cultivars, and this effect was mapped to the *ZmBx10–ZmBx12* locus (22), lending first support to the hypothesis that the caterpillar-induced conversion of DIMBOA-Glc to HDMBOA-Glc reduces aphid resistance.

While the ecological relevance of herbivore specificity in defense induction is well established, much less is known about the evolution of the underlying mechanisms for that specificity. Analysis of the recent literature suggests that the negative interaction between JA and SA is a conserved trait that was likely already present in the ancestor of angiosperms (5). To what extent secondary metabolite switches are evolutionarily conserved is currently unknown. Some secondary metabolites have evolved independently several times (23). In general, the rapid evolution and variation in plant secondary metabolites (24, 25) may favor convergent evolution of secondary metabolite switches mediating specific herbivore resistance.

In this study, we characterized the specificity, functional architecture, and genetic basis of aphid and caterpillar resistance in wheat. On the basis of current knowledge on caterpillar and aphid resistance in maize, we focused on benzoxazinoids as direct and indirect regulators of resistance. The core benzoxazinoid pathway is conserved among different cereals and likely to be of monophyletic origin within the Poaceae (26). Furthermore, the induction of HDMBOA-Glc at the expense of DIMBOA-Glc upon caterpillar attack occurs in both wheat and maize (12, 27). We therefore hypothesized that the switch between aphid and caterpillar resistance should be conserved between the two species as well. To test this hypothesis, we first explored the functional architecture of benzoxazinoid-dependent defense and resistance by overexpressing a maize DIMBOA-Glc OMT in wheat. This approach allowed us to explore the importance of HDMBOA-Glc accumulation for caterpillar resistance in vivo and to quantify the contribution of DIMBOA-Glc methylation to caterpillar-induced aphid susceptibility. To evaluate the specificity of callose regulation by benzoxazinoids, we conducted complementation experiments with benzoxazinoids and glucosinolates in wheat and *Arabidopsis*. Last, we analyzed the genetic architecture of the benzoxazinoid switch by transcriptional profiling, heterologous expression, and genome-based phylogenetic analyses.

RESULTS

Influence of DIMBOA-Glc O-methylation on wheat defense

To explore the role of DIMBOA-Glc O-methylation in wheat, we generated transgenic plants harboring the DIMBOA-Glc OMT gene *ZmBx12* from maize under the control of a constitutive maize *UBIQUITIN1* promoter. Experiments were carried out using two T2 homozygous transgenic lines (OeBx12_1 and OeBx12_2), which constitutively expressed *ZmBx12* (Fig. 1A). Compared with wild-type plants, OeBx12 leaves accumulated high amounts of HDMBOA-Glc at the expense of DIMBOA-Glc and DIMBOA, which were almost entirely depleted (Fig. 1B). The HDMBOA-Glc breakdown product MBOA also accumulated in higher amounts in OeBx12 lines, while HMBOA-Glc, which is likely formed from DIMBOA-Glc or DIMBOA-Glc, was present in lower concentrations (fig. S1). Levels of the other benzoxazinoids in the leaves did not change significantly, apart from a slight increase in DIM₂BOA-Glc in one of the OeBx12 lines

(fig. S1). Similar patterns were found in phloem sap collected through aphid styletometry (Fig. 1C). While DIMBOA-Glc and DIMBOA were dominant in the phloem of wild-type plants, OeBx12 lines accumulated high amounts of HDMBOA-Glc at the expense of DIMBOA-Glc and DIMBOA (Fig. 1C). OeBx12 plants grew similar to their wild-type counterparts (Fig. 1D) and accumulated similar amounts of sugars, starch, and soluble protein in their leaves (fig. S1). We also did not find any consistent changes in free amino acids in the leaves and phloem of wild-type and OeBx12 plants (fig. S1). Higher amounts of ferulic acid were observed in OeBx12 plants compared with wild-type plants (fig. S2). Furthermore, OeBx12 plants displayed less callose induction following treatment with the fungal elicitor chitosan (Fig. 1E) and aphid infestation (Fig. 1F). Thus, the functional architecture of benzoxazinoid regulation of callose seems to be similar in wheat and maize.

To better understand the relationship between benzoxazinoids and callose induction, we infiltrated wild-type and OeBx12 plants with DIMBOA, DIMBOA-Glc, and HDMBOA-Glc. DIMBOA and DIMBOA-Glc treatments induced significant callose deposition in the leaves of wild-type plants, while HDMBOA-Glc had no effect (Fig. 2A). Unexpectedly, complementation of OeBx12 plants with DIMBOA or DIMBOA-Glc did not result in any callose induction (Fig. 2A). We devised two hypotheses to explain this result. First, we postulated that the high levels of HDMBOA-Glc in OeBx12 plants may inhibit callose induction. To test this hypothesis, we infused wild-type leaves with combinations of DIMBOA, DIMBOA-Glc, and HDMBOA-Glc. Co-infusion of HDMBOA-Glc did not suppress callose induction by DIMBOA and DIMBOA-Glc (Fig. 2C). As an alternative hypothesis, we tested whether the infused DIMBOA and DIMBOA-Glc are rapidly metabolized in OeBx12 lines. Infusion of DIMBOA and DIMBOA-Glc increased DIMBOA-Glc levels in wild-type plants, but not in OeBx12 lines (Fig. 2D), where levels remained constantly low. The levels of two likely metabolic products, HDMBOA-Glc and MBOA, were not significantly increased in the infiltrated leaves in any of the lines upon DIMBOA or DIMBOA-Glc infiltration (fig. S3). These results suggest that either rapid transformation to yet unidentified, inactive catabolites or rapid transport of HDMBOA-Glc or MBOA into systemic tissues may have prevented the induction of callose by DIMBOA and DIMBOA-Glc in OeBx12 lines.

Specificity of callose induction by benzoxazinoids and glucosinolates

To better understand the specificity of DIMBOA and DIMBOA-Glc as callose inducers, we infused the metabolites into *Arabidopsis* leaves. As a cross-comparison, we infused the glucosinolate 4MO-I3M, which is known to induce callose in *Arabidopsis* (15), into *Arabidopsis* and wheat. 4MO-I3M, but not DIMBOA or DIMBOA-Glc, induced callose in *Arabidopsis* (fig. S4A). 4MO-I3M did not induce callose in wheat (fig. S4B). Overall, we did not detect any callose induction in cross-infusions. Thus, the induction of callose by secondary metabolites is specific for the respective plant species.

Influence of DIMBOA-Glc O-methylation on caterpillar and aphid resistance

In maize, high DIMBOA-Glc levels are required for aphid resistance (13), while HDMBOA-Glc has been shown to act as a deterrent for caterpillars in vitro (12). To test whether DIMBOA-Glc O-methylation affects aphid and caterpillar resistance in wheat, we conducted a series

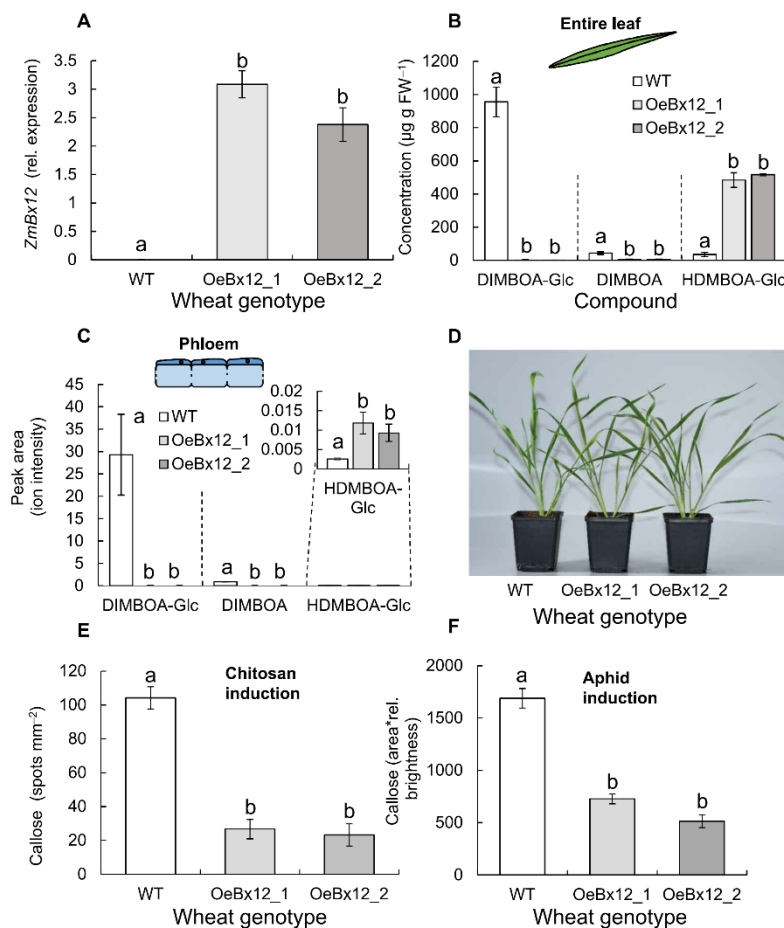


Fig. 1. Phenotype of *ZmBx12*-overexpressing wheat lines. (A) Relative (rel.) expression of the maize DIMBOA-Glc OMT *ZmBx12* in wild-type (WT) and *ZmBx12*-overexpressing plants ($n = 3$). (B) Major benzoxazinoids in the leaves of the different lines ($n = 5$). FW, fresh weight. (C) Major benzoxazinoids in the phloem of the different lines ($n = 3$ to 4). (D) Representative photograph of WT and transgenic lines. (E) Chitosan-induced callose deposition ($n = 9$ to 12). (F) Aphid-induced callose deposition ($n = 23$ to 39). Because of irregular shapes and brightness of callose induction spots following aphid attack, area*rel. brightness were used to assess callose deposition. Different letters indicate significant differences between wheat lines [analysis of variance (ANOVA) followed by Holm-Sidak post hoc tests, $P < 0.05$]. Photo credit for (D): B. Li and T. Züst, University of Bern.

of preference and performance tests. When given a choice, *Spodoptera littoralis* caterpillars preferred to feed on wild-type plants rather than on OeBx12 lines (Fig. 3A). Furthermore, they consumed more leaf biomass on wild-type plants (Fig. 3B). Caterpillar growth in no-choice experiments was not significantly affected (Fig. 3C). *Sitobion avenae* aphids, on the other hand, grew better on OeBx12 than wild-type plants (Fig. 3D). Thus, DIMBOA-Glc *O*-methylation increases caterpillar resistance through antixenosis but decreases aphid resistance in the form of antibiosis. To test whether DIMBOA-Glc *O*-methylation affects resistance against two common fungal pathogens, we quantified infection by powdery mildew (*Blumeria graminis* f. sp. *tritici*) and leaf rust (*Puccinia recondita* f. sp. *tritici*). OeBx12 expression did not affect wheat resistance against these pathogens (fig. S5).

Caterpillar attack increases DIMBOA-Glc *O*-methylation, and the resulting suppression of callose through DIMBOA-Glc depletion may weaken aphid resistance. To test this hypothesis, we first profiled changes in benzoxazinoids in the leaves of wild-type and OeBx12 plants, which were induced by *S. littoralis* for 24 hours. In wild-type plants, HDMBOA-Glc levels increased sixfold within 24 hours, and DIMBOA-Glc levels dropped threefold within 72 hours (Fig. 4A). By contrast, no significant changes were observed in OeBx12 plants, apart from a slight reduction in HDMBOA-Glc over time (Fig. 4A). In contrast to caterpillar attack, infestation with *S. avenae* aphids did not change DIMBOA-Glc, DIMBOA, or HDMBOA-Glc levels in wheat leaves (fig. S6). Chitosan-induced callose deposition was significantly suppressed upon *S. littoralis* attack in wild-type plants. By contrast, no changes in callose inducibility

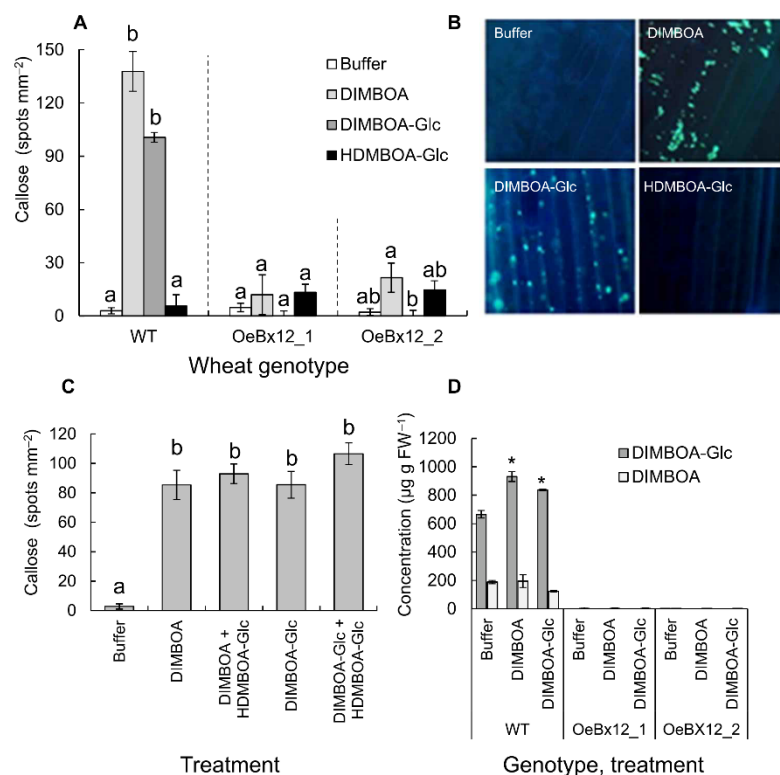


Fig. 2. Callose suppression through DIMBOA-Glc O-methylation. (A) Induction of callose in WT and *ZmBx12*-overexpressing lines after infiltration with DIMBOA, DIMBOA-Glc, or HDMBOA-Glc ($n = 4$ to 11). (B) Representative photographs of callose induction in WT plants after aniline blue staining. (C) Callose induction in WT plants treated with different benzoxazinoid mixtures ($n = 5$ to 11). (D) Concentration of DIMBOA-Glc (dark gray bars) and DIMBOA (light gray bars) in the leaves of WT and transgenic plants infused with DIMBOA-Glc or DIMBOA ($n = 3$). Different letters and asterisks indicate significant differences between treatments within lines (ANOVA followed by Holm-Sidak post hoc tests, $P < 0.05$). Photo credit for (B): B. Li, University of Bern.

were observed upon *S. littoralis* attack in OeBx12 plants (Fig. 4B). These results suggest that the *S. littoralis*-mediated suppression of DIMBOA-Glc leads to a reduction in callose inducibility.

To test whether DIMBOA-Glc O-methylation affects the interaction between caterpillars and aphids on the same plant, aphids were left to grow on *S. littoralis*-induced leaves of wild-type and OeBx12 plants in two different experiments. Overall, *S. littoralis* attack had a negative effect on aphid growth. The magnitude of this effect varied between experiments (Fig. 4C). In both experiments, the negative influence of *S. littoralis* attack on aphid performance was slightly more pronounced in OeBx12 plants than in wild-type plants (Fig. 4, C and D). Thus, the absence of callose suppression in OeBx12 plants is associated with a slight accentuation of caterpillar-induced resistance to aphids.

Identification of the wheat DIMBOA-Glc OMT TaBX10

As the core pathway of benzoxazinoid biosynthesis is conserved between wheat and maize (26), we hypothesized the wheat DIMBOA-Glc OMT might be an ortholog of maize *ZmBx10*–*ZmBx12* or *ZmBx14* (14, 28). However, initial BLAST analysis revealed no orthologs of these genes in the wheat genome. We therefore sequenced the transcriptomes of *S. littoralis*-damaged and *S. littoralis*-undamaged

wheat leaves to identify potential herbivore-induced OMT genes (fig. S7). Mapping of the obtained Illumina reads to the wheat gene model version 2.2 (29) and subsequent analysis of digital gene expression (EDGE) identified eight OMT gene candidates that were differentially expressed in the two treatments (fig. S7B and table S1). While none of the eight genes were homologous to *ZmBx10*/11/12/14, five of them showed a moderate sequence similarity to *ZmBx7*, an OMT involved in the methylation of hydroxyl groups on the aromatic ring of the benzoxazinoid core structure (fig. S8) (28, 30). The remaining three candidates were only distantly related to benzoxazinoid OMTs and grouped together with SABATH methyltransferase genes from maize, suggesting a function as benzenoid carboxyl methyltransferases (31, 32). Sequence comparison of the five wheat OMT genes similar to *ZmBx7* revealed that only two of them encoded full-length OMT proteins (fig. S9). These two genes, *Traes 4AL C467B516F* and *Traes 2BL C467B516F*, showed 100% nucleotide identity to each other. Quantitative reverse transcription polymerase chain reaction (qRT-PCR) analysis confirmed that they were strongly up-regulated after herbivory (fig. S7C). Construction of a de novo transcriptome based on the Illumina reads from *S. littoralis*-damaged wheat leaves revealed no further herbivore-induced

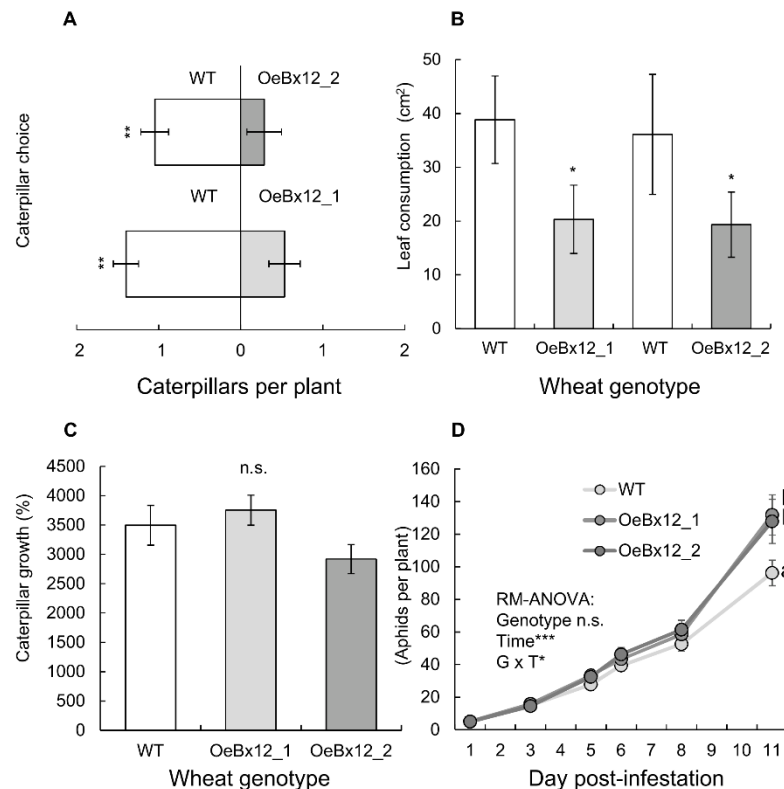


Fig. 3. DIMBOA-Glc O-methylation changes aphid and caterpillar resistance in opposite directions. (A) Preference of *S. littoralis* caterpillars for WT or *ZmBx12*-overexpressing plants ($n = 15$ to 21). (B) Leaf damage in a choice situation ($n = 8$). Asterisks indicate significant differences between lines (one-sample t tests on pairwise differences, $*P < 0.05$, $**P < 0.01$, $***P < 0.001$). (C) Caterpillar growth in a no-choice experiment. (D) *S. avenae* aphid reproduction on different lines. Different letters indicate differences between plant lines (repeated-measures ANOVA followed by Holm-Sidak post hoc tests, $P < 0.05$). Significance levels for repeated-measure ANOVA factors are shown. n.s., not significant.

ZmBx10/11/12/14-like OMT genes in comparison to those found in the gene model version 2.2 (fig. S10).

To characterize the enzymatic activity of the OMT protein encoded by Traes 4AL C467B516F/Traes 2BL C467B516F, the complete open reading frame, designated as *TaBx10*, was amplified from complementary DNA (cDNA) made from herbivore-damaged wheat leaves and heterologously expressed in *Escherichia coli*. In the presence of the OMT cosubstrate *S*-adenosyl-L-methionine, purified recombinant *TaBx10* was able to convert DIMBOA-Glc and DIM₂BOA-Glc into HDMBOA-Glc and HDM₂BOA-Glc, respectively (Fig. 5A). Maize *ZmBx10* was used as positive control and showed exclusively DIMBOA-Glc OMT activity, as previously reported (13, 28). No product formation was observed when the substrates were incubated with an empty vector control (fig. S11). *TaBx10* expression was similarly induced by *S. littoralis* in wild-type and *OeBx12* lines (fig. S12).

Independent evolution of benzoxazinoid OMT activity in maize and wheat

Maize and wheat belong to the Panicoideae (PACMAD lineage) and Pooideae (BEP lineage), respectively, two major grass sub-

families that diverged 50 to 70 Ma ago (33). Our initial sequence comparison of maize and wheat OMT genes revealed that the two *TaBx10* gene copies have only 54 to 58% nucleotide sequence identity to *ZmBx10/11/12/14* and are not directly related to the *ZmBx10/11/12/14* gene cluster in maize (fig. S8), suggesting independent evolution of DIMBOA-Glc OMT activity in the Panicoideae and Pooideae. To study this evolutionary scenario in more detail, we extracted full-length OMT gene sequences with similarity to *Bx7* from all Poaceae genomes available in the Phytozome database and included them into our phylogenetic analysis. The resulting phylogenetic tree showed that maize *ZmBx10/11/12/14* clustered within a well-defined clade (PACMAD lineage-specific *Bx10* clade), which comprised exclusively genes from Panicoideae and Chloridoideae species (Fig. 5B and fig. S13). In contrast, the sister clade contained genes from various Pooideae/Chloridoideae and Panicoideae species including wheat and maize. This indicates that the ancestors of the PACMAD lineage-specific *Bx10* clade and its sister clade must have existed before the separation of the Panicoideae/Chloridoideae and Pooideae and that the *Bx10* clade ancestor was probably lost early in the evolution of the

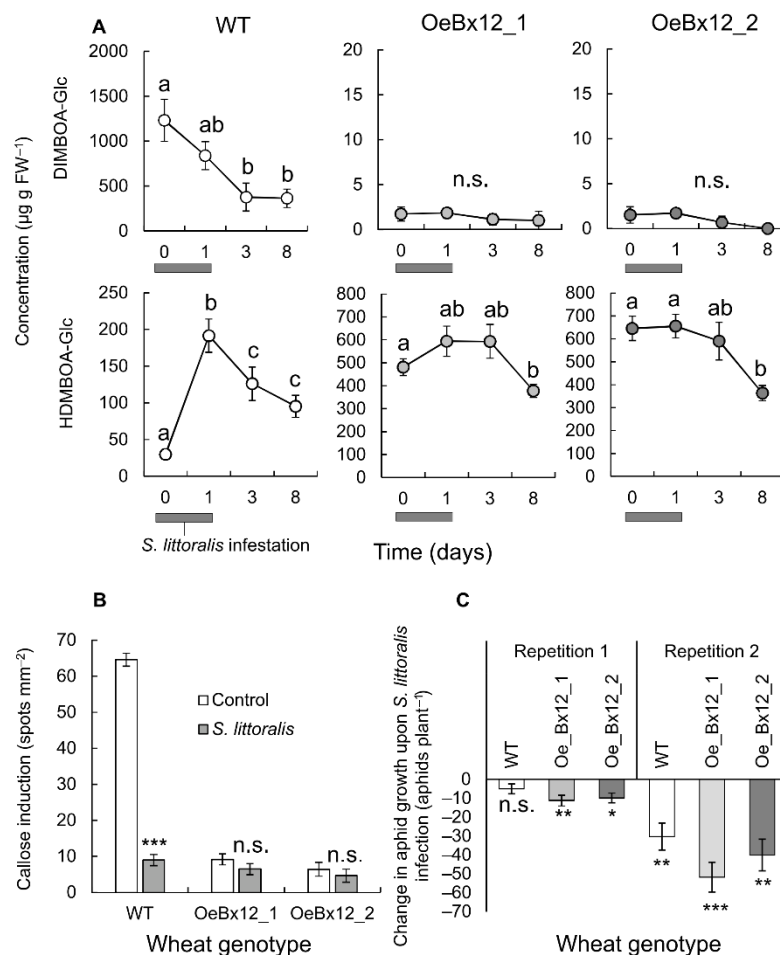


Fig. 4. DIMBOA-Glc O-methylation mediates a trade-off between induced caterpillar and aphid resistance. (A) Changes in major benzoxazinoids in WT and *ZmBx12*-overexpressing lines at different time points following 24 hours of *S. littoralis* attack ($n = 5$ to 7). Different letters indicate significant differences in concentrations over time (ANOVA followed by Holm-Sidak post hoc tests, $P < 0.05$). (B) Callose inducibility in control and *S. littoralis*-attacked wheat plants ($n = 12$ to 20). Asterisks indicate significant differences between treatments (two-way ANOVA followed by Holm-Sidak post hoc tests, * $P < 0.05$, ** $P < 0.01$, *** $P < 0.001$). (C) Aphid performance on *S. littoralis*-attacked wheat plants relative to nonattacked controls ($n = 9$ to 11). Results from two repetitions of the experiments are shown side by side. Stars indicate a significant reduction of aphid growth induced by *S. littoralis* caterpillar feeding relative to *S. littoralis*-unattacked plants (two-way ANOVA followed by Holm-Sidak post hoc tests).

Pooideae. The fact that the two *TaBx10* gene copies grouped together with other Pooideae and Panicoideae genes in a clade that was separated from the *Bx10* clade and its sister clade (Fig. 5B) confirms our initial hypothesis of independent evolution of DIMBOA-Glc OMT activity within the grasses.

Independent evolution of benzoxazinoid and glucosinolate OMT

To test whether benzoxazinoid OMT genes are related to glucosinolate OMT genes, we included indole glucosinolate O-methyltransferase 1 (IGMT1) and IGMT2, two recently identified OMTs from *Arabidopsis* that catalyze the methylation of 4-hydroxy-indol-3-yl-methyl gluco-

sinolate (4OH-I3M) to 4MO-I3M (37), into our phylogenetic analysis. As expected, IGMT1 and IGMT2 grouped together with other *Arabidopsis* OMT genes and were separated from *TaBx10* or *ZmBx10/11/12/14* (fig. S14), suggesting independent evolution of benzoxazinoid and glucosinolate OMT activity.

DISCUSSION

Plants can use secondary metabolites to deploy herbivore-specific defense responses. This study illustrates that a single, herbivory inducible methylation step serves as a switch and trade-off point between aphid and caterpillar resistance in wheat. Unexpectedly, while the core

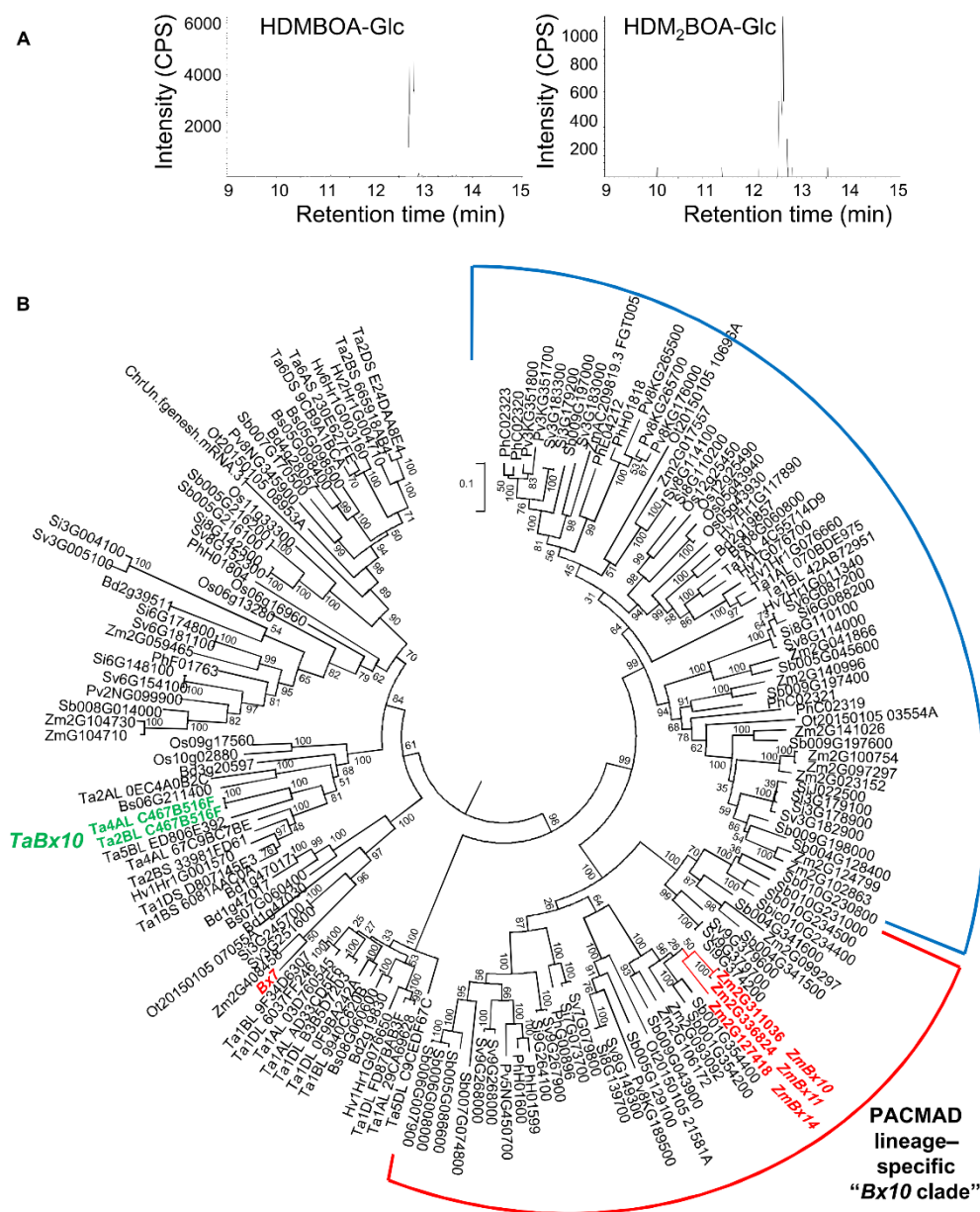


Fig. 5. Identification and characterization of TaBX10 as a functional DIMBOA-Glc OMT. (A) Recombinant TaBX10 methylates DIMBOA-Glc and DIM₂BOA-Glc. The enzyme was heterologously expressed in *E. coli*, purified, and incubated with a mixture of DIMBOA-Glc and DIM₂BOA-Glc. Enzyme products were analyzed using liquid chromatography–tandem mass spectrometry (LC-MS/MS). CPS, counts per second (electron multiplier). (B) Phylogenetic tree of Poaceae OMT genes similar to Bx7. Maize Bx7, 10, 11, 14 and wheat TaBX10 are shown in red and green, respectively. The tree represents a subclade of a larger Poaceae OMT tree that is given in fig. S13. The tree was inferred by using the maximum likelihood method based on the Tamura 3-parameter model. Bootstrap values are shown next to each node. The tree is drawn to scale, with branch lengths measured in the number of substitutions per site. Zm, *Zea mays*; Sb, *Sorghum bicolor*; Sv, *Setaria viridis*; Si, *S. italica*; Pv, *Panicum virgatum*; Ph, *P. hallii*; Ot, *Oropetium thomaeum*; Ta, *T. aestivum*; Hv, *Hordeum vulgare*; Bd, *Brachypodium distachyon*; Bs, *B. stacei*; Os, *Oryza sativa*. The PACMAD lineage-specific Bx10 clade is marked in red, and its sister clade is marked in blue.

SCIENCE ADVANCES | RESEARCH ARTICLE

biosynthesis pathway and the functional architecture of the defense switch are similar in wheat and maize, the responsible enzymes have evolved independently from each other. Below, we discuss these results from physiological, ecological, and evolutionary points of view.

The role of benzoxazinoids, including the methylation of DIMBOA-Glc to HDMBOA-Glc, in plant-herbivore interactions has been studied in detail in maize (12–14, 22, 28, 34). In vitro experiments with DIMBOA and HDMBOA-Glc suggested that HDMBOA-Glc may be more potent as a feeding deterrent, as it is rapidly deglycosylated and converted into unstable breakdown products (35), which precludes its detoxification by reglycosylation (12). Our results support this hypothesis by showing that the overproduction of HDMBOA-Glc renders plants less attractive and reduces leaf damage by *S. littoralis*. Apparently, HDMBOA-Glc acts as a strong antixenotic rather than an antibiotic, as caterpillar growth was not reduced in the transgenic lines. How caterpillars avoid negative consequences of HDMBOA-Glc on their digestive physiology remains to be determined. The increased levels of ferulic acid in HDMBOA-Glc-overproducing lines suggest that other secondary metabolites may be regulated by DIMBOA-Glc O-methylation. While the mechanisms behind this phenomenon remain unclear, it is possible that the increased levels of other defenses in HDMBOA-Glc-overproducing lines may have contributed to the reduction in caterpillar feeding.

Although HDMBOA-Glc is also toxic to aphids (14), aphids grow better on maize cultivars with high HDMBOA-Glc levels and low DIMBOA-Glc levels, which coincides with lower callose inducibility in these genotypes (14). Together with the fact that caterpillar attack induces HDMBOA-Glc production and depletes DIMBOA-Glc reserves (12), this led to the hypothesis that caterpillar feeding should induce aphid susceptibility by suppressing callose accumulation (22). Our experiments not only confirm this hypothesis but also demonstrate that callose inducibility only partially explains the interaction between *S. littoralis* and *S. avenae* in wheat. Aphid performance was decreased on caterpillar-attacked leaves even in the absence of DIMBOA-Glc depletion, suggesting that other inducible defenses increase aphid resistance. Caterpillar attack leads to substantial transcriptional and metabolic reprogramming of a plant's primary and secondary metabolism (36–39), and it is therefore not unusual that physiological changes other than benzoxazinoid-dependent callose deposition contribute to the overall outcome of the interaction between caterpillars and aphids. In maize, genetic mapping revealed substantial variation and multiple quantitative trait loci associated with caterpillar-induced resistance and susceptibility against aphids (22), which may provide a path toward the functional characterization of these additional factors.

The resistance of wheat to fungal pathogens has been associated with callose deposition (40). In this context, it is unexpected that the suppressed callose inducibility in Oe_Bx12 lines did not affect their resistance to two fungal pathogens. We propose three hypotheses to explain this result. First, it is possible that the fungi are more susceptible to HDMBOA-Glc than DIMBOA-Glc, which may have counterbalanced resistance in the transgenic lines. Second, the higher production of other defenses in HDMBOA-Glc-overproducing lines may have offset the effects of reduced callose deposition. Third, the two pathogens may suppress or avoid callose induction. In maize, fungal pathogen attack leads to a marked increase of HDMBOA-Glc levels (27, 41), and it is possible that such an induction, similar to caterpillar attack, suppresses callose inducibility in wheat and thereby allows the fungus to suppress effective defenses.

Overall, our experiments and the current literature reveal that the architecture of benzoxazinoid-dependent defense regulation is notably similar in maize and wheat (Fig. 6). In both species, DIMBOA-Glc is generally the dominant constitutively produced benzoxazinoid, and HDMBOA-Glc is strongly induced and becomes dominant upon caterpillar and pathogen attack (12, 27, 41). Furthermore, callose deposition is induced by DIMBOA and DIMBOA-Glc, but not by HDMBOA-Glc (11). Genetic analyses revealed that the core biosynthetic pathway that converts indole-3-glycerol phosphate to DIBOA-Glc via several intermediate steps is largely conserved between wheat and maize (26). The fact that the DIMBOA-Glc OMT genes in wheat and maize are analogs rather than orthologs is an unexpected finding in this context. Phylogenetic analysis suggests that the capacity to produce HDMBOA-Glc and to use the DIMBOA-Glc OMT as a regulatory switch between aphid and caterpillar resistance evolved independently in maize and wheat. The functional validation of the wheat DIMBOA-Glc OMT TaBX10 in planta would shed further light on its contribution to HDMBOA-Glc biosynthesis relative to other potential wheat OMTs. Although HDMBOA-Glc has also been found in Job's tears (*Coix lacryma-jobi*) (42), nothing is known about HDMBOA-Glc production in the other benzoxazinoid-producing plant species. Investigating and comparing the evolutionary relationships and defense regulation of benzoxazinoids in additional species are exciting prospects of this work.

Comparing callose induction of benzoxazinoids and glucosinolates revealed a high degree of specificity. While the benzoxazinoid-producing wheat responds strongly to DIMBOA and DIMBOA-Glc, it does not respond to the glucosinolate 4MO-I3M. Conversely, the glucosinolate-producing *Arabidopsis* responds strongly to 4MO-I3M, but not to DIMBOA or DIMBOA-Glc. As expected, the OMTs involved in the production of 4MO-I3M (43) and HDMBOA-Glc (14) are only distantly related to each other. Thus, callose regulation by benzoxazinoids and glucosinolates as illustrated in Fig. 6 does not proceed via the same mechanism, and it is likely that the two phenomena evolved independently from each other. Glucosinolate hydrolysis is required for callose induction in *Arabidopsis* (15), while DIMBOA seems to induce callose in the absence of any measurable increase in known breakdown products. As glucosinolate breakdown products are structurally distinct from benzoxazinoids and their catabolites, they would likely require a different mechanism of perception to be integrated into defense signaling (Fig. 6). Nevertheless, it is theoretically possible that the signaling cascades elicited by benzoxazinoids and glucosinolates share a common ancestor and diverged since the split of the mono- and dicotyledons 140 Ma ago (44). A better understanding of the molecular and genetic basis of callose regulation by benzoxazinoids and glucosinolates will be required to disentangle these hypotheses.

Convergence is an important force in evolution (45), and plants provide many fascinating examples in this context (46). Caffeine biosynthesis, for instance, evolved at least five times within the flowering plants, partially by co-opting enzymes with different ancestral functions (47). In general, plant secondary metabolism can evolve rapidly due to enzyme promiscuity and frequent gene duplications (25, 48, 49). Secondary metabolites may thus allow plants to rapidly and specifically adapt their defense signaling systems to different herbivore and pathogen pressures. The finding that maize and wheat co-opted the same secondary metabolite pathway to specifically regulate defenses against aphids and caterpillars is suggestive of an important adaptive role of this form of herbivore-specific defense regulation.

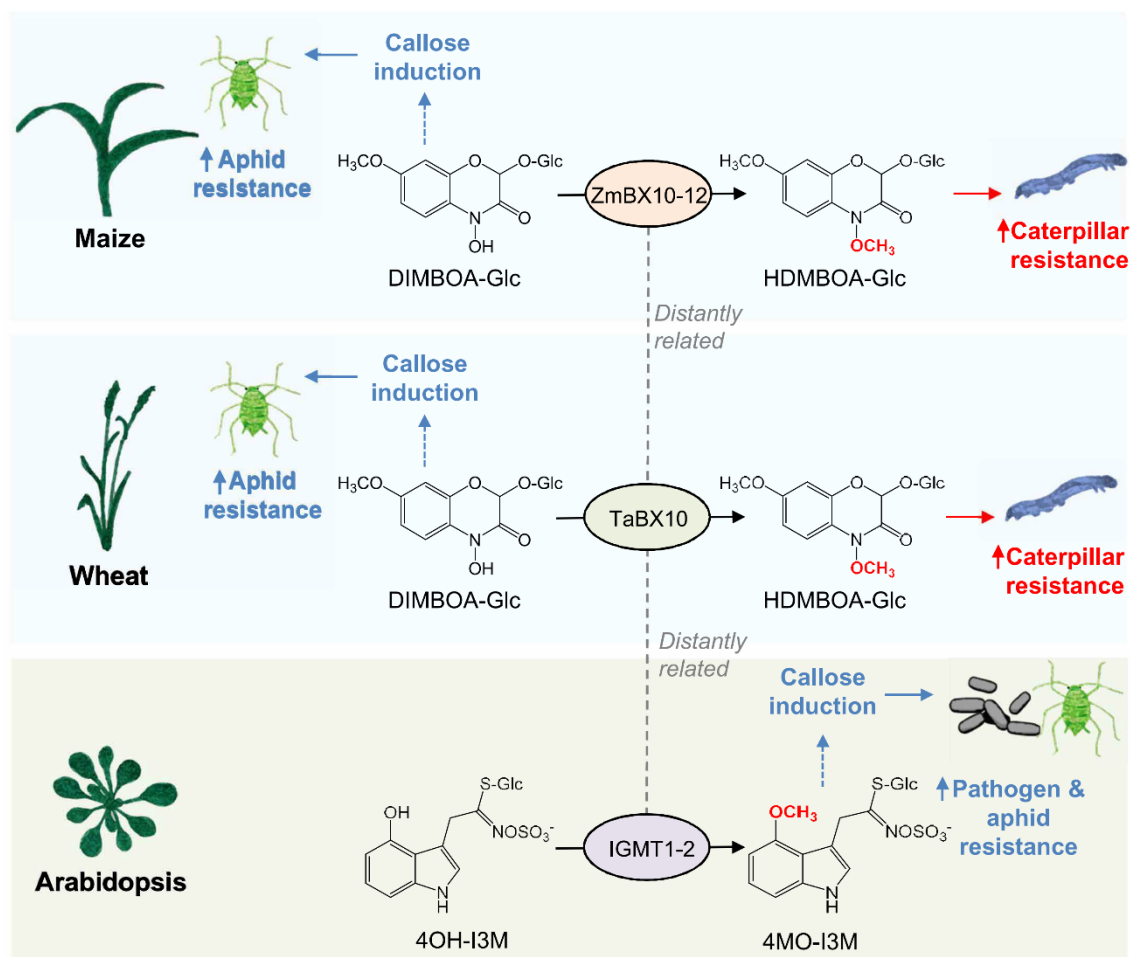


Fig. 6. Independently evolved O-methylation of benzoxazinoids and glucosinolates regulates defense and resistance. DIMBOA-Glc is required for callose induction in wheat and maize. Methylation of DIMBOA-Glc to HDMBOA-Glc reduces the DIMBOA-Glc pool and subsequently suppresses callose formation. The responsible OMTs, TaBX10 and ZmBX10–ZmBX12, evolved independently from each other. HDMBOA-Glc repels caterpillars, while DIMBOA-Glc reduces aphid growth, most likely by promoting callose formation. In *Arabidopsis*, methylation of the glucosinolate 4OH-I3M by IGMT1 and IGMT2 leads to the formation of 4MO-I3M, which is required for callose deposition in this species. 4MO-I3M increases aphid and pathogen resistance, most likely by promoting callose formation. IGMT1 and IGMT2 are only distantly related to cereal benzoxazinoid OMTs.

MATERIALS AND METHODS

Note that the numbers of replicates for the individual experiments are provided in the respective figure legends.

Plant and insect material

The wheat (*Triticum aestivum*) CYMMIT breeding line Bobwhite SH 98 26 (50) was used in this study. Plants were grown in a climate-controlled room with 16 hours photoperiod, 300 $\mu\text{mol m}^{-2} \text{s}^{-1}$ of photosynthetically active radiation, and a temperature cycle of 22°C/18°C (light/dark). *S. littoralis* caterpillars were provided by T. Turlings (FARCE Laboratory, University of Neuchâtel, Switzerland) and were

kept on artificial diet at 22°C. The English grain aphid (*S. avenae*) was obtained from Andermatt Biocontrol AG (Switzerland) and maintained on barley seedlings in a growth chamber with 16:8 light/dark photoperiod at 24°C.

Generation of ZmBx12-expressing transgenic wheat

The complete open reading frame of ZmBx12-CML322 was amplified with the primers ZmBx12_SpeI-fwd (GACTAGTCATGCAAGA-GAGCAGTAGC) and ZmBx12_EcoRI-rev (GGAATTCCTCAAG-GATAGACCTCGATGATGA) from the previously described vector pASK-IBA37plus::ZmBx12 (13). The amplification product was

SCIENCE ADVANCES | RESEARCH ARTICLE

digested with Spe I and Eco RI (Fast digest, Thermo Fisher Scientific) and subcloned into the linearized vector pUbi-AB downstream of the maize UBIQUITIN 1 promoter (*ZmUbi1*) (51). The resulting construct pUbi-AB::*ZmBx12* was digested with Sfi I (Fast digest, Thermo Fisher Scientific), and the digestion products were separated by gel electrophoresis. The fragment containing *ZmUbi1::ZmBx12* was subsequently extracted from the gel, purified, and subcloned into the binary vector p6i-d35S (51) that was linearized by Sfi I digestion. The insertion of *ZmUbi1::ZmBx12* into p6i-d35S was confirmed by a control digestion with Kpn I and Hind III (Fast digest, Thermo Fisher Scientific). The binary vector was transferred to the *Agrobacterium tumefaciens* strain AGL1 and used to inoculate immature Bobwhite SH 98 26 embryos. The generation of transgenic plants and their molecular analysis for transgene integration were conducted as previously described (52), with the exception of Southern blot analysis, which could not be completed successfully. The transgenic lines may therefore harbor single or multiple insertions of *ZmUbi1::ZmBx12*. Segregation analysis was conducted on T2 plants by using the ratio of DIMBOA-Glc to HDMBOA-Glc as a marker. T2 seeds of two homozygous T1 plants harboring at least one highly expressed, complete insertion of *ZmUbi1::ZmBx12* were used for biological experiments.

RNA extraction, cDNA synthesis, and quantitative real-time PCR

Total RNA was extracted from leaves of 14-day-old wild-type and *ZmBx12*-overexpressing plants using an RNA isolation kit (Thermo Fisher Scientific, USA). Two microgram of total RNA was used for reverse transcription with SuperScript II reverse transcriptase (Invitrogen, USA). The cDNA samples were diluted to 2 to 8 ng/μl. Triplicate quantitative assays were performed on 5 μl of each cDNA dilution with the Kapa SYBR Fast qPCR Master Mix (Sigma, USA) and a LightCycler96 detection system (Roche, Switzerland) according to the manufacturer's protocol. The relative quantification method (Delta-Delta CT) was used to evaluate quantitative variation between the replicates examined. The amplification of *T. aestivum* *Tubulin* was used as an internal control to normalize all data, and primers for *Tubulin* were ATCTGGTGC GGGAACAA (forward) and AAGTGGAGGCGAGGGAAT (reverse). Gene-specific primers for *ZmBx12* were ATGGCACTCATGCAAGAGAGC (forward) and TCAAGGATAGACCTCGATGATG (reverse).

For qRT-PCR analysis of *TaBx10*, RNA was extracted using the InviTrap Spin Plant RNA Mini Kit (Stratagene, Berlin, Germany) according to the manufacturer's instructions. cDNA was prepared from 1 μg of deoxyribonuclease-treated RNA using SuperScript III reverse transcriptase (Invitrogen, Carlsbad, CA, USA) and diluted 1:10 with water. Primers for *TaBx10* were TCCCCGATGGTGGGCA (forward) and GGTGGTGTCCCAAGACGTG (reverse). Primer specificity was confirmed by agarose gel electrophoresis, melting curve analysis, and standard curve analysis and by sequence verification of cloned PCR amplicons. Primer pair efficiency (98.5%) was determined using the standard curve method with twofold serial dilutions of cDNA. Samples were run in triplicate using the Brilliant III Ultra-Fast SYBR Green QPCR Master Mix (Agilent Technologies, Santa Clara, CA, USA). The following PCR conditions were applied for all reactions: initial incubation at 95°C for 3 min, followed by 40 cycles of amplification (95°C for 10 s, 60°C for 10 s). All samples were run on the same PCR machine (CFX Connect Real-Time System; Bio-Rad Laboratories, Hercules, CA, USA) in an optical 96-well plate. Six biological replicates for each treatment were analyzed as triplicates.

Collection of wheat fascicular phloem

Leaves of 14-day-old wheat plants were fixed inside a flat tray with double-sided adhesive tape. About 10 to 20 adult aphids (*S. avenae*) were placed onto the upper surface of each leaf and allowed to feed overnight. After cutting the aphid stylets with a microcautery device (CF-50, Syntech) according to Fisher and Frame (53), the flat tray with the fixed leaves and cut stylets was flooded with silicon oil (M 200, Roth) to prevent evaporation of the exudates. Twenty-four hours later, the phloem sap was collected under silicon oil using a microcapillary connected to a small syringe via a silicone tube with a side valve. Depending on the exudation time of the severed stylets, the sample amount was up to 1.4 μl per stylet during 24 hours. The samples of each plant were pooled and stored at -20°C. For LC-MS/MS analysis of benzoxazinoids (see below), phloem samples were diluted 1:7 with methanol:water (1:1, v/v).

Extraction and analysis of benzoxazinoids, phenolic acids, amino acids, proteins, sugars, and starch

Plant leaf tissue was ground into fine powder under liquid nitrogen. The frozen powder was weighed, and extraction buffer (50% methanol, 0.1% formic acid) was added immediately (1 mg, 10 μl). The plant sample was vortexed for 30 s and then centrifuged at 11,000g for 20 min at 4°C. The supernatant was transferred into a new Eppendorf tube and centrifuged once more to remove all particles.

Benzoxazinoid content was analyzed with an Acquity UPLC (Waters, USA) coupled to an ultraviolet (UV) detector and a QDa mass spectrometer (Waters, USA) using an Acquity BEH C18 column (2.1 mm by 100 mm, 1.7 μm; Waters, USA). The temperatures of the autosampler and column were set to 15° and 40°C, respectively. The mobile phase consisted of 99% water, 1% acetonitrile, and 0.1% formic acid (A), and acetonitrile and 0.1% formic acid (B). Flow rate was set to 0.4 ml min⁻¹ with 97% A and 3% B. The injection volume was 5 μl. The elution profile was: 0 to 9.65 min, 3 to 16.4% B; 9.65 to 13 min, 16.4 to 100% B; and 13.1 to 15 min at 100% B, followed by 2-min column reconditioning at 3% B. The extracted UV trace at 275 nm was used for benzoxazinoid quantification. The following extracted ion chromatograms were used for quantification with a mass window of ±0.01 D: 164 mass-to-charge ratio (*m/z*) for DIMBOA [retention time (RT), 5.62 min], 372 *m/z* for DIMBOA-Glc (RT, 5.64 min), 432 *m/z* for HDMBOA-Glc (RT, 8.19 min), 402 *m/z* for DIM₂BOA (RT, 5.81 min), 356 *m/z* for HMBOA-Glc (RT, 5.28 min), 342 *m/z* for DIBOA-Glc (RT, 4.29 min), 462 *m/z* HDM₂BOA-Glc (RT, 8.32 min), 164 *m/z* for MBOA (RT, 8.17 min), and 372 *m/z* for MOA-Glc (RT, 5.31 min). Benzoxazinoid concentrations were determined by external calibration curves obtained from purified DIMBOA-Glc, DIMBOA, and HDMBOA-Glc standards. Five calibration points (5, 10, 50, 150, and 200 μg/ml) were used.

Quantification of phenolic acids (chlorogenic acid, p-caffeic acid, p-coumaric acid, ferulic acid, and sinapic acid) was performed on an Acquity UPLC coupled to a Xevo G2 XS Q-TOF time-of-flight mass spectrometer (Waters, USA) equipped with an electrospray ionization (ESI) source. The compounds were separated on an Acquity BEH C18 ultra performance liquid chromatography (UPLC) column (2.1 mm by 50 mm internal diameter, 1.7 μm particle size). Water (0.1% formic acid) and acetonitrile (0.1% formic acid) were used as mobile phases A and B. The gradient profile was as follows: 0 to 1 min, 95% A in B; 1 to 5 min, 81% A in B; 5 to 5.2 min, 1% A in B; 5.2 to 6.5 min, 1% A in B; 6.6 to 8 min, 95% A. The mobile phase flow rate was 0.4 ml/min. The column temperature was maintained at 40°C,

and the injection volume was 1 μ l. The quadrupole orthogonal acceleration–time-of-flight (Q-TOF) was operated in ESI negative mode, and data were acquired in scan range (50 to 1200 m/z) using a cone voltage of 20 V. The elution order was as follows: 2.09 min, chlorogenic acid; 2.22 min, p-cafeic acid; 3.18 min, p-coumaric acid; 3.83 min, ferulic acid; and 4 min, sinapic acid. Chromatograms were acquired in MS^E mode using a collision energy ramping of 10 to 30 V. Quantification of the compounds was performed on the basis of their exact masses: chlorogenic acid, 353.0872 m/z ; p-cafeic acid, 179.0344 m/z ; p-coumaric acid, 163.0395 m/z ; ferulic acid, 3.83 min and 193.050 m/z ; and sinapic acid, 4 min and 223.0606 m/z . Calibration solutions containing the different phenolic acids were prepared between 0 and 5 μ g ml⁻¹ to establish linear regressions.

To determine amino acid concentrations in wheat phloem, phloem samples were diluted 1:7000 with methanol:water (1:1, v/v) and spiked with ¹³C, ¹⁵N-labeled amino acids (algal amino acids ¹³C, ¹⁵N; Isotec, Miamisburg, OH, USA) at a concentration of 9 μ g of the mix per milliliter. Amino acids were directly analyzed by LC-MS/MS as recently described (54). Amino acid concentrations in wheat leaves were determined using an AccQ-Tag kit (Waters, Milford, USA). Five hundred microliters of extract buffer (20 mM norleucine in MeOH) was added to 10 mg of dry and ground leaf powder. After the solution was thoroughly mixed for 15 min, 250 μ l of chloroform and 500 μ l Milli-Q water were added. The mixture was centrifuged at 11,000g for 5 min at room temperature (20° to 23°C). Fifty microliters of supernatant was freeze dried into dry residue and then suspended with 50 μ l of Milli-Q water. Five microliters of sample was briefly mixed with 35 μ l of borate buffer and 10 μ l of derivatization buffer from an AccQ-Tag Ultra Derivatization kit (Waters, USA) and then placed in a 55°C water bath for 10 min. Amino acid content was analyzed with a UPLC coupled to a UV detector and a QDa mass spectrometer (Waters, Milford, USA). Mixtures of 20 amino acids at 100, 50, 10, and 1 μ g ml⁻¹ were used as external standards for quantification. Soluble sugars, starch, and total soluble proteins were extracted and quantified as described previously (38).

Callose induction

To determine callose deposition induced by chitosan, DIMBOA, DIMBOA-Glc, HDMBOA-Glc, and 4MO-I3M, callose abundance after chemical infiltration was analyzed from 15 randomly collected leaf segments from five different 10-day-old wheat seedlings and six 5-week-old *Arabidopsis* accession Columbia-0 (Col-0) plants per treatment. Each leaf was infiltrated with 500 μ l of 0.2% (w/v) low viscous chitosan (Sigma, USA), which has a molecular weight of approximately 190 kDa. Chitosan was dissolved to 1% in 1% acetic acid and diluted to 0.2% by distilled water. DIMBOA, DIMBOA-Glc, and HDMBOA-Glc were dissolved to 80 μ g/ml by 1.96% methanol and 0.04% acetic acid. 4MO-I3M (Phytoplan, Germany) was dissolved to 80 μ g/ml by distilled water. Twenty-four hours after infiltration, leaf segments around the infiltration spots (approximately 4 cm²) were collected and destained by 96% ethanol to remove chlorophyll. Leaf segments with cell death symptoms were excluded. Destained leaf segments were stained with 70 mM phosphate buffer (pH 9.0) containing 0.01% aniline blue (Sigma, USA). Callose deposition was observed by epifluorescence microscopy (Zeiss, Germany), and callose spots were counted by eye. To determine callose deposition induced by aphid feeding, five aphid adults were placed in cages (2-cm diameter) on the leaves of 14-day-old wheat plants. After 7 days, all aphids were removed. Aphid-infested leaf segments were

collected from 10 different plants per line. Leaf segment destaining and callose staining were performed as described above. As callose deposition following aphid infestation showed variable shapes and intensity, we first determined the total area of callose per plant (μ m²) using Digimizer (MedCalc Software, Belgium). We then assessed the intensity of the staining on a relative scale from 1 (weak intensity) to 5 (strong intensity). Then, to obtain an integrated measure of callose induction, we multiplied intensity with callose area for each plant individually.

Transcriptome sequencing and analysis

To identify herbivore-induced OMT genes in wheat, we sequenced the transcriptomes of three *S. littoralis*-undamaged and three *S. littoralis*-damaged wheat seedlings using Illumina HiSeq 2500. Total RNA was extracted from leaf material as described above, TruSeq RNA-compatible libraries were prepared, and PolyA enrichment was performed before sequencing the six transcriptomes on an Illumina HiSeq 2500 with 21 Mio reads per library, 100 base pairs, paired end. Trimming of the obtained Illumina reads and mapping to the wheat gene model version 2.2 (29) were performed with the program CLC Genomics Workbench (Qiagen Bioinformatics) (mapping parameters: length fraction, 0.7; similarity fraction, 0.9; max number of hits, 25). Empirical analysis of digital gene expression (EDGE) implemented in the program CLC Genomics Workbench was used for gene expression analysis. A de novo transcriptome based on the Illumina reads from *S. littoralis*-damaged wheat leaves (~63 Mio reads in total) was constructed using the CLC Genomics Workbench (word size, auto; bubble size, 200) and was used for remapping with the same parameters as described above. Raw reads were deposited in the National Center for Biotechnology Information Sequence Read Archive under the accession no. SRP148745.

Sequence analysis and tree reconstruction

OMTs were identified using a BLASTP analysis with maize BX7 as query and all available Poaceae protein datasets in Phytozome 12.1 (<https://phytozome.jgi.doe.gov>) as template. Genes with open reading frames >1000 nucleotides were considered as “full length” and used for phylogenetic analysis. Multiple sequence alignments were computed using the MUSCLE codon algorithm implemented in MEGA6 (55). On the basis of these alignments, trees were reconstructed with MEGA6 using a maximum likelihood algorithm. Codon positions included were 1st + 2nd + 3rd + noncoding. All positions with <90% site coverage were eliminated. Ambiguous bases were allowed at any position. A bootstrap resampling analysis with 1000 replicates was performed to evaluate the topology of the generated trees. A substitution model test was performed with MEGA6 to identify the best-fit substitution model for each dataset. The substitution models used for tree reconstructions are indicated in the respective figure legends.

Cloning and expression of TaBx10

The complete open reading frame of *TaBx10* was amplified from cDNA with the primers ATGGTACGTCTCAGCGCATGCCGGC-CGCGCAGCACAT (forward) and ATGGTACGTCTCATATCAAG-GGTATACTTCGATAATTGATCGA (reverse) and inserted as Bsm BI fragment into the vector pASK-IBA37plus (IBA-GmbH, Göttingen), which allows the expression of *TaBx10* in *E. coli* NEB 10-beta cells (New England Biolabs) as N-terminal fusion protein. For expression, liquid cultures of bacteria harboring the expression construct were grown at 37°C and 220 rpm in lysogeny broth medium to an OD₆₀₀

SCIENCE ADVANCES | RESEARCH ARTICLE

(optical density at 600 nm) of 0.6 to 0.8. Anhydrotetracycline was added to a final concentration of 200 $\mu\text{g liter}^{-1}$, and the cultures were incubated for 20 hours at 18°C and 220 rpm. The cells were sedimented for 10 min at 5000g and 4°C. For breaking up the cells, the pellet was resuspended in ice-cold 4 ml of 50 mM tris-HCl (pH 8.0) containing 0.5 M NaCl, 20 mM imidazole, 20 mM 2-mercaptoethanol, and 10% glycerol and subsequently subjected to ultrasonication (4×20 s; Bandelin UW2070). The debris was separated by centrifugation for 20 min at 16,100g and 4°C. The N-terminal His-tagged TaBX10 was purified using Ni-NTA spin columns (Qiagen) according to the manufacturer's instructions. The purified proteins were eluted with 50 mM tris-HCl (pH 8.0) containing 0.5 M NaCl, 250 mM imidazole, and 10% glycerol. The salt was removed by gel filtration using Illustra NAP-5 columns (GE Healthcare), and the protein was redissolved in 50 mM tris-HCl (pH 7.0) containing 10% glycerol.

OMT enzyme assays

OMT activity of TaBX10 was tested using enzyme assays containing 0.5 mM dithiothreitol, 0.5 mM S-adenosyl-L-methionine, substrate (DIMBOA-Glc + DIM₂BOA-Glc; 25 $\mu\text{g ml}^{-1}$), and 35 μl of desalted enzyme in a volume of 100 μl . The assays were incubated overnight in glass vials at 25°C at 300 rpm using a ThermoMixer comfort 5355 (Eppendorf). The reaction was stopped with 1 volume 100% methanol and centrifuged for 5 min at 5000g. Product formation was monitored by the analytical methods described above.

Insect bioassays

For caterpillar performance assays, 14-day-old wheat seedlings were infested with five second-instar *S. littoralis* larvae. The whole plants were covered by breathable cellophane bags (Celloclair AG, Switzerland) to prevent larvae from escaping. After 11 days, caterpillar weight gain (mg) was measured by microbalance (Mettler Toledo, USA). The leaf consumption (cm^2) was calculated by Digimixer software (MedCalc Software, Belgium).

For caterpillar preference assays, one *ZmBx12*-overexpressing wheat plant and one wild-type plant were sown together in the same pot. Five second-instar *S. littoralis* larvae were put in the middle of the pot. Each pot was covered with transparent plastic film (Kodak, USA) to prevent larvae from escaping. The number of larvae feeding on each plant was recorded every 2 days for 8 days.

For aphid performance assays, 14-day-old wheat seedlings were infested with five adult *S. avenae* aphids. The whole seedling was covered with a breathable cellophane bag. Aphid progenies on the whole plants were counted during 11 days at regular time intervals.

To measure the effect of caterpillar feeding on aphid progeny production, five second-instar *S. littoralis* larvae were introduced onto the second leaf of 14-day-old wheat seedlings in clip cages. *S. littoralis* larvae were removed from plants after 24 hours. Five adult aphids were confined on the same leaves using clip cages for 7 days, and total aphid progenies were counted at the end.

Pathogen bioassays

For the wheat leaf rust infection assay, 12-day-old wheat seedlings were infected with the virulent isolate 90035. After incubation for 24 hours in the dark, the whole seedlings were covered with permeable plastic hoods until the end of the experiment. Disease symptoms were assessed 11 days after inoculation.

For the wheat powdery mildew infection assay, infection tests were performed on detached segments of the first leaves of 9-day-old wheat seedlings, inoculated with the virulent isolates 96224 and JIM2. Disease levels were evaluated 6 days later by measuring the percentage of infected leaf area.

Temporal effect of local induction by *S. littoralis* larvae and *S. avenae* on benzoxazinoids

Three second-instar *S. littoralis* larvae were attached in the second leaf of 14-day-old wheat seedlings by the clip cage and fed for 24 hours. After 24 hours, caterpillars were removed from the plants. Small leaf segments adjacent to the feeding sites were collected at several time points over a period of 7 days. After weighing, leaf segments were stored in the lysis tube containing ceramic beads and flash frozen with liquid nitrogen. The benzoxazinoid extraction buffer was added into the lysis tube (1 mg, 10 μl). Plant tissue was ground thoroughly by SpeedMill Plus (Analytik Jena, Germany) and then centrifuged at 13,200g for 20 min at 4°C twice to remove the pellet. Benzoxazinoids were analyzed as described above. To determine benzoxazinoid induction by aphids, five *S. avenae* adults were placed in cages (2-cm diameter) on the leaves of 14-day-old wheat plants. After 7 days, all aphids were removed. Aphid-infested leaf segments were collected from four to six different plants per line and analyzed as described above.

Statistical analyses

Data were analyzed by ANOVA followed by Holm-Sidak post hoc tests implemented in Sigma Plot 13.0. Normality and error variance were determined, and datasets were \log_{10} transformed to meet assumptions of ANOVAs where necessary.

SUPPLEMENTARY MATERIALS

Supplementary material for this article is available at <http://advances.sciencemag.org/cgi/content/full/4/12/eaat6797/DC1>

- Fig. S1. Phenotyping of *ZmBx12*-overexpressing plants I.
- Fig. S2. Phenotyping of *ZmBx12*-overexpressing plants II.
- Fig. S3. DIMBOA-Glc and MBOA levels upon DIMBOA and DIMBOA-Glc infiltration.
- Fig. S4. Specificity of benzoxazinoid- and glucosinolate-induced callose deposition.
- Fig. S5. Impact of DIMBOA-Glc O-methylation on wheat pathogen resistance.
- Fig. S6. Aphids do not induce benzoxazinoids in wheat leaves.
- Fig. S7. Identification of DIMBOA-Glc OMT candidate genes.
- Fig. S8. Phylogenetic tree of maize OMT genes similar to *Bx7* and wheat OMT genes that were found to be up-regulated after herbivory in wheat seedlings (RNA sequencing).
- Fig. S9. Sequence comparison of maize *Bx7* and *Bx10* with herbivore-induced OMT proteins from wheat.
- Fig. S10. Phylogenetic tree of maize and wheat OMT genes similar to *Bx7*.
- Fig. S11. Identification of *TaBx10* as a functional DIMBOA-Glc OMT.
- Fig. S12. No influence of *ZmBx12* overexpression on *TaBx10* expression.
- Fig. S13. Phylogenetic tree of Poaceae OMT genes similar to *Bx7*.
- Fig. S14. Phylogenetic tree of maize, wheat, and *Arabidopsis* OMT genes similar to *Bx7*.
- Table S1. Wheat OMT genes up-regulated after herbivory (RNA sequencing).

REFERENCES AND NOTES

1. R. A. R. Machado, M. McClure, M. R. Hervé, I. T. Baldwin, M. Erb, Benefits of jasmonate-dependent defenses against vertebrate herbivores in nature. *eLife* **5**, e13720 (2016).
2. G. A. Howe, G. Jander, Plant immunity to insect herbivores. *Annu. Rev. Plant Biol.* **59**, 41–66 (2008).
3. T. Züst, A. A. Agrawal, Mechanisms and evolution of plant resistance to aphids. *Nat. Plants* **2**, 15206 (2016).
4. T. Will, A. C. U. Furch, M. R. Zimmermann, How phloem-feeding insects face the challenge of phloem-located defenses. *Front. Plant Sci.* **4**, 336 (2013).
5. J. S. Thaler, P. T. Humphrey, N. K. Whiteman, Evolution of jasmonate and salicylate signal crosstalk. *Trends Plant Sci.* **17**, 260–270 (2012).

SCIENCE ADVANCES | RESEARCH ARTICLE

6. L. G. Barrett, M. Heil, Unifying concepts and mechanisms in the specificity of plant–enemy interactions. *Trends Plant Sci.* **17**, 282–292 (2012).
7. E. A. Schmelz, Impacts of insect oral secretions on defoliation-induced plant defense. *Curr. Opin. Insect Sci.* **9**, 7–15 (2015).
8. M. Erb, S. Meldau, G. A. Howe, Role of phytohormones in insect-specific plant reactions. *Trends Plant Sci.* **17**, 250–259 (2012).
9. Y. Li, M. Dicke, A. Kroes, W. Liu, R. Gols, Interactive effects of cabbage aphid and caterpillar herbivory on transcription of plant genes associated with phytohormonal signalling in wild cabbage. *J. Chem. Ecol.* **42**, 793–805 (2016).
10. R. Li, J. Zhang, J. Li, G. Zhou, Q. Wang, W. Bian, M. Erb, Y. Lou, Prioritizing plant defence over growth through WRKY regulation facilitates infestation by non-target herbivores. *eLife* **4**, e04805 (2015).
11. S. Ahmad, N. Veyrat, R. Gordon-Weeks, Y. Zhang, J. Martin, L. Smart, G. Glauser, M. Erb, V. Flors, M. Frey, J. Ton, Benzoxazinoid metabolites regulate innate immunity against aphids and fungi in maize. *Plant Physiol.* **157**, 317–327 (2011).
12. G. Glauser, G. Marti, N. Villard, G. A. Doyen, J.-L. Wolfender, T. C. J. Turlings, M. Erb, Induction and detoxification of maize 1,4-benzoxazin-3-ones by insect herbivores. *Plant J.* **68**, 901–911 (2011).
13. L. N. Mehlis, V. Handrick, G. Glauser, H. Barbier, H. Kaur, M. M. Haribal, A. E. Lipka, J. Gershenzon, E. S. Buckler, M. Erb, T. G. Köllner, G. Jander, Natural variation in maize aphid resistance is associated with 2,4-dihydroxy-7-methoxy-1,4-benzoxazin-3-one glucoside methyltransferase activity. *Plant Cell* **25**, 2341–2355 (2013).
14. D. Maag, A. Köhler, C. A. M. Robert, M. Frey, J.-L. Wolfender, T. C. J. Turlings, G. Glauser, M. Erb, Highly localized and persistent induction of *Bx1*-dependent herbivore resistance factors in maize. *Plant J.* **88**, 976–991 (2016).
15. N. K. Clay, A. M. Adio, C. Denoux, G. Jander, F. M. Ausubel, Glucosinolate metabolites required for an *Arabidopsis* innate immune response. *Science* **323**, 95–101 (2009).
16. H. Frerigmann, M. Pišlewski-Bednarek, A. Sánchez-Vallet, A. Molina, E. Glowacki, T. Gigolashvili, P. Bednarek, Regulation of pathogen-triggered tryptophan metabolism in *Arabidopsis thaliana* by MYB transcription factors and indole glucosinolate conversion products. *Mol. Plant* **9**, 682–695 (2016).
17. D. Maag, M. Erb, T. G. Köllner, J. Gershenzon, Defensive weapons and defense signals in plants: Some metabolites serve both roles. *Bioessays* **37**, 167–174 (2015).
18. P.-J. Zhang, S.-J. Zheng, J. J. A. van Loon, W. Bolland, A. David, R. Mumm, M. Dicke, Whiteflies interfere with indirect plant defense against spider mites in Lima bean. *Proc. Natl. Acad. Sci. U.S.A.* **106**, 21202–21207 (2009).
19. G. Zhou, J. Qi, N. Ren, J. Cheng, M. Erb, B. Mao, Y. Lou, Silencing *OsHL-LOX* makes rice more susceptible to chewing herbivores, but enhances resistance to a phloem feeder. *Plant J.* **60**, 638–648 (2009).
20. J. Lu, J. Li, H. Ju, X. Liu, M. Erb, X. Wang, Y. Lou, Contrasting effects of ethylene biosynthesis on induced plant resistance against a chewing and a piercing-sucking herbivore in rice. *Mol. Plant* **7**, 1670–1682 (2014).
21. L. Hu, M. Ye, R. Li, Y. Lou, *OsWRKY53*, a versatile switch in regulating herbivore-induced defense responses in rice. *Plant Signal. Behav.* **11**, e1169357 (2016).
22. V. Tzin, P. L. Lindsay, S. A. Christensen, L. N. Mehlis, L. B. Blue, G. Jander, Genetic mapping shows intraspecific variation and transgressive segregation for caterpillar-induced aphid resistance in maize. *Mol. Ecol.* **24**, 5739–5750 (2015).
23. E. Pichersky, E. Lewinsohn, Convergent evolution in plant specialized metabolism. *Annu. Rev. Plant Biol.* **62**, 549–566 (2011).
24. R. Milo, R. L. Last, Achieving diversity in the face of constraints: Lessons from metabolism. *Science* **336**, 1663–1667 (2012).
25. B. J. Leong, R. L. Last, Promiscuity, impersonation and accommodation. *Curr. Opin. Struct. Biol.* **47**, 105–112 (2017).
26. M. Frey, K. Schullehner, R. Dick, A. Fiesselmann, A. Gierl, Benzoxazinoid biosynthesis, a model for evolution of secondary metabolic pathways in plants. *Phytochemistry* **70**, 1645–1651 (2009).
27. A. Oikawa, A. Ishihara, C. Tanaka, N. Mori, M. Tsuda, H. Iwamura, Accumulation of HDMBOA-Glc is induced by biotic stresses prior to the release of MBOA in maize leaves. *Phytochemistry* **65**, 2995–3001 (2004).
28. V. Handrick, C. A. M. Robert, K. R. Ahern, S. Zhou, R. A. R. Machado, D. Maag, G. Glauser, F. E. Fernandez-Penny, J. N. Chandran, E. Rodgers-Melnik, B. Schneider, E. S. Buckler, W. Bolland, J. Gershenzon, G. Jander, M. Erb, T. G. Köllner, Biosynthesis of 8-O-methylated benzoxazinoid defense compounds in maize. *Plant Cell* **28**, 1682–1700 (2016).
29. International Wheat Genome Sequencing Consortium (IWGSC), A chromosome-based draft sequence of the hexaploid bread wheat (*Triticum aestivum*) genome. *Science* **345**, 1251788 (2014).
30. R. Janczyk, H. Schmidt, A. Osterrieder, A. Fiesselmann, K. Schullehner, M. Haslbeck, D. Sicker, D. Hofmann, N. Yalpani, C. Simmons, M. Frey, A. Gierl, Elucidation of the final reactions of DIMBOA-glucoside biosynthesis in maize: Characterization of *Bx6* and *Bx7*. *Plant Physiol.* **146**, 1053–1063 (2008).
31. U. Effmert, S. Saschenbrecker, J. Ross, F. Negre, C. M. Fraser, J. P. Noel, N. Dudareva, B. Piechulla, Floral benzenoid carboxyl methyltransferases: From in vitro to in planta function. *Phytochemistry* **66**, 1211–1230 (2005).
32. T. G. Köllner, C. Lenk, N. Zhao, I. Seidl-Adams, J. Gershenzon, F. Chen, J. Degenhardt, Herbivore-induced SABATH methyltransferases of maize that methylate anthranilic acid using S-adenosyl-L-methionine. *Plant Physiology* **153**, 1795–1807 (2010).
33. C. A. E. Strömberg, Evolution of grasses and grassland ecosystems. *Annu. Rev. Earth Planet. Sci.* **39**, 517–544 (2011).
34. F. C. Wouters, B. Blanchette, J. Gershenzon, D. G. Vassão, Plant defense and herbivore counter-defense: Benzoxazinoids and insect herbivores. *Phytochem. Rev.* **15**, 1127–1151 (2016).
35. J. Maresh, J. Zhang, D. G. Lynn, The innate immunity of maize and the dynamic chemical strategies regulating two-component signal transduction in *Agrobacterium tumefaciens*. *ACS Chem. Biol.* **1**, 165–175 (2006).
36. G. Marti, M. Erb, J. Boccia, G. Glauser, G. R. Doyen, N. Villard, C. A. M. Robert, T. C. J. Turlings, S. Rudaz, J.-L. Wolfender, Metabolomics reveals herbivore-induced metabolites of resistance and susceptibility in maize leaves and roots. *Plant Cell Environ.* **36**, 621–639 (2013).
37. J. Gulati, I. T. Baldwin, E. Gaquerel, The roots of plant defenses: Integrative multivariate analyses uncover dynamic behaviors of gene and metabolic networks of roots elicited by leaf herbivory. *Plant J.* **77**, 880–892 (2014).
38. R. A. R. Machado, C. C. M. Arce, A. P. Ferrieri, I. T. Baldwin, M. Erb, Jasmonate-dependent depletion of soluble sugars compromises plant resistance to *Manduca sexta*. *New Phytol.* **207**, 91–105 (2015).
39. C. Bonnet, S. Lassueur, C. Ponzo, R. Gols, M. Dicke, P. Raymond, Combined biotic stresses trigger similar transcriptomic responses but contrasting resistance against a chewing herbivore in *Brassica nigra*. *BMC Plant Biol.* **17**, 127 (2017).
40. R. Tiburzy, H. J. Reisener, Resistance of wheat to *Puccinia graminis* f.sp. *tritici*: Association of the hypersensitive reaction with the cellular accumulation of lignin-like material and callose. *Physiol. Mol. Plant Pathol.* **36**, 109–120 (1990).
41. A. Huffaker, F. Kaplan, M. M. Vaughan, N. J. Dafoe, X. Ni, J. R. Rocca, H. T. Alborn, P. E. A. Teal, E. A. Schmelz, Novel acidic sesquiterpenoids constitute a dominant class of pathogen-induced phytoalexins in maize. *Plant Physiol.* **156**, 2082–2097 (2011).
42. A. Oikawa, A. Ishihara, H. Iwamura, Induction of HDMBOA-Glc accumulation and DIMBOA-Glc 4-O-methyltransferase by jasmonic acid in poaceous plants. *Phytochemistry* **61**, 331–337 (2002).
43. M. Pfalz, M. D. Mikkelsen, P. Bednarek, C. E. Olsen, B. A. Halkier, J. Kroymann, Metabolic engineering in *Nicotiana benthamiana* reveals key enzyme functions in *Arabidopsis* indole glucosinolate modification. *Plant Cell* **23**, 716–729 (2011).
44. S.-M. Chaw, C.-C. Chang, H.-L. Chen, W.-H. Li, Dating the monocot–dicot divergence and the origin of core eudicots using whole chloroplast genomes. *J. Mol. Evol.* **58**, 424–441 (2004).
45. S. J. Gould, *Wonderful Life: Burgess Shale and the Nature of History* (W.W. Norton, 1990).
46. A. Bennis, The convergent evolution in plants. *Riv. Biol.* **96**, 485–489 (2003).
47. R. Huang, A. J. O'Donnell, J. J. Barbolino, T. J. Barkman, Convergent evolution of caffeine in plants by co-option of exapted ancestral enzymes. *Proc. Natl. Acad. Sci. U.S.A.* **113**, 10613–10618 (2016).
48. P. Fan, A. M. Miller, X. Liu, A. D. Jones, R. L. Last, Evolution of a flipped pathway creates metabolic innovation in tomato trichomes through BAHD enzyme promiscuity. *Nat. Commun.* **8**, 2080 (2017).
49. S. Xu, T. Brockmüller, A. Navarro-Quezada, H. Kuhl, K. Gase, Z. Ling, W. Zhou, C. Kreitzer, M. Stanke, H. Tang, E. Lyons, P. Pandey, S. P. Pandey, B. Timmermann, E. Gaquerel, I. T. Baldwin, Wild tobacco genomes reveal the evolution of nicotine biosynthesis. *Proc. Natl. Acad. Sci. U.S.A.* **114**, 6133–6138 (2017).
50. A. Pellegrineschi, L. M. Noguera, B. Skovmand, R. M. Brito, L. Velazquez, M. M. Salgado, R. Hernandez, M. Warburton, D. Hoisington, Identification of highly transformable wheat genotypes for mass production of fertile transgenic plants. *Genome* **45**, 421–430 (2002).
51. A. Himmelbach, U. Zierold, G. Hensel, J. Riechen, D. Douchkov, P. Schweizer, J. Kümlehn, A set of modular binary vectors for transformation of cereals. *Plant Physiol.* **145**, 1192–1200 (2007).
52. G. Hensel, C. Kastner, S. Oleszczuk, J. Riechen, J. Kümlehn, *Agrobacterium*-mediated gene transfer to cereal crop plants: Current protocols for barley, wheat, triticale, and maize. *Int. J. Plant Genomics* **2009**, 835608 (2009).
53. D. B. Fisher, J. M. Frame, A guide to the use of the exuding-stylet technique in phloem physiology. *Planta* **161**, 385–393 (1984).
54. S. Irmisch, A. C. McCormick, G. A. Boeckler, A. Schmidt, M. Reichelt, B. Schneider, K. Block, J.-P. Schnitzler, J. Gershenzon, S. B. Unsicker, T. G. Köllner, Two herbivore-induced cytochrome P450 enzymes CYP79D6 and CYP79D7 catalyze the formation of volatile aldoximes involved in poplar defense. *Plant Cell* **25**, 4737–4754 (2013).

SCIENCE ADVANCES | RESEARCH ARTICLE

55. K. Tamura, D. Peterson, N. Peterson, G. Stecher, M. Nei, S. Kumar, MEGA5: Molecular Evolutionary Genetics Analysis Using Maximum Likelihood, Evolutionary Distance, and Maximum Parsimony Methods. *Mol. Biol. Evol.* **28**, 2731–2739 (2011).

Acknowledgments: We thank C. Marthe for excellent technical assistance. **Funding:** This study was supported by the Swiss National Science Foundation (grant nos. 164480 to B.L., 157884 to M.E., and 160786 to M.E. and J.G.), the United States National Science Foundation (award IOS-1339237 to G.J.), the Max Planck Society, and the University of Bern. **Author contributions:** M.E., T.G.K., and G.J. conceived the study. All authors designed the experiments and analyzed the data. B.L., C.F., C.A.M.R., T.Z., R.A.R.M., L.H., J.-D.B., V.H., T.K., G.H., W.C., P.Y., and T.G.K. performed the experiments. M.E. and T.G.K. wrote the first draft. All authors contributed to the final version of the manuscript. **Competing interests:** The authors declare that they have no competing interests. **Data and materials availability:** All data needed

to evaluate the conclusions in the paper are present in the paper and/or the Supplementary Materials. Raw reads of the RNA sequencing experiment can be downloaded from the NCBI Sequence Read Archive (SRA accession: SRP148745). Additional data related to this paper may be requested from the authors.

Submitted 27 March 2018
Accepted 7 November 2018
Published 5 December 2018
10.1126/sciadv.aat6797

Citation: B. Li, C. Förster, C. A. M. Robert, T. Züst, L. Hu, R. A. R. Machado, J.-D. Berset, V. Handrick, T. Knauer, G. Hensel, W. Chen, J. Kumlehn, P. Yang, B. Keller, J. Gershenzon, G. Jander, T. G. Köllner, M. Erb, Convergent evolution of a metabolic switch between aphid and caterpillar resistance in cereals. *Sci. Adv.* **4**, eaat6797 (2018).

3.2 Manuscript II

Manuscript title: Biosynthesis and antifungal activity of fungus-induced O-methylated flavonoids in maize

Authors: Christiane Förster, Vinzenz Handrick, Yezhang Ding, Yoko Nakamura, Christian Paetz, Bernd Schneider, Gabriel Castro-Falcón, Chambers C. Hughes, Katrin Luck, Sowmya Poosapati, Grit Kunert, Alisa Huffaker, Jonathan Gershenzon, Eric A. Schmelz, and Tobias. G. Köllner

Bibliographic information: Förster, C., Handrick, V., Ding, Y., Nakamura, Y., Paetz, C., Schneider, B., Castro-Falcón, G., Hughes, C.C., Luck, K., Poosapati, S., Kunert, G., Huffaker, A., Gershenzon, J., Schmelz, E.A., and Köllner, T.G. (2021). Biosynthesis and antifungal activity of fungus-induced O-methylated flavonoids in maize. Plant Physiol, kiab496.

The candidate is

☒ First author, ☐ Co-first author, ☐ Corresponding author, ☐ Co-author.


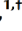

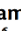
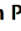



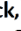
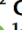





Status: published October 27 (2021) in Plant Physiology

Authors' contributions (in %) to the publication (indicated from 20%)

Author	Conceptual	Data analysis	Experimental	Writing the manuscript	Supply of material
Christiane Förster	20	75	70	70	/
Jonathan Gershenzon	5	/	/	10	80
Eric A. Schmelz	30	/	/	10	20
Tobias G. Köllner	35	/	/	10	/



Biosynthesis and antifungal activity of fungus-induced O-methylated flavonoids in maize

Christiane Förster ¹, Vinzenz Handrick ^{1,†}, Yezhang Ding ^{2,*}, Yoko Nakamura ³, Christian Paetz ³, Bernd Schneider ³, Gabriel Castro-Falcón ⁴, Chambers C. Hughes ^{4,§}, Katrin Luck ¹, Sowmya Poosapati ², Grit Kunert ¹, Alisa Huffaker ², Jonathan Gershenzon ¹, Eric A. Schmelz ² and Tobias G. Köllner ^{1,*§}

¹ Department of Biochemistry, Max Planck Institute for Chemical Ecology, Jena D-07745, Germany

² Section of Cell and Developmental Biology, University of California, San Diego, California 92093-0380, USA

³ Research Group Biosynthesis/NMR, Max Planck Institute for Chemical Ecology, Jena D-07745, Germany

⁴ Scripps Institution of Oceanography, University of California, San Diego, California 92093, USA

*Author for communication: koellner@ice.mpg.de

[†]Present address: Leibniz Institute of Plant Biochemistry, Department Biochemistry of Plant Interactions, D-06120 Halle (Saale), Germany.

[§]Present address: Environmental Genomics and Systems Biology, Lawrence Berkeley National Laboratory, Berkeley, California, USA.

[§]Present address: Interfaculty Institute of Microbiology and Infection Medicine, University of Tübingen, Tübingen, D-72076, Germany.

These authors contributed equally (E.A.S. and T.G.K.).

[§]Senior author

T.G.K., E.A.S., C.F., V.H., and J.G. designed the research. C.F., V.H., Y.D., Y.N., K.L., and S.P. performed the research. C.P., Y.N., B.S., C.C.H., and G.C.F. performed NMR analysis and structure elucidation. C.F., V.H., A.H., G.K., E.A.S., Y.D., and T.G.K. analyzed the data. C.F., T.G.K., E.A.S., and J.G. wrote the article with input from all other authors.

The author responsible for distribution of materials integral to the findings presented in this article in accordance with the policy described in the Instructions for Authors (<https://academic.oup.com/plphys/pages/general-instructions>) is Tobias G. Köllner (koellner@ice.mpg.de).

Abstract

Fungal infection of grasses, including rice (*Oryza sativa*), sorghum (*Sorghum bicolor*), and barley (*Hordeum vulgare*), induces the formation and accumulation of flavonoid phytoalexins. In maize (*Zea mays*), however, investigators have emphasized benzoxazinoid and terpenoid phytoalexins, and comparatively little is known about flavonoid induction in response to pathogens. Here, we examined fungus-elicited flavonoid metabolism in maize and identified key biosynthetic enzymes involved in the formation of O-methylflavonoids. The predominant end products were identified as two tautomers of a 2-hydroxynaringenin-derived compound termed xilonenin, which significantly inhibited the growth of two maize pathogens, *Fusarium graminearum* and *Fusarium verticillioides*. Among the biosynthetic enzymes identified were two O-methyltransferases (OMTs), flavonoid OMT 2 (FOMT2), and FOMT4, which demonstrated distinct regiospecificity on a broad spectrum of flavonoid classes. In addition, a cytochrome P450 monooxygenase (CYP) in the CYP93G subfamily was found to serve as a flavanone 2-hydroxylase providing the substrate for FOMT2-catalyzed formation of xilonenin. In summary, maize produces a diverse blend of O-methylflavonoids with antifungal activity upon attack by a broad range of fungi.

Received June 02, 2021. Accepted September 30, 2021. Advance access publication October 27, 2021

© The Author(s) 2021. Published by Oxford University Press on behalf of American Society of Plant Biologists.

This is an Open Access article distributed under the terms of the Creative Commons Attribution License (<https://creativecommons.org/licenses/by/4.0/>), which permits unrestricted reuse, distribution, and reproduction in any medium, provided the original work is properly cited.

Open Access

Introduction

Plants dynamically deploy a suite of low-molecular weight metabolites to protect against pathogen infection that is chemically diverse and often species-specific. When these compounds are produced in response to microbial challenge or other environmental stresses, they have been termed phytoalexins (VanEtten et al., 1994; Hammerschmidt, 1999). Rapid phytoalexin biosynthesis is often associated with enhanced pathogen resistance (Hain et al., 1993; He and Dixon, 2000). Phytoalexins have representatives from many known classes of specialized metabolites (Jeandet et al., 2014), including the stilbene resveratrol in grapes (*Vitis vinifera*; Langcake and Pryce, 1976) and an indole thiazole alkaloid, termed camalexin, in *Arabidopsis thaliana* (Browne et al., 1991). In maize (*Zea mays*), complex networks of sesquiterpenoid and diterpenoid phytoalexins have been described, which include zealexins, kauralexins, and dolabrallexins (Huffaker et al., 2011; Schmelz et al., 2011; Mafu et al., 2018; Ding et al., 2020).

Many phytoalexins are flavonoids, a large group of phenylpropanoid and polyketide-derived metabolites present in all plants (Tohge et al., 2017; de Souza et al., 2020; Ube et al., 2021). The accumulation of flavonoids after pathogen infection has been demonstrated to play a role in disease resistance in several plants, such as for the 3-deoxyanthocyanidins of sorghum (*Sorghum bicolor*) (Nicholson et al., 1987; Snyder et al., 1991; Liu et al., 2010) and the flavan-3-ols of poplar (Ullah et al., 2017).

The core pathways of flavonoid biosynthesis are well conserved among plant species (Grotewold, 2006; Tohge et al., 2017). The first step is the condensation of a phenylpropanoid derivative, 4-coumaroyl-CoA, with three malonyl-CoA subunits catalyzed by a polyketide synthase, chalcone synthase. The naringenin chalcone produced is then cyclized by chalcone isomerase to form flavanones, which are converted successively to dihydroflavonols and flavonols by soluble Fe^{2+} /2-oxoglutarate-dependent dioxygenases (2-ODDs). Flavanones can also be desaturated to form flavones via different mechanisms. While flavone synthases of type I (FNSI) belong to the 2-ODDs, FNSII are membrane-bound oxygen- and nicotinamide adenine dinucleotide phosphate (NADPH)-dependent cytochrome P450 monooxygenases (CYPs; Martens and Mithofer, 2005; Jiang et al., 2016).

Other common modifications of the flavonoid backbone include C- and O-glycosylation, acylation, and O-methylation (Grotewold, 2006). O-Methylation of flavonoids is catalyzed by O-methyltransferases (OMTs), which transfer the methyl group of the cosubstrate S-adenosyl-L-methionine (SAM) to a specific hydroxyl group of the flavonoid. Two major classes of plant phenylpropanoid OMTs exist: the caffeoyl-CoA OMTs (CCoAOMTs) of low-molecular weight (26–30 kDa) that require bivalent ions for catalytic activity, and the higher molecular weight (40–43 kDa) and bivalent ion-independent caffeic acid OMTs (COMTs). Flavonoid OMTs (FOMTs) are members of the COMT class (Kim et al., 2010). O-Methylation modifies the chemical properties of

flavonoids and can alter biological activity, depending on the position of reaction (Kim et al., 2010). In general, the reactivity of hydroxyl groups is reduced coincident with increased lipophilicity and antimicrobial activity (Ibrahim et al., 1998).

Many FOMT genes have been cloned from dicot species and the corresponding enzymes biochemically characterized (Kim et al., 2010; Berim et al., 2012; Liu et al., 2020). In contrast, only a few FOMT genes from monocotyledons, all belonging to the grass family (*Poaceae*), have been functionally characterized so far. Four FOMTs from rice (*Oryza sativa*), wheat (*Triticum aestivum*), barley (*Hordeum vulgare*), and maize are flavonoid 3'-/5'-OMTs that prefer the flavone trisetin as substrate (Kim et al., 2006; Zhou et al., 2006a, 2006b, 2008). The other two known *Poaceae* FOMTs are flavonoid 7-OMTs from barley and rice that mainly utilize apigenin and naringenin as substrates, respectively (Christensen et al., 1998; Shimizu et al., 2012). In both cases, the gene transcripts or FOMT reaction products, namely 7-methoxyapigenin (genkwanin) and 7-methoxynaringenin (sakuranetin) accumulated in leaves following challenge with pathogenic fungi or abiotic stress (Gregersen et al., 1994; Rakwal et al., 1996). Moreover, genkwanin and sakuranetin were shown to possess antibacterial and antifungal activity in vitro (Kodama et al., 1992; Martini et al., 2004; Park et al., 2014). Sakuranetin also inhibits the growth of the rice blast fungus (*Magnaporthe oryzae*) in vivo (Hasegawa et al., 2014). Despite our knowledge of the key pathogen protection roles of O-methylflavonoids in rice, their biosynthesis has not been previously described in maize.

To investigate fungal-induced defenses in maize, we used untargeted and targeted liquid chromatography/mass spectrometry (LC-MS) to identify and quantify flavonoids in leaves of different inbred lines infected with a necrotrophic fungus, southern leaf blight (SLB; *Bipolaris maydis*). O-Methylflavonoids were especially plentiful with the most abundant compound being a tautomeric O-dimethyl-2-hydroxynaringenin termed xilonenin, which exhibited small but significant in vitro antifungal activity against *Fusarium graminearum* and *Fusarium verticillioides*. Association mapping and RNA-Seq-based transcriptome analyses enabled the selection of candidate pathway genes encoding a CYP93G and three highly regiospecific OMTs.

Results

Fungal elicitation of maize results in the accumulation of a complex mixture of flavonoids, especially O-methylflavonoids

To identify flavonoids induced by fungal infection in maize, we used untargeted LC-MS to screen for metabolites present in the leaves of two inbred lines (B75 and W22) infected with the pathogenic fungus *B. maydis*, termed SLB (Figure 1A). Based on the accurate mass ($\Delta m/z \leq 2$ ppm), we identified a collection of 38 known and putative flavonoids showing increased accumulation following fungal infection (Figure 1B; Supplemental Table S1). Flavonoid levels

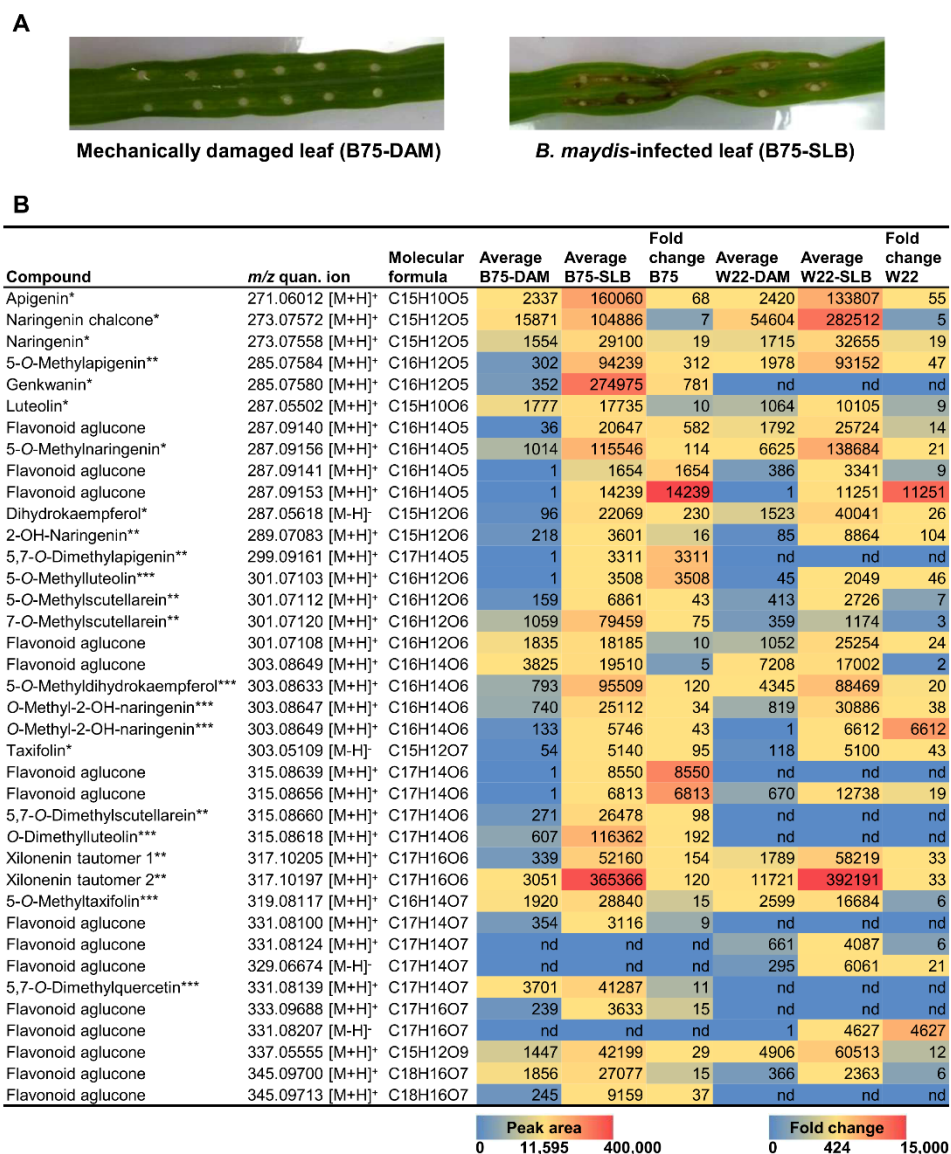


Figure 1 Flavonoids induced in maize leaves upon fungal infection. Damaged and water treated leaves (DAM) or damaged and *B. maydis*-infected leaves (SLB) of the maize lines B75 and W22 were harvested 4 d after inoculation. Methanol extracts made from ground leaf material were screened for putative non-O-methyl- and O-methylflavonoids by untargeted LC–MS based on the expected exact masses. A, Representative photographs of water control (DAM) and *B. maydis*-infected (SLB) B75 leaves. B, Potential flavonoids were tentatively identified using their exact masses. Only compounds with $\Delta m/z \leq 2$ ppm, a peak area more than 3,000, and a fold change of ≥ 5 after fungal infection were included in the candidate list. Mean relative abundances and fold changes are shown ($n = 6-8$). The differences between treatments are statistically significant ($P < 0.05$) for all compounds in both lines (t test implemented in MetaboScape version 4.0 software; for P-values see Supplemental Table S1). The identities of compounds were confirmed by commercially available standards (*), purification followed by NMR analysis (**), or inferred from specific enzymatic activities investigated in this study (***, see below).

differed qualitatively and quantitatively between the two inbreds; however, MS/MS fragmentation patterns indicated that flavonoids with methoxy groups at positions 5 and 7 of the A-ring predominated in both lines (Figure 1B; Supplemental Figure S1). We were able to confirm the structures of 7 non-O-methylated flavonoids and 16 O-methyl- or O-dimethylflavonoids by authentic standards, nuclear magnetic resonance (NMR) analysis, or by deducing their O-methylation patterns from specific enzymatic activities as detailed below.

Two maize OMT genes on chromosome 9 are genetically associated with O-methylflavonoid accumulation

To identify candidate OMTs involved in the formation of fungus-elicited O-methylflavonoids, we performed association analyses using the mapping traits 5-O-methylapigenin and genkwanin (7-O-methylapigenin), two of the compounds identified in our survey (Figure 1). Using the B73 × Ky21 recombinant inbred line (RIL) population (McMullen et al., 2009) and 5-O-methylapigenin levels, we performed association mapping with the general linear model (GLM) and 80,440 single-nucleotide polymorphisms (SNPs) that identified highly significant SNPs on chromosome 9 (B73 RefGen_v2) (Figure 2A; Supplemental Figure S2). The corresponding chromosomal region contained two putative OMT genes named FOMT2 (Zm00001d047192) and FOMT3 (Zm00001d047194). For clarity, unless otherwise noted, gene and protein abbreviations refer to line B73 (RefGen_v4) reference sequences. In addition, a genome-wide association study (GWAS) using the Goodman association panel (mixed linear model (MLM), 25,457,708 SNPs; Flint-Garcia et al., 2005) was performed using genkwanin or the apigenin/genkwanin ratio as traits (Figure 2B; Supplemental Figure S3), which revealed a second genomic region on chromosome 9 containing a third putative OMT gene named FOMT4 (Zm00001d048087).

Initial sequence analyses of the identified OMT genes in different maize inbred lines revealed that W22 has a second copy of FOMT2 (Zm00004b033403 and Zm00004b033399, W22 RefGen_v2) on chromosome 9, differing only in a single synonymous nucleotide (Supplemental Figures S4 and S5). Furthermore, FOMT2 and FOMT3 are closely related and encode proteins with 79% amino acid sequence identity. RNA sequencing (RNA-seq) of W22 leaves, damaged and treated with either water (control) or *B. maydis* hyphae for 4 d, showed significantly increased accumulation of transcripts encoding both copies of FOMT2 and FOMT4 as predicted for their involvement in flavonoid O-methylation (Figure 2C; Supplemental Table S2; Supplemental Data Set S1). In contrast, FOMT3 displayed dramatically lower expression levels that did not show statistically significant differences between the treatments.

Phylogenetic analyses demonstrated that FOMT2/3 are closely related to maize BX10/11/12/14, which catalyze various O-methylations of benzoxazinoid (BX) defense

compounds (Meihls et al., 2013), and to an uncharacterized maize OMT named FOMT5 (Zm00001d051934) (Figure 2D; Supplemental Figure S6; Supplemental Table S3). Notably, BX10/11/14 and FOMT5 transcripts also increased after fungal elicitation in our experiments (Figure 2C; Supplemental Figure S7; Supplemental Table S2). In contrast to FOMT2/3, FOMT4 showed the closest relation to OsNOMT, responsible for production of the phytoalexin sakuranetin in rice, and other Poaceae FOMTs, including maize OMT1 (FOMT1), which has been described to O-methylate the B-ring of various flavonoids (Figure 2D; Supplemental Figure S6).

FOMT2/3, FOMT4, and FOMT5 catalyze the regiospecific O-methylation of diverse flavonoids in vitro

To characterize the enzymatic activity of FOMT2, FOMT3, FOMT4, and FOMT5, we expressed the complete open reading frames in *Escherichia coli* and tested the purified recombinant proteins in enzyme assays with potential flavonoid substrates in the presence of the cofactor SAM. Using scutellarein as a substrate, LC-MS/MS analysis revealed that FOMT2, FOMT4, and FOMT5 each produced a different single product peak that was not present in the empty vector (EV) control (Figure 2E). Product purification followed by NMR structure elucidation (Supplemental Table S4; Supplemental Data Set S2) or comparison with commercially available standards confirmed regiospecific O-methylation on positions 5, 7, and 6 of the flavonoid A-ring catalyzed by FOMT2, FOMT4, and FOMT5, respectively. In an enzyme assay containing both FOMT2 and FOMT4, a 5,7-O-dimethylated product was detected (Figure 2E). Interestingly, the 5-O-methylated product (RT = 4.61 min), as well as the 5,7-O-dimethylated product (RT = 5.20 min), were retained less by the LC column than the non-O-methylated substrate (RT = 5.22 min; Supplemental Figure S8), suggesting that the carbonyl group on the C-ring can form a hydrogen bond to a solvent molecule, which likely makes the two products more polar compared to the substrate. The regiospecificity of FOMT2 and FOMT4 and the distinct elution patterns of their products were confirmed with enzyme assays using naringenin and apigenin as substrates (Supplemental Figure S8), followed by NMR structure verification (Supplemental Table S4; Supplemental Data Set S2), which was used as the basis for the identification of additional 5-/7-O-methylflavonoids given in Figure 1B. FOMT3 displayed the same enzymatic activity as FOMT2, producing the 5-O-methyl derivative of different flavonoid substrates, but exhibited much lower relative activity (Supplemental Table S5).

Despite their strict regiospecificity, FOMT2/3 and FOMT4 demonstrated an ability to functionalize a range of flavonoid skeletons (Figure 3). Preferred substrates for FOMT2 were flavanones (2-hydroxynaringenin, naringenin) and flavonols (quercetin, kaempferol), while FOMT4 showed highest activity with flavonols (kaempferol, quercetin) and flavones

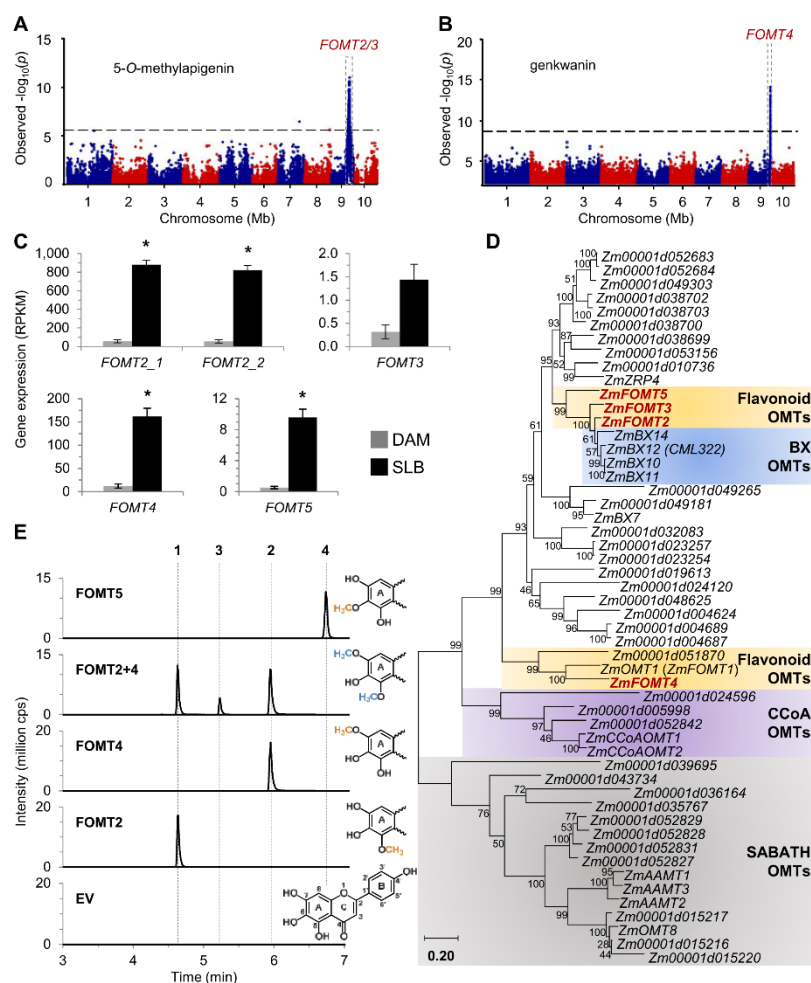


Figure 2 Association mapping reveals novel O-methyltransferases involved in maize O-methylflavonoid production. A, Manhattan plot of the association analysis of fungus-elicited 5-O-methylapigenin using the B73 × Ky21 RIL population with the GLM and 80,440 SNPs. The most statistically significant SNPs are located within the region of the maize *FOMT2/3* genes on chromosome 9 (*FOMT2*, Chr9:119,779,040–119,780,565 bp; *FOMT3*, Chr9:119,838,646–119,840,122 bp; B73 RefGen_v2). The black dashed line denotes the false discovery rate (< 0.05 at $-\log_{10}(P)$) using a Bonferroni correction. B, Manhattan plot of the association analysis (MLM) of genkwanin in the stems of maize plants from the Goodman diversity panel following 3 d of fungal elicitation. The most statistically significant SNPs are located within the region of the maize *FOMT4* gene on chromosome 9 (Chr9: 147,148,251–147,149,436 bp; B73 RefGen_v3). The black dashed line denotes the 5% Bonferroni corrected threshold for 25,457,708 SNP markers. C, Transcript abundance of identified OMT genes in damaged and water-treated (DAM) or damaged and *B. maydis*-infected (SLB) W22 leaves harvested after 4 d of inoculation. Gene expression is given as reads per kilobase per million reads mapped (RPKM; means \pm SE; $n = 4$). Asterisks indicate statistically significant differences ($P < 0.05$) between treatments using a Bonferroni correction (for statistical values, see Supplemental Table S2). D, Phylogenetic tree showing maize OMT genes similar to mapped *FOMT2/3*, previously characterized *AAMT1*, and *CCoAOMT1*. The tree was inferred using the maximum likelihood method based on the General Time Reversible model, including gamma distributed rate variation among sites (+ G, 4.3129). Bootstrap values ($n = 1,000$) are shown next to each node. The tree is drawn to scale, with branch lengths measured in the number of substitutions per site. All positions with $< 80\%$ site coverage were eliminated. Maize OMTs investigated in this study are highlighted in red. Gene accession numbers and references are provided in Supplemental Table S3. E, Enzymatic activity of purified recombinant *FOMT2*, *FOMT4*, *FOMT5*, and an EV control using scutellarein as substrate in the presence of the cosubstrate SAM. Reaction products were analyzed by LC–MS/MS. The structure of the substrate scutellarein (depicting flavonoid ring structure and numbering) and partial structures of the different enzymatic products highlighting the added methyl groups on the flavonoid A-ring are shown on the right side. 1, 5-O-methylscutellarein; 2, 7-O-methylscutellarein; 3, 5,7-O-dimethylscutellarein; 4, hispidulin; cps, counts per second.

(scutellarein, chrysin, luteolin, apigenin). All three enzymes showed activity, albeit rather low, with *O*-methylflavonoids as substrates. The structurally similar stilbenoid resveratrol was also a substrate for FOMT2/3. Neither the tested glycosylated flavonoids nor the phenolic compounds caffeic acid and DIMBOA-Glc were accepted as substrates by any of the assayed FOMTs (Figure 3). Altogether, the in vitro characterization demonstrated that FOMT2 and FOMT4 in combination are capable of generating the majority of the *O*-methylflavonoids observed in maize.

The phylogenetically related OMTs from BX biosynthesis BX10/11/14 are also induced upon fungal infection (Supplemental Figure S7). To investigate whether these enzymes might also play a role in *O*-methylflavonoid formation, we included BX10/11/12/14 in our OMT characterization. Besides the expected conversion of DIMBOA-Glc to HDMBOA-Glc (Supplemental Table S5), all four enzymes showed fairly low, but unspecific 5- and/or 7-*O*-methylation activity (<0.9% product formation of FOMT2 or 4) with flavonoid substrates such as naringenin, apigenin, and scutellarein (Supplemental Table S5). The only exception was the direct 5,7-*O*-dimethylation of apigenin by BX10, BX11, and BX12, which exhibited up to 60% of the activity of FOMT2 + 4 (Supplemental Table S5).

Two predominant fungal-induced *O*-dimethylated flavonoids are 2-hydroxynaringenin derivatives associated with FOMT2

Two of the most abundant *O*-methylflavonoids detected in our LC-MS profiles of fungal-infected maize leaves had identical accurate masses of m/z 317.102 $[M + H]^+$ (Figure 1; Supplemental Figure S9), suggesting both were di-*O*-methylated derivatives of a hydroxynaringenin (proposed molecular formula: $C_{17}H_{16}O_6$, $\Delta m/z \leq 0.14$ ppm). In addition, the fragmentation pattern (main fragments: m/z 181.050 $[M + H]^+$ and m/z 121.028 $[M + H]^+$), indicated that the hydroxyl group must be connected to a position on the flavonoid C-ring (Supplemental Figure S9). These two major unknowns were accompanied by two other unidentified flavonoids with m/z 303.086 $[M + H]^+$ (proposed molecular formula: $C_{16}H_{14}O_6$, $\Delta m/z \leq 0.72$ ppm), whose accurate mass and fragmentation pattern were consistent with being mono-*O*-methylated derivatives of a hydroxynaringenin. Moreover, there was also a peak for a non-*O*-methylated flavonoid in SLB-infected W22 leaves that was a potential precursor of these unknowns, which had m/z 289.071 $[M + H]^+$ (proposed molecular formula: $C_{15}H_{12}O_6$, $\Delta m/z = 0.43$ ppm; Supplemental Figure S9). The fragmentation pattern of this precursor candidate was consistent with that reported for 2-hydroxynaringenin (Supplemental Figure S9), which interconverts between closed-ring and open-ring tautomers at room temperature (Zhang et al., 2007; Du et al., 2010a, 2010b). Importantly, in the GWAS as well as the association analysis using the B73 \times Ky21 RIL population, FOMT2 was associated with the occurrence of the two major unknown compounds of m/z 317.102 (Figure 4A; Supplemental

Figures S2 and S10). We thus hypothesized that the open ring form of 2-hydroxynaringenin could serve as a substrate for two sequential *O*-methylation reactions catalyzed by FOMT2 since rotation of the A-ring creates two equivalent hydroxyl groups.

A fungal-induced flavanone 2-hydroxylase provides 2-hydroxynaringenin for the production of two open ring tautomeric di-*O*-methylated flavonoid derivatives termed xilonenin

To test whether 2-hydroxynaringenin can act as substrate for FOMT2, we first investigated the formation of this precursor. A flavanone 2-hydroxylase (F2H) converting naringenin to its 2-hydroxy derivative was previously characterized in maize (CYP93G5, F2H1; Morohashi et al., 2012); however, F2H1 transcript levels in W22 (Zm00004b033614) were low and not increased following fungal elicitation (Figures 4, B and C). We, therefore, performed a BLAST analysis of F2H1 in the W22 (NRGene_V2) genome to identify related genes. This search revealed five additional putative flavanone hydroxylases belonging to the CYP93G subfamily that clustered with characterized monocot F2Hs or FNSII in a phylogenetic tree (Figure 4B; Supplemental Table S6; Supplemental Figure S11), but were only distantly related to dicot F2H/FNSII enzymes belonging to the CYP93B subfamily (Du et al., 2010a, 2010b; Morohashi et al., 2012; Lam et al., 2014). Two of these CYP93G genes, Zm00004b010826 (CYP93G15) and Zm00004b039148 (CYP93G7), the latter recently characterized as a FNSII (Righini et al., 2019), were found to be upregulated after fungal infection (Figure 4C; Supplemental Table S2).

To determine the enzymatic activity of Zm00004b010826 (CYP93G15), we expressed the yeast codon-optimized full-length open reading frame in *Saccharomyces cerevisiae* and performed enzyme assays with the microsomal fraction, the cosubstrate NADPH, and the potential substrates naringenin or eriodictyol. The characterized F2H1 from B73 was included as positive control. LC-MS/MS analysis showed that both F2H1 and Zm00004b010826 (CYP93G15) converted naringenin and eriodictyol to 2-hydroxynaringenin and 2-hydroxyeriodictyol, respectively, while the EV control did not show any product peak (Figure 4D; Supplemental Figure S12). Among the other putative F2Hs, Zm00004b033614 (CYP93G5) exhibited F2H activity, converting naringenin and eriodictyol to their respective 2-hydroxy derivatives (Supplemental Figure S12), while Zm00004b008124 (CYP93G10) converted naringenin and eriodictyol to the corresponding flavones apigenin and luteolin, respectively, thus exhibiting FNSII activity (Supplemental Figure S12). Notably, we also detected low amounts of 2-hydroxynaringenin in the CYP93G10 reaction (insert in Supplemental Figure S12), indicating that this compound is likely an intermediate in flavone formation. No in vitro activity with naringenin or eriodictyol was found for Zm00004b039147 (CYP93G6) and Zm00004b033036 (CYP93F6; Supplemental Figure S12). Based on their in vitro activity, Zm00004b010826

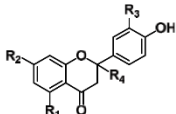
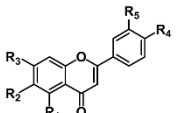
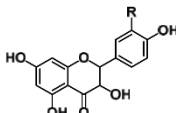
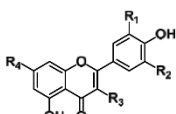
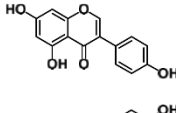
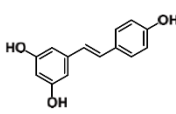
Category / Structure	Substrate	Composition	Relative activity (%)		
			FOMT2	FOMT3	FOMT4
Flavonone 	Naringenin	R ₁ =OH, R ₂ =OH, R ₃ =H, R ₄ =H	86.2 ± 2.8	91.8 ± 2.1	42.9 ± 0.3
	2-Hydroxynaringenin	R ₁ =OH, R ₂ =OH, R ₃ =H, R ₄ =OH	100 ± 1.8	67.2 ± 3.0	2.7 ± 0.8
	Eriodictyol	R ₁ =OH, R ₂ =OH, R ₃ =OH, R ₄ =H	57.1 ± 2.1	8.9 ± 0.7	39.2 ± 1.8
	5-O-Methylnaringenin	R ₁ =OCH ₃ , R ₂ =OH, R ₃ =H, R ₄ =H	-	-	4.6 ± 1.0
	Sakuranetin	R ₁ =OH, R ₂ =OCH ₃ , R ₃ =H, R ₄ =H	3.5 ± 0.4	18.5 ± 2.1	-
Flavone 	Chrysin	R ₁ =OH, R ₂ =H, R ₃ =OH, R ₄ =H, R ₅ =H	16.3 ± 0.9	traces	81.9 ± 1.5
	Apigenin	R ₁ =OH, R ₂ =H, R ₃ =OH, R ₄ =OH, R ₅ =H	47.3 ± 1.8	92.2 ± 2.8	71.3 ± 2.7
	Luteolin	R ₁ =OH, R ₂ =H, R ₃ =OH, R ₄ =OH, R ₅ =OH	65.0 ± 0.6	traces	72.2 ± 0.0
	5-O-Methylapigenin	R ₁ =OCH ₃ , R ₂ =H, R ₃ =OH, R ₄ =OH, R ₅ =H	-	-	49.0 ± 1.1
	Genkwanin	R ₁ =OH, R ₂ =H, R ₃ =OCH ₃ , R ₄ =OH, R ₅ =H	7.1 ± 1.3	100.0 ± 0.4	-
	Acacetin	R ₁ =OH, R ₂ =H, R ₃ =OH, R ₄ =OCH ₃ , R ₅ =H	traces	nd	31.2 ± 0.6
	Scutellarein	R ₁ =OH, R ₂ =OH, R ₃ =OH, R ₄ =OH, R ₅ =H	27.9 ± 1.6	4.9 ± 0.1	82.1 ± 2.0
	Hispidulin	R ₁ =OH, R ₂ =OCH ₃ , R ₃ =OH, R ₄ =OH, R ₅ =H	traces	nd	13.6 ± 0.9
Dihydroflavonol 	Dihydrokaempferol	R=H	47.3 ± 0.1	traces	6.2 ± 2.7
	Taxifolin	R=OH	51.9 ± 0.4	traces	traces
Flavonol 	Kaempferol	R ₁ =H, R ₂ =H, R ₃ =OH, R ₄ =OH	81.5 ± 2.5	traces	100.0 ± 1.5
	Quercetin	R ₁ =OH, R ₂ =H, R ₃ =OH, R ₄ =OH	91.8 ± 1.1	traces	74.0 ± 1.7
	Myricetin	R ₁ =OH, R ₂ =OH, R ₃ =OH, R ₄ =OH	16.7 ± 2.3	27.6 ± 0.9	58.0 ± 1.7
	Isokaempferide	R ₁ =H, R ₂ =H, R ₃ =OCH ₃ , R ₄ =OH	24.2 ± 0.3	3.1 ± 0.9	25.1 ± 1.6
	Kaempferol-7-O-β-D-glucopyranoside	R ₁ =H, R ₂ =H, R ₃ =OH, R ₄ =glucopyranosyl	nd	nd	nd
	Kaempferol-3-O-β-rutinoside	R ₁ =H, R ₂ =H, R ₃ =rutinosyl, R ₄ =OH	nd	nd	nd
Isoflavone 	Genistein		traces	nd	traces
	Caffeic acid		nd	nd	nd
Stilbenoid 	Resveratrol		14.1 ± 0.6	13.8 ± 0.6	nd
	DIMBOA-Glc		nd	nd	nd

Figure 3 Relative activities of the flavonoid O-methyltransferases FOMT2, FOMT3, and FOMT4 with various substrates in vitro. The purified recombinant enzymes as well as the EV control were incubated with the respective substrates in presence of the cosubstrate SAM. Substrate turnover was analyzed by LC-MS/MS and used to estimate the relative activity of each enzyme with different substrates. Product formation in the absence of altered substrate turnover was considered as trace activity. Data are shown as means ± SE (*n* = 2–3). nd, not detectable.

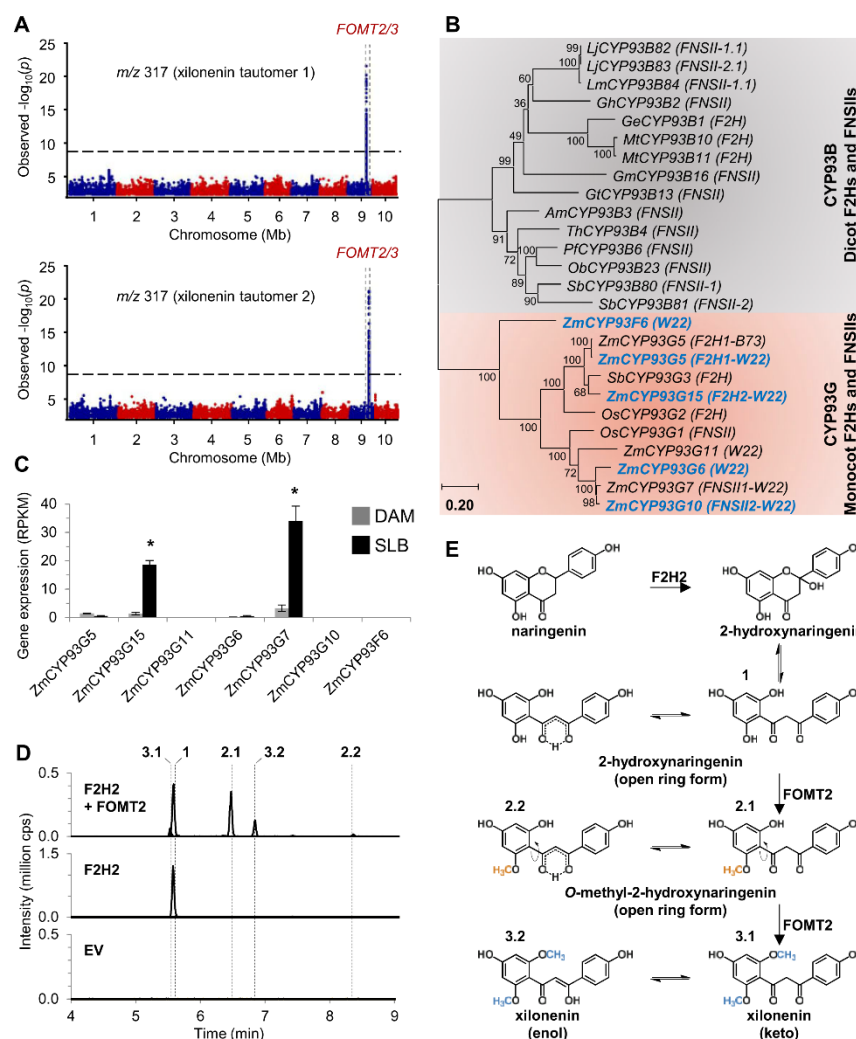


Figure 4 FOMT2 converts 2-hydroxynaringenin to the tautomeric O-dimethylated derivative xilonenin. **A**, Manhattan plots of the association analysis (MLM) of the two novel flavonoids with m/z 317 in the stems of maize plants from the Goodman diversity panel following 3 d of fungal elicitation. The most statistically significant SNPs are located within the region of the maize *FOMT2/3* genes on chromosome 9 (*FOMT2*, Chr9: 120,033,582–120,035,107 bp; *FOMT3*, Chr9: 120,093,188–120,094,664 bp; B73 RefGen_v3). The black dashed line denotes the 5% Bonferroni corrected threshold for 25,457,708 SNP markers. **B**, Phylogenetic analysis of maize genes (W22 NRGene_V2) similar to *F2H1* (B73 RefGen_V3) and additional *F2H* and *FNSII* genes from other monocots and dicots. The tree was inferred using the maximum likelihood method based on the General Time Reversible model, including gamma distributed rate variation among sites (+ G, 1.4700) and allowing invariable sites (+ I, 8.71% sites). Bootstrap values ($n = 1,000$) are shown next to each node. The tree is drawn to scale, with branch lengths measured in the number of substitutions per site. All positions with < 80% site coverage were eliminated. Maize CYP93Gs investigated in this study are highlighted in blue. Accession numbers and references are provided in Supplemental Table S6. **C**, Transcript accumulation of *F2H* candidates in damaged and water-treated leaves (DAM) or damaged and *B. maydis*-infected leaves (SLB) of W22 harvested after 4 d of inoculation. Gene expression is given as RPKM (Means \pm SE; $n = 4$). Asterisks indicate statistically significant differences ($P < 0.05$) between treatments using a Bonferroni correction (for statistical values, see Supplemental Table S2). **D**, Enzymatic activity of *F2H2* (CYP93G15, Zm00004b010826) alone and in combination with purified recombinant *FOMT2* using naringenin as substrate and NADPH and SAM, respectively, as cosubstrates. *F2H2* was heterologously expressed in yeast and the microsomal fraction was used in the enzyme assays. Reaction products were analyzed by LC–MS/MS. 1, 2-hydroxynaringenin; 2.1 and 2.2, O-methyl-2-hydroxynaringenin; 3.1 and 3.2, xilonenin (keto and enol form, respectively). **E** Proposed reaction scheme for the biosynthesis of xilonenin. RPKM, reads per kilobase per million reads mapped; cps, counts per second.

(CYP93G15) and Zm00004b008124 (CYP93G10) were designated as F2H2 and FNSII2, respectively.

To test whether the 2-hydroxynaringenin formed by F2H2 is a precursor of the two unknown compounds of m/z 317.102 $[M + H]^+$, F2H2 and FOMT2 were incubated together in the presence of naringenin, NADPH, and SAM. In addition to

2-hydroxynaringenin, two pairs of peaks were detected consistent with the keto and enol tautomers of mono-*O*-methylated 2-hydroxynaringenin (m/z 303.086) and di-*O*-methylated 2-hydroxynaringenin (m/z 317.102), respectively (Figure 4D). In order to verify the structure of the m/z 317.102 $[M + H]^+$ compounds, we purified them from a FOMT2-overexpressing *E. coli* culture incubated with chemically synthesized 2-hydroxynaringenin as substrate. NMR analyses confirmed the dominant FOMT2 products as *O*-dimethylated 2-hydroxynaringenins, which occur in both the keto and enol forms in a 1:2 ratio, at room temperature (Supplemental Figure S13; Supplemental Data Set S2). UV measurements confirmed predictions that the two tautomer peaks have different UV absorption maxima at 283 nm for the first peak (3.1; RT = 5.51 min in Figure 4D) and 352 nm for the second peak (3.2; RT = 6.81 min in Figure 4D; Supplemental Figure S14). Given that the conjugated enol system usually absorbs at longer wavelengths than the diketone system, we propose that the first peak (3.1 in Figure 4D) corresponds to the keto tautomer, while the second peak (3.2 in Figure 4D) corresponds to the enol tautomer (Figure 4E). As *O*-dimethylated 2-hydroxynaringenin appears to be an undescribed compound, we have named it xilonenin in reference to the Aztec maize goddess Xilonen. Our data thus reveal the fungus-elicited production of two di-*O*-methylated 2-hydroxynaringenin tautomers that are derived from the sequential activity of a F2H (F2H2), to produce 2-hydroxynaringenin, and FOMT2. Importantly, the free rotation of the A-ring in the chalcone-like open-ring form of 2-hydroxynaringenin allows FOMT2 to catalyze two sequential *O*-methylation reactions on the hydroxyl groups in *ortho*-position of ring A (Figure 4E).

Flavonoids accumulate locally at the site of pathogen infection

A defining feature of phytoalexins is their rapid and local accumulation at pathogen infection sites (Nicholson and Hammerschmidt, 1992; Hammerschmidt, 1999). To investigate the spatial distribution of fungal-induced flavonoids in maize leaves, we wounded and inoculated leaves of the inbred line B75 and hybrid maize “Sweet Nugget” in a defined leaf area with *B. maydis* (SLB) hyphae and quantified non-*O*-methylated and *O*-methylated flavonoids in three different leaf segments of which only the middle segment was SLB-infected (Supplemental Tables S7 and S8). The infected middle leaf segments of B75 accumulated much larger amounts of non-*O*-methyl and *O*-methylflavonoids than the noninfected upper and lower leaf segments (Figure 5A; Supplemental Table S9). Induced accumulation was already

significant 2 d post-inoculation, but was further increased at day 4. Similar results were obtained for the hybrid maize “Sweet Nugget” (Supplemental Figure S15; Supplemental Table S9).

The induction of flavonoids is a general pathogen response

To test whether the production of maize flavonoids is elicited by diverse fungal pathogens and thus represents a common defense response, we analyzed leaves (*Z. mays* “Sweet Nugget” hybrid) treated with six different maize fungal pathogens, including necrotrophs and hemibiotrophs, and the elicitor chitosan (CHT; Supplemental Table S10). Despite remarkable quantitative differences in flavonoid content for the different fungal treatments, which are in line with the manifestation of disease symptoms (Supplemental Figure S16), all of the fungi as well as CHT significantly induced the production of both *O*-methylated and non-*O*-methylated flavonoids (Figure 5B; Supplemental Table S10). Overall non-*O*-methyl and *O*-methylflavonoid content and composition were consistent with our previous data obtained for this maize line (Supplemental Figure S15; Supplemental Tables S7 and S8). These results demonstrate that the production of flavonoids, especially *O*-methylflavonoids is part of a general maize response to fungal pathogens.

The fungus-induced formation of O-methylflavonoids is accompanied by large-scale transcriptomic and metabolomic changes in the flavonoid and BX pathways

A broader investigation of transcriptomic and metabolomic data sets from SLB-infected and noninfected W22 leaves revealed many differences between the treatments beyond the *O*-methylation of flavonoids and their accumulation (Supplemental Figure S17). Apart from FOMT2/3, FOMT4, and FOMT5, a majority of known or predicted gene transcripts associated with flavonoid pathways increased significantly in response to the fungal elicitation (Figure 6A; Supplemental Table S2). Transcript abundance was associated with increased production of flavonoids belonging to different subclasses, mainly flavanones, flavones, and dihydroflavonols (Figure 6B; Supplemental Tables S7 and S8). In the BX pathway, transcript changes were more diverse. While genes encoding the core pathway (BX1-BX8) were downregulated after fungal infection, the terminal steps catalyzed by the OMTs BX10/11/14 were upregulated at both the transcript and metabolite levels (Supplemental Figure S18; Supplemental Tables S2 and S11). A RT-qPCR analysis of selected flavonoid and BX pathway genes confirmed the broad transcriptomic data, which was obtained from the RNA-seq experiment (Supplemental Figure S19).

Xilonenin and other maize flavonoids have antifungal activity

Xilonenin was the most abundant FOMT product detected in our experiments (Figure 1; Supplemental Table S8). To

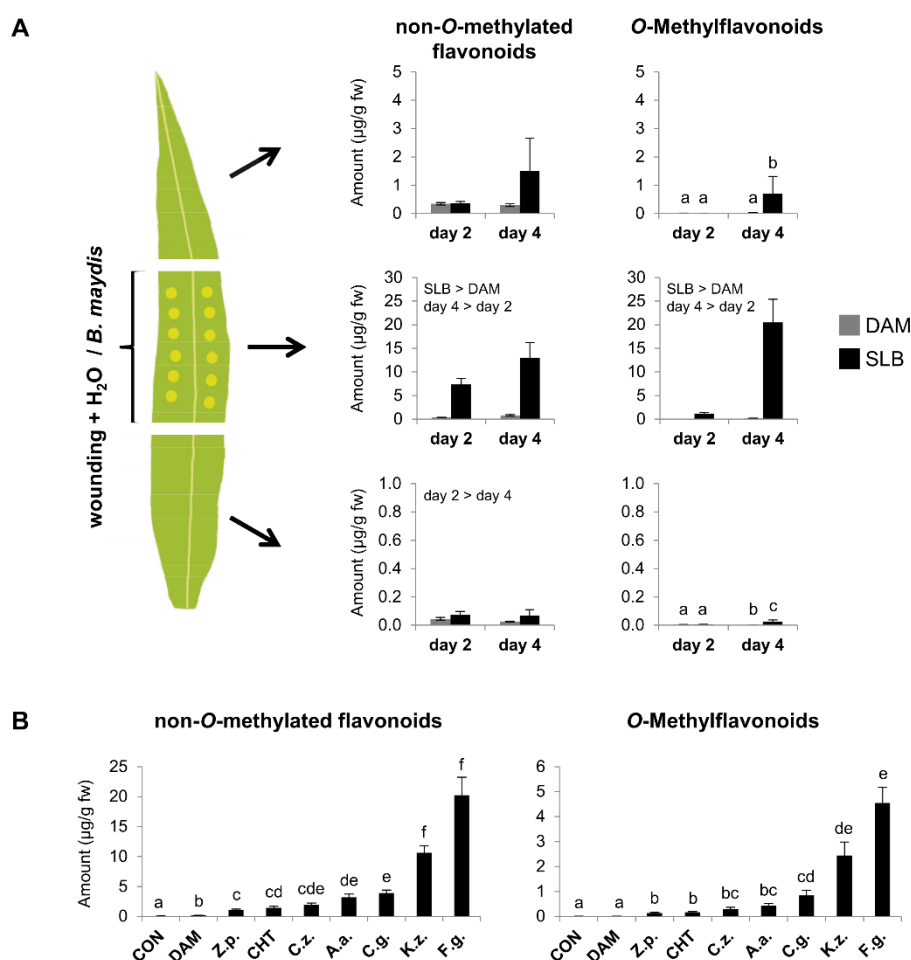


Figure 5 The accumulation of flavonoids is a general pathogen response in maize and occurs locally at the site of pathogen infection. A, Spatial distribution of non-O-methylated and O-methylated flavonoids in “upper,” “middle,” and “lower” (top down) segments of leaves of the inbred line B75. The middle leaf segment was mechanically damaged and either treated with water as control (DAM) or a mycelial suspension of *B. maydis* (SLB) for 2 or 4 d. Compounds were quantified in the three leaf parts using LC–MS/MS. Shown are the total amounts of all analyzed non-O-methylated and O-methylated flavonoids (left and right parts, respectively; Means \pm SE; $n = 6$). Significant differences for the factors treatment or day are stated. Different letters indicate significant differences between treatments and days (for statistical values, see [Supplemental Table S9](#)). Results for individual analyses are given in [Supplemental Tables S7 and S8](#). B, Concentrations of non-O-methylated flavonoids (left) and O-methylflavonoids (right) in leaves of hybrid maize (“Sweet Nugget”) 4 d after wounding and treatment with different fungal pathogens and CHT. Controls included undamaged (CON) as well as damaged and water-treated (DAM) leaves. Shown are the total amounts of all analyzed non-O-methylated and O-methylated flavonoids (means \pm SE; $n = 8$). Different letters indicate significant differences ($P < 0.05$) between treatments (one-way ANOVA followed by Tukey’s honestly significant difference (HSD) *post hoc* test; non-O-methylated flavonoids ($F = 198.700$, $P < 0.001$); O-methylflavonoids ($F = 113.500$, $P < 0.001$)). Results for individual analyses are given in [Supplemental Table S10](#). CHT, chitosan; Z.p., *Z. pseudotritici*; C.z., *C. zeae-maydis*; A.a., *A. alternata*; C.g., *C. graminicola*; K.z., *K. zea*; F.g., *F. graminearum*.

examine its impact on the growth of specific maize fungal pathogens, we conducted in vitro bioassays using *F. graminearum*, *F. verticillioides*, *Rhizopus microsporus*, and *B. maydis*, responsible for disease in diverse tissues. After 48 h, xilonenin significantly reduced the growth of *F. graminearum* in a dose-dependent manner (Figure 7). A similar but less pronounced growth inhibition activity was observed against *F. verticillioides* at a concentration of 100 µg/mL. In contrast, xilonenin showed no antifungal activity against *R. microsporus* or *B. maydis* but rather trended toward growth promotion; however, this effect was not statistically significant at 48 h (Figure 7).

Genkwanin, another O-methylflavonoid highly abundant in fungus-infected maize, negatively affected the growth of *F. verticillioides* but not *F. graminearum* (Figure 7). However, this compound showed strong dose-dependent activity against *R. microsporus*, while growth of *B. maydis* was slightly, but not significantly, reduced (Figure 7).

Interestingly, the non-O-methylated flavonoid naringenin also reduced the growth of all tested fungi, while its 5-O-methyl derivative showed no statistical effects at 48 h (Supplemental Figure S20). Apigenin slightly inhibited the growth of *R. microsporus*, and 5-O-methylapigenin reduced the growth of both *F. verticillioides* and *R. microsporus* (Supplemental Figure S21). In contrast, apigenin and 5-O-methylapigenin did not result in statistically significant differences in the growth *F. graminearum* and *B. maydis* (Supplemental Figure S21).

Discussion

Previous research has implicated O-methylflavonoids in grass species as anti-pathogen defenses (Kodama et al., 1992; Christensen et al., 1998; Zhou et al., 2006a; Hasegawa et al., 2014). In maize, infection studies with *Colletotrichum graminicola* first hinted that O-methylflavonoid pathways might play a role in maize–pathogen interactions (Balmer et al., 2013). However, the enzymes underlying the relevant biosynthetic pathways have remained unknown. In this effort, we undertook a comprehensive analysis of fungal-elicited maize O-methylflavonoids and pathway enzymes, resulting in the characterization of a CYP F2H and multiple OMTs with distinct product regiospecificity that produce the major inducible products. Moreover, we showed significant in vitro antifungal activity for the most abundant product, the O-dimethyl-2-hydroxynaringenin tautomer xilonenin, and for additional abundant O-methylated and non-O-methylated flavonoids.

Association studies and enzyme analyses demonstrate that FOMT2 and FOMT4 are responsible for the formation of maize O-methylflavonoids

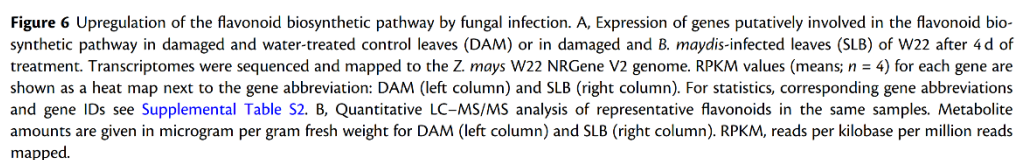
FOMTs have been characterized from dicot and a few monocot species (Kim et al., 2010); however, only two FOMTs active on the flavonoid A-ring have been reported in grasses (Christensen et al., 1998; Shimizu et al., 2012).

Here, we identified and characterized four maize OMT genes, namely FOMT2, FOMT3, FOMT4, and FOMT5 that were able to convert different flavonoids regiospecifically to their respective 5-, 7-, and 6-O-methyl derivatives (Figures 2 and 3; Supplemental Table S5). Several lines of evidence suggest that two of these OMTs, FOMT2 and FOMT4, are responsible for the formation of the bulk of the O-methylflavonoids detected in planta. First, metabolite-based association mapping efforts identified FOMT2 and FOMT4 as key biosynthetic candidates (Figure 2, A and B; Supplemental Figures S2 and S3). Second, transcripts of FOMT2 and FOMT4 and their corresponding enzymatic products (5- and 7-O-methylflavonoids, respectively) accumulated significantly after fungal elicitation, while FOMT3 encoding another 5-OMT displayed low levels of expression (Figures 1, 2C, and 6; Supplemental Table S2). Third, biochemical characterization not only confirmed the regiospecific activity of the FOMTs, but further demonstrated that FOMT2 and FOMT4 prefer flavanones and flavones, respectively, as substrates, mirroring the qualitative and quantitative abundance of the corresponding 5- and 7-O-methylflavonoids in planta (Figures 2E and 3; Supplemental Figure S8; Supplemental Table S8).

To understand defense pathway specificity, we also examined the BX pathway OMTs BX10, BX11, BX12, and BX14 that are closely related to FOMT2/3 (Figure 2D). All four BX OMTs displayed only trace activities for specific subsets of the tested flavonoid substrates, with 5- and/or 7-O-methyl derivatives produced in unspecific amounts (Supplemental Table S5). However, BX10, BX11, and BX12 each catalyzed the 5,7-O-dimethylation of apigenin (Supplemental Table S5), at a rate up to 60% of that of the FOMT2 and FOMT4 combination, demonstrating that BX OMTs could contribute to the biosynthesis of specific O-methylflavonoids in a limited way.

F2H2 and FOMT2 are the key enzymes in the biosynthesis of xilonenin tautomers

Previously, F2H1 (CYP93G5) was demonstrated to catalyze the conversion of flavanones (naringenin and eriodictyol) to their corresponding 2-hydroxy derivatives, which are intermediates in the production of maize C-glycosyl flavone anti-herbivore defenses such as maysin (Morohashi et al., 2012; Falcone-Ferreira et al., 2013; Casas et al., 2016). Our results demonstrate that the homologous enzyme F2H2 (CYP93G15) together with FOMT2 is involved in fungus-elicited production of the tautomeric xilonenin (Figure 4). F2H2 catalyzes the same reaction as F2H1 in vitro, converting naringenin and eriodictyol to 2-hydroxynaringenin and 2-hydroxyeriodictyol, respectively (Figure 4D; Supplemental Figure S12); however, only F2H2 expression occurs upon fungal elicitation (Figure 4C; Supplemental Figure S19). Closely related to the F2Hs are the FNSIIs (Figure 4B), which are proposed to generate the flavone double bond via a reaction where initial hydrogen abstraction from C-2 is followed by hydroxylation at this position and finally dehydration between C-2 and C-3. F2H activity is similar but with the loss



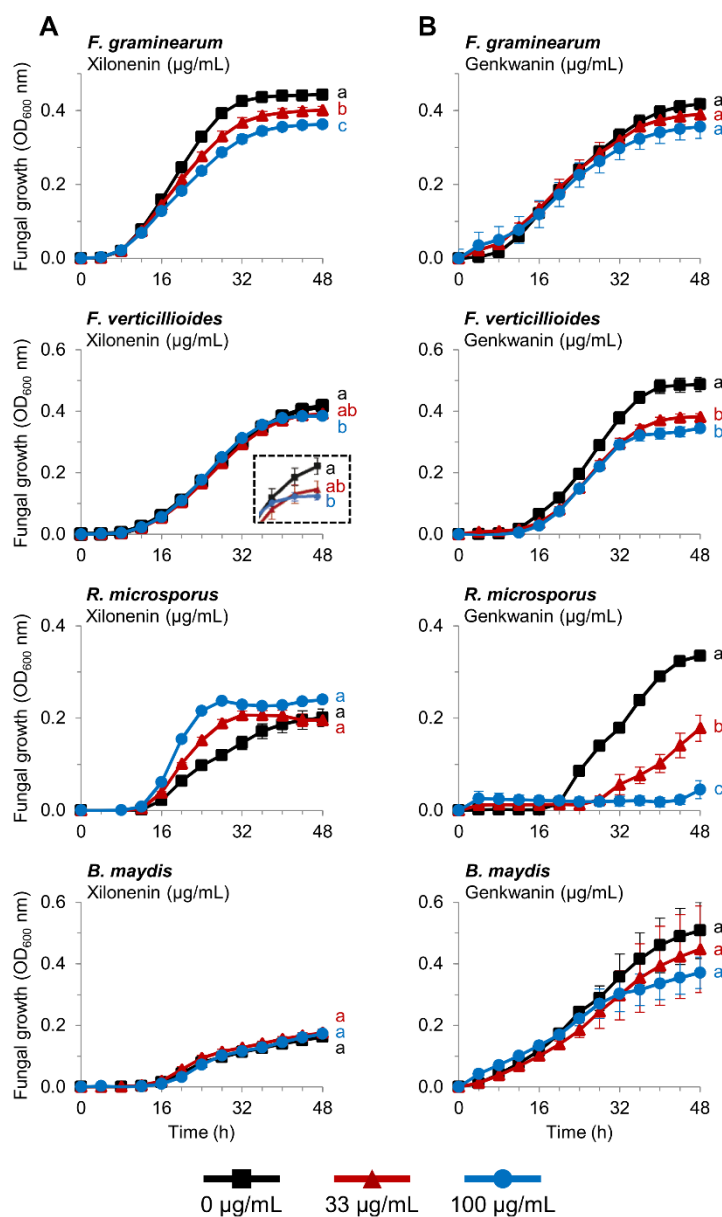


Figure 7 Antifungal activity of xilonenin and genkwanin. Growth (optical density (OD) at 600 nm) of *F. graminearum*, *F. verticillioides*, *R. microsporus*, and *B. maydis* in the absence and presence of purified xilonenin (A) and genkwanin (B) measured over a 48-h time course in a defined minimal broth medium using a microtiter plate assay. Data are shown as means \pm SE ($n = 4-5$). Different letters indicate significant differences ($P < 0.05$) between treatments at 48 h (one-way ANOVA followed by Tukey–Kramer's *post hoc* test). *Fusarium graminearum*: xilonenin ($F = 20.359$, $P < 0.001$); genkwanin ($F = 1.669$, $P = 0.242$); *F. verticillioides*: xilonenin ($F = 4.710$, $P = 0.031$); genkwanin ($F = 19.373$, $P < 0.001$); *R. microsporus*: xilonenin ($F = 3.386$, $P = 0.068$); genkwanin ($F = 47.766$, $P < 0.001$); *B. maydis*: xilonenin ($F = 0.485$, $P = 0.627$); genkwanin ($F = 0.460$, $P = 0.645$).

of the dehydratase activity (Akashi et al., 1998; Sawada et al., 2002). The close similarity between these two enzyme groups was seen in our work with FNSII2, a close relative to the recently characterized FNSII1 (CYP93G7; Righini et al., 2019). FNSII2 produced apigenin and low yet detectable levels of 2-hydroxynaringenin (Supplemental Figure S12), supporting 2-hydroxyflavanones as intermediates in the FNSII reaction mechanism. However, whether 2-hydroxyflavanones are accepted as substrates by FNSII1/2 remains to be elucidated.

Association mapping analyses using the B73 × Ky21 RIL population and the Goodman diversity panel linked FOMT2 with the occurrence of 2-hydroxynaringenin-derived xilonenin tautomers (Figure 4A; Supplemental Figures S2 and S10). Heterologous enzyme expression assays confirmed that recombinant FOMT2 utilizes 2-hydroxynaringenin as a substrate to catalyze the production of xilonenin in vitro (Figure 4, D and E). Furthermore, the extensive list of substrates used for comprehensive biochemical characterization demonstrates that 2-hydroxynaringenin is the preferred substrate of FOMT2 (Figure 3). Our results parallel the identification of xilonenin as most abundant FOMT2 product in both W22 and B75 inbred lines (Supplemental Table S8). Besides xilonenin tautomers, we detected two other products of FOMT2 in the enzyme assays and in the plant that are likely keto-enol tautomers of O-methyl-2-hydroxynaringenin (Figure 4D; Supplemental Figure S9). However, the rather low abundance of the precursor 2-hydroxynaringenin and its mono-O-methyl derivatives compared to xilonenin tautomers indicate a rapid and efficient turnover by FOMT2 in planta (Figure 1; Supplemental Tables S7 and S8). The presence of the first methoxyl group in O-methyl-2-hydroxynaringenin does not seem to influence the occurrence of the second O-methylation reaction considerably. This is in contrast to other mono-O-methylflavonoids such as sakuranetin, genkwanin, acacetin, or hispidulin that are only marginally accepted by FOMT2 as substrates for a second O-methylation (Figure 3).

Although xilonenin has apparently not been previously described, chalcone-like O-methylflavonoids are known and proposed as intermediates in the biosynthesis of echinatin, a retrochalcone with antibacterial activity from licorice (*Glycyrrhiza* spp.; Ayabe et al., 1980; Haraguchi et al., 1998).

Maize O-methylflavonoids are induced by fungal infection and contribute to plant defense

Flavonoids, including O-methylflavonoids have been previously shown to increase pathogen resistance in several plant species (Kodama et al., 1992; Skadhauge et al., 1997; Hasegawa et al., 2014). The complex flavonoid blends we measured in maize upon fungal attack (Figure 1; Supplemental Tables S7 and S8) accumulated largely at the sites of pathogen infection (Figure 5A; Supplemental Figure S15), consistent with the response of other phytoalexins (Nicholson and Hammerschmidt, 1992; Hammerschmidt, 1999). Moreover, several of the O-methylflavonoids detected

in fungus-elicited maize, such as genkwanin or 7-O-methylscutellarein (Figure 1; Supplemental Table S8), have previously been shown to possess antimicrobial activity (Martini et al., 2004; Balmer et al., 2013; Zhanzhaxina et al., 2020), suggesting that the maize flavonoid blend contributes to plant defense against pathogens. Interestingly, xilonenin, the most prominent FOMT product in the investigated maize lines (Figure 1; Supplemental Table S8), and other abundant O-methylated and non-O-methylated flavonoids exhibited contrasting effects on the growth of different maize pathogenic fungi in our experiments. While xilonenin had significant antifungal activity against two *Fusarium* species but did not inhibit the growth of *B. maydis* and *R. microsporus*, genkwanin affected the growth of *R. microsporus* and *F. verticillioides* but not *F. graminearum* and *B. maydis* (Figure 7). This suggests that the complex flavonoid blend comprising more than 35 different compounds may provide a defense barrier against a multitude of diverse maize pathogens. Moreover, additive and synergistic effects might mediate or even enhance the activity of single blend components. However, the mixed antifungal properties observed in our bioassays may also indicate that the maize pathogen defense response relies on several biochemical layers. For example, flavonoids may not be the predominant antifungal compounds, but may induce signaling pathways that trigger the formation of other antifungal defenses by, for example, acting as scavengers for reactive oxygen species (Zhang et al., 2015). On the other hand, some maize pathogens may have adapted to the toxic arsenal of their host plant by detoxifying their phytoalexins as is the case for other plant pathogens (Pedras and Ahiachonu, 2005), and this might explain the mixed antifungal effects seen in our bioassays. Recently, two rice pathogenic fungi have been reported to detoxify and tolerate 7-methoxynaringenin (sakuranetin) by hydroxylation, O-demethylation or glycosylation (Katsumata et al., 2017, 2018). Maize may still respond to fungal attack with the accumulation of flavonoid phytoalexins even if these are not effective since we demonstrated that flavonoid induction occurs in response to a broad range of necrotrophic and hemibiotrophic pathogens (Figure 5B).

Maize has been previously reported to biosynthesize complex mixtures of other pathogen-induced defense compounds including BXs, sesquiterpenoids, and diterpenoids (Oikawa et al., 2004; Rostas, 2007; Ahmad et al., 2011; Huffaker et al., 2011; Mafu et al., 2018; Ding et al., 2019, 2020). These substances have been demonstrated to reduce fungal diseases in experiments with defined biosynthetic mutants of the BX, kauralexin, and zealexin pathways (Ahmad et al., 2011; Ding et al., 2019, 2020). Here we highlight the role of another class of fungal-induced metabolites, the O-methylflavonoids, in innate immune responses that likely contribute to pathogen resistance in maize. Further investigation is required to understand if these different groups of phytoalexins have separate or joint roles in maize defense.

Materials and methods

Plants and growth conditions

Seeds of maize (*Z. mays*) inbred line W22 (NSL 30053), B73 (PI 550473), B75 (PI 608774), and Nested association mapping (NAM; McMullen et al., 2009) parental line seeds were provided by the US Department of Agriculture, Agricultural Research Service (USDA-ARS). Maize seeds for the Goodman diversity panel (Flint-Garcia et al., 2005) and the NAM RILs B73 × Ky21 subpopulation (McMullen et al., 2009) were provided by G. Jander (Boyce Thompson Institute) and P. Balint-Kurti (USDA-ARS), respectively. Seeds of the maize hybrid “Sweet Nugget” were purchased from N.L. Chrestensen Samen- und Pflanzenzucht GmbH (Erfurt, Germany). Plants were potted in soil (mix of 70 L Tonsubstrat with 200 L Kultursubstrat TS 1, Klasmann-Deilmann, Geeste, Germany) and grown in a climate-controlled chamber (Snijders Labs, Tilburg, Netherlands) under a 16-h light/8-h dark photoperiod, 1 mmol m⁻²s⁻¹ photosynthetically active radiation, a temperature cycle of 24°C/20°C (day/night), and 70% relative humidity.

Fungi and growth conditions

Fungal cultures of *B. maydis* (Belgian Co-ordinated Collections of Micro-Organisms, Institute of Hygiene, Epidemiology and Mycology, strain no. 5881), *C. graminicola* (Leibniz-Institut, Deutsche Sammlung von Mikroorganismen und Zellkulturen GmbH (DSMZ), strain (DSM) no. 63127), *F. graminearum* (DSM 4528), and *Kabatella zeae* (DSM 62737) were grown on potato dextrose agar (Sigma-Aldrich, St Louis, MO, USA) for 7 d at 25°C or 28°C (*B. maydis*) in the dark prior to use and subcultured if necessary (see below) to induce sporulation. *Alternaria alternata* (DSM 62006) and *Cercospora zeae-maydis* (Westerdijk Fungal Biodiversity Institute, strain no. 117755) were grown on modified V8 agar (V8 replaced by tomato juice, pH 6.5) for 7 and 14 d, respectively, at 25°C in the dark. To obtain mycelial inoculum, sterile water was added to an agar plate; the mycelium gently scraped off, and homogenized using a tissue homogenizer (Potter-Elvehjem, Carl Roth, Karlsruhe, Germany). Sporulation of *C. graminicola* was induced by subculturing on oatmeal agar (Sigma-Aldrich) at 25°C in the dark for 5–7 d. *Kabatella zeae* sporulation was enhanced using liquid K. zeae medium (KZM; Reifschneider and Amy, 1979). Briefly, 50 mL KZM were inoculated with a colony plug and incubated at 25°C and 150 rpm for 4 d. Afterwards, 400 µL of the liquid culture were plated on corn meal agar (Sigma-Aldrich) and grown for another 4 d. To promote sporulation of *C. zeae-maydis*, the mycelium (~2 cm²) was cut in little pieces, suspended in 10 mL sterile water, mixed vigorously and pipetted on V8 agar (2 mL/plate). After 15 min, remaining liquid was decanted and the plate was incubated at room temperature and 12-h d light for 5 d. Spores of *C. zeae-maydis* could not be separated from the mycelial fragments and hence a mixed spore and mycelial inoculum was used for experiments. All other spores were harvested in sterile water, filtered through a 40-µm cell strainer and

quantified for use. *Zymoseptoria pseudotritici* (STIR04 2.2.1) was kindly provided by Eva Stukenbrock (Stukenbrock et al., 2011, 2012) and grown on yeast-malt agar (4 g/L yeast extract, 4 g/L malt extract, 4 g/L sucrose, 15 g/L agar) at 18°C in the dark for 7 d. Then, colonies were picked, used to inoculate liquid yeast-malt sucrose (4 g/L yeast extract, 4 g/L malt extract, 4 g/L sucrose), and incubated at 18°C and 150 rpm for 4–5 d. Spores were harvested by centrifugation and resuspended in sterile water for quantification.

Plant inoculations with live fungi and CHT

All experiments were performed on the third fully developed leaf of 14-d-old maize plants. To analyze the content and spatial distribution of flavonoids in different maize lines after *B. maydis* infection, the middle segments of leaves were wounded on both sides of the midrib using modified pliers (punch-inoculation method; Matsuyama and Rich, 1974), producing a crushed spot, but without punching out a hole. Usually, 12 crushed spots per middle segment of about 10-cm length were made. Afterwards, a mycelial suspension of *B. maydis* containing 0.02% (v/v) Tween-20 was applied with a sterile cotton swab to each wounded spot ($n = 6–8$). Control plants were wounded and treated with water containing 0.02% (v/v) Tween-20 ($n = 6–8$). Whole plants were wrapped in plastic oven bags (“Bratschlauch,” Toppits, Minden, Germany) left open at the top to allow moderate air circulation, but prevent direct contact between plants of different treatments, and incubated for two or 4 d. For the general pathogen response experiment, hybrid maize (var. “Sweet Nugget”) plants were treated as described above, except that *C. graminicola*, *K. zeae*, and *Z. pseudotritici* were used as spore suspensions (1×10^6 /mL), while all other fungi were applied as a mycelial suspension. In addition, control treatments included undamaged plants. CHT was used as an artificial elicitor. Therefore low viscous CHT (50–190 kDa; Sigma-Aldrich) was dissolved to 1% (w/v) in 1% (v/v) acetic acid in water and further diluted with sterile water to 0.1% (w/v). Control plants were treated with 0.1% (v/v) acetic acid in water, respectively. In all experiments, different leaf segments were collected separately by cutting the leaf on both sides of the wounded and inoculated area (1.5 cm distant from the outer spots), flash-freezing in liquid nitrogen (N₂), and storing at –80°C until further processing.

Maize stem treatments with heat-killed fungal elicitors

Treatment of NAM inbred line parents and plants of the Goodman association panel follow from previous efforts (Ding et al., 2017, 2019). Plants of the Goodman diversity panel (260 analyzed inbred lines) were grown in greenhouses while the NAM RIL B73 × Ky21 subpopulation (156 analyzed lines) was grown in the field (2016, UCSD). Using a scalpel, 35-d-old plants were slit in the center, spanning both sides of the stem, to create an 8-cm long parallel longitudinal incision spanning the upper nodes, internodes, and basal portion of unexpanded leaves. To activate antifungal defenses, 500 µL of the heat-killed fungal hyphae

(commercial *Fusarium venenatum*, strain PTA-2684, Monde Nissin Corporation, Santa Rosa, Philippines) was placed into each slit stem and sealed with clear plastic packing tape to minimize tissue desiccation. Three or 5 d after elicitation (for plants of the Goodman panel and B73 × Ky21 RILs, respectively), reacted stem tissues were harvested in liquid N₂, ground to fine power, weighed out in 50 mg aliquots and stored at −80°C for analyses.

Methanol extraction of plant material

Maize leaf tissue was ground to a fine powder under liquid N₂ using a Geno/Grinder tissue homogenizer (SPEX SamplePrep). The frozen powder (50–70 mg) was weighed in a 2 mL microcentrifuge tube, and five volumes of 100% methanol (LC–MS grade, Merck) were added. The plant samples were immediately vortexed, and then further extracted using a ThermoMixer C (Eppendorf, Hamburg, Germany) for 5 min at 2,000 rpm and 20°C. Cell debris was sedimented by centrifugation at 16,000 g and 20°C for 25 min and the supernatant was transferred to a new 1.5-mL microcentrifuge tube. The sediment was extracted a second time with five volumes of 100% methanol and finally the combined supernatant was centrifuged again to remove all remaining particles. All samples were stored at −20°C before analysis.

LC–MS analysis of flavonoids and BXs

Untargeted LC–MS analysis with accurate mass determination

Chromatography was performed on a Dionex UltiMate 3000 RS pump system (Thermo Fisher Scientific, Waltham, MA, USA) equipped with a ZORBAX RRHD Eclipse XDB-C18 column (2.1 × 100 mm, 1.8 µm; Agilent Technologies, Santa Clara, CA, USA). Aqueous formic acid (0.1% (v/v)) and acetonitrile were used as mobile phases A and B, respectively, with a flow rate of 0.3 mL/min. The column temperature was maintained at 25°C. The following elution profile was used: 0–0.5 min, 5% B; 0.5–11 min, 5–60% B; 11.1–12 min, 100% B; 12.1–15 min, 5% B. The injection volume was 2 µL. The LC system was coupled to a timsTOF mass spectrometer (Bruker Daltonics, Billerica, MA, USA) equipped with an ESI ion source. Both positive and negative ionization were used for the analysis in full scan and auto MS/MS modes, scanning masses from *m/z* 50–1,500 (detailed parameters are provided in Supplemental Table S12). Sodium formate adducts were used for internal calibration. The software programs Bruker otof control version 5.1.107 and HyStar 4.1.31.1 (Bruker Daltonics) were used for data acquisition, and DataAnalysis version 5.1.201 (Bruker Daltonics) and MetaboScape version 4.0 (Bruker Daltonics) were used for data processing.

Targeted LC–MS/MS analysis for quantification of compounds in plant extracts and analysis of enzyme assays

Chromatographic separation was achieved on an Agilent 1260 Infinity II LC system (Agilent Technologies) equipped

with a ZORBAX Eclipse XDB-C18 column (50 × 4.6 mm, 1.8 µm; Agilent Technologies), using aqueous formic acid (0.05% (v/v)) and acetonitrile as mobile phases A and B, respectively. The flow rate was 1.1 mL/min and the column temperature was maintained at 20°C. The injection volume was 2 µL for maize leaf extracts and 1–4 µL for enzyme assays. The following gradient was used for the separation of flavonoids and flavonoid glycosides: 0–0.5 min, 10% B; 0.5–8.0 min, 10–55% B; 8.5–9.0 min, 100% B; 9.02–11 min, 10% B. The LC system was coupled to a QTRAP 6500+ tandem mass spectrometer (Sciex, Framingham, MA, USA) equipped with a turbospray ESI ion source, operated in positive or negative ionization mode, for the analysis of flavonoids or flavonoid glycosides, respectively (detailed parameters are provided in Supplemental Table S13). For the analysis of BXs, the chromatography was performed as described above, except that the following elution profile was used: 0–0.5 min, 5% B; 0.5–6.0 min, 5–32.5% B; 6.02–7.0 min, 100% B; 7.10–9.5 min, 5% B. The mass spectrometer was operated in negative ionization mode (detailed settings are provided in Supplemental Table S13). Multiple reaction monitoring was used to monitor analyte precursor ion → product ion transitions of flavonoids, flavonoid glycosides and BXs (Supplemental Tables S4, S15, and S16, respectively). Flavonoids were quantified using external calibration curves (0.5, 1, 2, 5, 10, 25, 50, 100, 200, 400, 1,000, 2,000, and 4,000 ng/mL) composed of commercially available standards as well as self-purified and NMR-quantified O-methylflavonoids (for all standards used, see Supplemental Table S17). Analyst version 1.6.3 software (Sciex) was used for data acquisition and processing. In addition, MultiQuant version 3.0.3 software (Sciex) was used for quantitative analysis.

Untargeted LC–UV–MS analysis for purification

The O-methylflavonoid content of *E. coli* culture extracts was analyzed using an Agilent 1100 Series LC system (Agilent Technologies) coupled to an ultraviolet diode array detector (UV-DAD, Agilent Technologies) and an Esquire 6000 ESI-Ion trap mass spectrometer (Bruker Daltonics). Chromatographic separation was performed on an EC 250/4.6 Nucleodur Sphinx column (RP 5 µm, Macherey-Nagel, Düren, Germany), with 0.2% (v/v) formic acid in water (A) and acetonitrile (B) as mobile phases. The flow rate was 1 mL/min and the column temperature was set to 25°C. The following elution profile was used: 0–15 min, 30–60% B; 15.1–16 min, 100% B; 16.1–20 min, 30% B. The mass spectrometer was run in alternating ion polarity (positive/negative) mode with a skimmer voltage of +40 V/−40 V, a capillary voltage of −3,500 V/+3,000 V and a capillary exit voltage of 113.5 V/−113.5 V, to scan masses from *m/z* 50–3,000. N₂ was used as drying gas (11 L/min, 330°C) and nebulizer gas (35 psi). The software programs esquireControl version 6.1 (Bruker Daltonics) and HyStar version 3.2 (Bruker Daltonics) were used for data acquisition, while DataAnalysis version 3.4 was used for data processing. The UV absorption

of individual O-methylflavonoids was analyzed using the post-processing software included in the HyStar version 3.2 package (Bruker Daltonics).

Semi-preparative high performance liquid chromatography with ultraviolet detector (HPLC-UV) for purification

For the purification of O-methylflavonoids, an Agilent 1100 series LC system (Agilent Technologies) coupled to an UV/VIS-detector and connected to an SF-2120 Super Fraction Collector (Advantec MSF, Inc., Dublin, CA, USA), was used. Chromatography was performed as described above in the section “Untargeted LC–MS analysis coupled with UV for purification,” except that 0.05% (v/v) formic acid in water was used as mobile phase A. Depending on the O-methylflavonoid to be purified, UV absorption was monitored at a single wavelength between 280 and 335 nm and used to determine the respective peak(s) for collection. HP ChemStation for LC (Rev. A.06.03, Hewlett Packard) was used for data acquisition.

Analyses of fungus-elicited flavonoids in stems

Analysis of fungus-elicited tissue from the NAM RIL B73 × Ky21 subpopulation and Goodman diversity panel employed LC/MS parameters and settings previously described (Ding et al., 2017). Stem tissue samples were sequentially bead homogenized in a series of solvents resulting in final volume of 450 µL and mixture of 1-propanol:acetonitrile:ethyl acetate:water (11:39:28:22). Approximately 150 µL of the particulate-free supernatant was used for LC/MS analyses using 5-µL injections. The LC consisted of an Agilent 1260 Infinitely Series HP Degasser (G4225A), 1260 binary pump (G1312B), and 1260 autosampler (G1329B). The binary gradient mobile phase consisted of 0.1% (v/v) formic acid in water (solvent A) and 0.1% (v/v) formic acid in methanol (solvent B). Chromatographic separation was performed on a Zorbax Eclipse Plus C18 Rapid Resolution HD column (Agilent; 1.8 µm, 50 × 2.1 mm) using a 0.35 mL/min flow rate. The mobile phase gradient was: 0–2 min, 5% B constant ratio; 3 min, 24% B; 18 min, 98% B; 25 min, 98% B; and 26 min, 5% B for column re-equilibration before the next injection. Electrospray ionization was accomplished with an Agilent Jet Stream Source with the following parameters: nozzle voltage (500 V), N₂ nebulizing gas (flow, 12 L/min, 379 kPa, 225°C) and sheath gas (350°C, 12 L/min). The transfer inlet capillary was 3,500 V and both MS1 and MS2 heaters were at 100°C. Negative ionization [M-H][−] mode scans (0.1-atomic mass unit steps, 2.25 cycles/s) from *m/z* 100–1,000 were acquired. The compounds identified in order of relative retention times and [M-H][−] parent ions are: xilonenin keto tautomer (9.00 min, *m/z* 315), apigenin-5-methyl ether (10.37 min, *m/z* 283), xilonenin enol tautomer (10.71 min, *m/z* 315), apigenin (11.78 min, *m/z* 269), and genkwanin (13.77 min, *m/z* 283).

Genetic mapping of O-methylflavonoid biosynthetic genes

A list of Goodman diversity panel inbred lines and NAM B73 × Ky21 subpopulation RILs used for mapping in this study is given in Supplemental Table S18. Flavonoid levels were used as traits for the association analyses. Genotypic data for the NAM B73 × Ky21 RIL subpopulation (NAM imputed ALLZea GBS Build July 2012 FINAL, AGPv2) and Goodman Diversity panel (Maize HapMapV3.2.1 genotypes with imputation, AGPv3) were downloaded (www.panzea.org). SNPs with <20% missing genotype data and minor allele frequencies >5% were employed in the association analysis resulting in the final use of 80,440 SNPs and 25,457,708 SNPs for the RIL and diversity panel, respectively. Analyses were initially conducted in TASSEL version 5.0 using the GLM for the NAM RIL B73 × Ky21 subpopulation and the unified mixed linear model (MLM) for the Goodman association panel (Yu et al., 2006; Bradbury et al., 2007; Zhang et al., 2010). This was done to minimize false positives arising from differential population structures and familial relatedness (Yu et al., 2006). Differential population structure and familial relatedness are less common features in biparental RIL populations and enable GLM analyses for the B73 × Ky21 RILs (Ding et al., 2017, 2020). To improve GWAS analysis, the kinship matrix (K) was used jointly with population structure (Q). Final analyses were conducted with the R package GAPIT (Lipka et al., 2012). Manhattan plots were constructed in the R package qqman (version 0.1.4) (<http://cran.rproject.org/web/packages/qqman/>; Turner, 2014).

RNA and cDNA preparation

Total RNA was extracted from approximately 50-mg frozen plant powder using the InviTrap Spin Plant RNA Kit (Stratagene) according to the manufacturer's instructions. The RNA concentration and purity was assessed with a spectrophotometer (NanoDrop 2000c; Thermo Fisher Scientific). RNA (1 µg) was treated with DNaseI (Thermo Fisher Scientific), followed by cDNA synthesis using SuperScript III reverse transcriptase and oligo (dT)₂₀ primers (Invitrogen) according to the manufacturer's instructions.

RNA-seq

To investigate gene expression changes after fungal infection in W22, total RNA was extracted from leaf tissue (*n* = 4) as described above and sent to Novogene (Cambridge, UK) for RNA-seq library construction (polyA enrichment) and sequencing (NovaSeq PE150, paired reads, 6 G of raw data per sample). Trimming of the obtained sequencing reads and mapping to the maize W22 NRGene_V2 genome were performed with the program CLC Genomics Workbench (Qiagen Bioinformatics, Hilden, Germany; mapping parameter: length fraction, 0.8; similarity fraction, 0.9; max number of hits, 25). Empirical analysis of digital gene expression implemented in the program CLC Genomics Workbench was used for gene expression analysis.

Raw reads were deposited in the NCBI Sequence Read Archive (SRA) under the BioProject accession PRJNA742147.

RT-qPCR analysis

To verify gene expression data of flavonoid and BX pathway genes from RNA-Seq, RT-qPCR was performed. For the amplification of gene fragments with a length of 100–250 bp, specific primers were designed having a $T_m \geq 60^\circ\text{C}$, a GC content between 40% and 60%, and a primer length of 20–23 nucleotides (Supplemental Table S19). The primer specificity was confirmed by agarose gel electrophoresis, melting curve analysis, and by sequence verification of cloned PCR amplicons. Primer pair efficiency (90%–112%) was determined using standard curve analysis with two-fold serial dilutions of cDNA. UBCP and MEP (Manoli et al., 2012) were used as reference genes. The measurements were performed using 1 μL 1:10 diluted cDNA in 20- μL reaction mixture containing Brilliant III Ultra-Fast SYBR[®] Green QPCR Master Mix (Agilent Technologies). All samples were run on a CFX Connect Real-Time PCR Detection System (Bio-Rad Laboratories, Hercules, CA, USA) in an optical 96-well plate. Four biological replicates per treatment were analyzed as triplicates. The following PCR conditions were applied for all reactions: Initial incubation at 95°C for 3 min followed by 40 cycles of amplification (95°C for 10 s, 60°C for 10 s). For all measurements, reads were taken during the extension step of each cycle and melting curve data were recorded at the end of cycling at 55 – 95°C . Cq values for the calculation of relative quantities were determined using CFX Manager version 3.1 software (Bio-Rad Laboratories).

Cloning and heterologous expression of OMT genes in *E. coli*

The complete open reading frames of FOMT2 (W22) and FOMT4 (W22) were amplified from cDNA obtained from *B. maydis*-infected W22 leaves with the primer pairs listed in Supplemental Table S20. FOMT3 and FOMT5 were amplified from plasmids containing the synthesized codon-optimized open reading frames (see paragraph below). The PCR products were cloned into the expression vector pET100/D-TOPO (Invitrogen, Waltham, MA, USA) or pASK-IBA37plus (IBA Lifesciences, Göttingen, Germany) and fully sequenced. BX10 (B73), BX11 (B73), BX12 (CML322), and BX14 (B73) were provided as pASK-IBA37plus constructs by Vinzenz Handrick (Meihls et al., 2013; Handrick et al., 2016). For heterologous expression, the expression constructs were transferred in *E. coli* strain BL21 (DE3; Invitrogen). Liquid cultures were grown in lysogeny broth at 37°C and 220 rpm until an optical density at 600 nm (OD_{600}) of 0.8–1, induced with a final concentration of 1 mM IPTG or 200 $\mu\text{g/L}$ anhydrotetracycline, and subsequently incubated at 18°C and 220 rpm for 15 h. The cells were harvested by centrifugation at 5,000 g and 4°C for 10 min, resuspended in refrigerated extraction buffer (50 mM Tris-HCl pH 8, 500 mM NaCl, 20 mM imidazole, 10% (v/v) glycerol, 1% (v/v) Tween20, and 25 U/mL Benzonase Nuclease (Merck, Kenilworth, NJ, USA;

freshly added)) and disrupted by sonication (4×20 s, with cooling on ice in between; Bandelin UW 2070). Cell debris was removed by centrifugation (16,000 g at 4°C for 20 min) and the N-terminal His-tagged proteins were purified from the supernatant using HisPur Cobalt Spin Columns (Thermo Fisher Scientific) according to the manufacturer's instructions. Tris-HCl buffer (pH 8, without Tween-20; see above) containing either 20 mM or 250 mM imidazole was used for equilibration/washing and elution steps, respectively. The buffer of the eluted protein samples was exchanged for assay buffer (50 mM Tris-HCl pH 7, 10% (v/v) glycerol) by gel filtration using illustra NAP Columns (GE Healthcare, Chicago, IL, USA). Protein concentrations were determined by the Bradford method using Quick Start Bradford 1 \times Dye Reagent (Bio-Rad Laboratories) and prediluted BSA protein standards (Thermo Scientific).

Gene synthesis

The complete open reading frames of FOMT3 (B73_V3) and FOMT5 (B73_V3) were synthesized after codon optimization for heterologous expression in *E. coli* by Eurofins MWG Operon (for sequences, see Supplemental Figure S22). CYP93G candidate genes (W22_V2) were codon optimized for *S. cerevisiae* and synthesized using the GeneArt gene synthesis service (Thermo Fisher Scientific) (for sequences, see Supplemental Figure S23). The synthetic genes were subcloned into the vector pUC57 (FOMT3 and FOMT5) or pMAT (CYP93G candidates), and the final constructs were verified by sequencing.

Cloning and heterologous expression of CYP93G genes in yeast

The complete open reading frames of F2H1 (W22), F2H2 (W22), FNSII2 (W22), Zm00004b039147 (CYP93G6-W22), and Zm00004b033036 (CYP93F6-W22) were synthesized as codon-optimized sequence (see above) and cloned as sticky-end fragments into the pESC-Leu 2d vector (Ro et al., 2008). F2H1 (B73) was amplified from cDNA (for primers used, see Supplemental Table S19). For heterologous expression in yeast, the resulting constructs were transformed into the engineered *S. cerevisiae* strain WAT11 (Pompon et al., 1996) using the S.c. EasyComp Transformation Kit (Invitrogen) according to the manufacturer's instructions. Subsequently, 30- mL Sc-Leu minimal medium (6.7 g/L yeast N₂ base without amino acids, but with ammonium sulfate; 100 mg/L of each l-adenine, l-arginine, l-cysteine, l-lysine, l-threonine, l-tryptophan, and uracil; 50 mg/L of each l-aspartic acid, l-histidine, l-isoleucine, l-methionine, l-phenylalanine, l-proline, l-serine, l-tyrosine, and l-valine; 20 g/L d-glucose) was inoculated with single yeast colonies and grown overnight at 28°C and 180 rpm. For main cultures, 100 mL YPGA (Glc) full medium (10 g/L yeast extract, 20 g/L bactopectone, 74 mg/L adenine hemisulfate, 20 g/L d-glucose) was inoculated with one unit OD_{600} of the overnight cultures and incubated under the same conditions for 30–35 h. After centrifugation (5,000 g, 16°C , 5 min), the expression was induced by resuspension of the cells in 100 mL YPGA (Gal)

medium (see above, but including 20 g/L galactose instead of d-glucose) and grown for another 15–18 h at 25°C and 160 rpm. The cells were harvested by centrifugation (7,500 g, 10 min, 4°C), resuspended in 30 mL TEK buffer (50 mM Tris–HCl pH 7.5, 1 mM EDTA, 100 mM KCl) and centrifuged again. Then, the cells were carefully resuspended in 2 mL TES buffer (50 mM Tris–HCl pH 7.5, 1 mM EDTA, 600 mM sorbitol; freshly added: 10 g/L bovine serum fraction V protein and 1.5 mM β -mercaptoethanol) and glass beads (0.45–0.50 mm diameter; Sigma-Aldrich) were added until they reached the upper level of the cell suspension. For cell disruption, the suspensions were shaken by hand 5 times for 1 min, with cooling on ice for 1 min in between. The crude extracts were recovered by washing the glass beads 4 times with 5 mL TES. The combined washes were centrifuged (7,500 g, 10 min, 4°C), and the supernatant containing the microsomes was transferred into an ultracentrifuge tube. After ultracentrifugation (100,000 g, 90 min, 4°C), the supernatant was carefully removed and the microsomal pellet was gently washed with 2.5 mL TES buffer, then with 2.5 mL TEG buffer (50 mM Tris–HCl pH 7.5, 1 mM EDTA, 30% glycerol). The microsomal fractions were homogenized in 2 mL TEG buffer using a glass homogenizer (Potter-Elvehjem, Carl Roth). Aliquots were stored at –20°C until further use.

In vitro enzyme assays

To test OMT activities, assays were set up containing 500 μ M dithiothreitol (DTT) and 100 μ M of the cosubstrate SAM. Substrates (flavonoids, caffeic acid, resveratrol, and DIMBOA-Glc) were added at 20 μ M from 400 μ M stock solutions made with 75% (v/v) dimethylsulfoxide (DMSO) in water. The assay buffer contained 50 mM Tris–HCl, pH 7, 10% (v/v) glycerol, and 0.8 μ g purified recombinant protein (equivalent to ~200 nM) was added in a total volume of 100 μ L. Incubations were carried out for 1 h at 25°C and 300 rpm on a ThermoMixer C (Eppendorf). All assays were conducted in technical triplicates. For combined OMT assays, the first OMT was incubated with the substrate in half of the assay volume for 1 h and then the second OMT was added and incubated for another hour (final reaction volume: 100 μ L). To obtain comparable activity estimates of the individual OMTs with different substrates, the decrease in substrate content compared to the EV control (substrate turnover) was used to calculate relative percent activity values. The highest percent substrate turnover per enzyme was set to 100% and the values for all other substrates were calculated accordingly.

CYP assays were performed with 1 mM cosubstrate NADPH, 20 μ M substrate (naringenin or eriodictyol), assay buffer, and 60 μ L microsomal fractions in a total volume of 300 μ L and incubated for 2 h at 25°C and 300 rpm. All assays were repeated at least twice. For combined CYP and OMT activity assays, CYPs were pre-incubated with the substrate (30 μ M) and NADPH (1 mM) in a 200 μ L reaction volume for 1 h, before addition of recombinant OMT protein, DTT, and SAM (final reaction volume: 300 μ L). All reactions were stopped by adding one volume of 100% methanol and

centrifuged at 4,000 g for 5–10 min to remove denatured proteins. Product formation was monitored by the analytical methods described above.

Purification of O-methylflavonoids from *E. coli* cultures

E. coli BL21 (DE3) harboring a *FOMT2* or *FOMT4* expression construct (described above in “Cloning and heterologous expression of OMT genes in *E. coli*”) were grown in terrific broth at 37°C and 220 rpm, induced at an OD₆₀₀ of 0.5 with a final concentration of 1 mM IPTG or 200 μ g/L anhydrotetracycline, and incubated for another 2–3 h at 37°C and 220 rpm. Subsequently, flavonoid substrate (naringenin, apigenin, and scutellarein; solved in 75% (v/v) DMSO in water) was added to yield a final concentration of 25 μ g/mL and the culture was incubated at 25°C and 220 rpm for 15 h. The culture was centrifuged at 5,000 g and 4°C for 20 min and the supernatant and the cell pellet were stored separately until further processing at 4°C and –20°C, respectively. For the production of 5,7-O-dimethylflavonoids, a *FOMT4* overexpressing culture was supplemented with the *FOMT2* culture supernatant in a ratio of 1:5 (e.g. 25 mL *FOMT2* culture supernatant/100 mL *FOMT4* overexpressing culture) and treated as described above. The culture supernatant was pre-purified by solid phase extraction (SPE) using a Chromabond HR-X column (15 mL, 500 mg, 83 μ m, Macherey-Nagel). The column was washed with 40% (v/v) methanol in water and, after drying for 30–60 min under vacuum, hydrophobic components were eluted thrice with 50:50 (v/v) methanol:acetonitrile followed by two elution steps with 100% acetonitrile. The *E. coli* pellet was extracted with 100% methanol (2.5–4 mL per pellet resulting from 100 mL culture) for 2 times 5 min in an ultrasonic bath, with vortexing in between. Cell fragments were removed by centrifugation at 5,000 g and 4°C for 20 min. The O-methylflavonoid content of SPE fractions and pellet extract was analyzed using LC–UV–MS as described in the section “Untargeted LC–UV–MS analysis for purification” and fractions containing the desired compound were combined and dried using a Rotavapor R-114 rotary evaporation system (Büchi, Flawil, Switzerland). After redissolving in 100% methanol, partially occurring precipitate was removed using a Minisart SRP syringe filter (Sartorius) and water was added to yield a solution of 50:50 (v/v) methanol:water. The resulting *E. coli* extract was separated by HPLC–UV as described above in chapter “Semi-preparative HPLC–UV for purification.” Collected fractions were dried using a rotary evaporator and subsequently a desiccator, and subjected to NMR and LC–MS/MS analysis.

Synthesis of 2-hydroxynaringenin

For synthesis of 2-hydroxynaringenin, we used a previously published method (Hao et al., 2016) and subsequently verified the structure by NMR.

NMR spectroscopy for structure elucidation and quantitative analysis

^1H NMR, ^{13}C NMR, ^1H - ^1H COSY, ^1H - ^{13}C ROESY, ^1H - ^{13}C HSQC, and ^1H - ^{13}C HMBC spectra were measured at 300 K (except for 2-hydroxynaringenin, which was measured at 268 K) on either a Bruker Avance III HD 500 NMR spectrometer, equipped with a cryogenically cooled 5 mm TCI $^1\text{H}\{^{13}\text{C}\}$ probe or an Avance III HD 700 NMR spectrometer, equipped with cryogenically cooled 1.7 mm TCI $^1\text{H}\{^{13}\text{C}\}$ probe. Samples were measured in acetone- d_6 and MeOH- d_3 , respectively. Chemical shifts were referenced using the residual solvent signals at $\delta_{\text{H}} 2.05/\delta_{\text{C}} 29.92$ for acetone- d_6 and $\delta_{\text{H}} 3.31/\delta_{\text{C}} 49.15$ for MeOH- d_3 . Spectrometer control, data acquisition, and processing were accomplished using Bruker TopSpin version 3.6.1. Standard pulse programs as implemented in Bruker TopSpin were used. For quantitative NMR measurements the Bruker ERETIC-2 protocol was used. (-)-Catechin was used as an external standard.

Sequence analysis and phylogenetic tree reconstruction

Maize OMT genes similar to *FOMT2* (B73), anthranilic acid methyltransferase 1 (*AAMT1*; B73), and *CCoAOMT1* (B73) or maize CYP93G candidates similar to *F2H1* (B73) were identified by BLASTP analysis available on MaizeGDB (<https://www.maizegdb.org/>), with B73 RefGen_V4 and W22 NRGene_V2 as search datasets, respectively. Multiple sequence alignments of maize OMT genes and characterized *FOMT* genes from several other species were generated using the MUSCLE codon algorithm implemented in the software MEGA version 7 (Kumar et al., 2016). Based on these alignments, phylogenetic trees were reconstructed with MEGA7 using a maximum likelihood method. Codon positions included were first + second + third + noncoding. All positions with < 80% site coverage (maize OMT phylogeny; Figure 2D) or < 90% site coverage (*FOMT* phylogeny; Supplemental Figure S6) were eliminated. Ambiguous bases were allowed at any position. A bootstrap resampling analysis with 1,000 replicates was performed to evaluate the topology of the generated trees. A substitution model test was performed with MEGA7 to identify the best-fitting substitution model for each dataset (for substitution model used, see respective figure legends). Phylogenetic analysis of maize genes similar to *F2H1* and characterized *F2H* and *FNSII* genes from other species was performed as described above, using all positions with $\geq 80\%$ site coverage. All corresponding accession numbers and references are provided in Supplemental Tables S3 and S6. Amino acid sequence alignments were visualized with the software BioEdit.

In vitro bioassays with O-methyl and non-O-methylflavonoids

Maize antifungal assays using self-purified or commercially available flavonoids (xilonenin, genkwanin, 5-O-methylapigenin, 5-O-methylnaringenin, apigenin, and naringenin; see Supplemental Table S17) were performed using the Clinical and Laboratory Standards Institute M38-A2 guidelines

(Schmelz et al., 2011). Fungal cultures of *R. microsporus* (Northern Regional Research Laboratory [NRRL] stock no. 54029), *F. verticillioides* (NRRL stock no. 7415), *F. graminearum* (NRRL stock no. 31084), and *B. maydis* were grown on V8 agar for 12 d before the quantification and final use as 2.5×10^4 conidia/mL (Huffaker et al., 2011). Using a 96-well microtiter plate, each well contained 200 μL of broth medium, fungal inoculum, and 0.5 μL of either pure ethanol or ethanol containing dilutions of flavonoids. All assays were conducted in four to five technical replicates. The flavonoid concentrations used in the bioassays (33 and 100 $\mu\text{g/mL}$) were chosen based on their abundance in fungal-infected tissue with the knowledge that (1) phytoalexin accumulation is highly localized to necrotic tissues and (2) that leaves used for metabolite quantification contained only 10–20% necrotic tissue (Figure 1A; Supplemental Figure S16). The actual flavonoid concentrations at the site of fungal attack are likely to be significantly higher than those measured at the whole leaf level. A Synergy4 (BioTek Instruments) reader was used to monitor fungal growth at 30°C through periodic measurements of changes in OD₆₀₀.

Statistical analysis

Statistical analyses were performed using SigmaPlot version 11.0 for Windows (Systat Software). The statistical test applied is indicated in the respective figure and table legends. Whenever necessary, the data were log-transformed to meet statistical assumptions such as normality and homogeneity of variances. Statistical significance of metabolomic data obtained by untargeted LC-MS was tested using the *t* test implemented in MetaboScape version 4.0 software (Bruker Daltonics).

To investigate whether the amount of flavonoids and O-methylflavonoids changed due to infection with *B. maydis* 2 or 4 d after infection, two-way analyses of variance (ANOVAs) were applied. In case of significant differences, Tukey's honestly significant difference (HSD) tests were performed. To account for the variance heterogeneity of the residuals, data were either log-transformed prior to the ANOVA or generalized least squares models (glms from the nlme library; Pinheiro et al., 2020) were applied. The varIdent variance structure was used. Whether the different variance of fungal treatment, time, or the combination of both factors should be incorporated into the model, was determined by comparing models with different variance structures with a likelihood ratio test and choosing the model with the smallest akaike information criterion (AIC). The influence (*P*-values) of the explanatory variables was determined by sequential removal of explanatory variables starting from the full model, and comparison of the simpler with the more complex model with a likelihood ratio test (Zuur et al., 2009). Differences between factor levels were determined by factor level reduction (Crawley, 2013). Data were analyzed with R version 4.0.3 (R Core Team, 2020).

Accession numbers

Sequence data for FOMT2-W22 (MZ484743) and FOMT4-W22 (MZ484744) can be found in the NCBI GenBank (<https://www.ncbi.nlm.nih.gov/genbank/>) under the corresponding identifiers. Raw reads of the RNA-seq experiment were deposited in the NCBI SRA under the BioProject accession PRJNA742147.

Supplemental data

The following materials are available in the online version of this article.

Supplemental Figure S1. MS/MS spectra of putative 5- and 7-O-methylflavonoids.

Supplemental Figure S2. Association mapping using B73 × Ky21 RIL with the GLM and 80,440 SNPs.

Supplemental Figure S3. GWAS mapping reveals association between the occurrence of genkwanin and FOMT4.

Supplemental Figure S4. Schematic chromosomal array of FOMT2 and FOMT3 in B73 and W22.

Supplemental Figure S5. Amino acid sequence alignment of FOMT2/3.

Supplemental Figure S6. Phylogenetic tree of maize FOMT genes characterized in this study, closely related maize OMT genes, and characterized FOMT genes from other monocots and dicots.

Supplemental Figure S7. Expression of BX OMT genes in W22 upon fungal infection.

Supplemental Figure S8. Regiospecific O-methylation and elution patterns of FOMT2 and FOMT4 products.

Supplemental Figure S9. Fragmentation patterns of 2-hydroxynaringenin and its O-methyl derivatives.

Supplemental Figure S10. GWAS mapping reveals association between the occurrence of xilonenin tautomers and FOMT2/3.

Supplemental Figure S11. Amino acid sequence alignment of Poaceae F2Hs belonging to the CYP93G subfamily.

Supplemental Figure S12. Enzymatic activity of CYP93G family members similar to F2H1 (CYP93G5) with naringenin or eriodictyol.

Supplemental Figure S13. NMR chemical shift data of xilonenin tautomers (in MeOH-*d*₃).

Supplemental Figure S14. The two xilonenin tautomers exhibit different UV absorption.

Supplemental Figure S15. De novo production of flavonoids in different maize lines after fungal infection.

Supplemental Figure S16. Visible signs of infection on hybrid maize after inoculation with different pathogenic fungi.

Supplemental Figure S17. Large-scale transcriptomic and metabolomic changes upon SLB infection.

Supplemental Figure S18. Expression of the BX biosynthetic pathway during fungal infection.

Supplemental Figure S19. RT-qPCR validation of flavonoid and BX pathway gene expression results in noninfected and fungus-infected W22 leaves.

Supplemental Figure S20. Antifungal activity of naringenin and 5-O-methylnaringenin.

Supplemental Figure S21. Antifungal activity of apigenin and 5-O-methylapigenin.

Supplemental Figure S22. Codon-optimized gene sequences of FOMT3-B73 and FOMT5-B73 synthesized for expression in *E. coli*.

Supplemental Figure S23. Codon-optimized gene sequences of CYP93G candidates synthesized for expression in *S. cerevisiae*.

Supplemental Table S1. *P*-values of *t* test analysis to determine statistical significant differences of flavonoid content between treatments obtained by the LC–MS measurements shown in Supplemental Figure 1B.

Supplemental Table S2. Expression of maize genes putatively involved in the phenylpropanoid pathway, flavonoid pathway, BX pathway or terpenoid biosynthesis.

Supplemental Table S3. MaizeGDB/GenBank accessions and references corresponding to Figure 2D and Supplemental Figure S6.

Supplemental Table S4. NMR structure elucidation of 5-/7-O-methyl and 5,7-O-dimethylflavonoids.

Supplemental Table S5. Product formation of maize OMTs with different substrates.

Supplemental Table S6. GenBank accessions and references corresponding to Figure 4B.

Supplemental Table S7. Quantification of flavonoids in leaf tissue of different maize inbred lines after infection with *B. maydis*.

Supplemental Table S8. Quantification of O-methylflavonoids in leaf tissue of different maize inbred lines after infection with *B. maydis*.

Supplemental Table S9. Statistical values for the analysis of the amount of non-O-methylated- and O-methylated flavonoids in different maize lines according to treatment, duration of treatment (day), and the interaction between treatment and its duration corresponding to the experiments shown in Figure 5A and Supplemental Figure S15.

Supplemental Table S10. Quantification of flavonoids and O-methylflavonoids in leaf tissue of hybrid maize ("Sweet Nugget") after treatment with different pathogenic fungi and CHT.

Supplemental Table S11. Relative quantification of BXs in leaf tissue of different maize inbred lines after infection with *B. maydis*.

Supplemental Table S12. MS settings used for the analysis on the timsTOF mass spectrometer.

Supplemental Table S13. MS settings used for the analysis on the QTRAP 6500+.

Supplemental Table S14. Mass analyzer settings used for the analysis of flavonoids and additional phenylpropanoids on the QTRAP 6500+.

Supplemental Table S15. Mass analyzer settings used for the analysis of flavonoid glycosides on the QTRAP 6500+.

Supplemental Table S16. Mass analyzer settings used for the analysis of BXs on the QTRAP 6500+.

Supplemental Table S17. Authentic standards used for identification and quantification.

Supplemental Table S18. Maize mapping lines used for GWASs in the Goodman diversity panel and Quantitative Trait Loci mapping in NAM subpopulation B73 × Ky21.

Supplemental Table S19. RT-qPCR primers.

Supplemental Table S20. PCR primers for the amplification of full-length open reading frames of investigated FOMTs and CYP93Gs.

Supplemental Data Set S1. Complete RNA-seq data set derived from damaged and water-treated control leaves (DAM) and damaged and *B. maydis*-infected leaves (SLB) of W22 after 4 d of treatment ($n = 4$).

Supplemental Data Set S2. NMR spectra.

Acknowledgments

We thank Elke Goschala and all gardeners of the Max Planck Institute for Chemical Ecology (MPICE) for their help in growing the maize plants. We thank Michael Reichelt (MPICE) for support concerning the analytical analyses, Bettina Raguschke (MPICE) for assistance in DNA sequencing, Paul Himmighofen and Laura Klement (MPICE) for assistance in plant experiments, and David R. Nelson (The University of Tennessee) for assigning the CYP names. For providing *Z. pseudotritici*, we thank Eva H. Stukenbrock (Christian-Albrechts University Kiel and Max Planck Institute of Evolutionary Biology).

Funding

The research was funded by the Max-Planck Society, the Swiss National Science Foundation (grant no. 160786, JG), the US Department of Agriculture, National Institute of Food and Agriculture (grant no. 2018-67013-28125, AH and EAS), and the National Science Foundation, Plant–Biotic Interactions Program (grant no. 1758976, EAS).

Conflict of interest statement. The authors declare that they have no conflict of interest.

References

- Ahmad S, Veyrat N, Gordon-Weeks R, Zhang YH, Martin J, Smart L, Glauser G, Erb M, Flors V, Frey M, et al. (2011) Benzoxazinoid metabolites regulate innate immunity against aphids and fungi in maize. *Plant Physiol* **157**: 317–327.
- Akashi T, Aoki T, Ayabe S (1998) Identification of a cytochrome P450 cDNA encoding (2S)-flavanone 2-hydroxylase of licorice (*Glycyrrhiza echinata* L.; Fabaceae) which represents licodione synthase and flavone synthase II. *FEBS Lett* **431**: 287–290.
- Ayabe SI, Yoshikawa T, Kobayashi M, Furuya T (1980) Studies on plant cultures. 34. biosynthesis of a retrochalcone, echinating - involvement of *O*-methyltransferase to licodione. *Phytochemistry* **19**: 2331–2336.
- Balmer D, de Papajewski DV, Planchamp C, Glauser G, Mauch-Mani B (2013) Induced resistance in maize is based on organ-specific defence responses. *Plant J* **74**: 213–225.
- Berim A, Hyatt DC, Gang DR (2012) A set of regioselective *O*-methyltransferases gives rise to the complex pattern of methoxylated flavones in sweet basil. *Plant Physiol* **160**: 1052–1069.
- Bradbury PJ, Zhang Z, Kroon DE, Casstevens TM, Ramdoss Y, Buckler ES (2007) TASSEL: software for association mapping of complex traits in diverse samples. *Bioinformatics* **23**: 2633–2635.
- Browne LM, Conn KL, Ayer WA, Tewari JP (1991) The camalexins - new phytoalexins produced in the leaves of *Camelina Sativa* (Cruciferae). *Tetrahedron* **47**: 3909–3914.
- Casas MI, Falcone-Ferreira ML, Jiang N, Mejia-Guerra MK, Rodriguez E, Wilson T, Engelmeier J, Casati P, Grotewold E (2016) Identification and characterization of maize salmon silks genes involved in insecticidal maysin biosynthesis. *Plant Cell* **28**: 1297–1309.
- Christensen AB, Gregersen PL, Olsen CE, Collinge DB (1998) A flavonoid 7-*O*-methyltransferase is expressed in barley leaves in response to pathogen attack. *Plant Mol Biol* **36**: 219–227.
- Crawley MJ (2013) *The R Book*, John Wiley and Sons Ltd, Hoboken, NJ.
- de Souza LP, Garbowski K, Brotman Y, Tohge T, Fernie AR (2020) The acetate pathway supports flavonoid and lipid biosynthesis in *Arabidopsis*. *Plant Physiol* **182**: 857–869.
- Ding Y, Murphy KM, Poretsky E, Mafu S, Yang B, Char SN, Christensen SA, Saldivar E, Wu MX, Wang Q, et al. (2019) Multiple genes recruited from hormone pathways partition maize diterpenoid defences. *Nat Plants* **5**: 1043–1056.
- Ding YZ, Huffaker A, Kollner TG, Weckwerth P, Robert CAM, Spencer JL, Lipka AE, Schmelz EA (2017) Selenene volatiles are essential precursors for maize defense promoting fungal pathogen resistance. *Plant Physiol* **175**: 1455–1468.
- Ding YZ, Weckwerth PR, Poretsky E, Murphy KM, Sims J, Saldivar E, Christensen SA, Char SN, Yang B, Tong AD, et al. (2020) Genetic elucidation of interconnected antibiotic pathways mediating maize innate immunity. *Nat Plants* **6**: 1375–1388.
- Du YG, Chu H, Chu IK, Lo C (2010a) CYP93G2 is a flavanone 2-hydroxylase required for *C*-glycosylflavone biosynthesis in rice. *Plant Physiol* **154**: 324–333.
- Du YG, Chu H, Wang MF, Chu IK, Lo C (2010b) Identification of flavone phytoalexins and a pathogen-inducible flavone synthase II gene (SbFNSII) in sorghum. *J Exp Bot* **61**: 983–994.
- Falcone-Ferreira ML, Rodriguez E, Casas MI, Labadie G, Grotewold E, Casati P (2013) Identification of a bifunctional maize *C*- and *O*-glucosyltransferase. *J Biol Chem* **288**: 31678–31688.
- Flint-Garcia SA, Thillet AC, Yu J, Pressoir G, Romero SM, Mitchell SE, Doebley J, Kresovich S, Goodman MM, Buckler ES (2005) Maize association population: a high-resolution platform for quantitative trait locus dissection. *Plant J* **44**: 1054–1064.
- Gregersen PL, Christensen AB, Sommerknudsen J, Collinge DB (1994) A putative *O*-methyltransferase from barley is induced by fungal pathogens and UV-light. *Plant Mol Biol* **26**: 1797–1806.
- Grotewold E (2006) *The Science of Flavonoids*, Springer, Berlin/Heidelberg, Germany.
- Hain R, Reif HJ, Krause E, Langebartels R, Kindl H, Vornam B, Wiese W, Schmelzer E, Schreier PH, Stocker RH, et al. (1993) Disease resistance results from foreign phytoalexin expression in a novel plant. *Nature* **361**: 153–156.
- Hammerschmidt R (1999) Phytoalexins: what have we learned after 60 years? *Annu Rev Phytopathol* **37**: 285–306.
- Handrick V, Robert CAM, Ahern KR, Zhou SQ, Machado RAR, Maag D, Glauser G, Fernandez-Penny FE, Chandran JN, Rodgers-Melnik E, et al. (2016) Biosynthesis of 8-*O*-methylated benzoxazinoid defense compounds in maize. *Plant Cell* **28**: 1682–1700.
- Hao B, Caulfield JC, Hamilton ML, Pickett JA, Midega CAO, Khan ZR, Wang J, Hooper AM (2016) Biosynthesis of natural and novel *C*-glycosylflavones utilising recombinant *Oryza sativa* *C*-glycosyltransferase (OsCGT) and *Desmodium incanum* root proteins. *Phytochemistry* **125**: 73–87.
- Haraguchi H, Tanimoto K, Tamura Y, Mizutani K, Kinoshita T (1998) Mode of antibacterial action of retrochalcones from *Glycyrrhiza inflata*. *Phytochemistry* **48**: 125–129.
- Hasegawa M, Mitsuhara I, Seo S, Okada K, Yamane H, Iwai T, Ohashi Y (2014) Analysis on blast fungus-responsive characters of a flavonoid phytoalexin sakuranetin; accumulation in infected rice

- leaves, antifungal activity and detoxification by fungus. *Molecules* **19**: 11404–11418
- He XZ, Dixon RA (2000) Genetic manipulation of isoflavone 7-O-methyltransferase enhances biosynthesis of 4'-O-methylated isoflavonoid phytoalexins and disease resistance in alfalfa. *Plant Cell* **12**: 1689–1702
- Huffaker A, Kaplan F, Vaughan MM, Dafoe NJ, Ni XZ, Rocca JR, Albarn HT, Teal PEA, Schmelz EA (2011) Novel acidic sesquiterpenoids constitute a dominant class of pathogen-induced phytoalexins in maize. *Plant Physiol* **156**: 2082–2097
- Ibrahim RK, Bruneau A, Bantignies B (1998) Plant O-methyltransferases: molecular analysis, common signature and classification. *Plant Mol Biol* **36**: 1–10
- Jandret P, Hebrard C, Deville MA, Cordelier S, Dorey S, Aziz A, Crouzet J (2014) Deciphering the role of phytoalexins in plant-microorganism interactions and human health. *Molecules* **19**: 18033–18056
- Jiang N, Doseff AI, Grotewold E (2016) Flavones: from biosynthesis to health benefits. *Plants (Basel)* **5**: 27
- Katsumata S, Toshima H, Hasegawa M (2018) Xylosylated detoxification of the rice flavonoid phytoalexin sakuranetin by the rice sheath blight fungus *Rhizoctonia solani*. *Molecules* **23**: 276
- Katsumata S, Hamana K, Horie K, Toshima H, Hasegawa M (2017) Identification of sternbin and naringenin as detoxified metabolites from the rice flavanone phytoalexin sakuranetin by *Pyricularia oryzae*. *Chem Biodivers* **14**: e1600240
- Kim BG, Lee Y, Hur HG, Lim Y, Ahn JH (2006) Flavonoid 3'-O-methyltransferase from rice: cDNA cloning, characterization and functional expression. *Phytochemistry* **67**: 387–394
- Kim BG, Sung SH, Chong Y, Lim Y, Ahn JH (2010) Plant flavonoid O-methyltransferases: substrate specificity and application. *J Plant Biol* **53**: 321–329
- Kodama O, Miyakawa J, Akatsuka T, Kiyosawa S (1992) Sakuranetin, a flavanone phytoalexin from ultraviolet-irradiated rice leaves. *Phytochemistry* **31**: 3807–3809
- Kumar S, Stecher G, Tamura K (2016) MEGA7: molecular evolutionary genetics analysis version 7.0 for bigger datasets. *Mol Biol Evol* **33**: 1870–1874
- Lam PY, Zhu FY, Chan WL, Liu HJ, Lo C (2014) Cytochrome P450 93G1 is a flavone synthase II that channels flavanones to the biosynthesis of Tricin O-linked conjugates in rice. *Plant Physiol* **165**: 1315–1327
- Langcake P, Pryce RJ (1976) Production of resveratrol by *Vitis Vinifera* and other members of Vitaceae as a response to infection or injury. *Physiol Plant Pathol* **9**: 77–86
- Lipka AE, Tian F, Wang Q, Peiffer J, Li M, Bradbury PJ, Gore MA, Buckler ES, Zhang Z (2012) GAPIT: genome association and prediction integrated tool. *Bioinformatics* **28**: 2397–2399
- Liu HJ, Du YG, Chu H, Shih CH, Wong YW, Wang MF, Chu IK, Tao YZ, Lo C (2010) Molecular dissection of the pathogen-inducible 3-deoxyanthocyanidin biosynthesis pathway in sorghum. *Plant Cell Physiol* **51**: 1173–1185
- Liu X, Wang Y, Chen Y, Xu S, Gong Q, Zhao C, Cao J, Sun C (2020) Characterization of a flavonoid 3'/5'/7-O-methyltransferase from *Citrus reticulata* and evaluation of the in vitro cytotoxicity of its methylated products. *Molecules* **25**: 858
- Mafu S, Ding YZ, Murphy KM, Yaacobi O, Addison JB, Wang Q, Shen ZX, Briggs SP, Bohlmann J, Castro-Falcon G, et al. (2018) Discovery, biosynthesis and stress-related accumulation of dolabradiene-derived defenses in maize. *Plant Physiol* **176**: 2677–2690
- Manoli A, Sturaro A, Trevisan S, Quaggiotti S, Nonis A (2012) Evaluation of candidate reference genes for qPCR in maize. *J Plant Physiol* **169**: 807–815
- Martens S, Mithofer A (2005) Flavones and flavone synthases. *Phytochemistry* **66**: 2399–2407
- Martini ND, Katerere DRP, Eloff JN (2004) Biological activity of five antibacterial flavonoids from *Combretum erythrophyllum* (Combretaceae). *J Ethnopharmacol* **93**: 207–212
- Matsuyama M, Rich S (1974) Punch inoculation for measuring resistance of corn leaf tissue to *Helminthosporium Maydis*. *Phytopathology* **64**: 429–430
- McMullen MD, Kresovich S, Villeda HS, Bradbury P, Li H, Sun Q, Flint-Garcia S, Thornsberry J, Acharya C, Bottoms C, et al. (2009) Genetic properties of the maize nested association mapping population. *Science* **325**: 737–740
- Meihls LN, Handrick V, Glauser G, Barbier H, Kaur H, Haribal MM, Lipka AE, Gershenzon J, Buckler ES, Erb M, et al. (2013) Natural variation in maize aphid resistance is associated with 2,4-dihydroxy-7-methoxy-1,4-benzoxazin-3-one glucoside methyltransferase activity. *Plant Cell* **25**: 2341–2355
- Morohashi K, Casas MI, Ferreyra LF, Mejia-Guerra MK, Pourcel L, Yilmaz A, Feller A, Carvalho B, Emiliani J, Rodriguez E, et al. (2012) A genome-wide regulatory framework identifies maize pericarp color1 controlled genes. *Plant Cell* **24**: 2745–2764
- Nicholson RL, Hammerschmidt R (1992) Phenolic-compounds and their role in disease resistance. *Annu Rev Phytopathol* **30**: 369–389
- Nicholson RL, Kollipara SS, Vincent JR, Lyons PC, Cadenagomez G (1987) Phytoalexin synthesis by the sorghum mesocotyl in response to infection by pathogenic and nonpathogenic fungi. *Proc Natl Acad Sci USA* **84**: 5520–5524
- Oikawa A, Ishihara A, Tanaka C, Mori N, Tsuda M, Iwamura H (2004) Accumulation of HDMBOA-Glc is induced by biotic stresses prior to the release of MBOA in maize leaves. *Phytochemistry* **65**: 2995–3001
- Park HL, Yoo Y, Hahn TR, Bhoo SH, Lee SW, Cho MH (2014) Antimicrobial activity of UV-induced phenylamides from rice leaves. *Molecules* **19**: 18139–18151
- Pedras MSC, Ahiaonu PWK (2005) Metabolism and detoxification of phytoalexins and analogs by phytopathogenic fungi. *Phytochemistry* **66**: 391–411
- Pinheiro J, Bates D, DebRoy S, Sarkar D; R Core Team (2020) nlme: linear and nonlinear mixed effects models. <https://cran.r-project.org/web/packages/nlme/index.html>
- Pompon D, Louerat B, Bronine A, Urban P (1996) Yeast expression of animal and plant P450s in optimized redox environments. *Cytochrome P450*: 51–64
- R Core Team (2020) R: a language and environment for statistical computing. R Foundation for Statistical Computing, R Core Team, Vienna, Austria
- Rakwal R, Tamogami S, Kodama O (1996) Role of jasmonic acid as a signaling molecule in copper chloride-elicited rice phytoalexin production. *Biosci Biotech Bioch* **60**: 1046–1048
- Reifschneider FJ, Army DC (1979) A liquid medium for the production of *Kabatiella zeae* conidia. *Can J Microbiol* **25**: 1100–1102
- Righini S, Rodriguez EJ, Berosich C, Grotewold E, Casati P, Falcone Ferreyra ML (2019) Apigenin produced by maize flavone synthase I and II protects plants against UV-B-induced damage. *Plant Cell Environ* **42**: 495–508
- Ro DK, Ouellet M, Paradise EM, Burd H, Eng D, Paddon CJ, Newman JD, Keasling JD (2008) Induction of multiple pleiotropic drug resistance genes in yeast engineered to produce an increased level of anti-malarial drug precursor, artemisinin acid. *BMC Biotechnol* **8**: 83
- Rostas M (2007) The effects of 2,4-dihydroxy-7-methoxy-1,4-benzoxazin-3-one on two species of *Spodoptera* and the growth of *Setosphaeria turcica* in vitro. *J Pest Sci* **80**: 35–41
- Sawada Y, Kinoshita K, Akashi T, Aoki T, Ayabe S (2002) Key amino acid residues required for aryl migration catalysed by the cytochrome P450 2-hydroxyisoflavanone synthase. *Plant J* **31**: 555–564
- Schmelz EA, Kaplan F, Huffaker A, Dafoe NJ, Vaughan MM, Ni XZ, Rocca JR, Albarn HT, Teal PE (2011) Identity, regulation, and activity of inducible diterpenoid phytoalexins in maize. *Proc Natl Acad Sci USA* **108**: 5455–5460
- Shimizu T, Lin FQ, Hasegawa M, Okada K, Nojiri H, Yamane H (2012) Purification and identification of naringenin

- 7-O-methyltransferase, a key enzyme in biosynthesis of flavonoid phytoalexin sakuranetin in rice. *J Biol Chem* **287**: 19315–19325
- Skadhauge B, Thomsen KK, von Wettstein D** (1997) The role of the barley testa layer and its flavonoid content in resistance to *Fusarium* infections. *Hereditas* **126**: 147–160
- Snyder BA, Leite B, Hipskind J, Butler LG, Nicholson RL** (1991) Accumulation of sorghum phytoalexins induced by *Colletotrichum Graminicola* at the infection site. *Physiol Mol Plant Pathol* **39**: 463–470
- Stukenbrock EH, Quaedylied W, Javan-Nikhah M, Zala M, Crous PW, McDonald BA** (2012) *Zymoseptoria ardabiliae* and *Z. pseudotritici*, two progenitor species of the *septoria tritici* leaf blotch fungus *Z. tritici* (synonym: *Mycosphaerella graminicola*). *Mycologia* **104**: 1397–1407
- Stukenbrock EH, Bataillon T, Dutheil JY, Hansen TT, Li RQ, Zala M, McDonald BA, Wang J, Schierup MH** (2011) The making of a new pathogen: insights from comparative population genomics of the domesticated wheat pathogen *Mycosphaerella graminicola* and its wild sister species. *Genome Res* **21**: 2157–2166
- Tohge T, de Souza LP, Fernie AR** (2017) Current understanding of the pathways of flavonoid biosynthesis in model and crop plants. *J Exp Bot* **68**: 4013–4028
- Turner SD** (2014) qqman: an R package for visualizing GWAS results using Q-Q and manhattan plots. Preprint at bioRxiv: <https://doi.org/10.1101/005165>.
- Ube N, Katsuyama Y, Kariya K, Tebayashi S, Sue M, Tohnooka T, Ueno K, Taketa S, Ishihara A** (2021) Identification of methoxyl-chalcones produced in response to CuCl₂ treatment and pathogen infection in barley. *Phytochemistry* **184**: 112650
- Ullah C, Unsicker SB, Fellenberg C, Constabel CP, Schmidt A, Gershenzon J, Hammerbacher A** (2017) Flavan-3-ols are an effective chemical defense against rust infection. *Plant Physiol* **175**: 1560–1578
- VanEtten HD, Mansfield JW, Bailey JA, Farmer EE** (1994) Two classes of plant antibiotics: phytoalexins versus “phytoanticipins”. *Plant Cell* **6**: 1191–1192
- Yu J, Pressoir G, Briggs WH, Vroh Bi I, Yamasaki M, Doebley JF, McMullen MD, Gaut BS, Nielsen DM, Holland JB, et al.** (2006) A unified mixed-model method for association mapping that accounts for multiple levels of relatedness. *Nat Genet* **38**: 203–208
- Zhang JA, Subramanian S, Zhang YS, Yu O** (2007) Flavone synthases from *Medicago truncatula* are flavanone-2-hydroxylases and are important for nodulation. *Plant Physiol* **144**: 741–751
- Zhang Y, De Stefano R, Robine M, Butelli E, Bulling K, Hill L, Rejzek M, Martin C, Schoonbeek HJ** (2015) Different reactive oxygen species scavenging properties of flavonoids determine their abilities to extend the shelf life of tomato. *Plant Physiol* **169**: 1568–1583
- Zhang Z, Ersoz, E, Lai CQ, Todhunter RJ, Tiwari HK, Gore MA, Bradbury PJ, Yu J, Arnett DK, Ordovas JM, et al.** (2010) Mixed linear model approach adapted for genome-wide association studies. *Nat Genet* **42**: 355–360
- Zhanzhaxina AS, Seilgazy M, Jalmakhanbetova RI, Ishmuratova MY, Seilkanov TM, Oyama M, Sarmurzina ZS, Tekebayeva ZB, Suleimen YM** (2020) Flavonoids from *Pulicaria vulgaris* and their antimicrobial activity. *Chem Nat Compd* **56**: 915–917
- Zhou JM, Fukushi Y, Wang XF, Ibrahim RK** (2006a) Characterization of a novel flavone O-methyltransferase gene in rice. *Nat Prod Commun* **1**: 981–984
- Zhou JM, Fukushi Y, Wollenweber E, Ibrahim RK** (2008) Characterization of two O-methyltransferase-like genes in barley and maize. *Pharm Biol* **46**: 26–34
- Zhou JM, Gold ND, Martin VJJ, Wollenweber E, Ibrahim RK** (2006b) Sequential O-methylation of trisetin by a single gene product in wheat. *Bba-Gen Subjects* **1760**: 1115–1124
- Zuur A, Ieno EN, Walker N, Saveliev AA, Smith GM** (2009) *Mixed Effects Models and Extensions in Ecology with R*, Springer, Berlin/Heidelberg, Germany

3.3 Manuscript III

Manuscript title: Evolution of DIMBOA-Glc O-methyltransferases from flavonoid O-methyltransferases in the grasses

Authors: Christiane Förster, Jonathan Gershenzon, and Tobias G. Köllner

Bibliographic information: not available

The candidate is

☒ First author, ☐ Co-first author, ☐ Corresponding author, ☐ Co-author.

Status: submitted for publication to Molecules (MDPI)

Authors' contributions (in %) to the publication (indicated from 20%)

Author	Conceptual	Data analysis	Experimental	Writing the manuscript	Supply of material
Christiane Förster	50	100	100	75	/
Jonathan Gershenzon	5	/	/	5	100
Tobias G. Köllner	45	/	/	20	/

Note: This manuscript was submitted to Molecules (MDPI) for possible open access publication on December 17 (2021) and is incorporated in this thesis under the terms of the Creative Commons Attribution (CC-BY 4.0) license, author Christiane Förster.

Evolution of DIMBOA-Glc O-methyltransferases from flavonoid O-methyltransferases in the grasses

Christiane Förster¹, Jonathan Gershenzon¹, and Tobias G. Köllner^{1,*}

¹ Department of Biochemistry, Max Planck Institute for Chemical Ecology, 07745 Jena, Germany; cfoerster@ice.mpg.de (C.F.); gershenzon@ice.mpg.de (J.G.)

* Correspondence: koellner@ice.mpg.de (T.G.K.); Tel.: +49(0)3641 57-1265

Abstract

O-Methylated benzoxazinoids (BXs) and flavonoids are widespread defenses against herbivores and pathogens in the grasses (Poaceae). Recently, two flavonoid O-methyltransferases (FOMTs), ZmFOMT2 and ZmFOMT3, have been reported to produce phytoalexins in maize (*Zea mays*). ZmFOMT2 and ZmFOMT3 are closely related to the BX O-methyltransferases (OMTs) ZmBX10-12 and ZmBX14, suggesting a common evolutionary origin in the Poaceae. Here, we studied the evolution and enzymatic requirements of flavonoid and BX O-methylation activities in more detail. Using BLAST searches and phylogenetic analyses, we identified enzymes homologous to ZmFOMT2 and ZmFOMT3, ZmBX10-12, and ZmBX14 in several grasses, with the most closely related candidates found almost exclusively in species of the Panicoideae subfamily. Biochemical characterization of candidate enzymes from sorghum (*Sorghum bicolor*), sugar cane (*Saccharum spp.*), and teosinte (*Zea nicaraguensis*) revealed either flavonoid 5-O-methylation activity or DIMBOA-Glc 4-O-methylation activity. However, the DIMBOA-Glc 4-OMTs from maize and teosinte also accepted flavonols as substrates and converted them to 3-O-methylated derivatives, suggesting an evolutionary relationship between these two activities. Homology modelling, sequence comparisons, and site-directed mutagenesis led to the identification of active site residues crucial for FOMT and BX OMT activity. However, a full conversion of ZmFOMT2 activity into BX OMT activity by switching these residues was not successful. Only trace O-methylation of BXs was observed, indicating that amino acids outside the active site cavity are also involved in determining the different substrate specificities. Altogether, our study suggests that BX OMTs have evolved from the ubiquitous FOMTs in the PACMAD clade of the grasses through a complex series of amino acid changes.

Key words

O-methyltransferase, benzoxazinoid, 5-O-methylflavonoid, isokaempferide, DIMBOA-Glc, FOMT2, BX10, *Zea mays*, Poaceae

Introduction

O-Methylation of plant specialized metabolites is a widespread biochemical transformation that creates structural diversity and forms products with modified chemical properties that help plants cope with different biotic and abiotic stresses. This tailoring reaction is catalyzed by S-adenosyl-L-methionine (SAM)-dependent O-methyltransferases (OMTs), which transfer the methyl group of the co-substrate SAM to a hydroxyl moiety of various acceptor molecules. The methyl ether derivatives produced often exhibit reduced reactivity of hydroxyl groups and altered solubility, which in turn affects their biological activity, stability, intracellular localization, and metabolic fate [1, 2]. O-Methylated specialized metabolites can fulfill important roles in plant defense acting, for example, as lignin precursors or as induced antimicrobial compounds [3, 4].

Plant OMTs have been classified into three major groups, based on phylogenetic analysis, conserved amino acid sequence features, protein structures, and substrate specificities: the caffeic acid OMTs (COMTs), caffeoyl-CoA OMTs (CCoAOMTs), and carboxylic acid OMTs [5-7]. The latter share only marginal sequence similarities with the other classes of OMTs and are involved, for instance, in the methylation of various organic acids such as salicylic acid, jasmonic acid, or indole-3-acetic acid [8]. CCoAOMTs are bivalent cation-dependent enzymes that mainly methylate coenzyme A (CoA) esters of phenylpropanoids to lignin precursors. All remaining plant OMTs belong to the large COMT class, which accepts a variety of different substrates, including phenylpropanoids, flavonoids, alkaloids, and coumarins. COMTs are larger (40-43 kDa) than CCoAOMTs (26-30 kDa) and do not require bivalent cations for activity [6, 9]. The majority of plant OMTs show remarkable substrate specificity as well as regiospecificity for certain hydroxyl groups [2]. However, multifunctional enzymes that are able to utilize structurally related compounds [10, 11] or exhibit non-selective positional activity [12-14] have also been described. In some cases, substrate specificity or regiospecificity has been associated with a single amino acid change [15, 16].

In the grasses (Poaceae), OMTs are involved, among other processes, in the biosynthesis of two important classes of defense compounds: flavonoids and benzoxazinoids (BXs). Flavonoids and their O-methyl derivatives are ubiquitously distributed in the plant kingdom and constitute one of the largest groups of plant natural products [17, 18]. The flavonoid core structure is derived from the acetate and phenylpropanoid pathways and can subsequently undergo numerous modifications [19], including O-methylation by flavonoid OMTs (FOMTs). O-methylated flavonoids have been described as potent antimicrobial

phytoalexins. For example, sakuranetin (7-O-methylnaringenin), produced by the FOMT OsNOMT in rice (*Oryza sativa*) leaves upon fungal infection or abiotic stress inhibits the growth of rice blast fungus (*Pyricularia oryzae*) *in vivo* and shows antifungal activity *in vitro* [20-24]. Similarly, pathogen-induced formation of O-methylflavonoids was also detected in other grasses such as sorghum (*Sorghum bicolor*), maize (*Zea mays*), and barley (*Hordeum vulgare*) [25-27]. Recently, we characterized four FOMTs from maize, ZmFOMT2 and ZmFOMT3, ZmFOMT4, and ZmFOMT5, that methylate the hydroxyl groups of various flavonoids regiospecifically at positions 5, 7, and 6 of the A ring, respectively, and are involved in the fungus-induced formation of complex O-methylflavonoid mixtures [28].

Unlike flavonoids, BXs are mostly restricted to the grass family and a few dicotyledonous species [29, 30]. The BX biosynthetic pathway branches off from tryptophan biosynthesis and has been elucidated in maize [29, 31, 32]. The O-methylated BXs usually show higher activity than their non- or less O-methylated precursors. 2-Hydroxy-4,7-dimethoxy-1,4-benzoxazin-3-one glucoside (HDMBOA-Glc), for example, was demonstrated to be more effective in deterring and reducing the growth of chewing herbivores [33, 34] and also more toxic to phloem-feeding aphids compared to its precursor 2,4-dihydroxy-7-methoxy-1,4-benzoxazin-3-one glucoside (DIMBOA-Glc) [31, 35]. The conversion of DIMBOA-Glc to HDMBOA-Glc is induced upon herbivory, fungal infection, or elicitor treatment in maize and other grasses [33, 36-38], and four OMTs ZmBX10, ZmBX11, ZmBX12 and ZmBX14 have been described to catalyze this reaction in maize [31, 32]. Notably, DIMBOA-Glc 4-OMT activity was also found in wheat; however, the corresponding enzyme TaBX10 is not related to ZmBX10-12 and ZmBX14, indicating an independent evolution of DIMBOA-Glc 4-OMT activity in maize and wheat [39]. Despite extensive knowledge on the biosynthesis and biological activity of O-methylated BXs, the evolutionary origin of the OMTs producing them remains unclear [40].

In this study, we investigated the evolution of DIMBOA-Glc 4-OMTs in maize. Because the recently identified flavonoid 5-OMTs ZmFOMT2 and ZmFOMT3 are closely related to ZmBX10-12 and ZmBX14 [28], we hypothesized that the DIMBOA-Glc 4-OMT activity evolved from FOMT activity in the PACMAD clade of the grasses, one of the two major clades of the Poaceae, named after the subfamilies Panicoideae, Aristidoideae, Chloridoideae, Micrairoideae, Arundinoideae, and Danthonioideae [41]. To investigate this evolutionary scenario, we performed phylogenetic analyses to identify ZmFOMT2 homologs in several Poaceae species, followed by *in vitro* enzyme characterization. In addition, comparative sequence analyses, homology modelling, and *in vitro* mutagenesis allowed us

to examine amino acid residues involved in the catalysis of flavonoid 5-OMTs and DIMBOA-Glc 4-OMTs. Our results suggest that DIMBOA-Glc OMTs evolved from FOMTs in the PACMAD clade of the grasses and that this change in activity was due to a complex series of amino acid mutations.

Results

Close homologs of the flavonoid 5-OMT *ZmFOMT2* are restricted to the Panicoideae subfamily

To identify *ZmFOMT2* homologs in the Poaceae family, we performed comprehensive BLAST and phylogenetic analyses including almost all the Poaceae genomes available in the Phytozome 13 and NCBI databases (Figures 1 and S1). The resulting phylogenetic tree showed that the closely related maize DIMBOA-Glc 4-OMT genes *ZmBX10-12* and *ZmBX14*, the flavonoid 5-OMT genes *ZmFOMT2* and *ZmFOMT3*, and the flavonoid 6-OMT gene *ZmFOMT5* clustered together with putative COMT genes from several other species in a well-defined subclade we designated as the “PACMAD-specific *FOMT2-BX10* clade”. This subclade is depicted in Figure 1, and the entire tree is shown in Figure S1. The *FOMT2-BX10* subclade consists entirely of genes from species belonging to the Panicoideae and Chloridoideae within the major PACMAD grass clade, with a clear preponderance of Panicoideae genes (Figure 1). To select the most relevant candidate genes, we subdivided this subtree and focused only on its upper part (hereafter referred to as the “*FOMT2*-like group”), which contains COMTs with 60-87% amino acid sequence identity to *ZmFOMT2*. The previously characterized wheat DIMBOA-Glc 4-OMT gene *TaBX10* [39], on the other hand, clustered in a clearly separated subclade, the “BOP-specific *BX10* clade”; Figure S1) named for the subfamilies Bambusoideae, Oryzoideae and Pooideae [41].

ZmFOMT2 homologs have DIMBOA-Glc 4-OMT or flavonoid 5-OMT activity

Six putative COMT genes that clustered in different subclades of the *FOMT2*-like group (Figure 1) were chosen for biochemical characterization. The complete open reading frames (ORFs) of *ShGCZX01092226* (from a *Saccharum* hybrid), *Sb001G354400* (from *Sorghum bicolor*), *ZnGBZQ01077209* (*ZnGBZQ*, from *Zea nicaraguensis*, teosinte), *ZnGCAA01001611*, *Pvag01G329400* (*Pvag9400*, from *Paspalum vaginatum*), and *Pvir9NG562300* (from *Panicum virgatum*), were either amplified from cDNA and cloned or synthesized. Because the cloned ORF of *Pvir9NG562300* had only 98% amino sequence identity with its respective database sequence, it was designated *Pvir2300-like*.

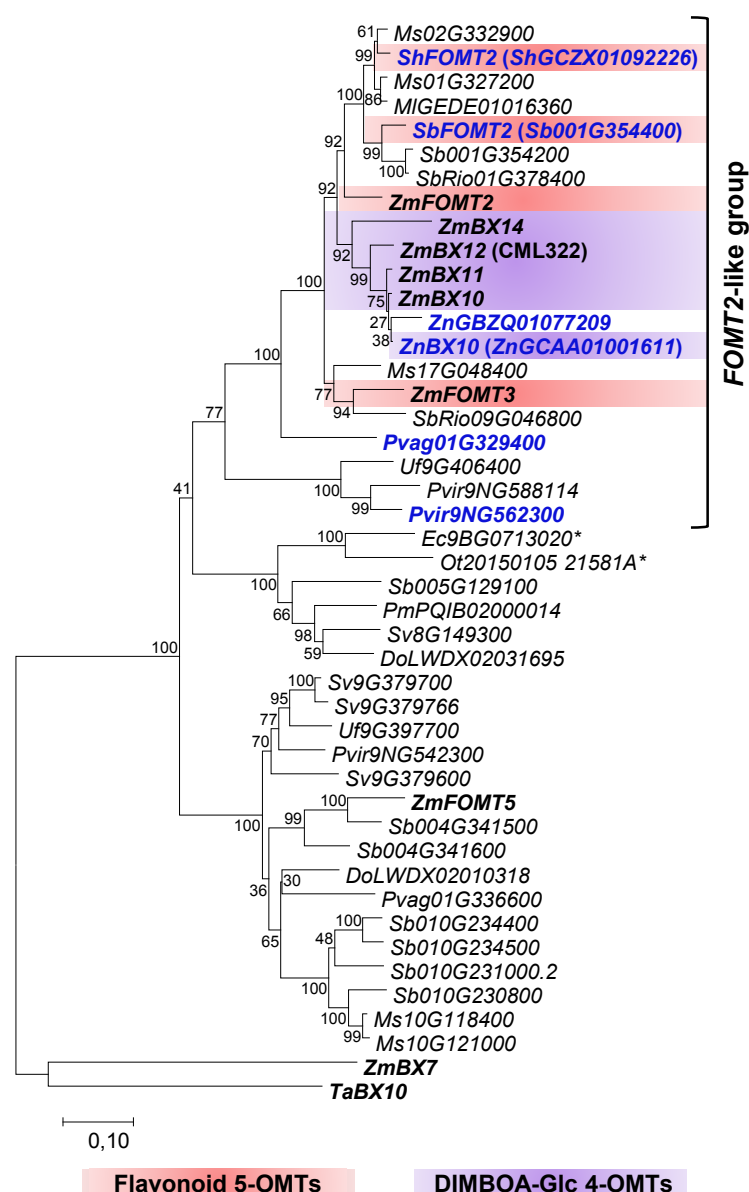


Figure 1. Phylogenetic analysis of putative FOMT and BX OMT genes similar to *ZmFOMT2* in diverse species of the Poaceae. The tree represents a subtree ("PACMAD-specific *FOMT2*-*BX10* clade") of a larger tree given in Figure S1. The tree was inferred using the maximum likelihood method based on the General Time Reversible model, including gamma distributed rate variation among sites (+G, 1.2811). Bootstrap values ($n = 1000$) are shown next to each node. The tree is drawn to scale, with branch lengths measured in the number of substitutions per site. All positions with $< 80\%$ site coverage were eliminated. *ZmBX7* (*Zm00001d049179*) and *TaBX10* (*4AL_C467B516F*) were used as an outgroup for rooting. OMTs investigated in this study are highlighted in bold blue text, and previously characterized genes are shown in bold black text. Genes marked with (*) belong to the Chloridoideae subfamily, all other genes belong to the Panicoideae subfamily. Species abbreviations: Do, *Dichanthelium oligosanthes*; Ec, *Eleusine coracana*; MI, *Miscanthus lutarioriparius*; Ms, *Miscanthus sinensis*; Ot, *Oropetium thomaeum*; Pm, *Panicum miliaceum*; Pvir, *Panicum virgatum*; Pvag, *Paspalum vaginatum*; Sh, *Saccharum hybrid*; Sb, *Sorghum bicolor*; SbRio, *Sorghum bicolor* Rio; Sv, *Setaria viridis*; Ta, *Triticum aestivum*; Uf, *Urochloa fusca*; Zm, *Zea mays*; Zn, *Zea nicaraguensis*.

ZnGCAA01001611, ShGCZX01092226, and Sb001G354400 were designated ZnBX10, ShFOMT2, and SbFOMT2, respectively, according to their *in vitro* activity described below.

To test for enzymatic activity, all genes were heterologously expressed in *Escherichia coli* and the purified His-tagged proteins were incubated with DIMBOA-Glc or different flavonoids as potential substrates in the presence of the cosubstrate SAM. Product formation was analyzed using liquid chromatography-tandem mass spectrometry (LC-MS/MS). The previously characterized flavonoid 5-OMT ZmFOMT2 and DIMBOA-Glc 4-OMTs ZmBX12 and ZmBX14 served as positive controls. Besides ZmBX14 and ZmBX12, ZnBX10 also converted DIMBOA-Glc to HDMBOA-Glc (Figure 2A, Table S1), while no product peak was observed in the empty vector (EV) control. However, DIMBOA-Glc was not accepted as a substrate by ZnGBZQ, the second enzyme from teosinte studied, or any other of the putative COMTs in the *FOMT2*-like group (Figure 2A, Table S1).

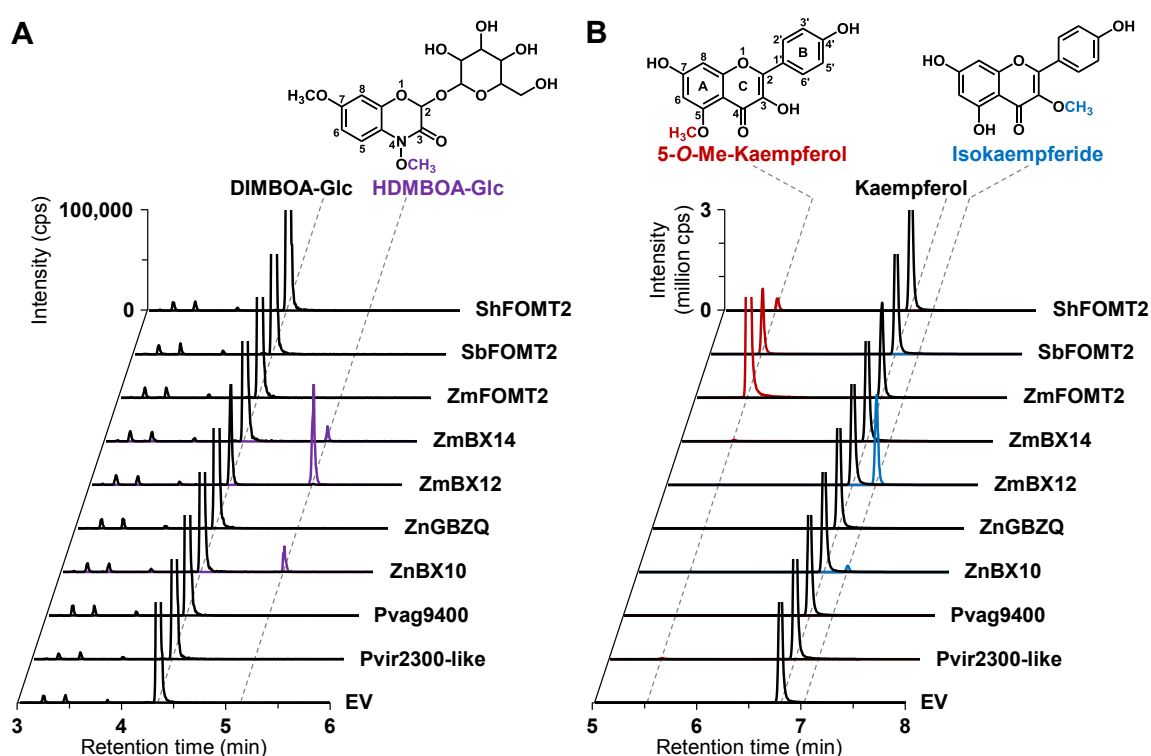


Figure 2. Activity of enzymes in the *FOMT2*-like group. The purified recombinant enzymes as well as an empty vector control (EV) were incubated with the potential substrates DIMBOA-Glc (**A**) and kaempferol (**B**) in the presence of the cosubstrate *S*-adenosyl-L-methionine (SAM). Reaction products were analyzed by LC-MS/MS. Chromatograms of specific MRM transitions (see methods section) are shown. In the upper part, the structures of the enzymatic products are shown with the attached methyl groups highlighted in purple (HDMBOA-Glc), red (5-O-methylkaempferol), and blue (isokaempferide), respectively. All assays were performed in technical triplicates. Abbreviations: Me, methyl; cps, counts per second.

Assays with various flavonoids including naringenin, 2-hydroxynaringenin, apigenin, scutellarein, dihydrokaempferol, kaempferol, and quercetin revealed flavonoid 5-OMT activity for ZmFOMT2, ShFOMT2, and SbFOMT2 (Figures 2B and S2; Table S1). However, compared to ZmFOMT2, the flavonoid O-methylation activities of ShFOMT2 and SbFOMT2 were rather low, ranging from 0.9 to 2.9% and 0.3 to 17.2% of the product formation rate of ZmFOMT2, respectively (Table S1). With 2-hydroxynaringenin as substrate, ShFOMT2 and SbFOMT2 showed higher product formation rates for the mono-O-methylated product but not for the di-O-methylated derivative xilonenin (Figure S2, Table S1). Pvag9400 showed trace 5-OMT activity with flavonoid substrates, while ZnGBZQ and Pv2300-like were not active at all (Table S1). Enzyme assays were also analyzed using untargeted LC-MS; however, no detectable activities were observed for any of the tested COMTs at other positions of the flavonoid skeleton.

The DIMBOA-Glc 4-OMTs ZmBX10-12 and ZnBX10 also possess flavonoid 3-OMT activity with flavonols

In a previous study, we showed that ZmBX10-12 and ZmBX14 exhibited nonspecific trace activity with various flavonoids such as naringenin, apigenin, and scutellarein [28]. However, when the flavonol kaempferol, which, in contrast to the above-mentioned flavonoids, contains an additional hydroxyl group at position 3 of the C ring, was tested as a substrate, ZmBX10-12 and ZnBX10 produced substantial amounts of the 3-O-methylated derivative isokaempferide (Figures 2B and S2; Table S1), while ZmFOMT2 and SbFOMT2 produced only trace amounts of this compound (Table S1). Notably, the catalytic efficiency of the BX OMTs towards kaempferol followed the same order as shown for DIMBOA-Glc [28, 31], with ZmBX12 as most active OMT, followed by ZmBX10, ZmBX11, and ZmBX14 (Figure S2). The flavonoid 6-OMT ZmFOMT5 [28] also accepted kaempferol as a substrate and produced minor amounts of isokaempferide (Figure S2). Untargeted LC-MS measurements with accurate mass determination showed that ZmBX12 and ZnBX10 were also active with quercetin, a flavonol similar to kaempferol, and both the MS/MS fragmentation pattern and the LC elution order indicated methylation at the 3-hydroxyl group of the C ring (Figure S3).

Identification of active site residues determining the substrate specificities and activities of flavonoid 5-OMTs and DIMBOA-Glc 4-OMTs

To identify amino acid residues that determine flavonoid 5-OMT and DIMBOA-Glc 4-OMT activity, respectively, we conducted homology modelling of ZmFOMT2 and amino acid sequence comparisons among all enzymes in the *FOMT2*-like group (Figure 3).

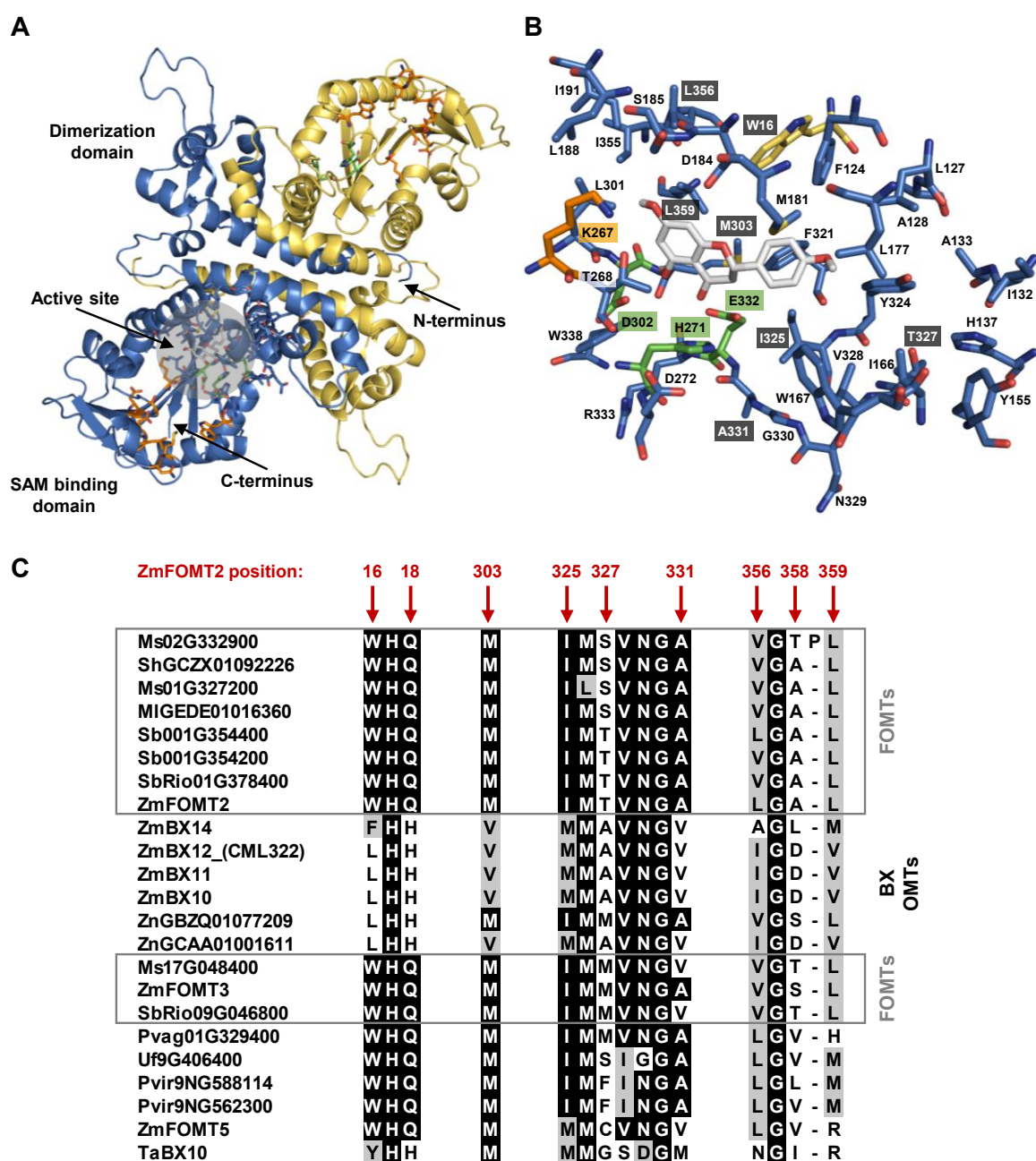


Figure 3. Structural model of ZmFOMT2 and alignment-based identification of putative active site residues. (A) Homology model of the biological homodimer of ZmFOMT2 (chain A: blue; chain B: gold) based on the template isoflavone 4'-OMT from *Medicago truncatula* (MtHI4OMT; PDB-ID: 1ZG3). Labels correspond to the monomer colored in blue. A close-up view of the putative active site is shown in (B), representing the 6 Å area around naringenin, docked in as a model flavonoid substrate. Amino acid residues (carbon atoms) are color-coded, with the catalytic triad in green, SAM binding residues in orange, naringenin in grey, and all other protein carbon atoms in blue (chain A) and gold (chain B). Oxygen atoms are red, nitrogen atoms are blue, and sulfur atoms are yellow. Mutation sites are labeled in dark grey. (C) Alignment of putative active site residues that differ between all ZmFOMT2-like FOMTs (grey boxes) and BX OMTs, respectively. The amino acid sequence sections are cut from the complete alignment given in Figure S5. Identical amino acids are shaded in black and similar amino acids in grey.

The crystal structure of an isoflavone 4'-OMT (MtHI4OMT) from *Medicago truncatula* [42], which shares 39% amino acid sequence identity with ZmFOMT2, was used as template for the construction of the ZmFOMT2 model (Figures 3A and S4). Docking of naringenin into the substrate binding pocket of ZmFOMT2 revealed 37 amino acids that were located at a distance of ≤ 6 Å around the docked substrate (Figure 3B, Table S2). Nine of these residues differed between all functional flavonoid 5-OMTs and DIMBOA-Glc 4-OMTs (Figures 3C and S5) and were therefore further analyzed by replacing them in ZmFOMT2 with the corresponding residues of ZmBX10. To reduce the number of mutants to be generated, nearby residues were combined in a single mutation step, resulting in three different double mutations and three single mutations (Figure 3C).

When fed with naringenin or kaempferol as substrate, the double mutant ZmFOMT2 W16L+Q18H, the triple mutant ZmFOMT2 W16L+Q18H+M303V, and the quadruple mutant ZmFOMT2 W16L+Q18H+I325M+T327A still showed flavonoid 5-OMT activity; however, with a successive decrease in activity compared to the wild type ZmFOMT2 enzyme (Figure 4). At the same time, a successively increased production of isokaempferide from kaempferol was observed (Figure 4). The introduction of two further mutations (A358D+L359V) into the quadruple mutant ZmFOMT2 W16L+Q18H+I325M+T327A almost completely abolished any enzymatic activity, and the simultaneous mutation of all nine residues also led to an inactive protein (Figure 4). Notably, none of the tested mutants was able to accept DIMBOA-Glc as substrate in our standard assay. However, when using 2.5-fold greater amounts of both the purified recombinant enzymes and DIMBOA-Glc, and a 5-fold greater amount of SAM, the triple mutant ZmFOMT2 W16L+Q18H+M303V and the quadruple mutant ZmFOMT2 W16L+Q18H+I325M+T327A produced small amounts of HDMBOA-Glc, while neither the EV control nor ZmFOMT2 showed any DIMBOA-Glc 4-OMT activity (Figure S6).

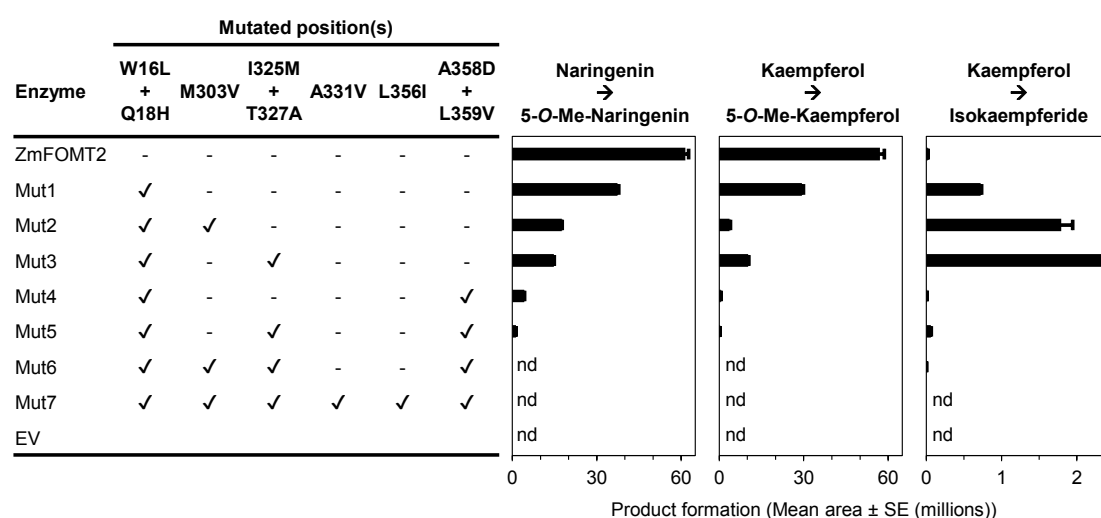


Figure 4. Enzymatic activity of ZmFOMT2 mutants with flavonoids. The purified recombinant enzymes as well as an empty vector control (EV) were incubated with the substrates naringenin or kaempferol in the presence of the cosubstrate SAM. Reaction products (5-O-methylnaringenin, 5-O-methylkaempferol, and isokaempferide) were analyzed by LC-MS/MS. Product formation is shown in bar charts (mean area ± SE ($n = 3$)). Abbreviations: Me, methyl; nd, not detected.

Discussion

O-methylated flavonoids and BXs are important anti-pathogen and anti-herbivore defense compounds widespread in the grasses [22, 33, 37, 39]. Recently, we identified two flavonoid 5-OMTs in maize, ZmFOMT2 and ZmFOMT3, and showed that they are closely related to the DIMBOA-Glc 4-OMTs ZmBX10-12 and ZmBX14, indicating a common OMT ancestor in the grasses [28]. To investigate the evolution of these enzymes in more detail, we characterized OMTs homologous to ZmFOMT2 from several other grass species. Our studies support the hypothesis that maize and teosinte DIMBOA-Glc 4-OMTs originated from FOMTs in the PACMAD clade. In addition, we identified amino acid residues in the active site of ZmFOMT2 that, when mutated to the corresponding residues of ZmBX10-12, altered the regiospecificity and catalytic activity of the enzyme.

The recently discovered DIMBOA-Glc 4-OMT gene *TaBX10* in wheat was shown not to be orthologous to *ZmBX10-12* and *ZmBX14* in maize. Therefore, DIMBOA-Glc 4-OMT activity is thought to have evolved independently in maize and wheat [39]. Our phylogenetic analyses, encompassing a larger set of Poaceae species, are consistent with this finding, as close homologs of *ZmFOMT2*, *ZmBX10-12*, and *ZmBX14* were found exclusively in the PACMAD clade, with the majority of genes belonging to the Panicoideae subfamily (PACMAD-specific *FOMT2-BX10* clade; Figures 1 and S1). Biochemical characterization of

selected candidate enzymes revealed good agreement between grouping within this subclade and actual OMT activity (Figures 2 and S2; Table S1). While ShFOMT2 and SbFOMT2 clustered with ZmFOMT2 and exhibited flavonoid 5-OMT activity, ZnBX10 clustered with ZmBX10-12 and ZmBX14 and showed DIMBOA-Glc 4-OMT activity. In contrast, Pvag01G329400 and Pvir2300-like clustered in smaller and more basal subclades of the phylogenetic tree and showed negligible or no flavonoid 5-OMT activity (Figures 1, 2, and S2; Table S1). However, whether these two enzymes accept other phenylpropanoids as substrates remains to be determined. Notably, DIMBOA-Glc 4-OMTs could only be identified in maize and its wild relative teosinte and not in the other species investigated, which is consistent with the distribution of BXs in these grasses [30]. Overall, our findings suggest that flavonoid 5-OMT activity is more widespread than DIMBOA-Glc 4-OMT activity, at least in the Panicoideae, and that DIMBOA-Glc 4-OMTs evolved from a flavonoid 5-OMT ancestor. Whether the wheat DIMBOA-Glc 4-OMT TaBX10 also evolved from an FOMT ancestor enzyme is still unclear. Thus, further studies are necessary to understand how these important plant defense genes have evolved independently in the grasses.

COMTs are known to generally catalyze the O-methylation of a variety of structurally diverse substrates; however, closely related COMTs often use structurally similar substrates [6]. BXs and flavonoids indeed share a similar basic chemical skeleton consisting of three six-membered rings, with the central ring being a heterocycle (Figure 2). Our results showed that the DIMBOA-Glc 4-OMTs, ZmBX10-12 and ZnBX10, are able to O-methylate the flavonols kaempferol and quercetin at position 3 of the C ring, which is close to position 4 in BXs (Figures 2, S2, and S3; Table S1). This indicates a similar orientation and binding mode for DIMBOA-Glc and flavonoid substrates in the active sites of these enzymes. Previous publications showed that the substrate preference, regiospecificity, and overall activity of FOMTs can be altered by a few amino acid mutations in the substrate binding pocket [16, 43, 44]. Using homology modelling and amino acid sequence comparisons, we identified nine putative active site residues that differ between flavonoid 5- and DIMBOA-Glc 4-OMTs (Figures 3, S4, and S5). Unexpectedly, the replacement of some of these residues in ZmFOMT2 with the corresponding residues of ZmBX10 gave only a very weak BX OMT activity, whereas the complete replacement of these residues resulted in an inactive enzyme. It thus appears that additional mutations are required for the switch from flavonoid 5-OMT to DIMBOA-Glc 4-OMT activity. Indeed, studies on terpene synthases from tobacco and maize have shown that amino acid residues near but not in the active site can also play a role in determining catalytic specificities [45, 46].

Interestingly, the stepwise and additive mutation of the nine identified active site residues in ZmFOMT2 led to mutants with altered catalytic efficiencies and substrate regiospecificities for flavonoids. While wild type ZmFOMT2 was highly regiospecific for position 5 on the A ring of flavonoids, even when using flavonols such as kaempferol or quercetin as substrates, the double mutant ZmFOMT2 W16L+Q18H showed flavonol 3-OMT activity at the expense of flavonoid 5-OMT activity (Figure 4). This effect was even stronger in the triple mutant ZmFOMT2 W16L+Q18H+M303V and the quadruple mutant ZmFOMT2 W16L+Q18H+I325M+T327A. Moreover, the triple mutant ZmFOMT2 W16L+Q18H+M303V and the quadruple mutant ZmFOMT2 W16L+Q18H+I325M+T327A both produced trace amounts of HDMBOA-Glc (Figure S6), indicating that the identified active site residues are involved in substrate binding and positioning. Previous studies [28, 31] and the biochemical data presented here show that the DIMBOA-Glc 4-OMTs and the flavonoid 5-OMTs exhibit different catalytic efficiencies despite generally comparable enzymatic functionality (Figures 2, S2, and S3; Table S1). All together, our study suggests that the evolution of DIMBOA-Glc 4-OMTs involved complex mutations that not only altered substrate specificity, but also fine-tuned catalytic efficiency. Follow-up studies based on structural data from a plant OMT more closely related to ZmFOMT2 are needed to unravel the enzymatic requirements for the substrate specificity of flavonoid 5-OMT and DIMBOA-Glc 4-OMT in more detail.

Materials and Methods

Plants and growth conditions

Seeds of *Sorghum bicolor* (L.) Moench subsp. *Bicolor* race *Bicolor* 'Lisorax' and *Panicum virgatum* L. were provided by the Leibniz-Institut für Pflanzengenetik und Kulturpflanzenforschung (IPK, Gatersleben, Germany). Plants were potted in soil (mix of 70 L Tonsubstrat with 200 L Kultursubstrat TS 1, Klasmann-Deilmann, Geeste, Germany) and grown in the greenhouse for two weeks.

RNA and cDNA preparation

Total RNA was extracted from approximately 50 mg frozen plant powder using the InviTrap Spin Plant RNA Kit (Stratec) according to the manufacturer's instructions. The RNA concentration and purity was assessed with a spectrophotometer (NanoDrop 2000c, Thermo Fisher Scientific). RNA (1 µg) was treated with DNaseI (Thermo Fisher Scientific),

followed by cDNA synthesis using SuperScript III reverse transcriptase and oligo (dT)₂₀ primers (Invitrogen) according to the manufacturer's instructions.

Gene Synthesis

The complete ORFs of *ShGCZX01092226* (*ShFOMT2*), *ZnGBZQ01077209*, *ZnGCAA01001611* (*ZnBX10*), and *Pvag01G329400* were synthesized after codon optimization for heterologous expression in *E. coli* and subcloned into the expression vector pET100/D-TOPO using the GeneArt gene synthesis and express cloning service (Thermo Fisher Scientific) (for sequences, see Figure S7).

Site-directed mutagenesis

For *in vitro* mutagenesis, 10-50 ng pET100/D-TOPO vector harboring the *ZmFOMT2* ORF was used as template for 18 cycles of mutagenesis PCR using the Q5 High-Fidelity DNA Polymerase (New England Biolabs) and the primers listed in Table S3. The primers used contained the desired mutations and the pairs were either designed completely overlapping or with only partially overlapping sequences, the latter allowing enhanced amplification efficiency from a smaller amount of plasmid template [47]. After PCR amplification, the plasmid template was digested with *DpnI*. The mutagenized PCR product was purified using the QIAquick PCR Purification Kit (Qiagen) according to the manufacturer's instructions and transferred into *E. coli* 10-beta cells (New England Biolabs) for recovery and amplification. All mutagenized plasmids were fully sequenced.

Cloning and heterologous expression of OMT genes in *E. coli*

The full-length ORFs of *Sb001G354400* (*SbFOMT2*) and *Pvir9NG562300* (*Pvir2300-like*) were amplified from cDNA derived from young leaves of *S. bicolor* and *P. virgatum*, respectively, with the primer pairs listed in Table S3. The resulting PCR products were cloned into the expression vector pET100/D-TOPO (Invitrogen) or pASK-IBA37plus (IBA Lifesciences) and fully sequenced. *ZmFOMT2* (W22; GenBank accession: MZ484743) was provided as a pET100/D-TOPO construct, while *ZmBX10* (B73), *ZmBX11* (B73), *ZmBX12* (CML322), *ZmBX14* (B73), and *E. coli* codon-optimized *ZmFOMT5* were available as pASK-IBA37plus constructs from our previous studies [28, 31, 32]. All OMTs were heterologously expressed in the *E. coli* strain BL21 (DE3) (Invitrogen) as previously described [28]. Liquid cultures were grown in lysogeny broth at 37°C and 220 rpm, induced at an OD₆₀₀ of 0.8 with a final concentration of 1 mM IPTG (pET100/D-TOPO) or 200 µg/L anhydrotetracycline (pASK-IBA37plus), and subsequently incubated at 18°C and 220 rpm for 15 h. The cells were harvested by centrifugation (5000 g, 4°C, 10 min), resuspended in

refrigerated extraction buffer (50 mM Tris-HCl pH 8, 500 mM NaCl, 20 mM imidazole, 10% (v/v) glycerol, 1% (v/v) Tween20, and 25 U/mL freshly added Benzonase Nuclease (Merck)) and disrupted by sonication (4 × 20 s; Bandelin UW 2070). Afterwards, cell debris were removed by centrifugation (16,000 g, 4°C, 20 min) and the N-terminal His-tagged proteins were purified from the supernatant using HisPur Cobalt Spin Columns (Thermo Fisher Scientific) according to the manufacturer's instructions. Tris-HCl buffer (pH 8, without Tween20; see above) containing either 20 mM or 250 mM imidazole was used for equilibration/washing and elution steps, respectively. The purified proteins were desalted by gel filtration using illustra NAP Columns (GE Healthcare) and eluted in assay buffer (50 mM Tris-HCl pH 7, 10% (v/v) glycerol). Alternatively, Amicon Ultra-0.5 centrifugal filter devices (Merck) were used for concentration and desalting of the His-purified proteins. Protein concentrations were determined by the Bradford method using Quick Start™ Bradford 1x Dye Reagent (Bio-Rad Laboratories) and pre-diluted BSA protein standards (Thermo Scientific) in a 96-well microtiter plate. The measurements were performed on a Tecan infinite 200 microplate reader (Tecan) using Magellan software (Tecan) for instrument control and data analysis.

***In vitro* enzyme assays**

To test OMT activities, assays were conducted as previously described [28]. Briefly, the 100 µL assay mixtures contained 500 µM dithiothreitol (DTT), 100 µM of the cosubstrate S-adenosyl-L-methionine (SAM), 20 µM of the substrate (DIMBOA-Glc or various flavonoids), and 0.8 µg purified recombinant protein in assay buffer (50 mM Tris-HCl, pH 7, 10% (v/v) glycerol). All assays were incubated for 1 h at 25°C and stopped by adding one volume of 100% methanol. Denatured proteins were removed by centrifugation (4000 g, 5 min) and product formation was monitored by the analytical methods described below.

Liquid chromatography mass spectrometry (LC-MS) analysis of BXs and flavonoids in enzyme assays

Targeted LC-MS/MS analysis

The analysis of BXs and flavonoids was performed as described previously in Förster et al. (2021). Briefly, an Agilent 1260 Infinity II LC system (Agilent Technologies) coupled to a QTRAP 6500+ tandem mass spectrometer (Sciex) was used for the analysis. Chromatographic separation was achieved on a ZORBAX Eclipse XDB-C18 column (50 × 4.6 mm, 1.8 µm; Agilent Technologies) using a 1.1 mL/min flow rate. Aqueous formic acid (0.05% (v/v)) and acetonitrile were used as mobile phases A and B, respectively. The

following gradients were used: BXs: 0 to 0.5 min, 5% B; 0.5 to 6.0 min, 5 to 32.5% B; 6.02 to 7.0 min, 100% B; 7.10 to 9.5 min, 5% B; flavonoids: 0 to 0.5 min, 10% B; 0.5 to 8.0 min, 10 to 55% B; 8.5 to 9.0 min, 100% B; 9.02 to 11 min, 10% B. The column temperature was maintained at 20°C. The injection volume was 4 μ L for enzyme assays with DIMBOA-Glc as substrate and 1 μ L for enzyme assays with flavonoid substrates. The mass spectrometer was equipped with a turbospray ESI ion source, operated in negative or positive ionization mode, for the analysis of BXs and flavonoids, respectively (detailed parameters are provided in Table S4). Multiple reaction monitoring (MRM) was used to monitor analyte parent ion \rightarrow product ion transitions as listed in Table S5. Product identities were confirmed by authentic standards or deduced from specific enzymatic activities as described previously in Förster et al. (2021). For data acquisition and processing, Analyst 1.6.3 (Sciex) and MultiQuant 3.0.3 software (Sciex) were used.

Untargeted LC-MS analysis with accurate mass determination

To screen for potential unknown enzymatic products, untargeted LC-MS was used as previously described [28]. Chromatography was performed on a Dionex UltiMate 3000 RS pump system (Thermo Fisher Scientific) equipped with a ZORBAX RRHD Eclipse XDB-C18 column (2.1 \times 100 mm, 1.8 μ m; Agilent Technologies), using aqueous formic acid (0.1% (v/v)) and acetonitrile as mobile phases A and B, respectively. The flow rate was 0.3 mL/min and the column temperature was maintained at 25°C. The elution profile was as follows: 0 to 0.5 min, 5% B; 0.5 to 11 min, 5 to 60% B; 11.1 to 12 min, 100% B; 12.1 to 15 min, 5% B. The injection volume was 4 μ L. The LC system was coupled to a timsTOF mass spectrometer (Bruker Daltonics) equipped with an ESI ion source, operated in positive ionization mode to scan masses from m/z 50 to 1500. The MS settings were as follows: capillary voltage, 4500 V; drying gas (nitrogen), 8 L/min, 280°C; nebulizer gas (nitrogen), 2.8 bar. In autoMS/MS mode, alternating collision energy (20/50 eV) was applied. Internal calibration was achieved using sodium formate adducts. Bruker otof control 6.0.115 and HyStar 5.1.8.1 software (Bruker Daltonics) were used for data acquisition, and DataAnalysis 5.3 (Bruker Daltonics) was used for data processing.

Sequence alignment and phylogenetic analysis

OMTs were identified by BLASTP analysis with ZmFOMT2 as query and using Poaceae protein datasets available in the Phytozome 13 (<https://phytozome-next.jgi.doe.gov/>; for all data sets used, see Table S6) and NCBI (<https://www.ncbi.nlm.nih.gov/>) databases. In addition, a local BLAST was performed with transcriptomic data from the NCBI

Transcriptome Shotgun Assembly (TSA, <https://www.ncbi.nlm.nih.gov/genbank/tsa/>) sequence database using the program BioEdit [48], and the full sequences of the resulting hits were retrieved from the NCBI database. Only genes (ORFs) with $\geq 80\%$ query coverage and a corresponding amino acid identity of $\geq 40\%$ were used for phylogenetic analysis. All sequences with ≤ 5 amino acid differences were excluded. Multiple sequence alignments were computed using the MUSCLE codon algorithm implemented in the software MEGA7 [49]. Based on these alignments, phylogenetic trees were reconstructed with MEGA7 using a maximum likelihood algorithm. Codon positions included were 1st+2nd+3rd+noncoding. All positions with $< 90\%$ site coverage (Poaceae OMT phylogeny, Figure S1) or $< 80\%$ site coverage (phylogeny of the *FOMT2-BX10* clade, Figure 1) were eliminated. Ambiguous bases were allowed at any position. To identify the best-fitting nucleotide substitution model for each dataset, a substitution model test was performed with MEGA7 (for substitution model used, see respective figure legends). A bootstrap resampling analysis with 1000 replicates was performed to evaluate the topology of the *FOMT2*-like subtree. Amino acid sequence alignments were generated with MEGA 7 and visualized with BioEdit.

Homology modeling and molecular docking

A homology model of ZmFOMT2 was generated using the Swiss Modell server (<https://swissmodel.expasy.org/>; [50]) based on isoflavone 4'-O-methyltransferase from *M. truncatula* (PDB-ID: 1ZG3; [42]). Docking of naringenin into the homology model of ZmFOMT2 was performed using AutoDock Vina (<http://vina.scripps.edu/>; [51]) with the grid box (size $x/y/z = 26 \text{ \AA}$) centered on His271 (C-2) of the catalytic triad and with the exhaustiveness set to 8. AutoDock Tools 1.5.7 (<https://ccsb.scripps.edu/mgltools/>) was used to prepare protein and ligand files for use in AutoDock Vina. Visualization was performed with PyMOL 0.99rc6 (<https://pymol.org/2/>). All binding modes of naringenin in the active site pocket (Table S2) were used in combination to represent the 6 \AA area shown in Figure 3B.

Accession numbers

Sequence data for the genes amplified and cloned in this study can be found in the NCBI GenBank (<https://www.ncbi.nlm.nih.gov/genbank/>) under the following identifiers: *SbFOMT2* (XXX) and *Pvir2300-like* (XXX).

Supplementary Materials: The following are available online, Figure S1: Phylogenetic tree of Poaceae OMT genes similar to *ZmFOMT2*, Figure S2: Enzymatic activity of *FOMT2*-like group members with different flavonoid substrates, Figure S3: BX OMTs catalyze the 3-O-methylation of flavonols, Figure S4: Amino acid sequence alignment of *ZmFOMT2* and *ZmBX10* with isoflavone OMTs, Figure S5: Amino acid sequence alignment of OMTs in the *FOMT2*-like group, Figure S6: Enzymatic activity of *ZmFOMT2* mutants with DIMBOA-Glc, Figure S7: Codon-optimized gene sequences of Poaceae OMTs synthesized for expression in *E. coli*, Table S1: Enzymatic activity of Poaceae OMTs in the *FOMT2*-like group with different substrates, Table S2: Resulting binding modes for docking of naringenin into the homology model of *ZmFOMT2* using AutoDock Vina (<http://vina.scripps.edu/>; Trott and Olson, 2010) with the grid box (size x/y/z = 26 Å) centered on His271 (C-2) base of the catalytic triad and with the exhaustiveness set to 8, Table S3: PCR primers for the amplification of full-length ORFs of investigated OMTs and for site-directed mutagenesis, Table S4: MS settings used for the analysis on the QTRAP 6500+, Table S5: Mass analyzer settings used for the analysis of BXs and flavonoids on the QTRAP 6500+, Table S6: Phytozome 13 (<https://phytozome-next.jgi.doe.gov/>) data sets used and corresponding references for the phylogenetic analysis shown in Figure 1 and Figure S1.

Author contributions: Conceptualization, T.G.K, C.F., and J.G.; investigation, C.F.; resources, J.G.; writing—original draft preparation, C.F.; writing—review and editing, T.G.K., J.G., and C.F.; visualization, C.F.; supervision, T.G.K. and J.G. All authors have read and agreed to the published version of the manuscript.

Funding: This research was funded by the Max-Planck Society and the Swiss National Science Foundation (grant no. 160786).

Institutional Review Board Statement: Not applicable.

Informed Consent Statement: Not applicable.

Data Availability Statement: Data are contained within the article and supplementary materials.

Acknowledgments: We thank all gardeners of the Max Planck Institute for Chemical Ecology (MPICE) for their help in growing the plants. We thank Michael Reichelt (MPICE) for support with the analytical analyses, Bettina Raguschke (MPICE) for assistance in DNA sequencing, and Elias Kalthoff (MPICE) for assistance in molecular biology work.

Conflicts of Interest: The authors declare no conflict of interest.

References

1. Ibrahim, R. K.; Deluca, V.; Khouri, H.; Latchinian, L.; Brisson, L.; Charest, P. M., Enzymology and Compartmentation of Polymethylated Flavonol Glucosides in *Chrysosplenium americanum*. *Phytochemistry* **1987**, 26, (5), 1237-1245.
2. Ibrahim, R. K.; Bruneau, A.; Bantignies, B., Plant O-methyltransferases: molecular analysis, common signature and classification. *Plant Mol Biol* **1998**, 36, (1), 1-10.
3. Dixon, R. A.; Paiva, N. L., Stress-Induced Phenylpropanoid Metabolism. *Plant Cell* **1995**, 7, (7), 1085-1097.
4. Hammerschmidt, R., Phytoalexins: What Have we Learned After 60 Years? *Annu Rev Phytopathol* **1999**, 37, 285-306.
5. Joshi, C. P.; Chiang, V. L., Conserved sequence motifs in plant S-adenosyl-L-methionine-dependent methyltransferases. *Plant Mol Biol* **1998**, 37, (4), 663-674.
6. Lam, K. C.; Ibrahim, R. K.; Behdad, B.; Dayanandan, S., Structure, function, and evolution of plant O-methyltransferases. *Genome* **2007**, 50, (11), 1001-1013.
7. Noel, J. P.; Dixon, R. A.; Pichersky, E.; Zubieta, C.; Ferrer, J. L., Structural, functional, and evolutionary basis for methylation of plant small molecules. In *Recent Adv Phytochem*, Romeo, J. T., Ed. Elsevier: 2003; Vol. 37, pp 37-58.
8. Qu, L. J.; Li, S. A.; Xing, S. F., Methylation of phytohormones by the SABATH methyltransferases. *Chinese Sci Bull* **2010**, 55, (21), 2211-2218.
9. Kim, B. G.; Sung, S. H.; Chong, Y.; Lim, Y.; Ahn, J. H., Plant Flavonoid O-Methyltransferases: Substrate Specificity and Application. *J Plant Biol* **2010**, 53, (5), 321-329.
10. Gauthier, A.; Gulick, P. J.; Ibrahim, R. K., Characterization of Two cDNA Clones Which Encode O-Methyltransferases for the Methylation of both Flavonoid and Phenylpropanoid Compounds. *Arch Biochem Biophys* **1998**, 351, (2), 243-249.
11. Frick, S.; Kutchan, T. M., Molecular cloning and functional expression of O-methyltransferases common to isoquinoline alkaloid and phenylpropanoid biosynthesis. *Plant J* **1999**, 17, (4), 329-339.
12. Deavours, B. E.; Liu, C. J.; Naoumkina, M. A.; Tang, Y. H.; Farag, M. A.; Sumner, L. W.; Noel, J. P.; Dixon, R. A., Functional analysis of members of the isoflavone and isoflavanone O-methyltransferase enzyme families from the model legume *Medicago truncatula*. *Plant Mol Biol* **2006**, 62, (4-5), 715-733.
13. Itoh, N.; Iwata, C.; Toda, H., Molecular cloning and characterization of a flavonoid-O-methyltransferase with broad substrate specificity and regioselectivity from *Citrus depressa*. *Bmc Plant Biol* **2016**, 16, 180.
14. Liu, X.; Wang, Y.; Chen, Y.; Xu, S.; Gong, Q.; Zhao, C.; Cao, J.; Sun, C., Characterization of a Flavonoid 3'/5'/7-O-Methyltransferase from *Citrus reticulata* and Evaluation of the In Vitro Cytotoxicity of Its Methylated Products. *Molecules* **2020**, 25, (4), 858.
15. Gang, D. R.; Lavid, N.; Zubieta, C.; Chen, F.; Beuerle, T.; Lewinsohn, E.; Noel, J. P.; Pichersky, E., Characterization of Phenylpropene O-Methyltransferases from Sweet Basil : Facile Change of Substrate Specificity and Convergent Evolution within a Plant O-Methyltransferase Family. *Plant Cell* **2002**, 14, (2), 505-519.
16. Zhou, J. M.; Lee, E.; Kanapathy-Sinnaiah, F.; Park, Y.; Kornblatt, J. A.; Lim, Y.; Ibrahim, R. K., Structure-function relationships of wheat flavone O-methyltransferase: Homology modeling and site-directed mutagenesis. *Bmc Plant Biol* **2010**, 10, 156.
17. Berim, A.; Gang, D. R., Methoxylated flavones: occurrence, importance, biosynthesis. *Phytochem Rev* **2016**, 15, (3), 363-390.

18. Yonekura-Sakakibara, K.; Higashi, Y.; Nakabayashi, R., The Origin and Evolution of Plant Flavonoid Metabolism. *Frontiers in plant science* **2019**, 10, 943.
19. Tohge, T.; de Souza, L. P.; Fernie, A. R., Current understanding of the pathways of flavonoid biosynthesis in model and crop plants. *J Exp Bot* **2017**, 68, (15), 4013-4028.
20. Kodama, O.; Miyakawa, J.; Akatsuka, T.; Kiyosawa, S., Sakuranetin, a Flavanone Phytoalexin from Ultraviolet-Irradiated Rice Leaves. *Phytochemistry* **1992**, 31, (11), 3807-3809.
21. Rakwal, R.; Tamogami, S.; Kodama, O., Role of Jasmonic Acid as a Signaling Molecule in Copper Chloride-elicited Rice Phytoalexin Production. *Biosci Biotech Bioch* **1996**, 60, (6), 1046-1048.
22. Hasegawa, M.; Mitsuhashi, I.; Seo, S.; Okada, K.; Yamane, H.; Iwai, T.; Ohashi, Y., Analysis on Blast Fungus-Responsive Characters of a Flavonoid Phytoalexin Sakuranetin; Accumulation in Infected Rice Leaves, Antifungal Activity and Detoxification by Fungus. *Molecules* **2014**, 19, (8), 11404-11418.
23. Murata, K.; Kitano, T.; Yoshimoto, R.; Takata, R.; Ube, N.; Ueno, K.; Ueno, M.; Yabuta, Y.; Teraishi, M.; Holland, C. K.; Jander, G.; Okumoto, Y.; Mori, N.; Ishihara, A., Natural variation in the expression and catalytic activity of a naringenin 7-O-methyltransferase influences antifungal defenses in diverse rice cultivars. *Plant J* **2020**, 101, (5), 1103-1117.
24. Shimizu, T.; Lin, F. Q.; Hasegawa, M.; Okada, K.; Nojiri, H.; Yamane, H., Purification and Identification of Naringenin 7-O-Methyltransferase, a Key Enzyme in Biosynthesis of Flavonoid Phytoalexin Sakuranetin in Rice. *J Biol Chem* **2012**, 287, (23), 19315-19325.
25. Lo, S. C.; Weiergang, I.; Bonham, C.; Hippskind, J.; Wood, K.; Nicholson, R. L., Phytoalexin accumulation in sorghum: Identification of a methyl ether of luteolinidin. *Physiol Mol Plant P* **1996**, 49, (1), 21-31.
26. Balmer, D.; de Papajewski, D. V.; Planchamp, C.; Glauser, G.; Mauch-Mani, B., Induced resistance in maize is based on organ-specific defence responses. *Plant J* **2013**, 74, (2), 213-225.
27. Ube, N.; Katsuyama, Y.; Kariya, K.; Tebayashi, S.; Sue, M.; Tohnooka, T.; Ueno, K.; Taketa, S.; Ishihara, A., Identification of methoxylchalcones produced in response to CuCl₂ treatment and pathogen infection in barley. *Phytochemistry* **2021**, 184, 112650.
28. Förster, C.; Handrick, V.; Ding, Y.; Nakamura, Y.; Paetz, C.; Schneider, B.; Castro-Falcón, G.; Hughes, C. C.; Luck, K.; Poosapati, S.; Kunert, G.; Huffaker, A.; Gershenzon, J.; Schmelz, E. A.; Köllner, T. G., Biosynthesis and antifungal activity of fungus-induced O-methylated flavonoids in maize. *Plant Physiol* **2021**, kiab496.
29. Frey, M.; Schullehner, K.; Dick, R.; Fiesselmann, A.; Gierl, A., Benzoxazinoid biosynthesis, a model for evolution of secondary metabolic pathways in plants. *Phytochemistry* **2009**, 70, (15-16), 1645-1651.
30. Kokubo, Y.; Nishizaka, M.; Ube, N.; Yabuta, Y.; Tebayashi, S.; Ueno, K.; Taketa, S.; Ishihara, A., Distribution of the tryptophan pathway-derived defensive secondary metabolites gramine and benzoxazinones in Poaceae. *Biosci Biotech Bioch* **2017**, 81, (3), 431-440.
31. Meihls, L. N.; Handrick, V.; Glauser, G.; Barbier, H.; Kaur, H.; Haribal, M. M.; Lipka, A. E.; Gershenzon, J.; Buckler, E. S.; Erb, M.; Köllner, T. G.; Jander, G., Natural Variation in Maize Aphid Resistance Is Associated with 2,4-Dihydroxy-7-Methoxy-1,4-Benzoxazin-3-One Glucoside Methyltransferase Activity. *Plant Cell* **2013**, 25, (6), 2341-2355.
32. Handrick, V.; Robert, C. A. M.; Ahern, K. R.; Zhou, S. Q.; Machado, R. A. R.; Maag, D.; Glauser, G.; Fernandez-Penny, F. E.; Chandran, J. N.; Rodgers-Melnik, E.; Schneider, B.; Buckler, E. S.; Boland, W.; Gershenzon, J.; Jander, G.; Erb, M.; Köllner, T. G., Biosynthesis of 8-O-Methylated Benzoxazinoid Defense Compounds in Maize. *Plant Cell* **2016**, 28, (7), 1682-1700.
33. Glauser, G.; Marti, G.; Villard, N.; Doyen, G. A.; Wolfender, J. L.; Turlings, T. C. J.; Erb, M., Induction and detoxification of maize 1,4-benzoxazin-3-ones by insect herbivores. *Plant J* **2011**, 68, (5), 901-911.

34. Maag, D.; Köhler, A.; Robert, C. A. M.; Frey, M.; Wolfender, J. L.; Turlings, T. C. J.; Glauser, G.; Erb, M., Highly localized and persistent induction of *Bx1*-dependent herbivore resistance factors in maize. *Plant J* **2016**, 88, (6), 976-991.
35. Cambier, V.; Hance, T.; De Hoffmann, E., Effects of 1,4-Benzoxazin-3-One Derivatives from Maize on Survival and Fecundity of *Metopolophium dirhodum* (Walker) on Artificial Diet. *J Chem Ecol* **2001**, 27, (2), 359-370.
36. Oikawa, A.; Ishihara, A.; Hasegawa, M.; Kodama, O.; Iwamura, H., Induced accumulation of 2-hydroxy-4,7-dimethoxy-1,4-benzoxazin-3-one glucoside (HDMBOA-Glc) in maize leaves. *Phytochemistry* **2001**, 56, (7), 669-675.
37. Oikawa, A.; Ishihara, A.; Tanaka, C.; Mori, N.; Tsuda, M.; Iwamura, H., Accumulation of HDMBOA-Glc is induced by biotic stresses prior to the release of MBOA in maize leaves. *Phytochemistry* **2004**, 65, (22), 2995-3001.
38. Oikawa, A.; Ishihara, A.; Iwamura, H., Induction of HDMBOA-Glc accumulation and DIMBOA-Glc 4-O-methyltransferase by jasmonic acid in poaceous plants. *Phytochemistry* **2002**, 61, (3), 331-7.
39. Li, B.; Förster, C.; Robert, C. A. M.; Züst, T.; Hu, L.; Machado, R. A. R.; Berset, J.-D.; Handrick, V.; Knauer, T.; Hensel, G.; Chen, W.; Kumlehn, J.; Yang, P.; Keller, B.; Gershenzon, J.; Jander, G.; Köllner, T. G.; Erb, M., Convergent evolution of a metabolic switch between aphid and caterpillar resistance in cereals. *Sci Adv* **2018**, 4, (12), eaat6797.
40. Makowska, B.; Bakera, B.; Rakoczy-Trojanowska, M., The genetic background of benzoxazinoid biosynthesis in cereals. *Acta Physiol Plant* **2015**, 37, (9), 176.
41. Soreng, R. J.; Peterson, P. M.; Romaschenko, K.; Davidse, G.; Teisher, J. K.; Clark, L. G.; Barbera, P.; Gillespie, L. J.; Zuloaga, F. O., A worldwide phylogenetic classification of the Poaceae (Gramineae) II: An update and a comparison of two 2015 classifications. *J Syst Evol* **2017**, 55, (4), 259-290.
42. Liu, C. J.; Deavours, B. E.; Richard, S. B.; Ferrer, J. L.; Blount, J. W.; Huhman, D.; Dixon, R. A.; Noel, J. P., Structural Basis for Dual Functionality of Isoflavonoid O-Methyltransferases in the Evolution of Plant Defense Responses. *Plant Cell* **2006**, 18, (12), 3656-3669.
43. Joe, E. J.; Kim, B. G.; An, B. C.; Chong, Y.; Ahn, J. H., Engineering of Flavonoid O-Methyltransferase for a Novel Regioselectivity. *Mol Cells* **2010**, 30, (2), 137-141.
44. Tang, Q.; Vianney, Y. M.; Weisz, K.; Grathwol, C. W.; Link, A.; Bornscheuer, U. T.; Pavlidis, I. V., Influence of Substrate Binding Residues on the Substrate Scope and Regioselectivity of a Plant O-Methyltransferase against Flavonoids. *Chemcatchem* **2020**, 12, (14), 3721-3727.
45. Greenhagen, B. T.; O'Maille, P. E.; Noel, J. P.; Chappell, J., Identifying and manipulating structural determinates linking catalytic specificities in terpene synthases. *P Natl Acad Sci USA* **2006**, 103, (26), 9826-9831.
46. Köllner, T. G.; Degenhardt, J.; Gershenzon, J., The Product Specificities of Maize Terpene Synthases TPS4 and TPS10 Are Determined Both by Active Site Amino Acids and Residues Adjacent to the Active Site. *Plants (Basel)* **2020**, 9, (5), 552.
47. Liu, H. T.; Naismith, J. H., An efficient one-step site-directed deletion, insertion, single and multiple-site plasmid mutagenesis protocol. *Bmc Biotechnol* **2008**, 8, 91.
48. Hall, T. A., BioEdit: a user-friendly biological sequence alignment editor and analysis program for Windows 95/98/NT. *Nucleic Acids Symposium Series* **1999**, 41, 95-98.
49. Kumar, S.; Stecher, G.; Tamura, K., MEGA7: Molecular Evolutionary Genetics Analysis Version 7.0 for Bigger Datasets. *Mol Biol Evol* **2016**, 33, (7), 1870-1874.
50. Waterhouse, A.; Bertoni, M.; Bienert, S.; Studer, G.; Tauriello, G.; Gumienny, R.; Heer, F. T.; de Beer, T. A. P.; Rempfer, C.; Bordoli, L.; Lepore, R.; Schwede, T., SWISS-MODEL: homology modelling of protein structures and complexes. *Nucleic Acids Res* **2018**, 46, (W1), W296-W303.
51. Trott, O.; Olson, A. J., Software News and Update AutoDock Vina: Improving the Speed and Accuracy of Docking with a New Scoring Function, Efficient Optimization, and Multithreading. *J Comput Chem* **2010**, 31, (2), 455-461.

4. Discussion

In this work, I investigated the formation and biochemical evolution of two important classes of induced specialized defense metabolites in grass species – benzoxazinoids (BXs) and flavonoids. I focused primarily on O-methyltransferases (OMTs), enzymes that transfer a methyl group to specific hydroxyl groups of these compounds; a modification that has been frequently described to enhance the activity of these compounds against attacking organisms compared to their non-O-methyl precursors. Since the individual results are largely discussed in the corresponding manuscripts, I will now highlight novel findings, discuss how our obtained results are connected and what general or further conclusions can be drawn. Moreover, I will provide additional data that shed light on the role of regiospecific enzyme catalysis in possible biological modes of action.

4.1 Evolution of OMTs in the grasses

BXs produced by the core pathway such as DIBOA-Glc and DIMBOA-Glc are widely distributed in the Poaceae family and are also found in a few dicotyledonous species (Frey et al., 2009; Kokubo et al., 2017). In contrast, late pathway products such as the N-O-methylated HDMBOA-Glc are so far only known to occur in the grasses, maize, wheat, and Job's tears (*Coix lacryma-jobi*) (Oikawa et al., 2002; Sicker and Schulz, 2002). DIMBOA-Glc 4-OMTs catalyzing the conversion of DIMBOA-Glc to HDMBOA-Glc have been identified in maize (ZmBX10, ZmBX11, ZmBX12, and ZmBX14) and wheat; however, the wheat enzyme had only been partially purified from JA-treated leaves (Oikawa et al., 2002) and the respective gene was unknown. We identified and characterized TaBX10 as functional wheat DIMBOA-Glc 4-OMT and could show that the gene encoding it is not an ortholog of maize *ZmBX10-ZmBX12*, or *ZmBX14* and therefore evolved independently of them (Manuscript I; Li et al., 2018). Interestingly, TaBX10 was able to O-methylate both DIMBOA-Glc and DIM₂BOA-Glc *in vitro*, suggesting that it likely covers a second reaction step in the BX pathway that is exclusively catalyzed by ZmBX14 in maize (Handrick et al., 2016). DIM₂BOA-Glc has been previously detected in wheat ears (Søltoft et al., 2008), and we also found both the precursor DIM₂BOA-Glc and the corresponding product HDM₂BOA-Glc in minor amounts in unchallenged leaves (Manuscript I). Thus, wheat appears to have, in principle, the entire BX pathway, and we could show that the functionality of converting DIMBOA-Glc to HDMBOA-Glc as switch between aphid and caterpillar resistance is

conserved in wheat as well (Manuscript I). However, whether HDM₂BOA-Glc formation is induced in specific plant tissues, in other wheat cultivars, or under certain conditions and plays a role in wheat defense remains to be elucidated.

The convergent evolution of the DIMBOA-Glc 4-OMTs in maize and wheat (Manuscript I) contrasts with the evolution of the BX core pathway (Makowska et al., 2015). Corresponding orthologous genes to maize *ZmBX1-ZmBX5* involved in DIBOA biosynthesis have been identified in several grass species including diploid (*T. boeoticum*) and hexaploid wheat (*T. aestivum*) (Nomura et al., 2002; Nomura et al., 2003; Nomura et al., 2007), rye (*S. cereale*) (Bakera et al., 2015; Tanwir et al., 2017), and a wild barley (*H. lechleri*) (Grün et al., 2005). Except for rye, functional similarity to the respective maize enzymes was demonstrated *in vitro* for all encoded enzymes. Thus, it was suggested that the genes of DIBOA biosynthesis diverged from a common ancestor within the grasses (Grün et al., 2005; Frey et al., 2009; Makowska et al., 2015). In addition, genes encoding BX6 and BX6-like enzymes have been isolated from wheat and rye, and phylogenetic clustering again indicates that they are orthologs of maize *ZmBX6* (Tanwir et al., 2017; Shavit et al., 2021; Sue et al., 2021). Gene orthology has also been proposed for the OMT BX7 responsible for DIMBOA-Glc formation (Bakera and Rakoczy-Trojanowska, 2020); however, the isolated rye gene *ScBX7* has not been functionally characterized and the amino acid sequence identity to *ZmBX7* is only 45%. A phylogenetic tree encompassing the *OMT* genes characterized in this thesis and other previously characterized or uncharacterized *OMT* genes of grass species shows that *ScBX7* clusters actually in a subclade with *TaBX10* and homologous genes of grass species belonging to the major BOP lineage and not with *ZmBX7* (Figure 5). This may indicate independent evolution of BX7 in rye and maize. Glucosyltransferases and β -glucosidases, which are important for BX stabilization and activation, respectively, again appear to be conserved within the Poaceae (Sue et al., 2006; Sue et al., 2011).

Thus, while the BX core pathway leading to the constitutively produced BXs DIBOA-Glc and DIMBOA-Glc is largely conserved within the Poaceae, the late decoration steps catalyzed by OMTs have likely evolved independently in different grasses. The ability to synthesize N-O-methyl derivatives such as HDMBOA-Glc appears to be a recent and, based on current knowledge, rare evolutionary adaptation. However, the fact that this happened independently in maize and wheat (Manuscript I), representatives of the two major grass clades PACMAD and BOP, emphasizes the importance of these compounds for plant defense.

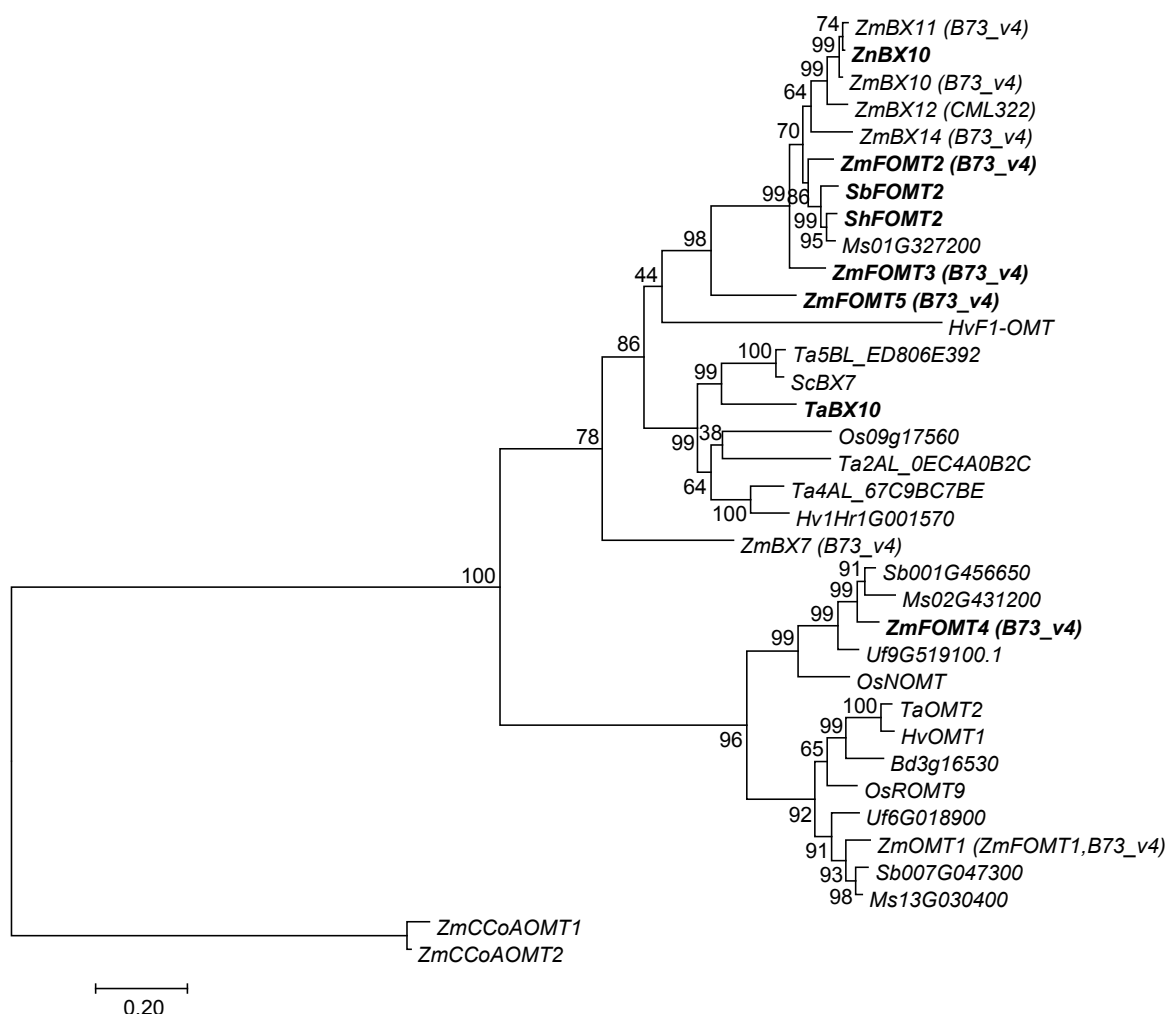


Figure 5. Phylogenetic tree of FOMT and BX OMT genes from diverse species of the Poaceae.

Genes characterized in this thesis are highlighted in bold. The tree was inferred using the maximum likelihood method based on the General Time Reversible model, including gamma distributed rate variation among sites (+G, 2.3845). Bootstrap values ($n = 1000$) are shown next to each node. The tree is drawn to scale, with branch lengths measured in the number of substitutions per site. All positions with $< 90\%$ site coverage were eliminated. *ZmCCoAOMT1* and *ZmCCoAOMT2* were used as outgroup for rooting. Species abbreviations: Bd, *Brachypodium distachyon*; Hv, *Hordeum vulgare*; Ms, *Miscanthus sinensis*; Os, *Oryza sativa*; Sc, *Secale cereale*; Sb, *Sorghum bicolor*; Ta, *Triticum aestivum*; Uf, *Urochloa fusca*; Zm, *Zea mays*; Zn, *Zea nicaraguensis*; Accession numbers: ScBX7, MG519859; for all others see Manuscripts I, II, and III.

In Manuscript II (Förster et al., 2021), we identified and characterized four maize FOMTs, termed *ZmFOMT2* and *ZmFOMT3*, *ZmFOMT4*, and *ZmFOMT5*, that catalyze the regiospecific O-methylation of various flavonoids at positions 5, 7, and 6 of the A ring, respectively, and are involved in the fungus-elicited production of a diverse O-methylflavonoid blend. Two of these FOMTs, *ZmFOMT2* and *ZmFOMT3*, were found to be closely related to the DIMBOA-Glc 4-OMTs *ZmBX10-12* and *ZmBX14* (Manuscript II;

Figure 5). Based on the characterization of homologous enzymes from sorghum (SbFOMT2), sugarcane (ShFOMT2), and teosinte (*Zea nicaraguensis*; ZnBX10), we could show that the flavonoid 5-OMT activity is more widespread in the Panicoideae subfamily of the grasses and that DIMBOA-Glc 4-OMTs likely evolved from FOMTs in the PACMAD clade of the grasses (Manuscript III; Figure 5). Regiospecific flavonoid 5-OMTs (Manuscript II and III) have not been isolated previously. However, presumably SbFOMT2 and/or another close homolog identified in our study (Manuscript III) catalyzes the formation of the sorghum phytoalexin 5-methoxyluteolinidin (Lo et al., 1996). Interestingly, we could also show that the DIMBOA-Glc 4-OMTs, ZmBX10-12 and ZnBX10, can accept flavonols such as kaempferol and quercetin as substrates and convert them into 3-O-methylated derivatives, another indicator of the close relationship between FOMTs and DIMBOA-Glc 4-OMTs (Manuscript III; Figure 5).

Despite clear evidence for the origin of the DIMBOA-Glc OMTs from the PACMAD clade (Manuscript III), the evolutionary origin of TaBX10 from the BOP clade remains unclear. We have cloned and expressed several genes homologous to *TaBX10* in *Escherichia coli*, but so far none of the enzymes showed activity with any of the tested compounds (data not shown). However, it is still likely that the ancestor of TaBX10 is also a FOMT or an OMT that utilizes another structurally similar compound (Lam et al., 2007). TaBX10 shows the highest similarity to another wheat OMT (Ta5BL_ED806E392), which shares high amino acid sequence similarity (95%) with putative ScBX7 (Figure 5). Thus, it could also be that TaBX10 and the wheat gene encoding BX7 share a common evolutionary origin.

ZmFOMT4, the other important FOMT identified in our study, is only distantly related to the gene cluster containing *ZmFOMT2* and *ZmFOMT3*, *ZmBX10-12*, and *ZmBX14* (Manuscript II; Figure 5). Instead it shares 70% amino acid identity with another flavonoid 7-OMT, OsNOMT from rice, that is involved in sakuranetin formation (Shimizu et al., 2012). Furthermore, ZmFOMT4 and OsNOMT cluster together with 3'/5'-FOMTs from maize, rice, wheat, and barley (Manuscript II; Figure 5; ZmOMT1, OsROMT9, TaOMT2, and HvOMT1) that all use the flavone tricetin as their preferred substrate (Kim et al., 2006; Zhou et al., 2006a; Zhou et al., 2006b; Zhou et al., 2008). 3'/5'-FOMTs are widely distributed in the plant kingdom and mostly share a common evolutionary origin (Kim et al., 2010). Thus, the 3'/5'-FOMTs and the related flavonoid 7-OMTs most likely evolved from a common ancestor earlier in the evolution of the grasses, whereas flavonoid 5-OMTs appear to be a later and unique adaptation in the Panicoideae that gave rise to the DIMBOA-Glc 4-OMTs in *Zea* species after gene duplication. However, the barley flavonoid 7-OMT, HvF1-OMT

(Christensen et al., 1998), shares only 30-33% amino acid identity with the two Poaceae flavonoid 7-OMTs mentioned above (ZmFOMT4 and OsNOMT) and clustered separately from them in the phylogenetic tree (Manuscript II; Figure 5), indicating convergent evolution of these enzymes. Several other grasses possess closely homologous genes to *ZmFOMT4*, but not barley (Figure 5). The flavonoid 7-OMT ancestor might have been lost during the evolution of barley.

Thus, both divergent and convergent processes play a role in the evolution of the grass (F)OMTs investigated in this work, as observed for many other OMTs belonging to the COMT class from species outside of the Poaceae (Lam et al., 2007). As with BX biosynthesis, genes for the flavonoid core pathway are well conserved in various plants (Yonekura-Sakakibara et al., 2019). Apart from flavonoid and BX OMTs, independent evolution of functionally similar enzymes (also known as repeated evolution) was found for several other classes of secondary metabolites (Pichersky and Lewinsohn, 2011 and references therein). For example, the terpene synthases (TPSs) linalool synthase from bergamot mint (*Mentha citrate*) (Crowell et al., 2002) and (*E*)- β -caryophyllene synthase from maize (Köllner et al., 2008), were more closely related to other mono- or sesquiterpene synthases, respectively, from the same species than to TPSs with the same function from other species. However, the *trans*-isoprenyl diphosphate synthases, which provide the terpene precursors (e.g. GPP and FPP) are highly conserved (Wang and Ohnuma, 1999; Wang and Ohnuma, 2000). Overall, modification reactions, including those catalyzed by OMTs, appear to evolve more frequently through convergent forces than their upstream reactions.

4.2 O-methylation of flavonoids: The position makes the difference

Modification of flavonoids by O-methylation commonly reduces the reactivity of their hydroxyl groups but makes them more lipophilic, which often seems to enhance their antimicrobial activity (Ibrahim et al., 1987; Ibrahim et al., 1998) (see chapter 1.7 for examples). We have isolated the FOMTs ZmFOMT2, SbFOMT2, and ShFOMT2 from maize, sorghum, and sugar cane, respectively, that regiospecifically O-methylate different flavonoids at position 5 of the A ring (Manuscript II and III). The resulting products showed an unusual elution pattern on C18 reversed phase-liquid-chromatography (RP-LC) columns, eluting considerably earlier than their non-O-methylated precursors (Manuscript II and III; Supplemental Figure 1). A second O-methylation largely compensates this effect, as 5,7-di-O-methylated flavonoids elute only shortly before the non-O-methylated

compound. Flavonoids that are O-methylated at any other than the 5 position are retained more by the RP-LC columns compared to the precursor (Manuscript II; Supplemental Figure 1), as expected for compounds with higher lipophilicity. We assume that the unusual elution behavior of 5-O-methylflavonoids is due to the elimination of intramolecular hydrogen bonding between the 5-hydroxyl group and the carbonyl-O at position 4, which decreases interactions of 5-O-methylated flavonoids with the alkyl chains of the C18 RP-LC column (Manuscript II). This is consistent with previous reports that the presence of a hydroxyl group at position 5 of the A ring versus hydroxyl groups at other positions, increases the lipophilicity of flavonoids (Selvaraj et al., 2015). Because of this intramolecular hydrogen bond, the 5-hydroxyl group is also considered difficult to methylate (Kim et al., 2010). Indeed, 5-O-methylated flavonoids have rarely been observed in nature and have been previously described almost exclusively from woody species such as yellow oleander (*Thevetia peruviana*), *Cistus laurifolius*, and *Citrus* (Voigtländer and Balsam, 1970; Harborne, 1977; Vogt et al., 1988; Kawaii et al., 1999).

In *in vitro* bioassays, 5-O-methylnaringenin and -apigenin showed only marginal antifungal activity against four maize fungal pathogens that was not higher than that of their non-O-methylated precursors, whereas genkwanin (7-O-methylapigenin), a product of ZmFOMT4, appeared to be a better growth inhibitor (Manuscript II). In addition to these published bioassays, I performed bioassays with a broader range of flavonoids and O-methylated derivatives against four other maize fungal pathogens (Supplemental Figures 1-5). Test compounds also included O-methylflavonoids that do not accumulate in maize but whose antifungal properties have been previously demonstrated, such as 5,7-O-dimethylflavone (Tomasbarberan et al., 1988), sakuranetin (Kodama et al., 1992), and tangeretin (Almada-Ruiz et al., 2003). A meta-analysis of these bioassays revealed that the *in vitro* antifungal activity of flavonoids appears to be related to their retention time (RT) on C18 RP-LC columns and thus to their lipophilicity (Figure 6). O-methylflavonoids with high RTs, such as sakuranetin, genkwanin and tangeretin, tend to be more effective in reducing fungal growth than more polar flavonoids (Figure 6; Supplemental Figures 1-5), such as 5-O-methylapigenin and -naringenin in particular, which may even slightly promote the growth of some fungi (Manuscript II; Figure 6). The xilonenin tautomers were the most abundant ZmFOMT2 products detected in our analyses of fungus-infected maize leaves and showed moderate antifungal activity (Manuscript II). This would fit the results of the meta-analysis (Figure 6), as the two tautomers would fall into the range of compounds with low (keto tautomer: RT = 7.0 min) and moderate (enol tautomer: RT = 8.5 min) activity.

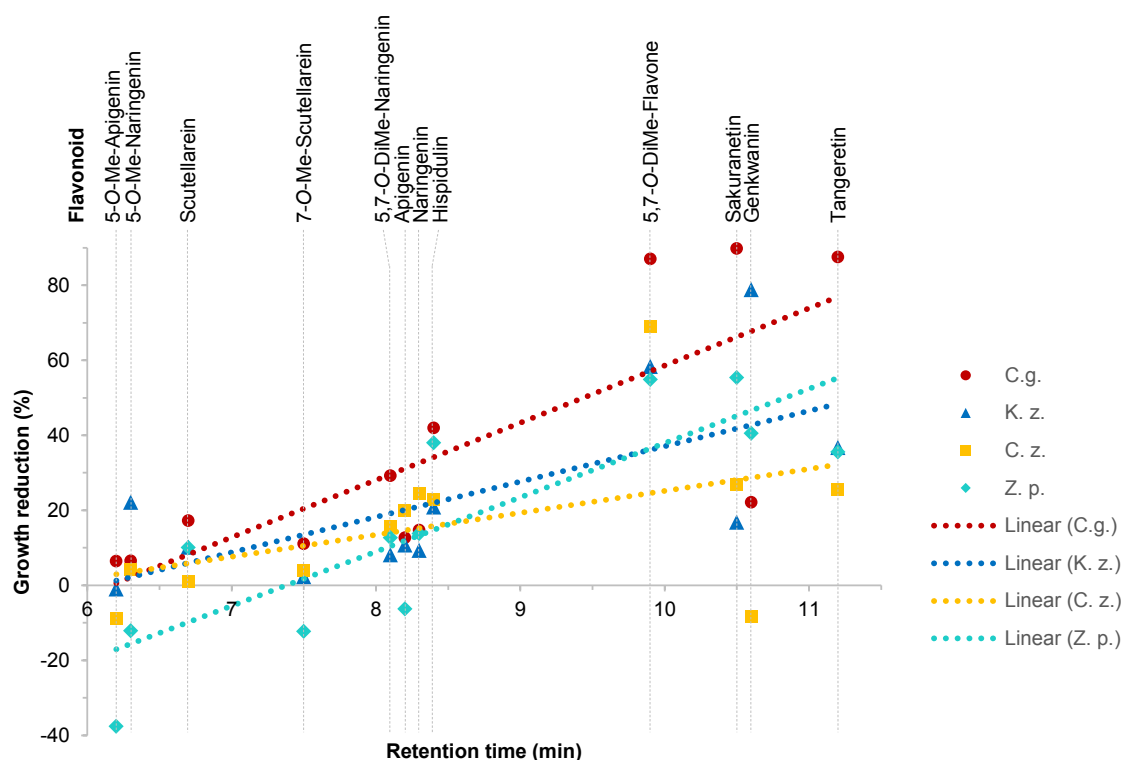


Figure 6. The *in vitro* antifungal activity of O-methyl- and non-O-methylflavonoids appears to be related to their retention time on C18 reversed phase liquid-chromatography (RP-LC) columns. Growth reduction (%) was calculated for four plant pathogenic fungi using the fungal growth (optical density at 600 nm; means, $n = 3$) in absence and presence (32 $\mu\text{g/mL}$) of different flavonoids at 40 h and blotted against the retention time of the corresponding O-methyl- and non-O-methylflavonoids on a RP-LC column. Linear regression was performed to assess a possible relationship between growth reduction and retention time ($P < 0.05$). C.g. (adjusted $R^2 = 0.581$; $F = 16.242$, $P = 0.002$); K.z. (adjusted $R^2 = 0.396$, $F = 8.223$, $P = 0.017$); C.z. (adjusted $R^2 = 0.149$, $F = 2.929$, $P = 0.118$); Z.p. (adjusted $R^2 = 0.673$, $F = 23.642$, $P < 0.001$). For graphical representation only, the retention time of 5,7-O-DiMe-Naringenin and Hispidulin was jittered by 0.1 min. The structures of the individual flavonoids are depicted in Supplemental Figure 1. The results of all fungal bioassays are shown in Supplemental Figures 2-5. Abbreviations: C.g., *Colletotrichum graminicola*; K.z., *Kabatiella zeae*; C.z., *Cercospora zeae-maydis*; Z.p., *Zymoseptoria pseudotritici*; Me, methyl; DiMe, dimethyl.

It should be noted, however, that the growth-inhibitory effects of the individual flavonoids were remarkably diverse among the different maize fungal pathogens in all our bioassays (Manuscript II; Figure 6), probably reflecting the adaptation of some fungi to these compounds. Recently, detoxification of sakuranetin by demethylation and/or conjugation to sugar moieties was shown for two rice pathogenic fungi (Katsumata et al., 2017; Katsumata et al., 2018). An analysis of the flavonoid composition after completion of my additional bioassays revealed that three of the four fungi, except *Zymoseptoria pseudotritici*, were able to demethylate both 7-O-methylated naringenin (sakuranetin) and apigenin (genkwanin),

but apparently not the corresponding 5-*O*-methylflavonoids (Supplemental Figures 6 and 7). Demethylation at the 7 position was also detected for 5,7-dimethoxynaringenin in fungus-containing assay mixtures (Supplemental Figure 6). Noteworthy, the amounts of naringenin and apigenin seem to be also reduced in the presence of some of the fungi (Supplemental Figures 6 and 7), which may indicate further detoxification reactions as previously described (Katsumata et al., 2017; Katsumata et al., 2018). These detoxification data indicate that 5- and 7-*O*-methylflavonoids are metabolized differently by fungal pathogens. Altogether, the comparisons of these specific compounds clearly show how regiospecific *O*-methylation can dramatically alter the chemical properties of flavonoids, which in turn likely alter their mode of action and thus their biological activity. Lipophilic flavonoids appear to be direct inhibitors of fungal growth, while the potential activity of more polar flavonoids is less elusive. However, it is possible that the more polar ZmFOMT2 products found in maize, especially xilonenin, may act as signaling molecules and therefore contribute more indirectly to pathogen defense (see below).

4.3 The flavonoid/*O*-methylflavonoid antifungal mode of action: direct inhibition versus signaling

The direct growth inhibition of fungal pathogens by lipophilic flavonoids such as genkwanin (Manuscript II; Figure 6; Supplemental Figures 1-5) can probably be attributed to their ability to interact with, penetrate and/or cross fungal membranes. Such interactions are mainly dependent on the lipophilicity of flavonoids and their structural features (e.g. planarity). Membrane-interacting flavonoids may localize either within the hydrophobic core or at the surface of the lipid bilayer, which alters the fluidity or rigidity of the membrane. This in turn can alter the permeability of the membrane for other compounds, influence membrane-associated proteins including influx and efflux transporters, and disturb membrane-mediated cell signaling pathways, leading to perturbation of the cell metabolism and eventually cell death (Selvaraj et al., 2015). Flavonoids that are able to cross the fungal membrane, which could be through passive diffusion and/or via membrane transport proteins (Esquivel and White, 2017; Galocha et al., 2020), can also reach specific targets inside the cell. Direct inhibition of resistance-conferring membrane proteins by lipophilic flavonoids, as proposed for bacterial efflux pumps (Maia et al., 2011), is also conceivable. Numerous studies in mammalian cell systems or artificial membrane systems have linked the ability of flavonoids to interact with membranes to their bioactivity (Hendrich, 2006;

Selvaraj et al., 2015; and references therein). In several cases, lipophilic O-methylated flavonoids had higher specific activity in direct comparison to more polar flavonoids. The O-methylflavonoids acacetin (4'-O-methylapigenin) and rhamnetin (7-O-methylquercetin), for example, were better inducers of calcein leakage from fluid egg phosphatidylcholine vesicles than apigenin, quercetin, and other non-O-methylflavonoids (Ollila et al., 2002). Gardenin B (5-demethyl tangeretin), which has a higher lipophilicity than tangeretin (Li et al., 2006), has also been shown to accumulate at higher intracellular concentrations and to have a stronger growth inhibitory effect on nonsmall cell lung cancer cells than tangeretin (Charoensinphon et al., 2013). However, another study showed that the non-O-methylated flavone chrysin had lower anti-inflammatory activity in Caco-2 cells than its derivative 5,7-O-dimethylflavone (During and Larondelle, 2013), which is expected to be a little bit less hydrophobic (see above). The authors suggested that the higher activity of 5,7-O-dimethylflavone may be due to more efficient transport through Caco-2 cell monolayers, higher metabolic stability, and consequently higher intracellular concentration and better inhibition of the NF- κ B signaling pathway (During and Larondelle, 2013). This might suggest that some degree of lipophilicity is required (e.g. to cross membranes), but that it is not the only driving force in such interactions with cells.

In contrast to the hydrophobic flavonoids included in the fungus-elicited maize flavonoid mixture, the considerably more polar ZmFOMT2 products (Manuscript II) may rather not act directly against invading fungal pathogens but modulate the plant-pathogen response by affecting signaling pathways within plant cells. It is well-known that flavonoids can act as signaling modulators in mammals, often by directly binding to and inhibiting protein and lipid kinases involved in phosphorylation-dependent signaling cascades (e.g. serine/threonine kinases such as protein kinase C (PKC), MAPKs, or phosphatidylinositol-3 kinases (PI3Ks)), leading to downstream transcriptional reprogramming (Williams et al., 2004; Mansuri et al., 2014; and references therein). To date, many studies have shown that flavonoids may modulate plant signaling pathways, including phytohormone signaling, in similar ways (Peer and Murphy, 2006; Brunetti et al., 2018; and references therein). A well-known example is the modulation of auxin (indole-3-acetic acid, IAA) transport, for instance, by flavonols such as quercetin (Peer and Murphy, 2007).

Amongst the ZmFOMT2 products (Manuscript II), xilonenin might be particularly interesting in terms of affecting signal transduction pathways. We could show that this tautomeric flavonoid derivative is formed in maize from the core pathway precursor naringenin by the consecutive action of the fungus-induced CYP ZmF2H2 and ZmFOMT2 (Manuscript II).

ZmF2H2 provides 2-hydroxynaringenin, which spontaneously interconverts between closed-ring and open-ring tautomers at room temperature (Manuscript II; Du et al., 2010a). In its open ring form, 2-hydroxynaringenin has two equivalent hydroxyl groups on the A ring that are subsequently O-methylated to xilonenin by ZmFOMT2 (Manuscript II). The two methoxy groups stabilize the chalcone-like open ring structure by precluding spontaneous ring closure. As the typical C6-C3-C6 carbon core structure is missing in xilonenin, it cannot be considered as flavonoid anymore. Chalcones are known for their diverse biological activities, which have been largely attributed to the reactive α,β -unsaturated carbonyl (enone) moiety, common to these compounds (Sahu et al., 2012). Roughly similar, xilonenin possesses a β -dicarbonyl moiety, representing an electrophilic site that could react with nucleophilic protein residues such as cysteine (thiol group), lysine (amino group), glutamic acid (carboxyl group), or tyrosine (hydroxyl group). This in turn might lead to the inhibition of regulatory or biosynthetic target enzymes or to a depletion of the redox-buffer glutathione (γ -glutamylcysteinylglycine; GSH), modulating or causing downstream signaling events (Noctor et al., 2012). As observed with most β -diketones (Urbaniak et al., 2011), the equilibrium between the ketone and enol forms of xilonenin was shifted towards the enol form (1:2 ratio; Manuscript II). In this enol form, xilonenin may also be able to complex metal ions (Urbaniak et al., 2011), which could additionally contribute to its potential to inhibit enzymes. Compounds with β -diketone groups are considered rare in nature; however, a well-known compound with this structural feature is curcumin, and many of its valuable properties for human health (e.g. anti-inflammatory and anti-carcinogenic) can be attributed to its ability to directly or indirectly regulate signaling pathways (Zhou et al., 2011; Kljun and Turel, 2017).

Thus, the structural features of xilonenin are in good agreement with a possible role as inhibitor or modulator of signal transduction pathways in plants. However, there are many other alternatives. For example, it might be also possible that xilonenin acts as direct inhibitor of fungal enzymes secreted by fungi to degrade plant cell walls, such as cellulases, xylanases, or pectinases (Skadhauge et al., 1997). Whether xilonenin and the various O-methylflavonoids detected in fungus-infected maize leaves can actually affect the activity of enzymes, modulate signal pathways, or interact with fungal membranes, respectively, remains to be elucidated.

Interestingly, there seem to be some parallels between O-methylflavonoids or xilonenin and BXs in terms of their potential mode of action. Similar to lipophilic O-methylflavonoids, hydrophobic BXs might have stronger direct antifungal activity than the more hydrophilic BXs (Wouters et al., 2016). In one study, MBOA was shown to be a better inhibitor of conidial germination and germ tube elongation of three plant fungal pathogens than its precursors. Therefore, the authors suggested that the accumulation of HDMBOA-Glc in maize leaves upon fungal infection might be advantageous due to its much faster degradation to MBOA (Oikawa et al., 2004). Xilonenin, on the other hand, shares structural features with BX hydroxamic acids, such as an electrophilic site and metal ion binding site, which are thought to be responsible for the enzyme inhibitory activity of BXs (Wouters et al., 2016). Moreover, DIMBOA has been demonstrated to induce callose in both maize (Ahmad et al., 2011) and wheat (Manuscript I) and thus to be involved in defense signaling.

A possible role of O-methylated flavonoid derivatives in plant signaling is also of interest because maize is known to produce many other phytoalexins upon fungal infection. This includes not only BXs (Oikawa et al., 2004), but also an enormous array of non-volatile terpenoids such as zealexins, kauralexins, and dolabralalexins (Huffaker et al., 2011b; Schmelz et al., 2011; Mafu et al., 2018). Especially the latter have been shown to be potent antifungal agents *in vitro* and resistance factors *in vivo* (Huffaker et al., 2011b; Schmelz et al., 2011; Mafu et al., 2018; Ding et al., 2019; Ding et al., 2020). Consistent with these earlier studies, we have observed large-scale transcriptomic and metabolomic changes in *Bipolaris maydis*-infected maize leaves beyond the mere accumulation of flavonoids, their O-methyl derivatives and late-pathway BXs (Manuscript II). It is important to consider that these different compounds and/or biosynthetic pathways could influence each other, and that flavonoids are not necessarily the predominant direct antifungal defense compounds. Such interactions have rarely been studied so far. However, it was shown, for instance, that functional CHI, a flavonoid core pathway enzyme, is necessary for terpenoid production in glandular trichomes of tomato (*Solanum lycopersicum*) (Kang et al., 2014).

4.4 Conclusion and future perspectives

O-methylation is an important mechanism contributing to the formation of the enormous structural and functional diversity of specialized metabolites in the plant kingdom. The reduced reactivity of hydroxyl groups and altered solubility of methyl ether derivatives also has implications for their metabolic stability, intracellular localization, and biological activity.

The results obtained in this work shed light on the formation of O-methylated flavonoids and BXs in grasses in the context of plant defense and unravel the evolutionary relationship and history of some of the OMTs that produce them. DIMBOA-Glc 4-OMTs have evolved independently in maize and wheat, and their ancestors in the PACMAD clade of the grasses seem to be FOMTs. Several lines of evidence demonstrate that the identified and characterized maize FOMTs are involved in the fungus-induced formation of a diverse O-methylflavonoid mixture. Moreover, the *in vitro* antifungal activity of some of the O-methylated flavonoids produced by these enzymes against maize fungal pathogens and/or their structural features suggest that these compounds should provide the plant with an advantage in defending against fungal pathogens. However, *in planta* data showing a clear relationship between the accumulation of the various O-methylflavonoids and the resistance of maize to fungal infections are not yet available. Thus, it is important to investigate this further in the future. The generation of specific biosynthetic mutant lines has already demonstrated such a relation for other maize phytoalexins, including BXs, kauralexins, and zealexins (Ahmad et al., 2011; Ding et al., 2019; Ding et al., 2020), and would therefore also be a favorable option with respect to ZmFOMT2- and ZmFOMT4-derived O-methylflavonoids. In addition, treating maize plants with low concentrations of O-methylflavonoids or xilonenin and studying their effects, for instance, on the levels of phytohormones and the other known phytoalexins might help to find out more about a possible role of these compounds in plant signaling. Determining the intra- or extracellular localization of O-methylflavonoids in maize could be another important component to elucidate the mode of action of these metabolites during fungal infection.

5. Summary

Depending on their specific ecological niches, plants produce distinct mixtures of low molecular weight specialized metabolites. Modification by O-methylation is one important mechanism that increases the structural diversity of such compounds and provides derivatives with altered chemical properties, which helps plants to cope with various ecological challenges, including defense against pathogens and insect pests. In the grass family (Poaceae), two important classes of defense metabolites are benzoxazinoids (BXs) and flavonoids. Their O-methyl derivatives often show higher specific activity against attacking organisms than their non-O-methylated precursors.

Therefore, the aims of my thesis were to identify and characterize O-methyltransferases (OMTs) in several grass species as key enzymes in the formation of O-methylated BXs and flavonoids, to investigate their evolutionary relationships, and to elucidate their possible role in plant defense.

The biosynthesis of BXs has been previously fully elucidated in maize. However, in other grass species, such as wheat, the late steps of the biosynthetic pathway have not been deciphered. These late steps lead to the valuable O-methyl derivatives including HDMBOA-Glc, which is known to be induced in wheat by herbivory. Using transcriptomic data derived from herbivore-damaged and -undamaged wheat leaves, we identified the herbivore-induced OMT gene *TaBX10*. Heterologous expression and functional characterization of the encoded enzyme *in vitro* revealed that TaBX10 catalyzes the conversion of DIMBOA-Glc and DIM₂BOA-Glc to their N-O-methyl derivatives HDMBOA-Glc and HDM₂BOA-Glc, respectively. Thus, TaBX10 was shown to be a functional homolog of the maize DIMBOA-Glc 4-OMTs ZmBX10-12 and ZmBX14. However, phylogenetic analyses demonstrated that the corresponding genes are only distantly related, suggesting convergent evolution of the DIMBOA-Glc 4-OMTs in wheat and maize. Nevertheless, we could show that their function in plant defense is conserved in wheat as well. The presence of these OMTs causes the production of HDMBOA-Glc, a resistance factor against caterpillars, while the absence of these enzymes leads to the accumulation of DIMBOA-Glc, which triggers callose deposition as a resistance factor against aphids.

A previous study showed that the O-methylflavonoid genkwanin is produced in maize following fungal infection and exhibits antifungal activity *in vitro*. This gave a first hint that O-methylated flavonoids may play a role in the defense of maize against fungal pathogens. However, the biosynthetic enzymes involved were unknown. We therefore comprehensively

investigated fungus-induced flavonoid metabolism in maize. Using association mapping and transcriptomics, we identified four maize OMT genes and a cytochrome P450 monooxygenase (CYP) gene associated with the fungus-elicited production of O-methylflavonoids. Biochemical characterization showed that the four OMT candidates ZmFOMT2 and ZmFOMT3, ZmFOMT4, and ZmFOMT5 were able to catalyze the regiospecific O-methylation of diverse flavonoids at positions 5, 7 and 6 of the A ring, respectively. The CYP candidate ZmF2H2 hydroxylated the core pathway intermediate naringenin to 2-hydroxynaringenin. Subsequent O-methylation of 2-hydroxynaringenin by ZmFOMT2 leads to the formation of a novel, tautomeric di-O-methylated flavonoid derivative termed xilonenin. Collectively, our data indicate that the identified enzymes contribute greatly to the formation of the diverse flavonoid blend detected *in planta*, which comprises 38 known and putative flavonoids and their O-methyl derivatives that are rapidly induced upon fungal infection in maize leaves. *In vitro* bioassays revealed significant but variable activity of xilonenin and other abundant O-methylated and non-O-methylated flavonoids against different maize pathogenic fungi. The 5-O-methylated flavonoids produced by ZmFOMT2 were found to be considerably less lipophilic compared to other O-methylflavonoids. I have speculated that hydrophobic flavonoids such as the 7-O-methylflavonoids produced by ZmFOMT4 are direct inhibitors of fungal growth due to their ability to interact with and/or cross fungal membranes. Xilonenin and other more polar O-methylflavonoids, on the other hand, might be more indirectly involved in plant defense by acting as signaling molecules.

Phylogenetic analyses revealed that ZmFOMT2 and ZmFOMT3 are closely related to the DIMBOA-Glc 4-OMTs (ZmBX10-12 and ZmBX14). To investigate the evolution of these maize OMTs, we identified and characterized ZmFOMT2 homologs from several other Poaceae species. We additionally isolated two functional flavonoid 5-OMTs from sorghum (SbFOMT2) and sugarcane (ShFOMT2), and a DIMBOA-Glc 4-OMT from teosinte (*Zea mays*; ZmBX10). Our findings indicate a broader distribution of flavonoid 5-OMTs compared to DIMBOA-Glc 4-OMTs in the Panicoideae subfamily of the grasses, and suggest that the DIMBOA-Glc 4-OMTs, which are so far known only from *Zea* species within the major PACMAD lineage, have evolved from a flavonoid 5-OMT ancestor. Based on sequence comparisons, homology modelling, and *in vitro* mutagenesis, we also could get first insights on the amino acid residues that determine the differential activity of these enzymes.

6. Zusammenfassung

In Abhängigkeit von ihren individuellen ökologischen Nischen produzieren Pflanzen unterschiedliche Mischungen spezialisierter Metaboliten mit niedrigem Molekulargewicht. Die Modifizierung durch O-Methylierung ist ein wichtiger Mechanismus, der die strukturelle Vielfalt solcher Verbindungen erhöht und Derivate mit veränderten chemischen Eigenschaften hervorbringt. Diese helfen den Pflanzen, verschiedene ökologische Herausforderungen zu bewältigen, einschließlich der Abwehr von Krankheitserregern und Insektenschädlingen. Zwei wichtige Klassen von Verteidigungsmetaboliten in der Familie der Gräser (Poaceae) sind Benzoxazinoide (BXs) und Flavonoide. Ihre O-Methyl-Derivate zeigen oft eine höhere spezifische Aktivität gegen angreifende Organismen als ihre nicht O-methylierten Vorläufer.

Ziel dieser Arbeit war es daher, O-Methyltransferasen (OMTs) in verschiedenen Grasarten als Schlüsselenzyme für die Bildung von O-methylierten BXs und Flavonoiden zu identifizieren und zu charakterisieren. Zudem sollten die evolutionären Beziehungen der isolierten OMTs untersucht und ihre mögliche Rolle in der Pflanzenabwehr aufgeklärt werden.

Die Biosynthese von BXs wurde in Mais bereits vollständig aufgeklärt. Bei anderen Grasarten, wie z. B. Weizen, sind die späten Schritte des Biosynthesewegs jedoch noch nicht entschlüsselt worden. Diese späten Schritte führen zu den wertvollen O-Methyl-Derivaten, einschließlich HDMBOA-Glc. Von diesem ist bekannt, dass es in Weizen durch Herbivorie induziert wird. Unter Nutzung von Transkriptomdaten, die von Herbivoren-geschädigten und -ungeschädigten Weizenblättern stammen, identifizierten wir das Herbivoren-induzierte OMT-Gen *TaBX10*. Die heterologe Expression und funktionelle Charakterisierung des kodierten Enzyms *in vitro* zeigte, dass TaBX10 die Umwandlung von DIMBOA-Glc und DIM₂BOA-Glc in ihre N-O-Methyl-derivate HDMBOA-Glc bzw. HDM₂BOA-Glc katalysiert. Folglich ist TaBX10 ein funktionelles Homolog der Mais-DIMBOA-Glc 4-OMTs ZmBX10-12 und ZmBX14. Phylogenetische Analysen zeigten jedoch, dass die entsprechenden Gene nur entfernt miteinander verwandt sind. Dies lässt auf eine konvergente Evolution der DIMBOA-Glc 4-OMTs in Weizen und Mais schließen. Dennoch konnten wir zeigen, dass ihre Funktion in der Pflanzenabwehr auch in Weizen konserviert ist. Das Vorhandensein dieser OMTs bewirkt die Produktion von HDMBOA-Glc, einem Resistenzfaktor gegen Raupen. Das Fehlen dieser Enzyme führt zur Akkumulation von DIMBOA-Glc, das die Ablagerung von Kallose als Resistenzfaktor gegen Blattläuse auslöst.

Eine frühere Studie zeigte, dass das O-Methylflavonoid Genkwanin in Mais nach einer Pilzinfektion gebildet wird und *in vitro* eine antimykotische Aktivität aufweist. Dies war ein erster Hinweis darauf, dass O-methylierte Flavonoide eine Rolle bei der Verteidigung von Mais gegen pilzliche Krankheitserreger spielen könnten. Die beteiligten biosynthetischen Enzyme waren jedoch unbekannt. Daher haben wir den durch Pilze induzierten Flavonoid-Stoffwechsel in Mais umfassend untersucht. Mithilfe von Assoziationskartierung und Transkriptomik identifizierten wir vier OMT-Gene und ein Cytochrom-P450-Monooxygenase (CYP)-Gen, welche mit der Pilz-induzierten Produktion von O-Methylflavonoiden in Verbindung stehen. Die biochemische Charakterisierung zeigte, dass die vier OMT-Kandidaten ZmFOMT2 und ZmFOMT3, ZmFOMT4 sowie ZmFOMT5 in der Lage sind, die regiospezifische O-Methylierung verschiedener Flavonoide an den Positionen 5, 7 bzw. 6 des A-Rings zu katalysieren. Der CYP-Kandidat ZmF2H2 hydroxylierte das Kernweg-Zwischenprodukt Naringenin zu 2-Hydroxynaringenin. Die anschließende O-Methylierung von 2-Hydroxynaringenin durch ZmFOMT2 führte zur Bildung eines neuartigen, tautomeren di-O-methylierten Flavonoid-Derivats, das als Xilonenin bezeichnet wurde. Insgesamt deuten die erhaltenen Daten darauf hin, dass die identifizierten Enzyme in hohem Maße zur Bildung der vielfältigen Flavonoid-Mischung beitragen, die in Pflanzen nachgewiesen wurde. Diese Mischung umfasst 38 bekannte und mutmaßliche Flavonoide und ihre O-Methyl-Derivate, welche bei einer Pilzinfektion in Maisblättern rasch induziert werden. *In-vitro*-Bioassays zeigten eine signifikante, aber unterschiedliche Aktivität von Xilonenin und anderen reichlich vorhandenen O-methylierten und nicht O-methylierten Flavonoiden gegen verschiedene Mais-pathogene Pilze. Die von ZmFOMT2 produzierten 5-O-methylierten Flavonoide erwiesen sich im Vergleich zu anderen O-Methylflavonoiden als deutlich weniger lipophil. Es ist zu vermuten, dass hydrophobe Flavonoide, wie die von ZmFOMT4 produzierten 7-O-Methylflavonoide, aufgrund ihrer Fähigkeit mit Pilzmembranen zu interagieren und/oder diese zu durchqueren, das Pilzwachstum direkt hemmen. Xilonenin und andere polarere O-Methylflavonoide könnten dagegen eher indirekt an der Pflanzenabwehr beteiligt sein, indem sie als Signalmoleküle wirken.

Im Weiteren zeigten phylogenetische Analysen, dass ZmFOMT2 und ZmFOMT3 eng mit den DIMBOA-Glc 4-OMTs (ZmBX10-12 and ZmBX14) verwandt sind. Um die Evolution dieser Mais-OMTs zu untersuchen, wurden ZmFOMT2-Homologe aus mehreren anderen Poaceae-Arten identifiziert und charakterisiert. Außerdem wurden zwei funktionelle Flavonoid-5-OMTs aus Sorghum (SbFOMT2) und Zuckerrohr (ShFOMT2) sowie eine

DIMBOA-Glc-4-OMT aus Teosinte (*Zea nicaraguensis*; ZnBX10) isoliert. Die Ergebnisse deuten auf eine größere Verbreitung von Flavonoid-5-OMTs im Vergleich zu DIMBOA-Glc-4-OMTs in der Panicoideae-Unterfamilie der Gräser hin. Das legt nahe, dass die DIMBOA-Glc-4-OMTs, die bisher nur von *Zea*-Arten innerhalb der großen PACMAD-Linie bekannt sind, sich aus einem Flavonoid-5-OMT-Vorläufer entwickelt haben. Auf der Grundlage von Sequenzvergleichen, Homologiemodellierung und *In-vitro*-Mutagenese konnten zudem erste Erkenntnisse über die Aminosäurereste gewonnen werden, welche die unterschiedliche Aktivität dieser Enzyme bestimmen.

7. References

- Ahmad, S., Veyrat, N., Gordon-Weeks, R., Zhang, Y.H., Martin, J., Smart, L., Glauser, G., Erb, M., Flors, V., Frey, M., and Ton, J. (2011). Benzoxazinoid Metabolites Regulate Innate Immunity against Aphids and Fungi in Maize. *Plant Physiol* **157**, 317-327.
- Akashi, T., Aoki, T., and Ayabe, S. (1998). Identification of a cytochrome P450 cDNA encoding (2S)-flavanone 2-hydroxylase of licorice (*Glycyrrhiza echinata* L.; Fabaceae) which represents licodione synthase and flavone synthase II. *FEBS letters* **431**, 287-290.
- Aktar, M.W., Sengupta, D., and Chowdhury, A. (2009). Impact of pesticides use in agriculture: their benefits and hazards. *Interdiscip Toxicol* **2**, 1-12.
- Al-Maharik, N. (2019). Isolation of naturally occurring novel isoflavonoids: an update. *Nat Prod Rep* **36**, 1156-1195.
- Almada-Ruiz, E., Martínez-Téllez, M.A., Hernández-Álamos, M.M., Vallejo, S., Primo-Yúfera, E., and Vargas-Arispuro, I. (2003). Fungicidal potential of methoxylated flavones from citrus for *in vitro* control of *Colletotrichum gloeosporioides*, causal agent of anthracnose disease in tropical fruits. *Pest Manag Sci* **59**, 1245-1249.
- Atanasova-Penichon, V., Pons, S., Pinson-Gadais, L., Picot, A., Marchegay, G., Bonnin-Verdal, M.N., Ducos, C., Barreau, C., Roucolle, J., Sehabiague, P., Carolo, P., and Richard-Forget, F. (2012). Chlorogenic Acid and Maize Ear Rot Resistance: A Dynamic Study Investigating *Fusarium graminearum* Development, Deoxynivalenol Production, and Phenolic Acid Accumulation. *Mol Plant Microbe In* **25**, 1605-1616.
- Bakera, B., and Rakoczy-Trojanowska, M. (2020). Isolation and structural analysis of the *Bx6* and *Bx7* genes controlling the biosynthesis of benzoxazinoids in rye (*Secale cereale* L.). *Acta Physiol Plant* **42**, 56.
- Bakera, B., Makowska, B., Groszyk, J., Niziolek, M., Orczyk, W., Bolibok-Bragoszewska, H., Hromada-Judycka, A., and Rakoczy-Trojanowska, M. (2015). Structural characteristics of *ScBx* genes controlling the biosynthesis of hydroxamic acids in rye (*Secale cereale* L.). *J Appl Genet* **56**, 287-298.
- Balmer, D., de Papajewski, D.V., Planchamp, C., Glauser, G., and Mauch-Mani, B. (2013). Induced resistance in maize is based on organ-specific defence responses. *Plant J* **74**, 213-225.
- Betsiashvili, M., Ahern, K.R., and Jander, G. (2015). Additive effects of two quantitative trait loci that confer *Rhopalosiphum maidis* (corn leaf aphid) resistance in maize inbred line Mo17. *J Exp Bot* **66**, 571-578.
- Brunetti, C., Fini, A., Sebastiani, F., Gori, A., and Tattini, M. (2018). Modulation of Phytohormone Signaling: A Primary Function of Flavonoids in Plant-Environment Interactions. *Frontiers in plant science* **9**, 1042.
- Bushman, B.S., Snook, M.E., Gerke, J.P., Szalma, S.J., Berhow, M.A., Houchins, K.E., and McMullen, M.D. (2002). Two Loci Exert Major Effects on Chlorogenic Acid Synthesis in Maize Silks. *Crop Sci* **42**, 1669-1678.
- Caasi-Lit, M.T., Tanner, G.J., Nayudu, M., and Whitecross, M.I. (2007). Isovitexin-2'-O-β-[6-O-E-p-coumaroylglucopyranoside] from UV-B irradiated Leaves of Rice, *Oryza sativa* L. Inhibits Fertility of *Helicoverpa armigera*. *Photochem Photobiol* **83**, 1167-1173.
- Cambier, V., Hance, T., and de Hoffmann, E. (1999). Non-injured Maize Contains Several 1,4-Benzoxazin-3-one Related Compounds but only as Glucoconjugates. *Phytochem Analysis* **10**, 119-126.
- Cambier, V., Hance, T., and De Hoffmann, E. (2001). Effects of 1,4-Benzoxazin-3-One Derivatives from Maize on Survival and Fecundity of *Metopolophium dirhodum* (Walker) on Artificial Diet. *J Chem Ecol* **27**, 359-370.

- Charoensinphon, N., Qiu, P.J., Dong, P., Zheng, J.K., Ngauv, P., Cao, Y., Li, S.M., Ho, C.T., and Xiao, H. (2013). 5-Demethyltangeretin inhibits human nonsmall cell lung cancer cell growth by inducing G2/M cell cycle arrest and apoptosis. *Mol Nutr Food Res* **57**, 2103-2111.
- Chen, Y.H., Gols, R., and Benrey, B. (2015). Crop Domestication and Its Impact on Naturally Selected Trophic Interactions. *Annu Rev Entomol* **60**, 35-58.
- Cheng, A.X., Han, X.J., Wu, Y.F., and Lou, H.X. (2014). The Function and Catalysis of 2-Oxoglutarate-Dependent Oxygenases Involved in Plant Flavonoid Biosynthesis. *International journal of molecular sciences* **15**, 1080-1095.
- Christensen, A.B., Gregersen, P.L., Olsen, C.E., and Collinge, D.B. (1998). A flavonoid 7-O-methyltransferase is expressed in barley leaves in response to pathogen attack. *Plant Mol Biol* **36**, 219-227.
- Cluzet, S., Mérillon, J.-M., and Ramawat, K.G. (2020). Specialized Metabolites and Plant Defence. In *Plant Defence: Biological Control*, J.-M. Mérillon and K.G. Ramawat, eds (Springer International Publishing), pp. 45-80.
- Cos, P., Ying, L., Calomme, M., Hu, J.P., Cimanga, K., Van Poel, B., Pieters, L., Vlietinck, A.J., and Vanden Berghe, D. (1998). Structure-Activity Relationship and Classification of Flavonoids as Inhibitors of Xanthine Oxidase and Superoxide Scavengers. *J Nat Prod* **61**, 71-76.
- Crowell, A.L., Williams, D.C., Davis, E.M., Wildung, M.R., and Croteau, R. (2002). Molecular cloning and characterization of a new linalool synthase. *Arch Biochem Biophys* **405**, 112-121.
- Cuevas, L., and Niemeyer, H.M. (1993). Effect of Hydroxamic Acids from Cereals on Aphid Cholinesterases. *Phytochemistry* **34**, 983-985.
- Cuevas, L., Niemeyer, H.M., and Pérez, F.J. (1990). Reaction of DIMBOA, a Resistance Factor from Cereals, with α -Chymotrypsin. *Phytochemistry* **29**, 1429-1432.
- Dawkins, R., and Krebs, J.R. (1979). Arms races between and within species. *Proc R Soc Ser B-Bio* **205**, 489-511.
- de Souza, L.P., Garbowicz, K., Brotman, Y., Tohge, T., and Fernie, A.R. (2020). The Acetate Pathway Supports Flavonoid and Lipid Biosynthesis in Arabidopsis. *Plant Physiol* **182**, 857-869.
- Deavours, B.E., Liu, C.J., Naoumkina, M.A., Tang, Y.H., Farag, M.A., Sumner, L.W., Noel, J.P., and Dixon, R.A. (2006). Functional analysis of members of the isoflavone and isoflavanone O-methyltransferase enzyme families from the model legume *Medicago truncatula*. *Plant Mol Biol* **62**, 715-733.
- Degenhardt, J. (2009). Indirect Defense Responses to Herbivory in Grasses. *Plant Physiol* **149**, 96-102.
- Dias, M.C., Pinto, D.C.G.A., and Silva, A.M.S. (2021). Plant Flavonoids: Chemical Characteristics and Biological Activity. *Molecules* **26**, 5377.
- Ding, Y., Murphy, K.M., Poretsky, E., Mafu, S., Yang, B., Char, S.N., Christensen, S.A., Saldivar, E., Wu, M.X., Wang, Q., Ji, L.X., Schmitz, R.J., Kremling, K.A., Buckler, E.S., Shen, Z.X., Briggs, S.P., Bohlmann, J., Sher, A., Castro-Falcon, G., Hughes, C.C., Huffaker, A., Zerbe, P., and Schmelz, E.A. (2019). Multiple genes recruited from hormone pathways partition maize diterpenoid defences. *Nat Plants* **5**, 1043-1056.
- Ding, Y.Z., Weckwerth, P.R., Poretsky, E., Murphy, K.M., Sims, J., Saldivar, E., Christensen, S.A., Char, S.N., Yang, B., Tong, A.D., Shen, Z.X., Kremling, K.A., Buckler, E.S., Kono, T., Nelson, D.R., Bohlmann, J., Bakker, M.G., Vaughan, M.M., Khalil, A.S., Betsiashvili, M., Dressano, K., Köllner, T.G., Briggs, S.P., Zerbe, P., Schmelz, E.A., and Huffaker, A. (2020). Genetic elucidation of interconnected antibiotic pathways mediating maize innate immunity. *Nat Plants* **6**, 1375-1388.
- Dixon, R.A. (2001). Natural products and plant disease resistance. *Nature* **411**, 843-847.
- Dixon, R.A., and Paiva, N.L. (1995). Stress-Induced Phenylpropanoid Metabolism. *Plant Cell* **7**, 1085-1097.

- Dixon, R.A., and Strack, D. (2003). Phytochemistry meets genome analysis, and beyond Phytochemistry **62**, 815-816.
- Du, Y.G., Chu, H., Chu, I.K., and Lo, C. (2010a). CYP93G2 Is a Flavanone 2-Hydroxylase Required for C-Glycosylflavone Biosynthesis in Rice. Plant Physiol **154**, 324-333.
- Du, Y.G., Chu, H., Wang, M.F., Chu, I.K., and Lo, C. (2010b). Identification of flavone phytoalexins and a pathogen-inducible flavone synthase II gene (*SbFNSII*) in sorghum. J Exp Bot **61**, 983-994.
- During, A., and Larondelle, Y. (2013). The O-methylation of chrysin markedly improves its intestinal anti-inflammatory properties: Structure-activity relationships of flavones. Biochem Pharmacol **86**, 1739-1746.
- Ejike, C.E.C.C., Gong, M., and Udenigwe, C.C. (2013). Phytoalexins from the Poaceae: Biosynthesis, function and prospects in food preservation. Food Res Int **52**, 167-177.
- Esquivel, B.D., and White, T.C. (2017). Accumulation of Azole Drugs in the Fungal Plant Pathogen *Magnaporthe oryzae* Is the Result of Facilitated Diffusion Influx. Front Microbiol **8**, 1320.
- Fahey, J.W., Zalcmann, A.T., and Talalay, P. (2001). The chemical diversity and distribution of glucosinolates and isothiocyanates among plants. Phytochemistry **56**, 5-51.
- Förster, C., Handrick, V., Ding, Y., Nakamura, Y., Paetz, C., Schneider, B., Castro-Falcón, G., Hughes, C.C., Luck, K., Poosapati, S., Kunert, G., Huffaker, A., Gershenzon, J., Schmelz, E.A., and Köllner, T.G. (2021). Biosynthesis and antifungal activity of fungus-induced O-methylated flavonoids in maize. Plant Physiol, kiab496.
- Frey, M., Schullehner, K., Dick, R., Fiesselmann, A., and Gierl, A. (2009). Benzoxazinoid biosynthesis, a model for evolution of secondary metabolic pathways in plants. Phytochemistry **70**, 1645-1651.
- Frey, M., Stettner, C., Pare, P.W., Schmelz, E.A., Tumlinson, J.H., and Gierl, A. (2000). An herbivore elicitor activates the gene for indole emission in maize. P Natl Acad Sci USA **97**, 14801-14806.
- Frey, M., Huber, K., Park, W.J., Sicker, D., Lindberg, P., Meeley, R.B., Simmons, C.R., Yalpani, N., and Gierl, A. (2003). A 2-oxoglutarate-dependent dioxygenase is integrated in DIMBOA-biosynthesis. Phytochemistry **62**, 371-376.
- Frey, M., Chomet, P., Glawischnig, E., Stettner, C., Grün, S., Winklmaier, A., Eisenreich, W., Bacher, A., Meeley, R.B., Briggs, S.P., Simcox, K., and Gierl, A. (1997). Analysis of a Chemical Plant Defense Mechanism in Grasses. Science **277**, 696-699.
- Frick, S., and Kutchan, T.M. (1999). Molecular cloning and functional expression of O-methyltransferases common to isoquinoline alkaloid and phenylpropanoid biosynthesis. Plant J **17**, 329-339.
- Galocha, M., Costa, I.V., and Teixeira, M.C. (2020). Carrier-Mediated Drug Uptake in Fungal Pathogens. Genes (Basel) **11**, 1324.
- Gang, D.R., Lavid, N., Zubieta, C., Chen, F., Beuerle, T., Lewinsohn, E., Noel, J.P., and Pichersky, E. (2002). Characterization of Phenylpropene O-Methyltransferases from Sweet Basil : Facile Change of Substrate Specificity and Convergent Evolution within a Plant O-Methyltransferase Family. Plant Cell **14**, 505-519.
- Gauthier, A., Gulick, P.J., and Ibrahim, R.K. (1998). Characterization of Two cDNA Clones Which Encode O-Methyltransferases for the Methylation of both Flavonoid and Phenylpropanoid Compounds. Arch Biochem Biophys **351**, 243-249.
- Glauser, G., Marti, G., Villard, N., Doyen, G.A., Wolfender, J.L., Turlings, T.C.J., and Erb, M. (2011). Induction and detoxification of maize 1,4-benzoxazin-3-ones by insect herbivores. Plant J **68**, 901-911.
- Grün, S., Frey, M., and Gierl, A. (2005). Evolution of the indole alkaloid biosynthesis in the genus *Hordeum*: Distribution of gramine and DIBOA and isolation of the benzoxazinoid biosynthesis genes from *Hordeum lechleri*. Phytochemistry **66**, 1264-1272.
- Hammerschmidt, R. (1999). Phytoalexins: What Have we Learned After 60 Years? Annu Rev Phytopathol **37**, 285-306.

- Handrick, V., Robert, C.A.M., Ahern, K.R., Zhou, S.Q., Machado, R.A.R., Maag, D., Glauser, G., Fernandez-Penny, F.E., Chandran, J.N., Rodgers-Melnik, E., Schneider, B., Buckler, E.S., Boland, W., Gershenzon, J., Jander, G., Erb, M., and Köllner, T.G. (2016). Biosynthesis of 8-O-Methylated Benzoxazinoid Defense Compounds in Maize. *Plant Cell* **28**, 1682-1700.
- Harborne, J.B. (1977). Flavonoids and the Evolution of the Angiosperms. *Biochem Syst Ecol* **5**, 7-22.
- Hasegawa, M., Mitsuhashi, I., Seo, S., Okada, K., Yamane, H., Iwai, T., and Ohashi, Y. (2014). Analysis on Blast Fungus-Responsive Characters of a Flavonoid Phytoalexin Sakuranetin; Accumulation in Infected Rice Leaves, Antifungal Activity and Detoxification by Fungus. *Molecules* **19**, 11404-11418.
- Heim, K.E., Tagliaferro, A.R., and Bobilya, D.J. (2002). Flavonoid antioxidants: chemistry, metabolism and structure-activity relationships. *J Nutr Biochem* **13**, 572-584.
- Hendrich, A.B. (2006). Flavonoid-membrane interactions: possible consequences for biological effects of some polyphenolic compounds. *Acta Pharmacol Sin* **27**, 27-40.
- Hodkinson, T. (2018). Evolution and Taxonomy of the Grasses (Poaceae): A Model Family for the Study of Species Rich Groups. In *Annual Plant Reviews Online*, J.A. Roberts, ed, pp. 255-294.
- Hodnick, W.F., Duval, D.L., and Pardini, R.S. (1994). Inhibition of Mitochondrial Respiration and Cyanide-stimulated Generation of Reactive Oxygen Species by Selected Flavonoids. *Biochem Pharmacol* **47**, 573-580.
- Huffaker, A., Dafoe, N.J., and Schmelz, E.A. (2011a). ZmPep1, an Ortholog of Arabidopsis Elicitor Peptide 1, Regulates Maize Innate Immunity and Enhances Disease Resistance. *Plant Physiol* **155**, 1325-1338.
- Huffaker, A., Kaplan, F., Vaughan, M.M., Dafoe, N.J., Ni, X.Z., Rocca, J.R., Alborn, H.T., Teal, P.E.A., and Schmelz, E.A. (2011b). Novel Acidic Sesquiterpenoids Constitute a Dominant Class of Pathogen-Induced Phytoalexins in Maize. *Plant Physiol* **156**, 2082-2097.
- Ibdah, M., Zhang, X.H., Schmidt, J., and Vogt, T. (2003). A Novel Mg²⁺-dependent O-Methyltransferase in the Phenylpropanoid Metabolism of *Mesembryanthemum crystallinum*. *J Biol Chem* **278**, 43961-43972.
- Ibrahim, R.K., Bruneau, A., and Bantignies, B. (1998). Plant O-methyltransferases: molecular analysis, common signature and classification. *Plant Mol Biol* **36**, 1-10.
- Ibrahim, R.K., Deluca, V., Khouri, H., Latchinian, L., Brisson, L., and Charest, P.M. (1987). Enzymology and Compartmentation of Polymethylated Flavonol Glucosides in *Chrysosplenium americanum*. *Phytochemistry* **26**, 1237-1245.
- Isman, M.B., and Duffey, S.S. (1982). Toxicity of Tomato Phenolic-Compounds to the Fruitworm, *Heliothis Zea*. *Entomol Exp Appl* **31**, 370-376.
- Itoh, N., Iwata, C., and Toda, H. (2016). Molecular cloning and characterization of a flavonoid-O-methyltransferase with broad substrate specificity and regioselectivity from *Citrus depressa*. *Bmc Plant Biol* **16**, 180.
- Jiang, N., Doseff, A.I., and Grotewold, E. (2016). Flavones: From Biosynthesis to Health Benefits. *Plants (Basel)* **5**, 27.
- Jonczyk, R., Schmidt, H., Osterrieder, A., Fiesselmann, A., Schullehner, K., Haslbeck, M., Sicker, D., Hofmann, D., Yalpani, N., Simmons, C., Frey, M., and Gierl, A. (2008). Elucidation of the Final Reactions of DIMBOA-Glucoside Biosynthesis in Maize: Characterization of Bx6 and Bx7. *Plant Physiol* **146**, 1053-1063.
- Joshi, C.P., and Chiang, V.L. (1998). Conserved sequence motifs in plant S-adenosyl-L-methionine-dependent methyltransferases. *Plant Mol Biol* **37**, 663-674.
- Kang, J.H., McRoberts, J., Shi, F., Moreno, J.E., Jones, A.D., and Howe, G.A. (2014). The Flavonoid Biosynthetic Enzyme Chalcone Isomerase Modulates Terpenoid Production in Glandular Trichomes of Tomato. *Plant Physiol* **164**, 1161-1174.

- Katsumata, S., Toshima, H., and Hasegawa, M. (2018). Xylosylated Detoxification of the Rice Flavonoid Phytoalexin Sakuranetin by the Rice Sheath Blight Fungus *Rhizoctonia solani*. *Molecules* **23**, 276.
- Katsumata, S., Hamana, K., Horie, K., Toshima, H., and Hasegawa, M. (2017). Identification of Sternbin and Naringenin as Detoxified Metabolites from the Rice Flavanone Phytoalexin Sakuranetin by *Pyricularia oryzae*. *Chem Biodivers* **14**, e1600240.
- Kawaii, S., Tomono, Y., Katase, E., Ogawa, K., and Yano, M. (1999). Quantitation of Flavonoid Constituents in *Citrus* fruits. *J Agr Food Chem* **47**, 3565-3571.
- Kim, B.G., Lee, Y., Hur, H.G., Lim, Y., and Ahn, J.H. (2006). Flavonoid 3'-O-methyltransferase from rice: cDNA cloning, characterization and functional expression. *Phytochemistry* **67**, 387-394.
- Kim, B.G., Sung, S.H., Chong, Y., Lim, Y., and Ahn, J.H. (2010). Plant Flavonoid O-Methyltransferases: Substrate Specificity and Application. *J Plant Biol* **53**, 321-329.
- Kljun, J., and Turel, I. (2017). β -Diketones as Scaffolds for Anticancer Drug Design - From Organic Building Blocks to Natural Products and Metallodrug Components. *Eur J Inorg Chem* **2017**, 1655-1666.
- Kodama, O., Miyakawa, J., Akatsuka, T., and Kiyosawa, S. (1992). Sakuranetin, a Flavanone Phytoalexin from Ultraviolet-Irradiated Rice Leaves. *Phytochemistry* **31**, 3807-3809.
- Köhler, A., Maag, D., Veyrat, N., Glauser, G., Wolfender, J.L., Turlings, T.C.J., and Erb, M. (2015). Within-plant distribution of 1,4-benzoxazin-3-ones contributes to herbivore niche differentiation in maize. *Plant Cell Environ* **38**, 1081-1093.
- Kokubo, Y., Nishizaka, M., Ube, N., Yabuta, Y., Tebayashi, S., Ueno, K., Taketa, S., and Ishihara, A. (2017). Distribution of the tryptophan pathway-derived defensive secondary metabolites gramine and benzoxazinones in Poaceae. *Biosci Biotech Bioch* **81**, 431-440.
- Köllner, T.G., Held, M., Lenk, C., Hiltbold, I., Turlings, T.C., Gershenzon, J., and Degenhardt, J. (2008). A Maize (*E*)- β -Caryophyllene Synthase Implicated in Indirect Defense Responses against Herbivores Is Not Expressed in Most American Maize Varieties. *Plant Cell* **20**, 482-494.
- Kong, C.H., Xu, X.H., Zhang, M., and Zhang, S.Z. (2010). Allelochemical triclin in rice hull and its aurone isomer against rice seedling rot disease. *Pest Manag Sci* **66**, 1018-1024.
- Kumar, S., and Pandey, A.K. (2013). Chemistry and Biological Activities of Flavonoids: An Overview. *The Scientific World Journal* **2013**, 162750.
- Lam, K.C., Ibrahim, R.K., Behdad, B., and Dayanandan, S. (2007). Structure, function, and evolution of plant O-methyltransferases. *Genome* **50**, 1001-1013.
- Lee, Y.J., Kim, B.G., Chong, Y., Lim, Y., and Ahn, J.H. (2008). Cation dependent O-methyltransferases from rice. *Planta* **227**, 641-647.
- Li, B., Förster, C., Robert, C.A.M., Züst, T., Hu, L., Machado, R.A.R., Berset, J.-D., Handrick, V., Knauer, T., Hensel, G., Chen, W., Kumlehn, J., Yang, P., Keller, B., Gershenzon, J., Jander, G., Köllner, T.G., and Erb, M. (2018). Convergent evolution of a metabolic switch between aphid and caterpillar resistance in cereals. *Sci Adv* **4**, eaat6797.
- Li, S.M., Lo, C.Y., and Ho, C.T. (2006). Hydroxylated Polymethoxyflavones and Methylated Flavonoids in Sweet Orange (*Citrus sinensis*) Peel. *J Agr Food Chem* **54**, 4176-4185.
- Liu, C.J., Deavours, B.E., Richard, S.B., Ferrer, J.L., Blount, J.W., Huhman, D., Dixon, R.A., and Noel, J.P. (2006). Structural Basis for Dual Functionality of Isoflavonoid O-Methyltransferases in the Evolution of Plant Defense Responses. *Plant Cell* **18**, 3656-3669.
- Liu, X., Wang, Y., Chen, Y., Xu, S., Gong, Q., Zhao, C., Cao, J., and Sun, C. (2020). Characterization of a Flavonoid 3'/5'/7-O-Methyltransferase from *Citrus reticulata* and Evaluation of the In Vitro Cytotoxicity of Its Methylated Products. *Molecules* **25**, 858.
- Lo, S.C., Weiergang, I., Bonham, C., Hipkind, J., Wood, K., and Nicholson, R.L. (1996). Phytoalexin accumulation in sorghum: Identification of a methyl ether of luteolinidin. *Physiol Mol Plant P* **49**, 21-31.

- Lo, S.C.C., De Verdier, K., and Nicholson, R.L. (1999). Accumulation of 3-deoxyanthocyanidin phytoalexins and resistance to *Colletotrichum sublineolum* in sorghum. *Physiol Mol Plant P* **55**, 263-273.
- Loayza-Muro, R., Figueroa, C.C., and Niemeyer, H.M. (2000). Effect of Two Wheat Cultivars Differing in Hydroxamic Acid Concentration on Detoxification Metabolism in the Aphid *Sitobion avenae*. *J Chem Ecol* **26**, 2725-2736.
- Maag, D., Köhler, A., Robert, C.A.M., Frey, M., Wolfender, J.L., Turlings, T.C.J., Glauser, G., and Erb, M. (2016). Highly localized and persistent induction of *Bx1*-dependent herbivore resistance factors in maize. *Plant J* **88**, 976-991.
- Maffei, M.E., Arimura, G.I., and Mithöfer, A. (2012). Natural elicitors, effectors and modulators of plant responses. *Nat Prod Rep* **29**, 1288-1303.
- Mafu, S., Ding, Y.Z., Murphy, K.M., Yaacoobi, O., Addison, J.B., Wang, Q., Shen, Z.X., Briggs, S.P., Bohlmann, J., Castro-Falcon, G., Hughes, C.C., Betsiashvili, M., Huffaker, A., Schmelz, E.A., and Zerbe, P. (2018). Discovery, Biosynthesis and Stress-Related Accumulation of Dolabradiene-Derived Defenses in Maize. *Plant Physiol* **176**, 2677-2690.
- Maia, G.L., Falcão-Silva, V.D.S., Aquino, P.G., de Araújo-Júnior, J.X., Tavares, J.F., da Silva, M.S., Rodrigues, L.C., de Siqueira-Júnior, J.P., and Barbosa-Filho, J.M. (2011). Flavonoids from *Praxelis clematidea* R.M. King and Robinson modulate bacterial drug resistance. *Molecules* **16**, 4828-4835.
- Makowska, B., Bakera, B., and Rakoczy-Trojanowska, M. (2015). The genetic background of benzoxazinoid biosynthesis in cereals. *Acta Physiol Plant* **37**, 176.
- Mansuri, M.L., Parihar, P., Solanki, I., and Parihar, M.S. (2014). Flavonoids in modulation of cell survival signalling pathways. *Genes Nutr* **9**, 400.
- Marais, J.P.J., Deavours, B., Dixon, R.A., and Ferreira, D. (2006). The Stereochemistry of Flavonoids. In *The Science of Flavonoids*, E. Grotewold, ed (Springer New York), pp. 1-46.
- Maresh, J., Zhang, J., and Lynn, D.G. (2006). The Innate Immunity of Maize and the Dynamic Chemical Strategies Regulating Two-Component Signal Transduction in *Agrobacterium tumefaciens*. *Acs Chem Biol* **1**, 165-175.
- Marmion, C.J., Parker, J.P., and Nolan, K.B. (2013). Hydroxamic Acids: An Important Class of Metalloenzyme Inhibitors. In *Comprehensive Inorganic Chemistry II: From Elements to Applications*, J. Reedijk and K. Poepelmeier, eds (Elsevier), pp. 683-708.
- Martens, S., and Mithöfer, A. (2005). Flavones and flavone synthases. *Phytochemistry* **66**, 2399-2407.
- Marti, G., Erb, M., Boccard, J., Glauser, G., Doyen, G.R., Villard, N., Robert, C.A.M., Turlings, T.C.J., Rudaz, S., and Wolfender, J.L. (2013). Metabolomics reveals herbivore-induced metabolites of resistance and susceptibility in maize leaves and roots. *Plant Cell Environ* **36**, 621-639.
- Meihls, L.N., Handrick, V., Glauser, G., Barbier, H., Kaur, H., Haribal, M.M., Lipka, A.E., Gershenzon, J., Buckler, E.S., Erb, M., Köllner, T.G., and Jander, G. (2013). Natural Variation in Maize Aphid Resistance Is Associated with 2,4-Dihydroxy-7-Methoxy-1,4-Benzoxazin-3-One Glucoside Methyltransferase Activity. *Plant Cell* **25**, 2341-2355.
- Mierziak, J., Kostyn, K., and Kulma, A. (2014). Flavonoids as Important Molecules of Plant Interactions with the Environment. *Molecules* **19**, 16240-16265.
- Mithöfer, A., and Boland, W. (2012). Plant Defense Against Herbivores: Chemical Aspects. *Annual Review of Plant Biology* **63**, 431-450.
- Morohashi, K., Casas, M.I., Ferreyra, L.F., Mejía-Guerra, M.K., Pourcel, L., Yilmaz, A., Feller, A., Carvalho, B., Emiliani, J., Rodriguez, E., Pellegrinet, S., McMullen, M., Casati, P., and Grotewold, E. (2012). A Genome-Wide Regulatory Framework Identifies Maize *Pericarp Color1* Controlled Genes. *Plant Cell* **24**, 2745-2764.
- Mukanganyama, S., Figueroa, C.C., Hasler, J.A., and Niemeyer, H.M. (2003). Effects of DIMBOA on detoxification enzymes of the aphid *Rhopalosiphum padi* (Homoptera : Aphididae). *J Insect Physiol* **49**, 223-229.

- Murata, K., Kitano, T., Yoshimoto, R., Takata, R., Ube, N., Ueno, K., Ueno, M., Yabuta, Y., Teraishi, M., Holland, C.K., Jander, G., Okumoto, Y., Mori, N., and Ishihara, A. (2020). Natural variation in the expression and catalytic activity of a naringenin 7-O-methyltransferase influences antifungal defenses in diverse rice cultivars. *Plant J* **101**, 1103-1117.
- Murphy, K.M., and Zerbe, P. (2020). Specialized diterpenoid metabolism in monocot crops: Biosynthesis and chemical diversity. *Phytochemistry* **172**, 112289.
- Nicholson, R.L., and Hammerschmidt, R. (1992). Phenolic-Compounds and Their Role in Disease Resistance. *Annu Rev Phytopathol* **30**, 369-389.
- Nicholson, R.L., Kollipara, S.S., Vincent, J.R., Lyons, P.C., and Cadenagomez, G. (1987). Phytoalexin synthesis by the sorghum mesocotyl in response to infection by pathogenic and nonpathogenic fungi. *P Natl Acad Sci USA* **84**, 5520-5524.
- Niculaes, C., Abramov, A., Hannemann, L., and Frey, M. (2018). Plant Protection by Benzoxazinoids—Recent Insights into Biosynthesis and Function. *Agronomy* **8**, 143.
- Niemeyer, H.M. (1988). Hydroxamic Acids (4-Hydroxy-1,4-Benzoxazin-3-Ones), Defense Chemicals in the Gramineae. *Phytochemistry* **27**, 3349-3358.
- Niemeyer, H.M. (2009). Hydroxamic Acids Derived from 2-Hydroxy-2H-1,4-Benzoxazin-3(4H)-one: Key Defense Chemicals of Cereals. *J Agr Food Chem* **57**, 1677-1696.
- Noctor, G., Mhamdi, A., Chaouch, S., Han, Y., Neukermans, J., Marquez-Garcia, B., Queval, G., and Foyer, C.H. (2012). Glutathione in plants: an integrated overview. *Plant Cell Environ* **35**, 454-484.
- Noel, J.P., Dixon, R.A., Pichersky, E., Zubieta, C., and Ferrer, J.L. (2003). Structural, functional, and evolutionary basis for methylation of plant small molecules. In *Integrative Phytochemistry: From Ethnobotany to Molecular Ecology*, J.T. Romeo, ed (Elsevier), pp. 37-58.
- Noman, A., Aqeel, M., and Lou, Y.G. (2019). PRRs and NB-LRRs: From Signal Perception to Activation of Plant Innate Immunity. *International journal of molecular sciences* **20**, 1882.
- Nomura, T., Ishihara, A., Iwamura, H., and Endo, T.R. (2007). Molecular characterization of benzoxazinone-deficient mutation in diploid wheat. *Phytochemistry* **68**, 1008-1016.
- Nomura, T., Ishihara, A., Imaishi, H., Endo, T.R., Ohkawa, H., and Iwamura, H. (2002). Molecular characterization and chromosomal localization of cytochrome P450 genes involved in the biosynthesis of cyclic hydroxamic acids in hexaploid wheat. *Mol Genet Genomics* **267**, 210-217.
- Nomura, T., Ishihara, A., Imaishi, H., Ohkawa, H., Endo, T.R., and Iwamura, H. (2003). Rearrangement of the genes for the biosynthesis of benzoxazinones in the evolution of Triticeae species. *Planta* **217**, 776-782.
- Oikawa, A., Ishihara, A., and Iwamura, H. (2002). Induction of HDMBOA-Glc accumulation and DIMBOA-Glc 4-O-methyltransferase by jasmonic acid in poaceous plants. *Phytochemistry* **61**, 331-337.
- Oikawa, A., Ishihara, A., Hasegawa, M., Kodama, O., and Iwamura, H. (2001). Induced accumulation of 2-hydroxy-4,7-dimethoxy-1,4-benzoxazin-3-one glucoside (HDMBOA-Glc) in maize leaves. *Phytochemistry* **56**, 669-675.
- Oikawa, A., Ishihara, A., Tanaka, C., Mori, N., Tsuda, M., and Iwamura, H. (2004). Accumulation of HDMBOA-Glc is induced by biotic stresses prior to the release of MBOA in maize leaves. *Phytochemistry* **65**, 2995-3001.
- Ollila, F., Halling, K., Vuorela, P., Vuorela, H., and Slotte, J.P. (2002). Characterization of Flavonoid-Biomembrane Interactions. *Arch Biochem Biophys* **399**, 103-108.
- Pappas, M.L., Baptista, P., Broufas, G.D., Dalakouras, A., Djibbi, W., Flors, V., Guerfali, M.M., Khayl, S., Mentag, R., Pastor, V., Pereira, J.A., Sánchez-Bel, P., and Papadopolou, K. (2020). Biological and Molecular Control Tools in Plant Defense. In *Plant Defence: Biological Control*, J.-M. Méillon and K.G. Ramawat, eds (Springer International Publishing), pp. 3-43.
- Paxton, J.D. (1980). A New Working Definition of the Term "Phytoalexin". *Plant Dis* **64**, 734.

- Pedras, M.S., and Yaya, E.E.** (2015). Plant Chemical Defenses: Are all Constitutive Antimicrobial Metabolites Phytoanticipins? *Nat Prod Commun* **10**, 209-218.
- Peer, W.A., and Murphy, A.S.** (2006). Flavonoids as Signal Molecules: Targets of Flavonoid Action. In *The Science of Flavonoids*, E. Grotewold, ed (Springer, New York, NY), pp. 239-268.
- Peer, W.A., and Murphy, A.S.** (2007). Flavonoids and auxin transport: modulators or regulators? *Trends Plant Sci* **12**, 556-563.
- Pentzold, S., Zagrobelny, M., Rook, F., and Bak, S.** (2014). How insects overcome two-component plant chemical defence: plant β -glucosidases as the main target for herbivore adaptation. *Biol Rev* **89**, 531-551.
- Perez, F.J., and Niemeyer, H.M.** (1989). Reaction of DIMBOA, a Resistance Factor from Cereals, with Papain. *Phytochemistry* **28**, 1597-1600.
- Pichersky, E., and Lewinsohn, E.** (2011). Convergent Evolution in Plant Specialized Metabolism. *Annu Rev Plant Biol* **62**, 549-566.
- Qu, L.J., Li, S.A., and Xing, S.F.** (2010). Methylation of phytohormones by the SABATH methyltransferases. *Chinese Sci Bull* **55**, 2211-2218.
- Rakwal, R., Tamogami, S., and Kodama, O.** (1996). Role of Jasmonic Acid as a Signaling Molecule in Copper Chloride-elicited Rice Phytoalexin Production. *Biosci Biotech Bioch* **60**, 1046-1048.
- Ramawat, K.G., and Goyal, S.** (2020). Co-evolution of Secondary Metabolites During Biological Competition for Survival and Advantage: An Overview. In *Co-Evolution of Secondary Metabolites*, J.-M. Mérillon and K.G. Ramawat, eds (Springer International Publishing), pp. 3-17.
- Reifschneider, F.J., and Arny, D.C.** (1979). A liquid medium for the production of *Kabatiella zeae* conidia. *Can J Microbiol* **25**, 1100-1102.
- Reimann, J.E., and Byerrum, R.U.** (1964). Studies on the Biosynthesis of 2,4-Dihydroxy-7-Methoxy-2h-1,4-Benzoxazin-3-One. *Biochemistry-U.S* **3**, 847-851.
- Sahu, N.K., Balbhadra, S.S., Choudhary, J., and Kohli, D.V.** (2012). Exploring Pharmacological Significance of Chalcone Scaffold: A Review. *Curr Med Chem* **19**, 209-225.
- Savary, S., Willcoquet, L., Pethybridge, S.J., Esker, P., McRoberts, N., and Nelson, A.** (2019). The global burden of pathogens and pests on major food crops. *Nat Ecol Evol* **3**, 430-439.
- Sawada, Y., and Ayabe, S.I.** (2005). Multiple mutagenesis of P450 isoflavonoid synthase reveals a key active-site residue. *Biochem Bioph Res Co* **330**, 907-913.
- Schmelz, E.A., Kaplan, F., Huffaker, A., Dafoe, N.J., Vaughan, M.M., Ni, X.Z., Rocca, J.R., Alborn, H.T., and Teal, P.E.** (2011). Identity, regulation, and activity of inducible diterpenoid phytoalexins in maize. *P Natl Acad Sci USA* **108**, 5455-5460.
- Schröder, G., Wehinger, E., and Schröder, J.** (2002). Predicting the substrates of cloned plant O-methyltransferases. *Phytochemistry* **59**, 1-8.
- Scordia, D., and Cosentino, S.L.** (2019). Perennial Energy Grasses: Resilient Crops in a Changing European Agriculture. *Agriculture* **9**, 169.
- Selvaraj, S., Krishnaswamy, S., Devashya, V., Sethuraman, S., and Krishnan, U.M.** (2015). Influence of membrane lipid composition on flavonoid-membrane interactions: Implications on their biological activity. *Prog Lipid Res* **58**, 1-13.
- Seybold, H., Trempel, F., Ranf, S., Scheel, D., Romeis, T., and Lee, J.** (2014). Ca^{2+} signalling in plant immune response: from pattern recognition receptors to Ca^{2+} decoding mechanisms. *New Phytol* **204**, 782-790.
- Sharma, A., Kumar, V., Shahzad, B., Tanveer, M., Sidhu, G.P.S., Handa, N., Kohli, S.K., Yadav, P., Bali, A.S., Parihar, R.D., Dar, O.I., Singh, K., Jasrotia, S., Bakshi, P., Ramakrishnan, M., Kumar, S., Bhardwaj, R., and Thukral, A.K.** (2019). Worldwide pesticide usage and its impacts on ecosystem. *Sn Appl Sci* **1**, 1446.

- Shavit, R., Batyrshina, Z.S., Yaakov, B., Florean, M., Köllner, T.G., and Tzin, V. (2021). The wheat dioxygenase BX6 is involved in the formation of benzoxazinoids *in planta* and contributes to plant defense against insect herbivores. Preprint at bioRxiv: <https://doi.org/10.1101/2021.09.25.461767>.
- Shimizu, T., Lin, F.Q., Hasegawa, M., Okada, K., Nojiri, H., and Yamane, H. (2012). Purification and Identification of Naringenin 7-O-Methyltransferase, a Key Enzyme in Biosynthesis of Flavonoid Phytoalexin Sakuranetin in Rice. *J Biol Chem* **287**, 19315-19325.
- Sicker, D., and Schulz, M. (2002). Benzoxazinones in plants: Occurrence, synthetic access, and biological activity. In *Studies in Natural Products Chemistry: Bioactive Natural Products (Part H)*, Atta-ur-Rahman, ed (Elsevier), pp. 185-232.
- Simmonds, M.S.J. (2003). Flavonoid-insect interactions: recent advances in our knowledge. *Phytochemistry* **64**, 21-30.
- Simmonds, M.S.J., and Stevenson, P.C. (2001). Effects of Isoflavonoids from *Cicer* on Larvae of *Helicoverpa armigera*. *J Chem Ecol* **27**, 965-977.
- Skadhauge, B., Thomsen, K.K., and von Wettstein, D. (1997). The role of the barley testa layer and its flavonoid content in resistance to *Fusarium* infections. *Hereditas* **126**, 147-160.
- Snyder, B.A., and Nicholson, R.L. (1990). Synthesis of Phytoalexins in Sorghum as a Site-Specific Response to Fungal Ingress. *Science* **248**, 1637-1639.
- Søltoft, M., Jørgensen, L.N., Svensmark, B., and Fomsgaard, I.S. (2008). Benzoxazinoid concentrations show correlation with Fusarium Head Blight resistance in Danish wheat varieties. *Biochem Syst Ecol* **36**, 245-259.
- Song, J., Liu, H., Zhuang, H.F., Zhao, C.X., Xu, Y.X., Wu, S.B., Qi, J.F., Li, J., Hettenhausen, C., and Wu, J.Q. (2017). Transcriptomics and Alternative Splicing Analyses Reveal Large Differences between Maize Lines B73 and Mo17 in Response to Aphid *Rhopalosiphum padi* Infestation. *Frontiers in plant science* **8**, 1738.
- Soreng, R.J., Peterson, P.M., Romaschenko, K., Davidse, G., Teisher, J.K., Clark, L.G., Barbera, P., Gillespie, L.J., and Zuloaga, F.O. (2017). A worldwide phylogenetic classification of the Poaceae (Gramineae) II: An update and a comparison of two 2015 classifications. *J Syst Evol* **55**, 259-290.
- Stobiecki, M., and Kachlicki, P. (2006). Isolation and Identification of Flavonoids. In *The Science of Flavonoids*, E. Grotewold, ed (Springer New York), pp. 47-69.
- Stukenbrock, E.H., Quaedvlieg, W., Javan-Nikhah, M., Zala, M., Crous, P.W., and McDonald, B.A. (2012). *Zymoseptoria ardabiliae* and *Z. pseudotritici*, two progenitor species of the *septoria tritici* leaf blotch fungus *Z. tritici* (synonym: *Mycosphaerella graminicola*). *Mycologia* **104**, 1397-1407.
- Stukenbrock, E.H., Bataillon, T., Dutheil, J.Y., Hansen, T.T., Li, R.Q., Zala, M., McDonald, B.A., Wang, J., and Schierup, M.H. (2011). The making of a new pathogen: Insights from comparative population genomics of the domesticated wheat pathogen *Mycosphaerella graminicola* and its wild sister species. *Genome Res* **21**, 2157-2166.
- Sue, M., Nakamura, C., and Nomura, T. (2011). Dispersed Benzoxazinone Gene Cluster: Molecular Characterization and Chromosomal Localization of Glucosyltransferase and Glucosidase Genes in Wheat and Rye. *Plant Physiol* **157**, 985-997.
- Sue, M., Fujii, M., and Fujimaki, T. (2021). Increased benzoxazinoid (Bx) levels in wheat seedlings via jasmonic acid treatment and etiolation and their effects on Bx genes including Bx6. *Biochem Biophys Rep* **27**, 101059.
- Sue, M., Yamazaki, K., Yajima, S., Nomura, T., Matsukawa, T., Iwamura, H., and Miyamoto, T. (2006). Molecular and Structural Characterization of Hexameric β -d-Glucosidases in Wheat and Rye. *Plant Physiol* **141**, 1237-1247.
- Tanwir, F., Dionisio, G., Adhikari, K.B., Fomsgaard, I.S., and Gregersen, P.L. (2017). Biosynthesis and chemical transformation of benzoxazinoids in rye during seed germination and the identification of a rye Bx6-like gene. *Phytochemistry* **140**, 95-107.

- Tipton, C.L., and Buell, E.L. (1970). Ferric Iron Complexes of Hydroxamic Acids from Maize. *Phytochemistry* **9**, 1215-1217.
- Tohge, T., de Souza, L.P., and Fernie, A.R. (2017). Current understanding of the pathways of flavonoid biosynthesis in model and crop plants. *J Exp Bot* **68**, 4013-4028.
- Tomasbarberan, F.A., Msonthi, J.D., and Hostettmann, K. (1988). Antifungal Epicuticular Methylated Flavonoids from *Helichrysum Nitens*. *Phytochemistry* **27**, 753-755.
- Tzin, V., Lindsay, P.L., Christensen, S.A., Meihls, L.N., Blue, L.B., and Jander, G. (2015). Genetic mapping shows intraspecific variation and transgressive segregation for caterpillar-induced aphid resistance in maize. *Mol Ecol* **24**, 5739-5750.
- Ube, N., Katsuyama, Y., Kariya, K., Tebayashi, S., Sue, M., Tohnooka, T., Ueno, K., Taketa, S., and Ishihara, A. (2021). Identification of methoxychalcones produced in response to CuCl₂ treatment and pathogen infection in barley. *Phytochemistry* **184**, 112650.
- Ullah, C., Unsicker, S.B., Fellenberg, C., Constabel, C.P., Schmidt, A., Gershenzon, J., and Hammerbacher, A. (2017). Flavan-3-ols Are an Effective Chemical Defense against Rust Infection. *Plant Physiol* **175**, 1560-1578.
- Urbaniak, W., Jurek, K., Witt, K., and Goraczko, A.J. (2011). Properties and application of diketones and their derivatives. *Chemik* **65**, 273-282.
- VanEtten, H.D., Mansfield, J.W., Bailey, J.A., and Farmer, E.E. (1994). Two Classes of Plant Antibiotics: Phytoalexins versus "Phytoanticipins". *Plant Cell* **6**, 1191-1192.
- Vogt, T., Gulz, P.G., and Wray, V. (1988). Epicuticular 5-O-Methyl Flavonols from *Cistus Laurifolius*. *Phytochemistry* **27**, 3712-3713.
- Voigtländer, H.-W., and Balsam, G. (1970). Apigenin-5-methyläther, ein neues Flavon aus *Thevetia peruviana*. *Arch Pharm* **303**, 785-864.
- von Rad, U., Hüttel, R., Lottspeich, F., Gierl, A., and Frey, M. (2001). Two glucosyltransferases are involved in detoxification of benzoxazinoids in maize. *Plant J* **28**, 633-642.
- Waiss, A.C., Chan, B.G., Elliger, C.A., Wiseman, B.R., Mcmillian, W.W., Widstrom, N.W., Zuber, M.S., and Keaster, A.J. (1979). Maysin, a Flavone Glycoside from Corn Silks with Antibiotic-Activity toward Corn Earworm. *J Econ Entomol* **72**, 256-258.
- Wang, K., and Ohnuma, S. (1999). Chain-length determination mechanism of isoprenyl diphosphate synthases and implications for molecular evolution. *Trends Biochem Sci* **24**, 445-451.
- Wang, K.C., and Ohnuma, S. (2000). Isoprenyl diphosphate synthases. *Bba-Mol Cell Biol L* **1529**, 33-48.
- Wang, W.X., Li, Y.Y., Dang, P.Q., Zhao, S.J., Lai, D.W., and Zhou, L.G. (2018). Rice Secondary Metabolites: Structures, Roles, Biosynthesis, and Metabolic Regulation. *Molecules* **23**, 3098.
- Williams, C.A., and Grayer, R.J. (2004). Anthocyanins and other flavonoids. *Nat Prod Rep* **21**, 539-573.
- Williams, R.J., Spencer, J.P., and Rice-Evans, C. (2004). Flavonoids: antioxidants or signalling molecules? *Free Radic Biol Med* **36**, 838-849.
- Winkel, B.S.J. (2006). The Biosynthesis of Flavonoids. In *The Science of Flavonoids*, E. Grotewold, ed (Springer New York), pp. 71-95.
- Wiseman, B.R., Snook, M.E., Isenhour, D.J., Mihm, J.A., and Widstrom, N.W. (1992). Relationship between Growth of Corn-Earworm and Fall Armyworm Larvae (Lepidoptera, Noctuidae) and Maysin Concentration in Corn Silks. *J Econ Entomol* **85**, 2473-2477.
- Wouters, F.C., Gershenzon, J., and Vassao, D.G. (2016). Benzoxazinoids: Reactivity and Modes of Action of a Versatile Class of Plant Chemical Defenses. *J Brazil Chem Soc* **27**, 1379-1397.
- Yonekura-Sakakibara, K., Higashi, Y., and Nakabayashi, R. (2019). The Origin and Evolution of Plant Flavonoid Metabolism. *Frontiers in plant science* **10**, 943.
- Zhan, J.S., Thrall, P.H., and Burdon, J.J. (2014). Achieving sustainable plant disease management through evolutionary principles. *Trends Plant Sci* **19**, 570-575.

- Zhang, Y., De Stefano, R., Robine, M., Butelli, E., Bulling, K., Hill, L., Rejzek, M., Martin, C., and Schoonbeek, H.J.** (2015). Different Reactive Oxygen Species Scavenging Properties of Flavonoids Determine Their Abilities to Extend the Shelf Life of Tomato. *Plant Physiol* **169**, 1568-1583.
- Zhou, H.Y., Beevers, C.S., and Huang, S.L.** (2011). Targets of curcumin. *Curr Drug Targets* **12**, 332-347.
- Zhou, J.M., and Ibrahim, R.K.** (2010). Tricin-a potential multifunctional nutraceutical. *Phytochem Rev* **9**, 413-424.
- Zhou, J.M., Fukushi, Y., Wang, X.F., and Ibrahim, R.K.** (2006a). Characterization of a Novel Flavone O-Methyltransferase Gene in Rice. *Nat Prod Commun* **1**, 981-984.
- Zhou, J.M., Fukushi, Y., Wollenweber, E., and Ibrahim, R.K.** (2008). Characterization of Two O-Methyltransferase-like Genes in Barley and Maize. *Pharm Biol* **46**, 26-34.
- Zhou, J.M., Gold, N.D., Martin, V.J.J., Wollenweber, E., and Ibrahim, R.K.** (2006b). Sequential O-methylation of tricetin by a single gene product in wheat. *Biochimica et Biophysica Acta (BBA) - General Subjects* **1760**, 1115-1124.
- Zhou, J.M., Lee, E., Kanapathy-Sinnaiaha, F., Park, Y., Kornblatt, J.A., Lim, Y., and Ibrahim, R.K.** (2010). Structure-function relationships of wheat flavone O-methyltransferase: Homology modeling and site-directed mutagenesis. *Bmc Plant Biol* **10**, 156.
- Zubieta, C., He, X.Z., Dixon, R.A., and Noel, J.P.** (2001). Structures of two natural product methyltransferases reveal the basis for substrate specificity in plant O-methyltransferases. *Nat Struct Biol* **8**, 271-279.
- Zubieta, C., Kota, P., Ferrer, J.L., Dixon, R.A., and Noel, J.P.** (2002). Structural Basis for the Modulation of Lignin Monomer Methylation by Caffeic Acid/5-Hydroxyferulic Acid 3/5-O-Methyltransferase. *Plant Cell* **14**, 1265-1277.

8. Acknowledgements

This work would not have been possible without the help and support of many people.

First of all, I would like to thank my supervisors Dr. Tobias G. Köllner and Prof. Jonathan Gershenzon for giving me the opportunity to work on this exciting and challenging project, for their great support, advice, scientific freedom, and patience over the past years. I would like to express my very special thanks to Tobias. Thank you that I could always come to you with my questions, ideas and doubts. I would also like to thank you for your trust in my work, for many inspiring scientific discussions, for sharing your experiences, and for your motivation in difficult times. Thank you, Jonathan, for your continued support and your interest and enthusiasm for my work. I would also like to thank my supervisor at the university, Prof. Günter Theißen, for agreeing to be my official first supervisor and also for his support.

I would like to thank Prof. Matthias Erb and Prof. Eric A. Schmelz for making joint projects possible and for pushing them forward. I thank them and of course all other collaborators for sharing ideas and data, as well as their help and patience on the way to publication of the manuscripts.

Thanks to all the thesis reviewers for taking the time to evaluate my work.

Many thanks to Dr. Vinzenz Handrick, who initiated the flavonoid project and never lost his interest and enthusiasm for it, shared his experiences with me and introduced me to some of the methods at the beginning of my PhD.

I would like to thank Dr. Grit Kunert, not only for being a great office mate, but also for her help and support during my final steps. I am especially grateful for the many, often very spontaneous, pieces of advice on statistics.

Thanks to all the people who actively helped with the daily lab work and/or contributed with their expertise and valuable discussions. I thank Dr. Michael Reichelt for his help and support in all analytical questions. Thanks also to Dr. Yoko Nakamura and Dr. Christian Paetz for their help and advice in the sometimes not so easy purification of O-methylated

flavonoids. I would also like to thank them both, as well as Dr. Bernd Schneider, for the many, many NMR measurements and structure verifications. My thanks also go to Katrin Luck, who gave great advice on molecular biology methods, generated many awesome RT-qPCRs results, and performed enzyme expressions in yeast for me. I would like to thank Bettina Raguschke for all the DNA sequencing. Thanks also to Natascha Rauch and my student assistants Elias Kalthoff, Paul Himmighofen, and Laura Klement for their help with time-consuming molecular biology work, plant treatments and harvests that I could not have done alone, and other sometimes boring, repetitive lab work.

I would like to thank the greenhouse team for taking good care of the plants and everything related to them. A special thanks goes to Elke Goschala, who grew many maize plants in phytochambers for me and kept them happy until the experiments. Thanks also to Daniel Veit from the workshop for providing specially needed equipment related to my plant inoculation experiments.

A big thank you to Angela Schneider for all the organization and her help with the sometimes tricky forms.

Thanks also to all other people from the administration, the IT, library, and IMPRS teams who keep things running smoothly and are always friendly and helpful.

Many thanks to all former and current members of the Cake group and the entire Department of Biochemistry for welcoming me to the department and the very nice working environment. Thank you for your support, the nice chats and sharing of cakes and other sweets. A special thanks to the more regular coffee break mates.

I also thank all my friends inside and outside the Institute for encouraging words, support, and distractions during free time.

I would also like to thank my parents and my brothers for always being there for me, always believing in me and supporting me. Thank you so much.

9. Eigenständigkeitserklärung

Hiermit erkläre ich, dass mir die aktuell geltende Promotionsordnung der Fakultät für Biowissenschaften der Friedrich-Schiller-Universität Jena bekannt ist. Nach § 5 Absatz 4 der Promotionsordnung bestätige ich, dass ich die Dissertation selbst angefertigt und keine Textabschnitte von Dritten oder eigener Prüfungsarbeiten ohne Kennzeichnung übernommen habe. Alle verwendeten Hilfsmittel, persönlichen Mitteilungen und Quellen sind in der Dissertation bzw. den entsprechenden Manuskripten eindeutig aufgeführt. Personen, die mich bei der Auswahl und Auswertung des Materials sowie der Erstellung der Manuskripte unterstützt haben, sind an den entsprechenden Stellen entweder als Autoren aufgelistet oder werden in der Danksagung genannt. Des Weiteren versichere ich, dass keine kommerzielle Promotionsvermittlung in Anspruch genommen wurde und dass Dritte weder unmittelbar noch mittelbar geldwerte Leistungen von mir für Arbeiten erhalten haben, die im Zusammenhang mit den Inhalten der vorgelegten Dissertation stehen. Die vorgelegte Dissertation wurde zu keinem früheren Zeitpunkt als staatliche oder wissenschaftliche Prüfungsarbeit eingereicht. Weiterhin wurde weder die gleiche, noch eine in wesentlichen Teilen ähnliche oder andere Abhandlung bei einer anderen Hochschule oder anderen Fakultät als Dissertation eingereicht.

Jena, den 29.06.2022

Christiane Förster

10. Curriculum Vitae

Christiane Förster

Place and date of birth: May 13, 1988 in Seligenstadt

Nationality: German

Work address: Max Planck Institute for Chemical Ecology, Department of Biochemistry, Hans-Knöll-Straße 8, 07745 Jena, Germany

Contact: cfoerster@ice.mpg.de

Education

- Mar. 2016 - present **Doctoral student**, Max Planck Institute for Chemical Ecology, Department of Biochemistry, Jena, Germany; Thesis title: “Biochemical, functional, and evolutionary aspects of flavonoid and benzoxazinoid O-methylation in grasses”; Supervision: Prof. Dr. Günter Theißen, Prof. Dr. Jonathan Gershenzon
- Oct. 2013 - Mar. 2016 **Master of Science (M. Sc.) degree in Biochemistry** (Grade 1.3), Martin Luther University of Halle-Wittenberg, Halle (Saale), Germany; Thesis title (originally in German): “Identification and characterization of a short-chain dehydrogenase and its role in the metabolism of monoterpenes in *Thymus vulgaris*” (Grade 1.0; Supervision: Prof. Dr. Jörg Degenhardt)
- Oct. 2009 - Oct. 2013 **Bachelor of Science (B. Sc.) degree in Biochemistry** (Grade 2.5), Martin Luther University of Halle-Wittenberg, Halle (Saale), Germany; Thesis title (originally in German): “Studies on the role of secretory phospholipase A2 α in auxin-dependent processes in *Arabidopsis thaliana*” (Grade 1.2; Supervision: Prof. Dr. Ingo Heilmann)
- May 2008 **Abitur** (Grade 2.4), Berufliches Gymnasium Hanau, Hanau, Germany

List of Publications

Förster, C., Gershenzon, J., and Köllner, T.G. (2022). Evolution of DIMBOA-Glc O-Methyltransferases from Flavonoid O-Methyltransferases in the Grasses. *Molecules* 27 (3), 1007.

Krause, S.T., Liao, P., Crocoll, C., Boachon, B., Förster, C., Leidecker, F., Wiese, N., Zhao, D., Wood, J.C., Buell, C.R., Gershenzon, J., Dudareva, N., and Degenhardt, J. (2021). The biosynthesis of thymol, carvacrol, and thymohydroquinone in Lamiaceae proceeds via cytochrome P450s and a short-chain dehydrogenase. *Proceedings of the National Academy of Sciences of the United States of America* 118 (52), e2110092118.

Förster, C., Handrick, V., Ding, Y., Nakamura, Y., Paetz, C., Schneider, B., Castro-Falcón, G., Hughes, C.C., Luck, K., Poosapati, S., Kunert, G., Huffaker, A., Gershenzon, J., Schmelz, E.A., and Köllner, T.G. (2021). Biosynthesis and antifungal activity of fungus-induced O-methylated flavonoids in maize. *Plant Physiology* 188 (1), 167-190, kiab496.

Gfeller, V., Huber, M., Förster, C., Huang, W., Köllner, T.G., and Erb, M. (2019). Root volatiles in plant–plant interactions I: High root sesquiterpene release is associated with increased germination and growth of plant neighbours. *Plant, Cell and Environment* 42 (6), 1950-1963.

Li, B., Förster, C., Robert, C.A.M., Züst, T., Hu, L., Machado, R.A.R., Berset, J.-D., Handrick, V., Knauer, T., Hensel, G., Chen, W., Kumlehn, J., Yang, P., Keller, B., Gershenzon, J., Jander, G., Köllner, T.G., and Erb, M. (2018). Convergent evolution of a metabolic switch between aphid and caterpillar resistance in cereals. *Science Advances* 4 (12), eaat6797.

List of Oral Presentations

- | | |
|------|---|
| 2020 | A phytoalexin story – Fungal infection induces O-methylation of flavonoids in maize. Talk presented at Institute Symposium, MPI for Chemical Ecology, Jena, Germany |
| 2019 | Fungal infection induces O-methylation of flavonoids in maize. Talk presented at 18th IMPRS Symposium, MPI for Chemical Ecology, IMPRS, Dornburg, Germany |

- 2018 Fungal infestation induces O-methylation of flavonoids in maize. Talk presented at Metabolism, biotechnology and ecology of plant natural products – Young scientists workshop of the ‘Natural Products’ section, Deutsche Botanische Gesellschaft, Technical University of Braunschweig, Institute of Pharmaceutical Biology, Warberg, Germany

List of Poster Presentations

- 2019 Förster, C., Handrick, V., Huffaker, A., Gershenzon, J., Schmelz, E.A., Köllner, T.G. Flavonoid O-methyltransferases as targets for engineering pathogen resistance in maize. Poster presented at Gordon Research Conference – Plant Metabolic Engineering, Barga, Italy
- 2018 Förster, C., Li, B., Robert, C., Züst, T., Hu, L., Machado, R.A.R., Handrick, V., Hensel, G., Kumlehn, J., Gershenzon, J., Erb, M., Köllner, T.G. Convergent evolution of a metabolic switch between aphid and caterpillar resistance in cereals. Poster presented at 17th IMPRS Symposium, MPI for Chemical Ecology, IMPRS, Dornburg, Germany
- 2017 Förster, C., Handrick, V., Schneider, B., Köllner, T.G. The evolution of DIMBOA-Glc O-methyltransferases in the grasses. Poster presented at 2nd European Molecular Maize Meeting, Ghent, Belgium

Scientific Activities

- Apr. 2018 presented at 9. Forsche-Schüler-Tag: Vom Geschmack und Duft der Kräuter
- Apr. 2017 presented at 8. Forsche-Schüler-Tag: Vom Geschmack und Duft der Kräuter

Jena, June 29, 2022

Christiane Förster

11. Supplemental Material

11.1 Manuscript I



advances.sciencemag.org/cgi/content/full/4/12/eaat6797/DC1

Supplementary Materials for

Convergent evolution of a metabolic switch between aphid and caterpillar resistance in cereals

B. Li, C. Förster, C. A. M. Robert, T. Züst, L. Hu, R. A. R. Machado, J.-D. Berset, V. Handrick, T. Knauer, G. Hensel, W. Chen, J. Kumlehn, P. Yang, B. Keller, J. Gershenzon, G. Jander, T. G. Köllner*, M. Erb*

*Corresponding author. Email: matthias.erb@ips.unibe.ch (M.E.); koellner@ice.mpg.de (T.G.K.)

Published 5 December 2018, *Sci. Adv.* **4**, eaat6797 (2018)
DOI: 10.1126/sciadv.aat6797

This PDF file includes:

- Fig. S1. Phenotyping of *ZmBx12*-overexpressing plants I.
- Fig. S2. Phenotyping of *ZmBx12*-overexpressing plants II.
- Fig. S3. HDMBOA-Glc and MBOA levels upon DIMBOA and DIMBOA-Glc infiltration.
- Fig. S4. Specificity of benzoxazinoid- and glucosinolate-induced callose deposition.
- Fig. S5. Impact of DIMBOA-Glc *O*-methylation on wheat pathogen resistance.
- Fig. S6. Aphids do not induce benzoxazinoids in wheat leaves.
- Fig. S7. Identification of DIMBOA-Glc OMT candidate genes.
- Fig. S8. Phylogenetic tree of maize *OMT* genes similar to *Bx7* and wheat *OMT* genes that were found to be up-regulated after herbivory in wheat seedlings (RNA sequencing).
- Fig. S9. Sequence comparison of maize *BX7* and *BX10* with herbivore-induced OMT proteins from wheat.
- Fig. S10. Phylogenetic tree of maize and wheat *OMT* genes similar to *Bx7*.
- Fig. S11. Identification of *TaBx10* as a functional DIMBOA-Glc OMT.
- Fig. S12. No influence of *ZmBx12* overexpression on *TaBx10* expression.
- Fig. S13. Phylogenetic tree of Poaceae *OMT* genes similar to *Bx7*.
- Fig. S14. Phylogenetic tree of maize, wheat, and *Arabidopsis* *OMT* genes similar to *Bx7*.
- Table S1. Wheat *OMT* genes up-regulated after herbivory (RNA sequencing).

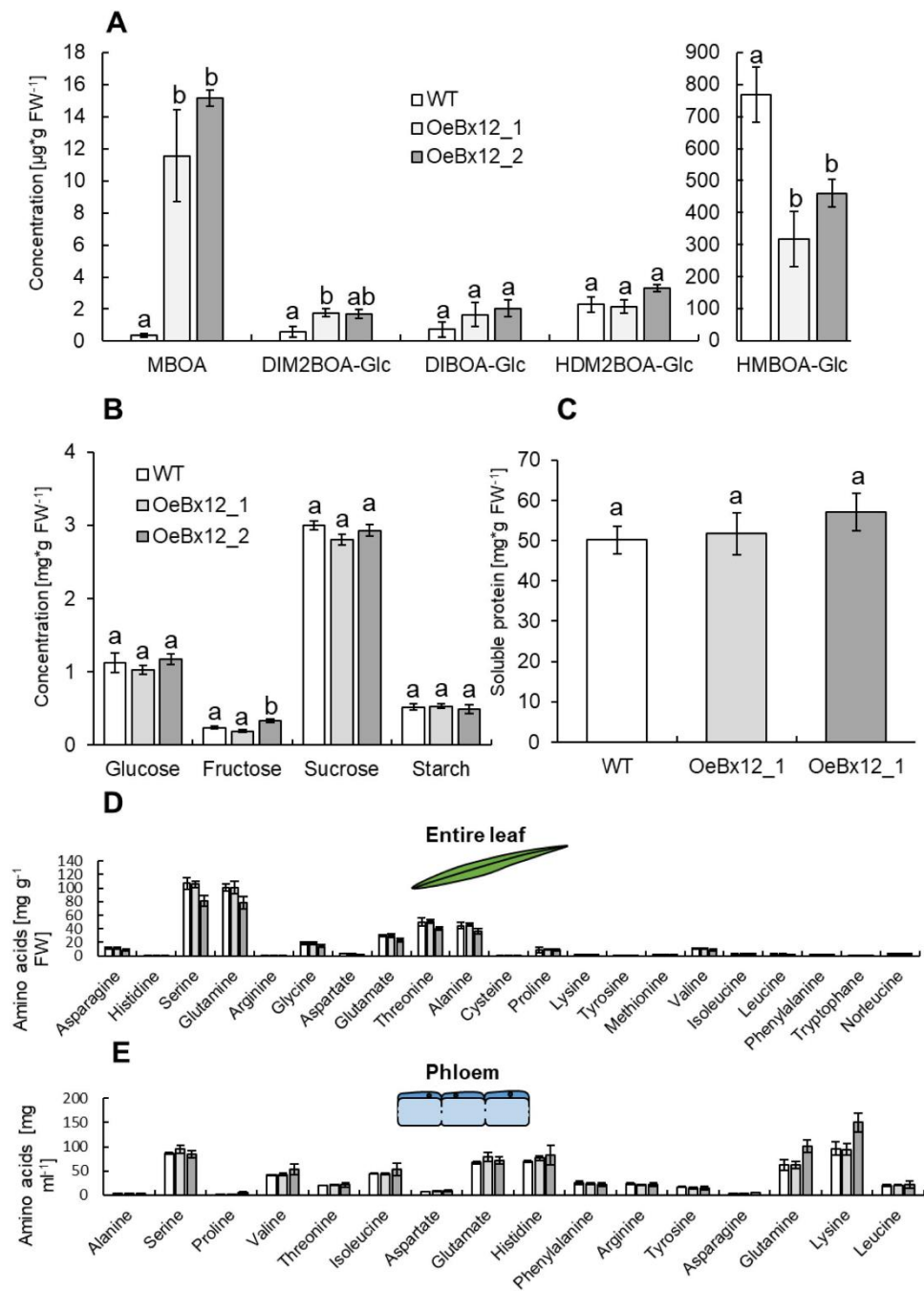


Fig. S1. Phenotyping of *ZmBx12*-overexpressing plants I. Concentrations of benzoxazinoids (A), sugars and starch (B), soluble protein (C), and free amino acids (D,E) in wild type (WT) and transgenic lines are shown. Different letters indicate significant differences between wheat lines (ANOVA followed by Holm-Sidak Post-Hoc tests, $p < 0.05$).

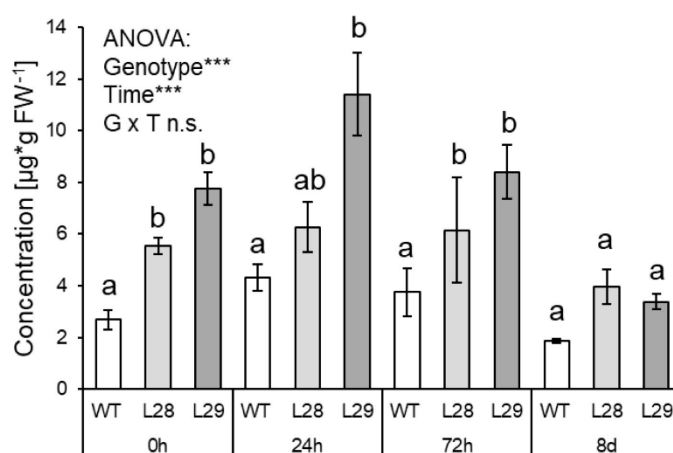


Fig. S2. Phenotyping of *ZmBx12*-overexpressing plants II. Concentrations of ferulic acid in wild type (WT) and transgenic lines in non-induced plants (0h) and *S. littoralis*-induced plants at different time points are shown. Chlorogenic acid, caffeic acid, coumaric acid and sinapic acid were below the limit of detection. Significance levels for Two-Way ANOVA factors are shown (* $p < 0.05$; ** $p < 0.01$; *** $p < 0.001$). Letters indicate significant differences between lines within time points (ANOVA followed by Holm-Sidak Post-Hoc tests, $p < 0.05$). N.s. not significant.

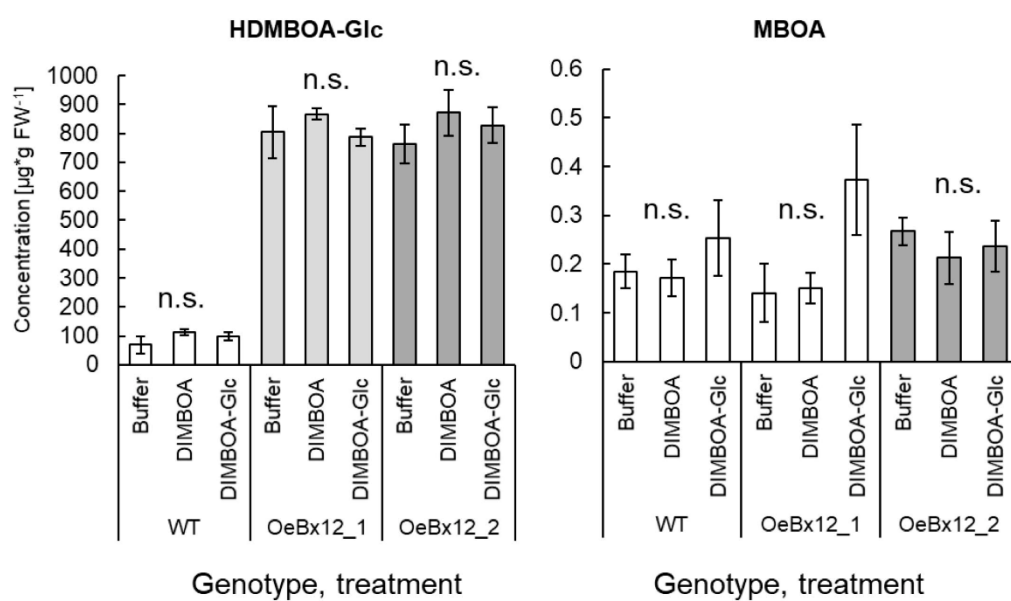


Fig. S3. HDMBOA-Glc and MBOA levels upon DIMBOA and DIMBOA-Glc infiltration. No significant differences between treatments within genotypes were detected.

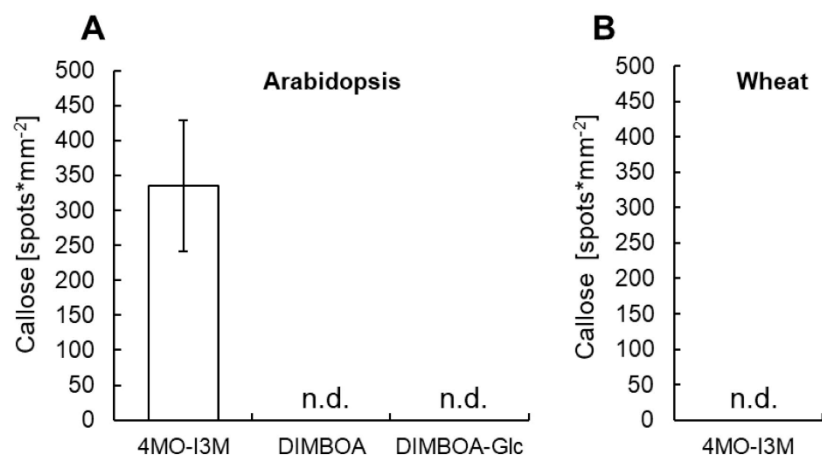


Fig. S4. Specificity of benzoxazinoid- and glucosinolate-induced callose deposition. Callose deposition in wheat (A) and *Arabidopsis thaliana* leaves (B) infused with the glucosinolate 4MO-I3M or the benzoxazinoids DIMBOA and DIMBOA-Glc (n=6). N.d. not detected.

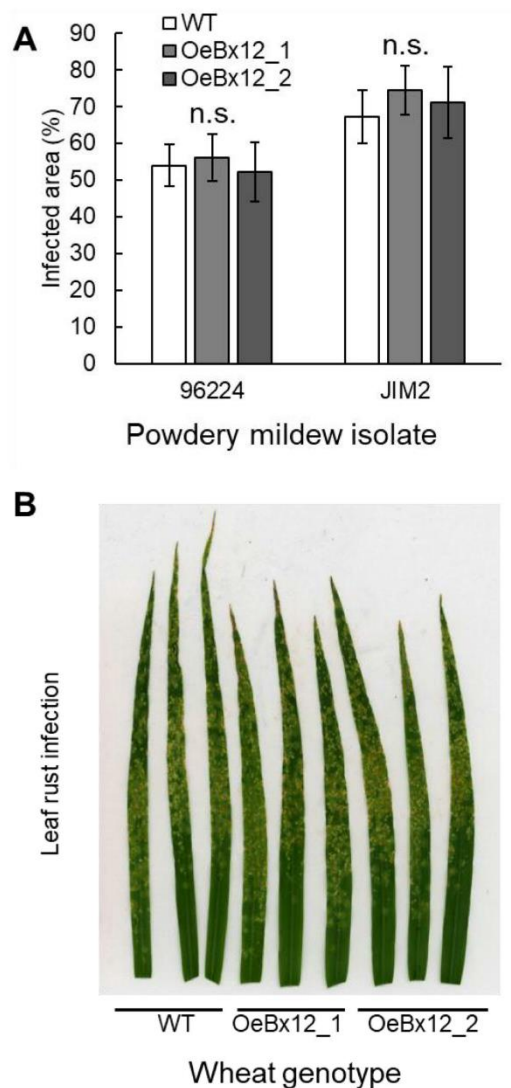


Fig. S5. Impact of DIMBOA-Glc O-methylation on wheat pathogen resistance. (A) infection severity caused by two powdery mildew (*Blumeria graminis* f. sp. tritici) isolates. No differences between wild type (WT) and transgenic lines were found (ANOVA followed by Holm-Sidak Post-Hoc tests, $p > 0.05$). (B) representative photographs of leaf rust (*Puccinia recondita* f.sp.tritici) infested wheat leaves. Visual inspection revealed no differences in infection severity between the different lines. Photo credit for (B): Ping Yang, University of Zürich.

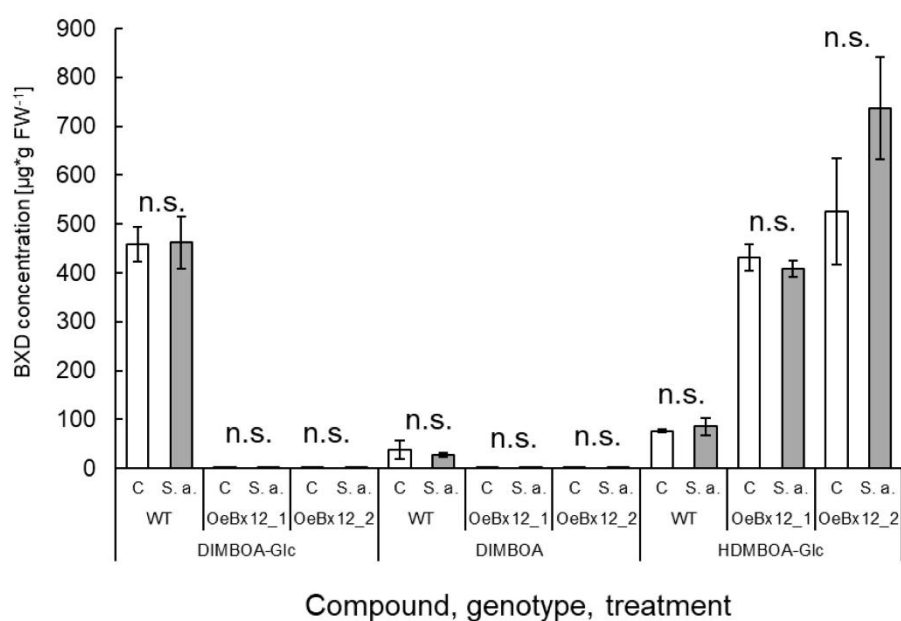


Fig. S6. Aphids do not induce benzoxazinoids in wheat leaves. Major benzoxazinoids in wild type (WT) and *ZmBx12* overexpressing leaves of control plants (C) and plants infested with *Sitobion avenae* aphids (S.a.). No significant differences between treatments within genotypes were detected.

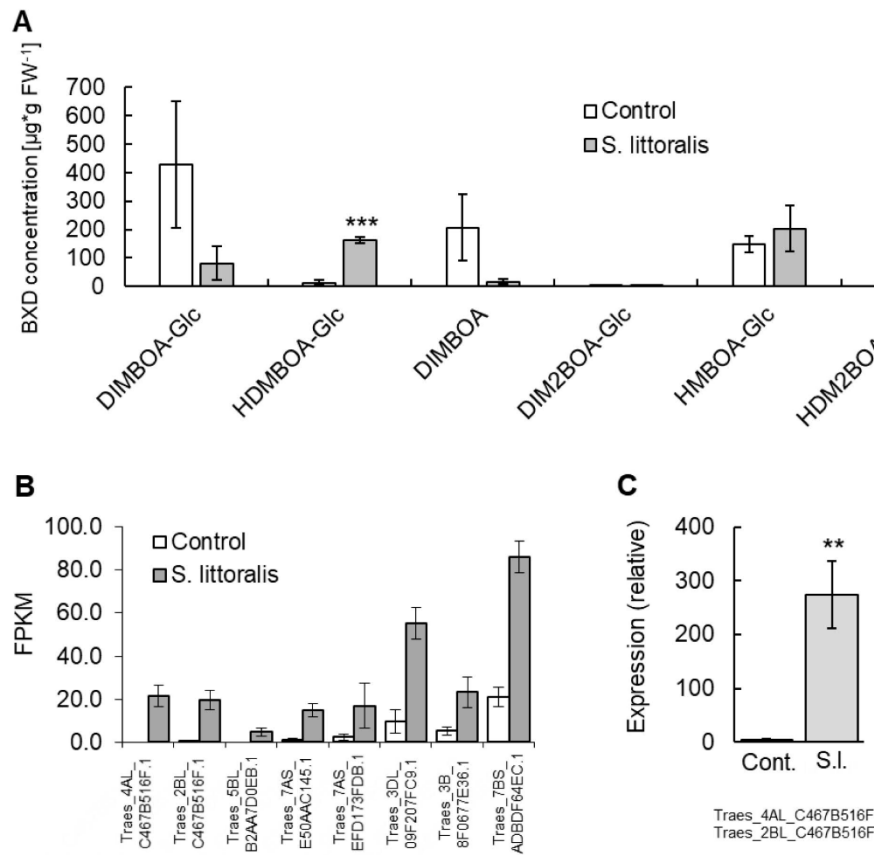


Fig. S7. Identification of DIMBOA-Glc OMT candidate genes. (A) Benzoxazinoid levels in control and *S. littoralis* induced wheat leaves (n=3). (B) The transcriptomes of the same samples were sequenced, and the obtained sequences were mapped to the primary gene models of the *T. aestivum* v2.2 genome. Differential gene expression was analyzed using the EDGE test implemented in the CLC genomics workbench package. Genes with a fold change > 3.5 and $P < 0.001$ were considered as upregulated. Means and SE are shown (n=3). (C) qRT-PCR analysis of Traes 4AL C467B516F/Traes 2BL C467B516F gene expression in herbivore-damaged wheat leaves. Means and SE are shown (n=6-7). Because 4AL C467B516F and Traes 2BL C467B516F share 100 % nucleotide identity, they could not be distinguished from each other in the qRT-PCR. Cont.: Control. S.I.: *Spodoptera littoralis*.

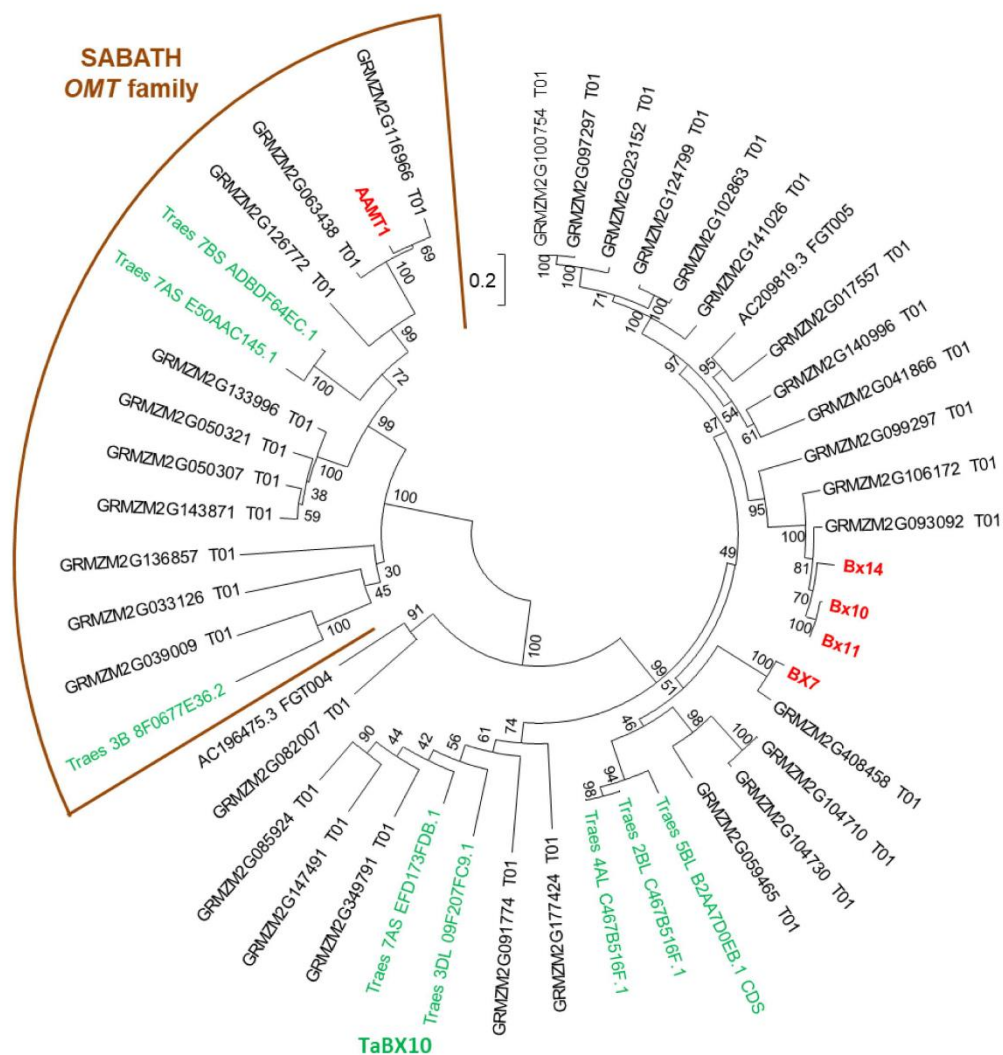


Fig. S8. Phylogenetic tree of maize *OMT* genes similar to *Bx7* and wheat *OMT* genes that were found to be up-regulated after herbivory in wheat seedlings (RNA sequencing). The tree was inferred by using the Maximum Likelihood method based on the General Time Reversible model. Bootstrap values ($n = 1000$ replicates) are shown next to each node. The tree is drawn to scale, with branch lengths measured in the number of substitutions per site. GRMZM, *Zea mays* genes (black); Traes, *Triticum aestivum* genes (green). Maize AAMT1 (anthranilic acid carboxyl methyltransferase 1) has been described as a member of the SABATH family (Köllner et al., 2010, Herbivore-Induced SABATH Methyltransferases of Maize That Methylate Anthranilic Acid Using *S*-Adenosyl-L-Methionine. *Plant Physiology* 153, 1795-1807).


```

BX7      GHQAQHTD-----DTEETAAHQRLWCPAFVYKSLALCLDLRIPTAFHRC--CAHTCEHAASETISASN
BX10     ALMQES-----SSQDLTCAHDELLHSCCFKSLALAVADLRIPPAHHHCAGGTLQALLAETALEHCK
Traes_2BL_C467B516F.1 PAHQHIERDQDLAM-----SSDELTCAOLELYHSCAFVKSALAKADLRIPPAHRC--CAHTCEHAASETISASN
Traes_4AL_C467B516F.1 PAHQHIERDQDLAM-----SSDELTCAOLELYHSCAFVKSALAKADLRIPPAHRC--CAHTCEHAASETISASN
Traes_5BL_B2AA7D0EB.1 -----GRSKQVAAASIPHSIDHTHTPCRPRSTSNKTKTELTCAOLELYHSCAFVKSALAKADLRIPPAHRC--CAHTCEHAASETISASN
Traes_7AS_E50AAC145.1 -----
Traes_7AS_EFD173FDB.1 -----
Traes_3DL_09F207FC9.1 -----
Traes_3B_8F0677E36.2 -----
Traes_7BS_ADBDF64EC.1 KEASGVMTG-----DGENSYANNSRIQKALLETREPLRKAIOEVCTSPSARE--STMVADLCSSC--ENT

BX7      HDYLRVRMRNTAMRISAAASH-----DPKADDAAAISYQTPASRLVSSSSVDDAAGASKENTTTPSILPNIAHLVRPNTIS
BX10     LRALRRMRVLTVTGHSVVEQPPAGGDDSTVHTSDDEAVVYRNTAASRFLVSD-----DVSTATLAPFVSLALQPIAAC
Traes_2BL_C467B516F.1 RSNLRVRMRVLTGTGFSIVQGKGS-----NDHAGDCAA--YKTRVSRLLV-----ERSPHNLSPMGTIVNTLCWT
Traes_4AL_C467B516F.1 RSNLRVRMRVLTGTGFSIVQGKGS-----NDHAGDCAA--YKTRVSRLLV-----ERSPHNLSPMGTIVNTLCWT
Traes_5BL_B2AA7D0EB.1 RSNLRVRMRVLTGTGFSIVQGKGS-----NDHAGD-----ERSPHNLSPMGTIVNTLCWT
Traes_7AS_E50AAC145.1 -----
Traes_7AS_EFD173FDB.1 -----
Traes_3DL_09F207FC9.1 -----
Traes_3B_8F0677E36.2 LALVSTAINAIHNHCL--QLQPPPEICVLLNDLPDPTDFNTVVKSLVTLRQS-----KNPVVTVGAPGSFYERLFTS
Traes_7BS_ADBDF64EC.1 LSFISEYIGAVRSCTRKEERRAVEVQFFLNDLPDPTDFNTVVKSLVTLRQS-----KNPVVTVGAPGSFYERLFTS

BX7      L-LFSMGEWMK----DESAASVSLYETVHRQGMWACVEDDAANRASFYESMDADTLVMQAVVRRCPHVFDGK-SVDVVCGRCTAANA
BX10     PHALGISAWFQEQHEPSYGLAFRQTP--TIWEHADDVN--ALLNKGMAADSFLMPTVRECGETFRGID-SVDVVCCHGGAART
Traes_2BL_C467B516F.1 S-LLKMFPEWFTQCGESASQSHSLVQLANGCTFWDTTKVDG---GLFNDGMAADSITAMKVLKEHGGAFGEVKSSVDICNKGATASA
Traes_4AL_C467B516F.1 S-LLKMFPEWFTQCGESASQSHSLVQLANGCTFWDTTKVDG---GLFNDGMAADSITAMKVLKEHGGAFGEVKSSVDICNKGATASA
Traes_5BL_B2AA7D0EB.1 -----
Traes_7AS_E50AAC145.1 -----
Traes_7AS_EFD173FDB.1 -----
Traes_3DL_09F207FC9.1 -----
Traes_3B_8F0677E36.2 NSLHVVCASNSLQWLSKAPEDLTRNIP--AFNIDEHARREMLPMVREAYEQQFKDFKLFELRAKELVSGGRMVISVCTRSDVIAS
Traes_7BS_ADBDF64EC.1 RSVHFFHSSYSILMRSKVPEELSSCTHLNEGNIYIGKTT----PMVIKLFQEQFKDFELFUTLRFKELVSGGRMLTFLCKNKEEMMT

BX7      VVAAPFHLQRCVTMDLPHVAAEPAGTAGLSHGGMDFEHPISADALMISLWLDWDEDKCIKIMERCKEATGGKPAAGKVITIDVVLSS
BX10     IAAAPFHL-KCSVLDPHVVAGAPSDGNV-QEVAGNMFEYPPATAVFLKTLHDWGDECVKIKDKCKEATSPRPAAGKVITIDVVLSS
Traes_2BL_C467B516F.1 VVAAPFHL-KCSVLDPHVVAAAPSDIIL-TEVAGNMFEYVPPADAVLLWLDWKKHEDCVKIMRCKEATPAKPAAGKVITIDVVLSS
Traes_4AL_C467B516F.1 VVAAPFHL-KCSVLDPHVVAAAPSDIIL-TEVAGNMFEYVPPADAVLLWLDWKKHEDCVKIMRCKEATPAKPAAGKVITIDVVLSS
Traes_5BL_B2AA7D0EB.1 -----GRVEKEKLDSNVPYITPSVKEVRELINSRHFG--DEHARLFESNWDQDDSDGDVVLVLA-SS
Traes_7AS_E50AAC145.1 -----SVLEHDSDEDCIKRLHACCKEATPPRGAAGKVITIDVVLSS
Traes_7AS_EFD173FDB.1 -----QLVHLWACDEDCIKRLHACCKEATPPRGAAGKVITIDVVLSS
Traes_3DL_09F207FC9.1 EFSIETSI--LAQILSVMAEGVIDKAKFDSYVPLHGPSIEEVREIIEKREGSFS--LREMVDHPTAE-----MNIALS
Traes_3B_8F0677E36.2 HGEVGTLYELVAESLSLILKGRVEKEKLDSNVPYITPSVKEVRELINSRHFG--DEHARLFESNWDQDDSDGDVVLVLA-SS
Traes_7BS_ADBDF64EC.1

BX7      RADDDDDKCTRETYVLDLHLLSFVNCASRSEHEWRRSLAAGSRVYKLTHTRC-IPSIIEVVE*
BX10     KQ--SNIKHCTQVMFDLYMMA-VNCGVDEQWKKLTPKAGKIVKILPVLDVSVVIEVVE*
Traes_2BL_C467B516F.1 PVTQPNHSK--BAQVLIDLYMNG-SDCMRRENEWSLISPAEGESIVKLTPTNG-IKRSIIEVVE*
Traes_4AL_C467B516F.1 PVTQPNHSK--BAQVLIDLYMNG-SDCMRRENEWSLISPAEGESIVKLTPTNG-IKRSIIEVVE*
Traes_5BL_B2AA7D0EB.1 -----GANVANCIKRAVMEPLIVDFEGEDIID----DLFVVVASIVAKHLEKAKAKYPIVLSLKKA*
Traes_7AS_E50AAC145.1 -----ASGLMLSTHLLVDMKLVMTRGRGRDEKDSDEHMKAGESEYKLPKKV-ARAVIEVVE*
Traes_7AS_EFD173FDB.1 -----SCEATYEPQVLADMLM-----PSKFWNLIALFEPIIVHGFGEVMEFVRAALHWSI--DVDLSLRQERARTSRAMLVSLAKA*
Traes_3DL_09F207FC9.1 -----GANVANCIKRAVLEPLIVDFEGEDIID----DLFVVVASIVAKHLEKAKAKYPIVLSLKKA*
Traes_3B_8F0677E36.2 -----
Traes_7BS_ADBDF64EC.1 -----

```

Fig. S9. Sequence comparison of maize BX7 and BX10 with herbivore-induced OMT proteins from wheat. Amino acids identical in at least 5 out of 10 sequences are marked by black boxes and amino acids with similar side chains are marked by gray boxes. The genes encoding Traes_2BL_C467B516F.1 and Traes_4AL_C467B516F.1 have identical nucleotide sequences and were both designated as *TaBX10* (shown in red).

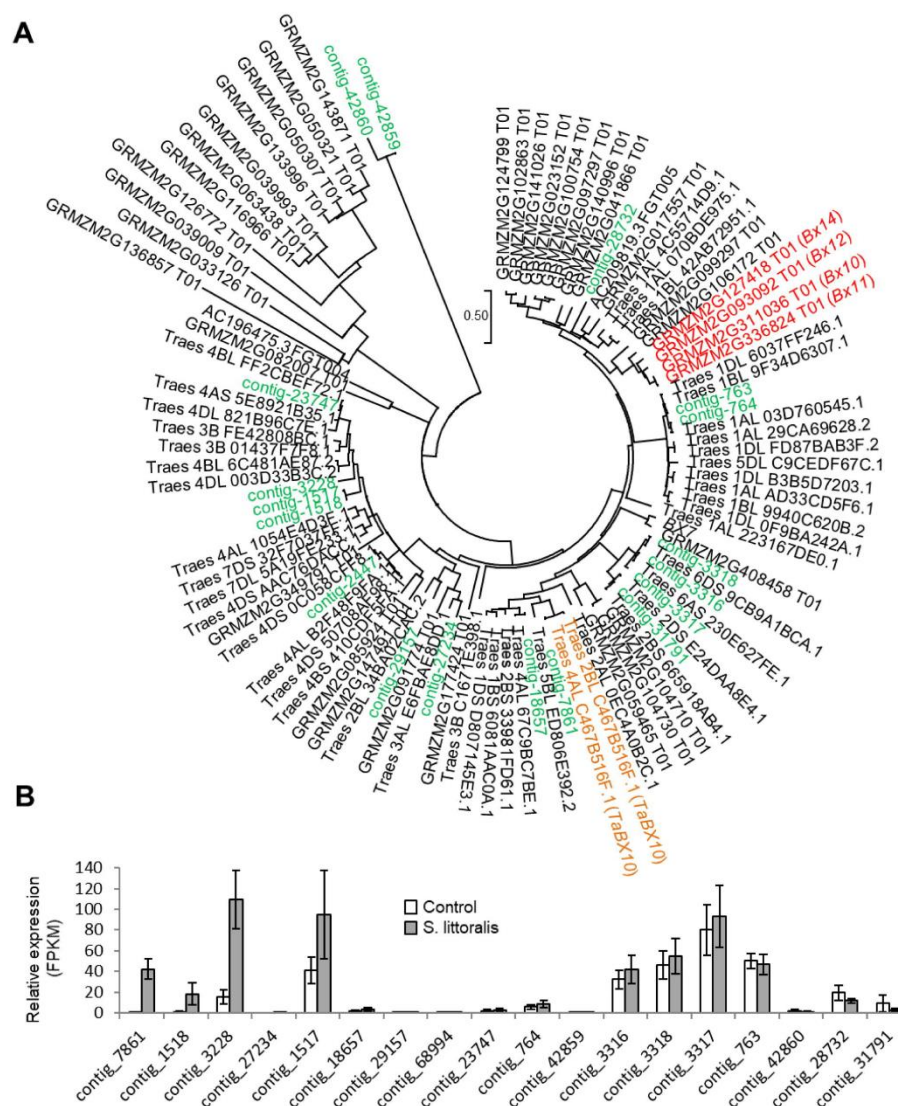


Fig. S10. Phylogenetic tree of maize and wheat *OMT* genes similar to *Bx7*. (A) and expression values of *OMT* contigs extracted from a *de novo* transcriptome of herbivore-damaged wheat leaves (B). *OMT*s were identified using a BLASTP analysis with maize *Bx7* as query and the maize and wheat protein datasets in Phytozome 12.1 (<https://phytozome.jgi.doe.gov>) as template. In addition, a *de novo* transcriptome of *Spodoptera littoralis* damaged wheat leaves was used as template for a TBLASTN analysis with *Bx10* as query. Genes with ORFs > 1000 nucleotides were considered as ‘full-length’ and used for phylogenetic analysis. Maize *Bx10,11,12,14*, wheat *TaBX10*, and wheat *OMT* contigs found in the *de novo* transcriptome are shown in red, brown, and green, respectively. The tree was inferred by using the Maximum Likelihood method based on the Tamura 3-parameter model. The tree is drawn to scale, with branch lengths measured in the number of substitutions per site. GRMZM, *Zea mays*; Traes, *Triticum aestivum*; contig, contig number in the *de novo* transcriptome.

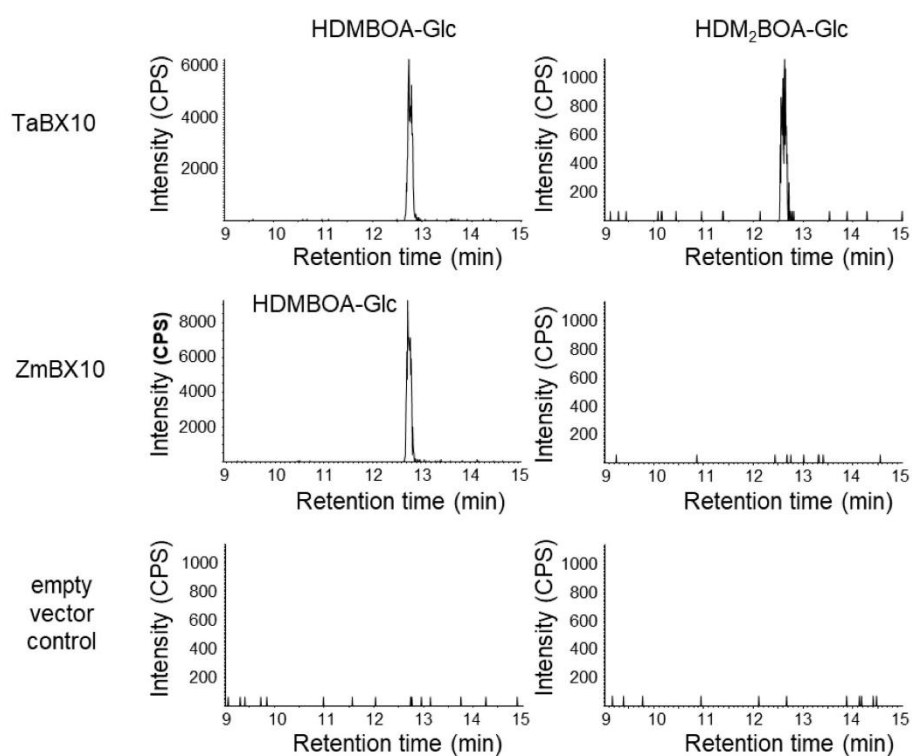


Fig. S11. Identification of *TaBx10* as a functional DIMBOA-Glc OMT. Recombinant Traes 4AL C467B516F (*TaBX10*) accepts DIMBOA-Glc and DIM₂BOA-Glc as substrate and produces HDMBOA-Glc and HDM₂BOA-Glc, respectively. The enzymes were heterologously expressed in *E. coli*. Purified recombinant proteins were incubated with a mixture of DIMBOA-Glc and DIM₂BOA-Glc as substrate and SAM as co-substrate. Enzyme products were analyzed using LC-MS/MS. Maize *ZmBX10* was included as positive control and an *E. coli* strain expressing an empty vector was used as negative control.

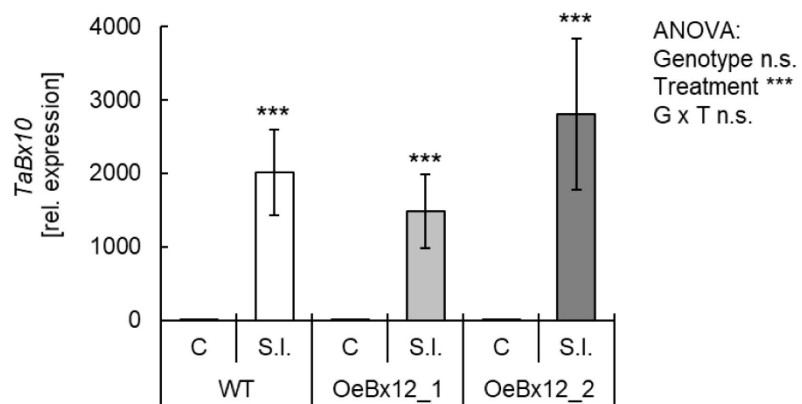


Fig. S12. No influence of *ZmBx12* overexpression on *TaBx10* expression. Relative expression of *TaBx10* in the leaves of WT and OeBx12 plants that were uninfested or infested with *S. littoralis* larvae for 24 h ($n=5-6$). Stars above bars indicate a significant difference between treatments within genotypes (Holm-Sidak Post-Hoc tests, * $p<0.05$; ** $p<0.01$; *** $p<0.001$). Significance levels for ANOVA factors are shown on the right (* $p<0.05$; ** $p<0.01$; *** $p<0.001$) C: Control. S.I.: *Spodoptera littoralis*.

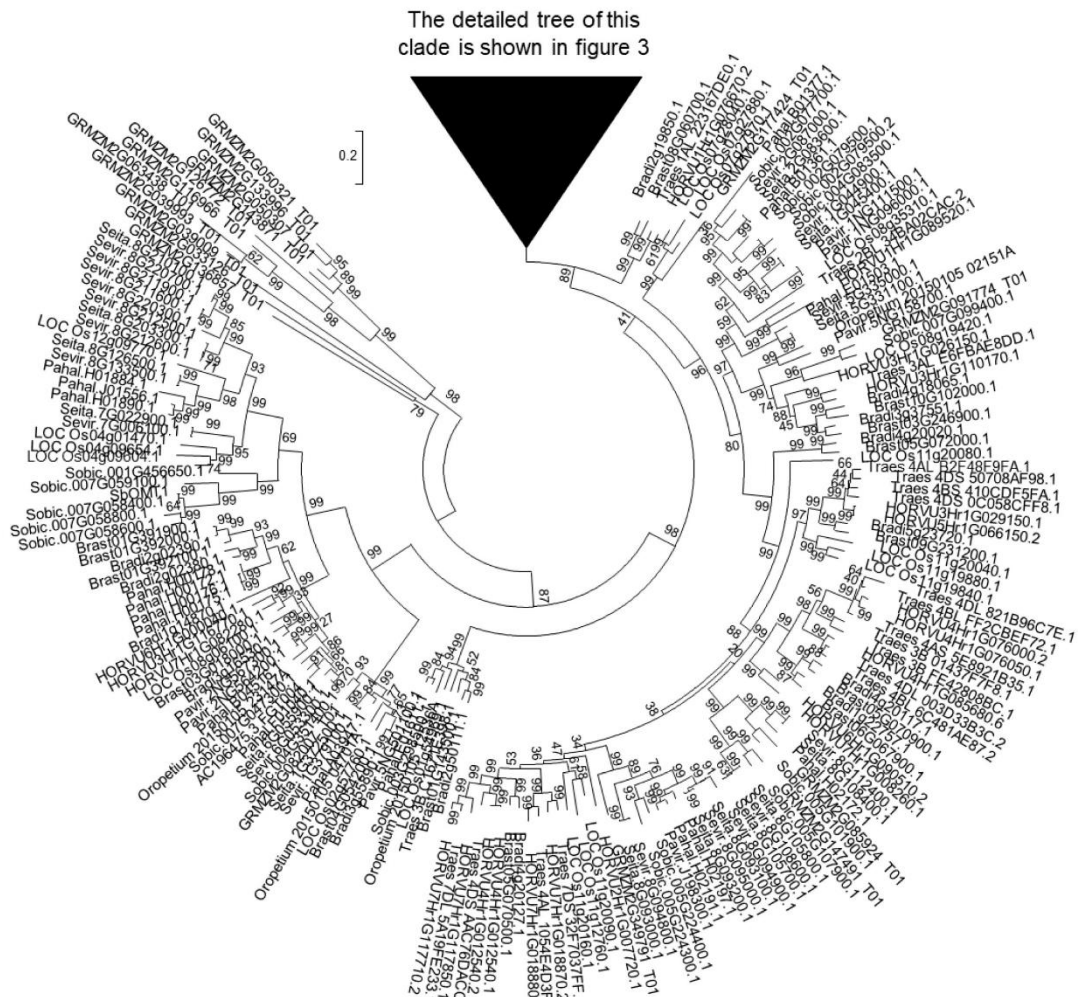


Fig. S13. Phylogenetic tree of Poaceae *OMT* genes similar to *Bx7*. OMTs were identified using a BLASTP analysis with maize *Bx7* as query and all available Poaceae protein datasets in Phytozome 12.1 (<https://phytozome.jgi.doe.gov>) as template. Genes with ORFs > 1000 nucleotides were considered as ‘full-length’ and used for dendrogram analysis. The tree was inferred by using the Maximum Likelihood method based on the Tamura 3-parameter model. Bootstrap values ($n = 1000$ replicates) are shown next to each node. The tree is drawn to scale, with branch lengths measured in the number of substitutions per site. GRMZM, *Zea mays*; Sobic, *Sorghum bicolor*; Sevir, *Setaria viridis*; Seita, *S. italica*; Pavir, *Panicum virgatum*; Pahal, *P. hallii*; Oropetium, *Oropetium thomaeum*; Traes, *Triticum aestivum*; HORVU, *Hordeum vulgare*; Bradi, *Brachypodium distachyon*; Brast, *B. stacei*; LOC Os, *Oryza sativa*.

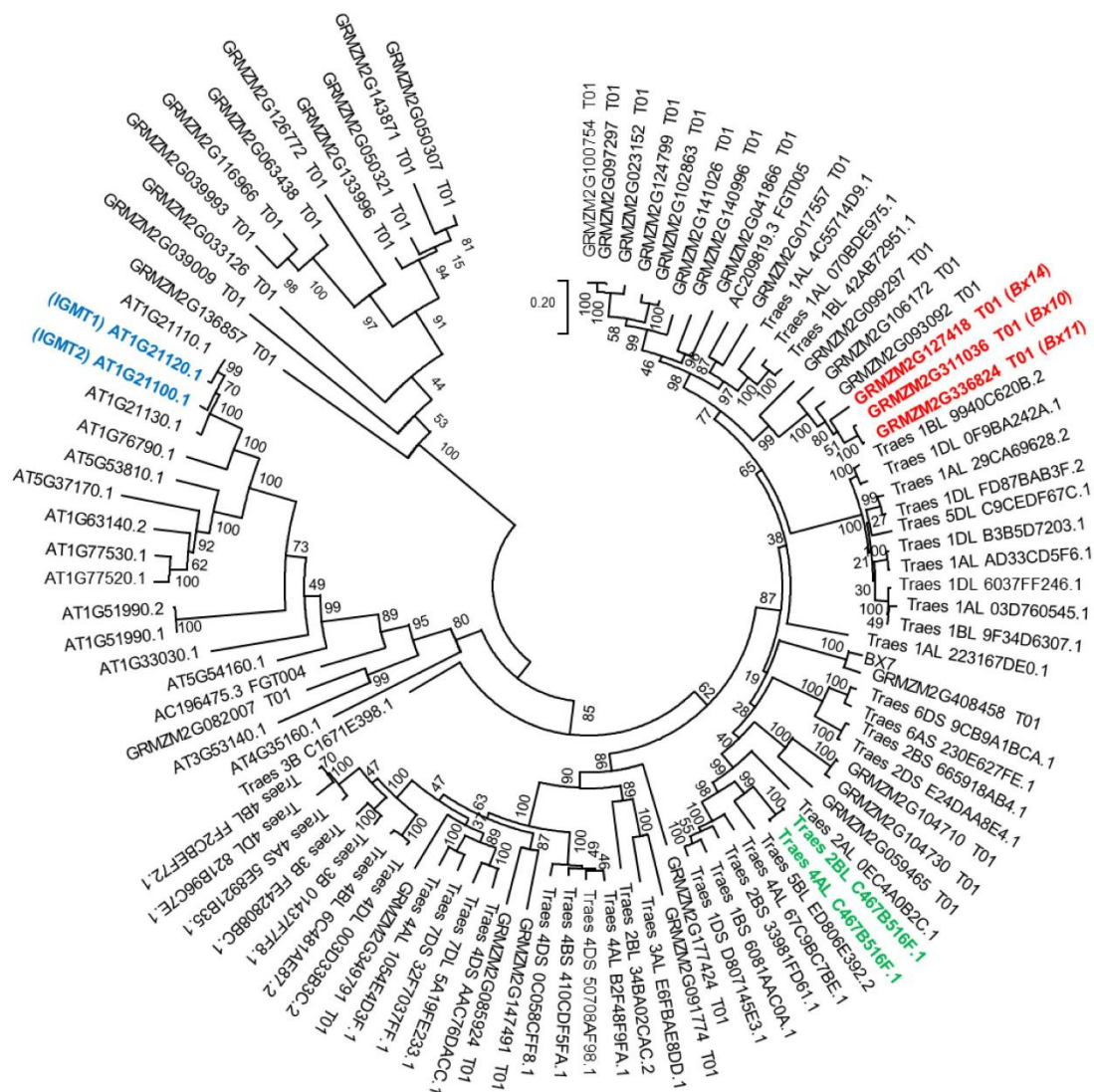


Fig. S14. Phylogenetic tree of maize, wheat, and *Arabidopsis* OMT genes similar to Bx7. OMTs were identified using a BLASTP analysis with maize BX7 as query and the maize, wheat, and *Arabidopsis thaliana* protein datasets in Phytozome 12.1 (<https://phytozome.jgi.doe.gov>) as template. Genes with ORFs > 1000 nucleotides were considered as ‘full-length’ and used for phylogenetic analysis. Maize *Bx10*, *11*, *14*, wheat *TaBX10*, and *Arabidopsis* IGMT1,2 are shown in red, green, and blue, respectively. The tree was inferred by using the Maximum Likelihood method based on the Tamura 3-parameter model. Bootstrap values (n = 1000 replicates) are shown next to each node. The tree is drawn to scale, with branch lengths measured in the number of substitutions per site. GRMZM, *Zea mays*; Traes, *Triticum aestivum*; AT, *Arabidopsis thaliana*.

Table S1. Wheat *OMT* genes up-regulated after herbivory (RNA sequencing). Wheat seedlings were subjected to herbivory by *Spodoptera littoralis*. The transcriptomes of three damaged and three undamaged plants were sequenced and compared to identify herbivory-induced *O*-methyltransferase genes. All identified *OMT* genes with a fold change > 3.0 and a *P*-value < 0.001 are shown.

Feature ID	EDGE test Fold change	EDGE test P-value	EDGE test Weighted difference	leaf ctr 2644_A FPKM	leaf ctr 2644_C FPKM	leaf ctr 2644_B FPKM	leaf 2644_E FPKM	leaf 2644_D FPKM	leaf 2644_F FPKM	leaf ctr Means FPKM	leaf herb Means FPKM	annotation
Traes_4AL_C467B516F.1	161.6	1E-13	1.58E-05	0.0	0.0	0.0	16.5	18.9	29.4	0.0	21.6	PTHR11746//PTHR11746:SF108 - O-METHYLTRANSFERASE
Traes_2BL_C467B516F.1	96.9	1E-11	1.44E-05	0.0	0.0	0.2	15.7	16.6	27.1	0.1	19.8	PTHR11746//PTHR11746:SF108 - O-METHYLTRANSFERASE
Traes_5BL_B2AA7D0EB.1	35.7	0.0001	3.42E-06	0.0	0.0	0.0	1.9	5.0	7.3	0.0	4.7	PTHR11746//PTHR11746:SF108 - O-METHYLTRANSFERASE
Traes_7AS_E50AAC145.1	11.5	5E-07	9.89E-06	2.1	0.6	0.3	14.1	10.9	19.4	1.0	14.8	PTHR31009//PTHR31009:SF16 - S-ADENOSYL-L-METHIONINE:CARBOXYL METHYLTRANSFERASE
Traes_7AS_EFD173FDB.1	6.3	0.0029	1.1E-05	2.5	0.0	4.4	0.8	19.8	30.4	2.3	17.0	2.1.1.240 - Trans-resveratrol di-O-methyltransferase / Resveratrol O-methyltransferase
Traes_3DL_09F207FC9.1	4.7	2E-07	3.19E-05	7.1	3.7	18.3	53.3	46.2	66.4	9.7	55.3	PTHR11746//PTHR11746:SF91 - O-METHYLTRANSFERASE
Traes_3B_8F0677E36.2	3.8	0.0002	1.28E-05	5.7	2.0	7.8	12.1	25.9	31.7	5.2	23.2	PTHR31009//PTHR31009:SF12 - S-ADENOSYL-L-METHIONINE:CARBOXYL METHYLTRANSFERASE

11.2 Manuscript II

The Supplemental Material for

Biosynthesis and antifungal activity of fungus-induced *O*-methylated flavonoids in maize

Förster, C., Handrick, V., Ding, Y., Nakamura, Y., Paetz, C., Schneider, B., Castro-Falcón, G., Hughes, C.C., Luck, K., Poosapati, S., Kunert, G., Huffaker, A., Gershenzon, J., Schmelz, E.A., and Köllner, T.G.

published October 27 (2021) in Plant Physiology

DOI:10.1093/plphys/kiab496

Originally the Supplemental includes the following files:

supplemental_figures

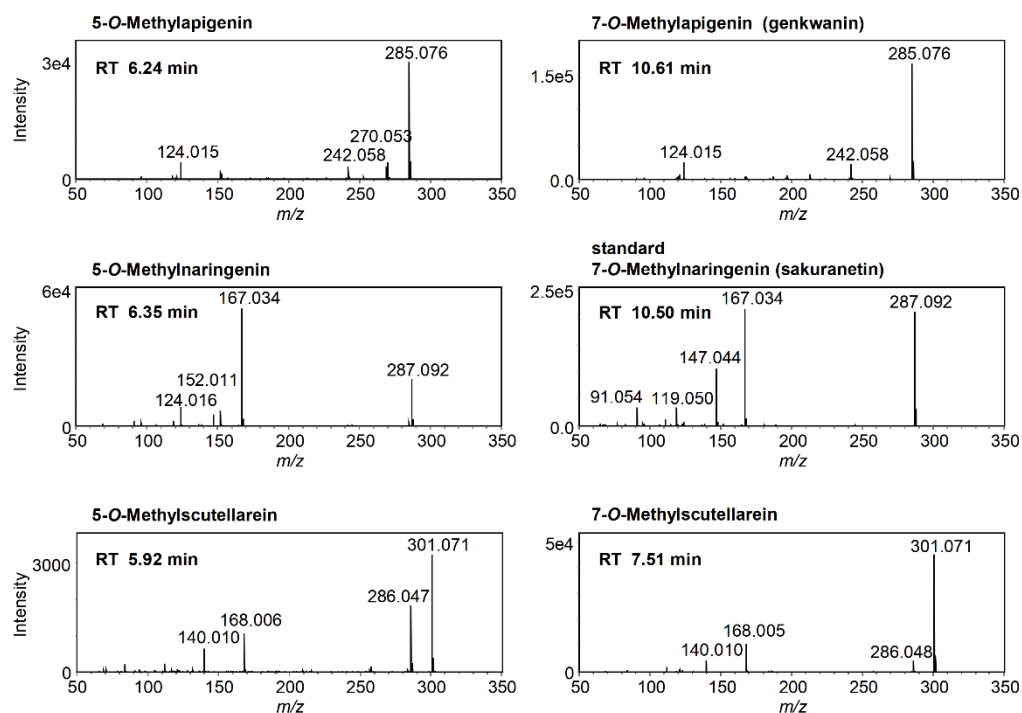
supplemental_tables_part1

supplemental_tables_part2 (Excel file)

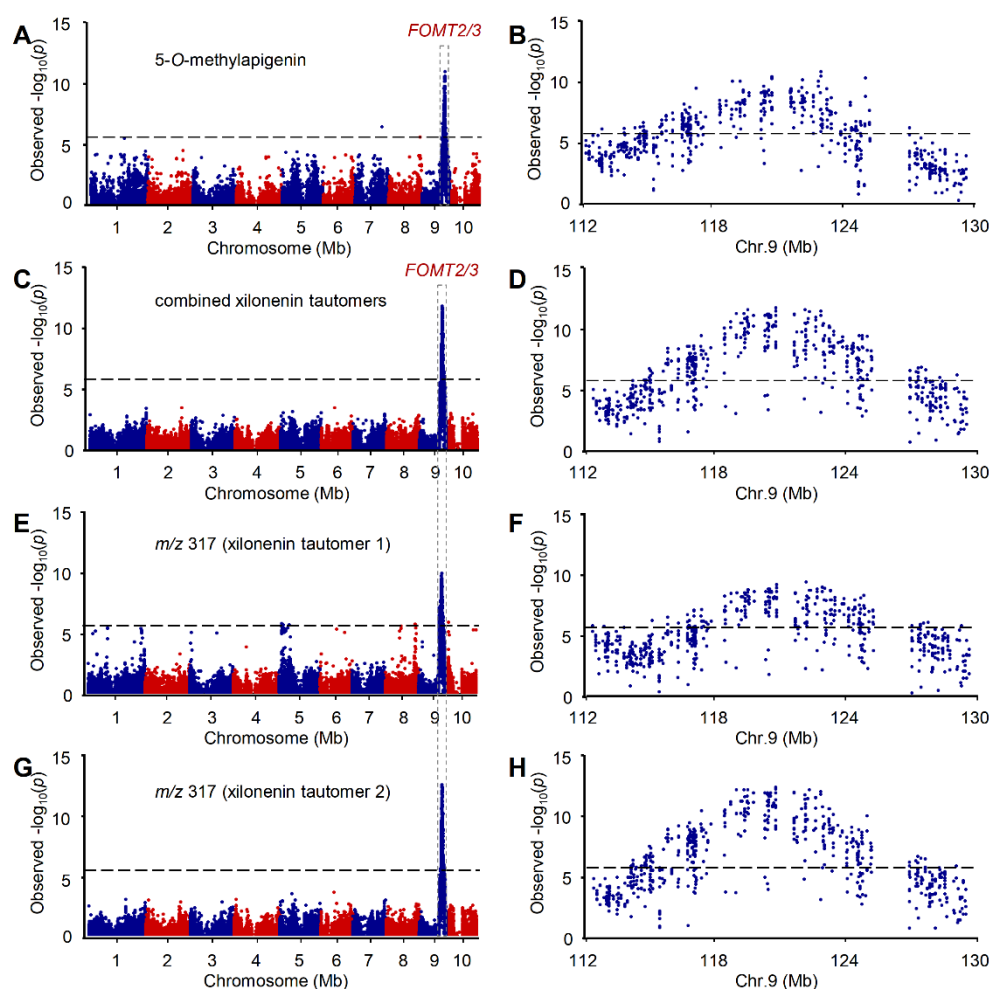
supplemental_data_set_S1 (Excel file)

Supplemental Dataset S2

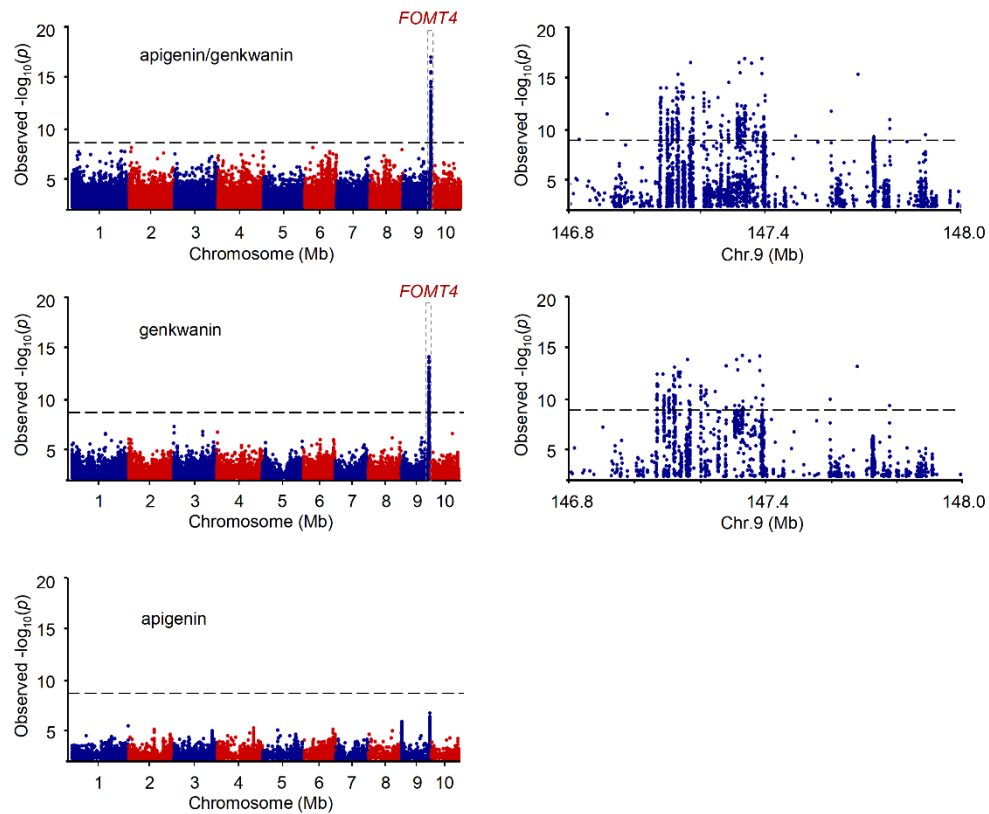
Note: supplemental_tables_part2 and the two Supplemental Datasets are not included in this thesis. This data is available online.



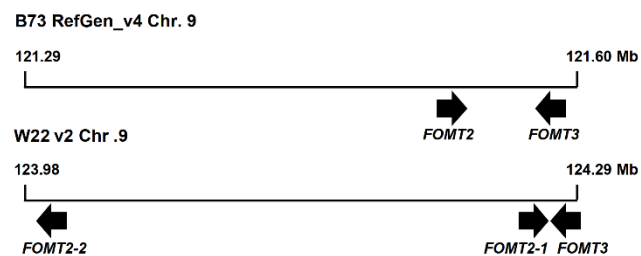
Supplemental Figure S1. MS/MS spectra of putative 5- and 7-O-methylflavonoids. The compounds were observed in *B. maydis*-infected W22 and/or B75 leaf tissue using untargeted LC-MS (full scan and auto MS/MS mode) as described in the methods section. The MS/MS spectrum of sakuranetin was obtained using a commercially available standard. 5- and 7-O-methyl derivatives have similar MS/MS spectra, but differ greatly in retention time (RT).



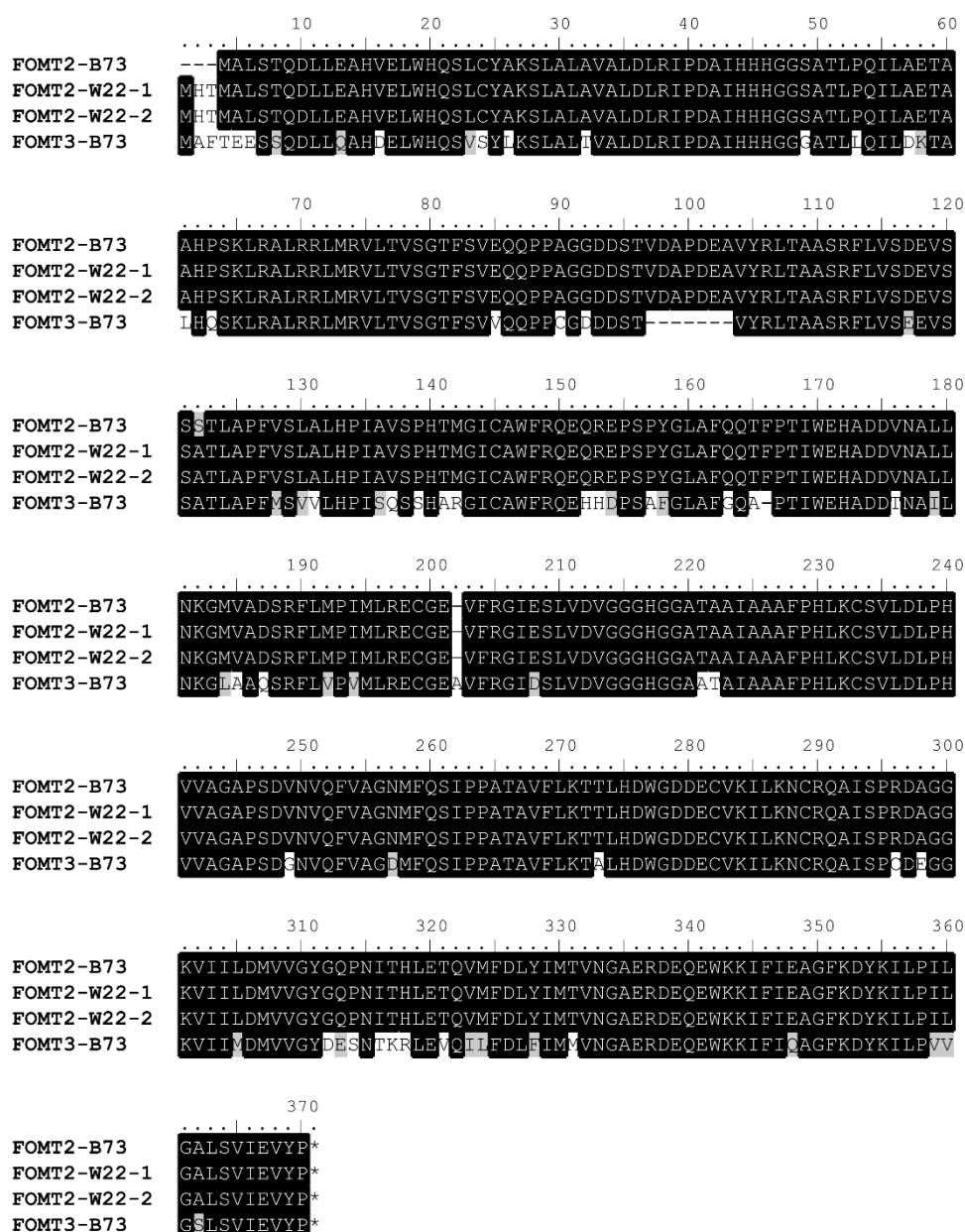
Supplemental Figure S2. Association mapping using B73 × Ky21 RIL with the GLM and 80,440 SNPs. Left panel (A,C,E,G): Manhattan plots of the association analysis of the indicated metabolites. The most statistically significant SNPs are located within the region of the maize FOMT2/3 on chromosome 9 (FOMT2, Chr.9:119,779,040-119,780,565 bp; FOMT3, Chr9: 119,838,646-119,840,122 bp; B73 RefGen_v2). The black dashed line denotes the false discovery rate (<0.05 at $-\log_{10}[P]$) using a Bonferroni correction. **Right panel (B, D, F, H):** Regional Manhattan plots representing a 'zoomed-in' view of the signal between 112.0 Mb and 130.0 Mb on chromosome 9, and each dot representing a single SNP.



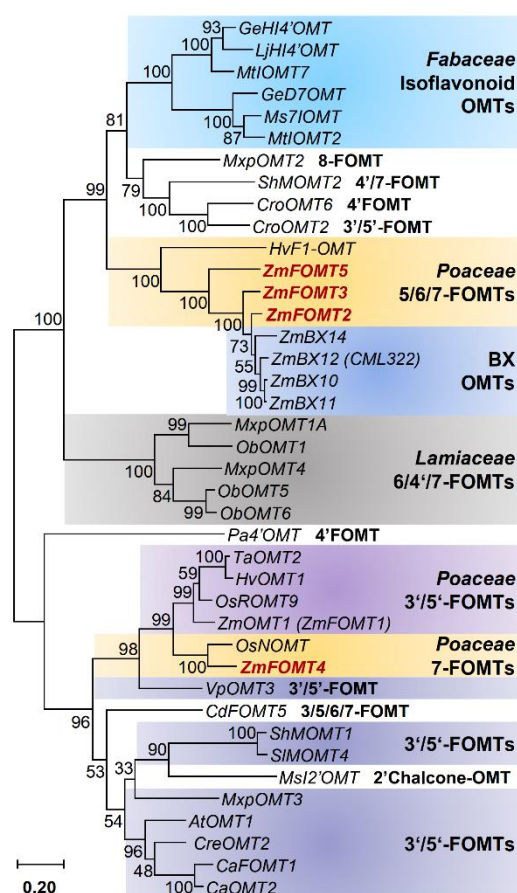
Supplemental Figure S3. GWAS mapping reveals association between the occurrence of genkwanin and *FOMT4*. **Left panel:** Manhattan plots of the association analysis (mixed linear model) of the indicated metabolites in the stems of maize plants from the Goodman diversity panel following 3 days of fungal elicitation. The most statistically significant SNPs associated with genkwanin and the ratio of apigenin to genkwanin are located within the region of the maize *FOMT4* on chromosome 9 (Chr9: 147,148,251-147,149,436 bp; B73 RefGen_v3), while no significant SNPs are associated with apigenin. The black dashed line denotes the false discovery rate (<0.05 at $-\log_{10}[P]$) using a Bonferroni correction. **Right panel:** Regional Manhattan plots representing a 'zoomed-in' view of the signal between 146.8 Mb and 148.0 Mb on chromosome 9, and each dot representing a single SNP.



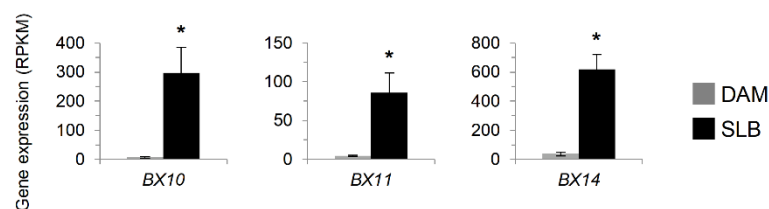
Supplemental Figure S4. Schematic chromosomal array of *FOMT2* and *FOMT3* in B73 and W22.
FOMT2-B73, Zm00001d047192; *FOMT3*-B73, Zm00001d047194; *FOMT2*-W22-1, Zm00004b033403;
FOMT2-W22-2, Zm00004b033399; *FOMT3*-W22, Zm00004b033404.



Supplemental Figure S5. Amino acid sequence alignment of FOMT2/3. The amino acid sequences encoded by *Zm00001d047192* (FOMT2-B73), *Zm00004b033403* (FOMT2-W22-1), *Zm00004b033399* (FOMT2-W22-2), and *Zm00001d047194* (FOMT3-B73) were aligned using the MUSCLE codon algorithm implemented in the software MEGA7 and visualized with the program BioEdit. Identical amino acids are shaded in black and similar amino acids in grey. FOMT2-B73 shares 99% and 79% amino acid identity with FOMT2-W22-1/2 and FOMT3-B73, respectively. **Note:** Unlike the W22 database sequences displayed here, the cloned FOMT2 sequence contains a D instead of an E on alignment position 17.

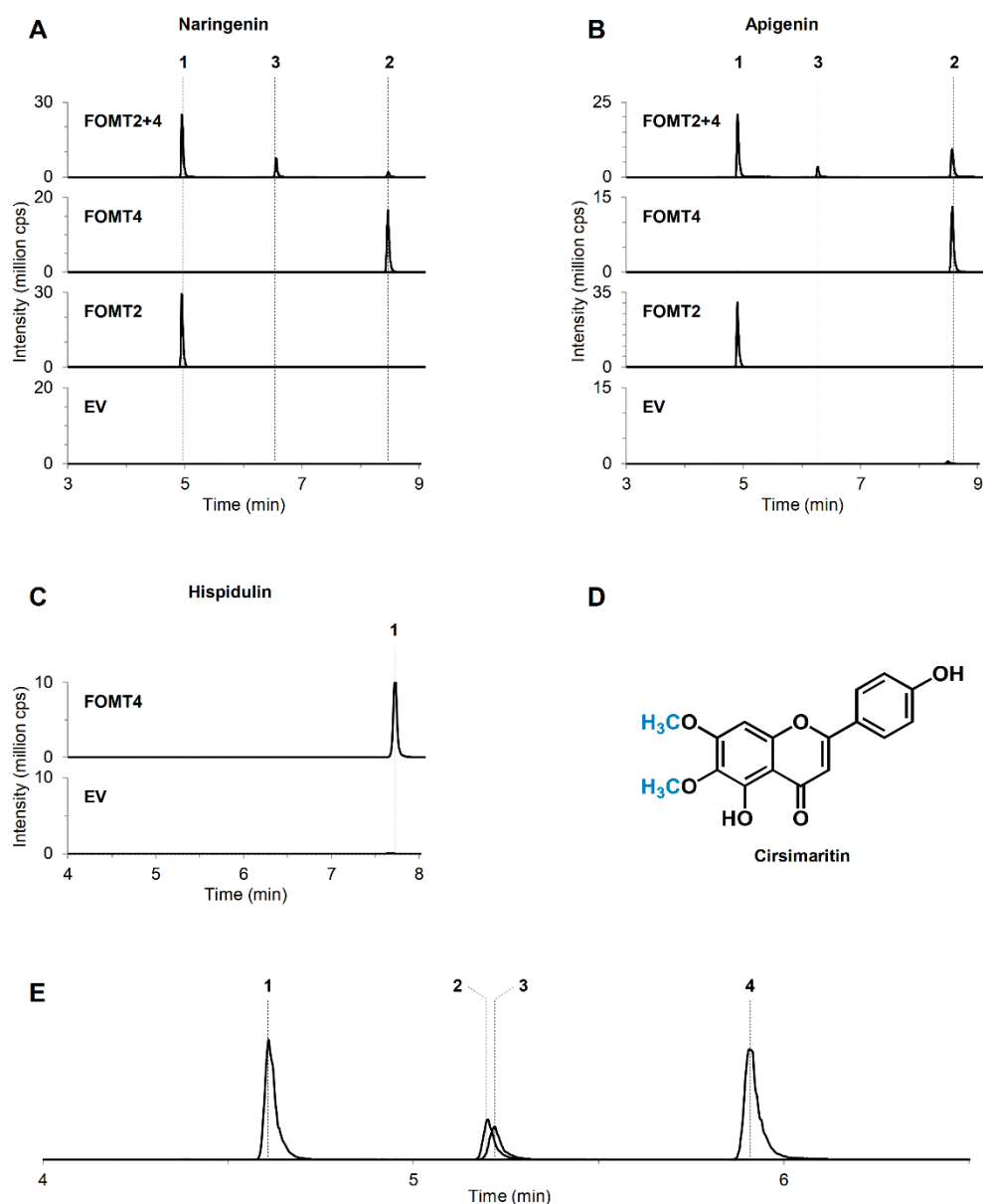


Supplemental Figure S6. Phylogenetic tree of maize *FOMT* genes characterized in this study, closely related maize *OMT* genes and characterized *FOMT* genes from other monocots and dicots. The tree was inferred using the maximum likelihood method based on the General Time Reversible model, including gamma distributed rate variation among sites (+G, 2.2239). Bootstrap values ($n = 1000$) are shown next to each node. The tree is drawn to scale, with branch lengths measured in the number of substitutions per site. All positions with $< 90\%$ site coverage were eliminated. Maize *FOMTs* investigated in this study are highlighted in red. The gene accession numbers and references are provided in Supplemental Table S3.

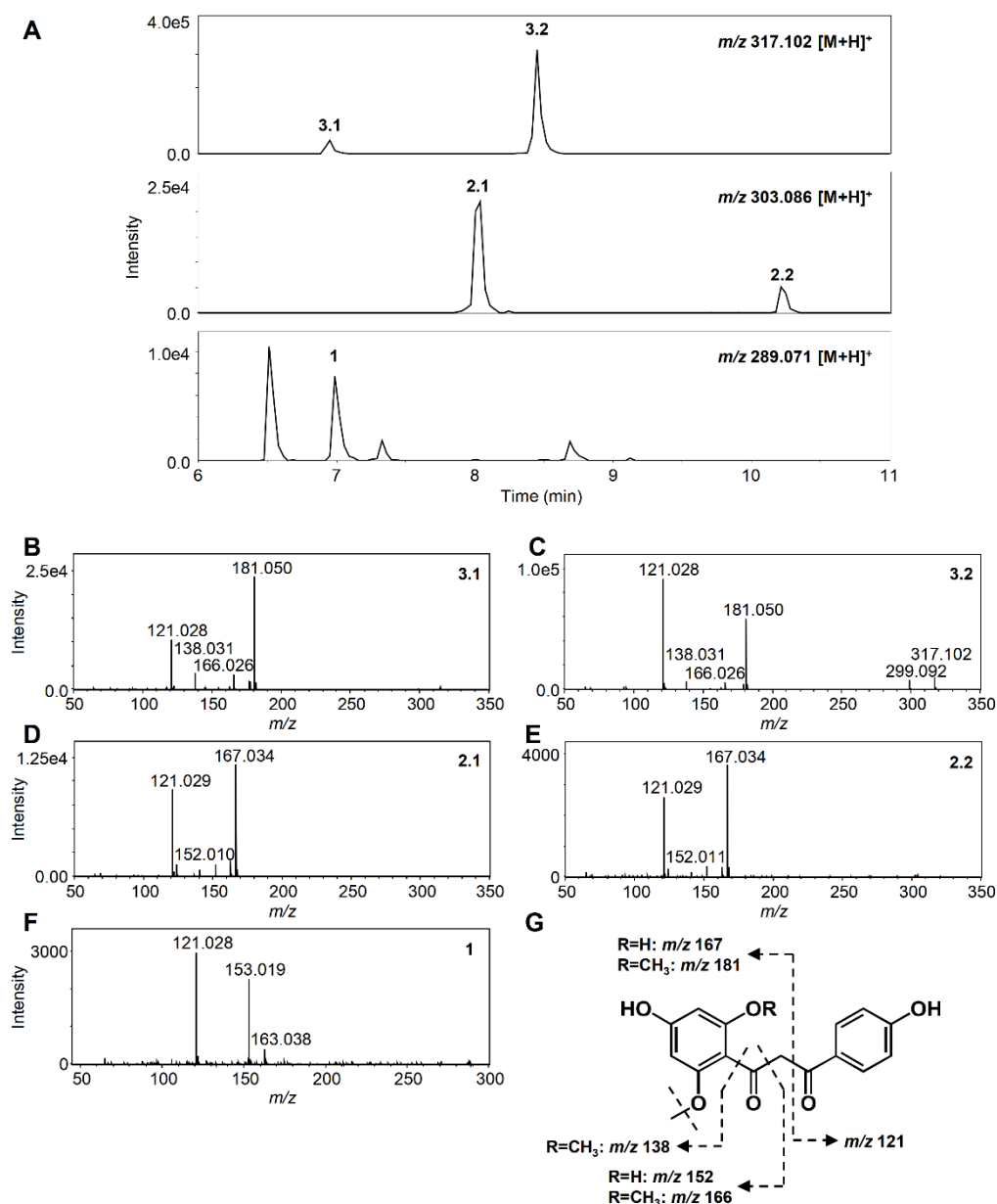


Supplemental Figure S7. Expression of *BX OMT* genes in W22 upon fungal infection.

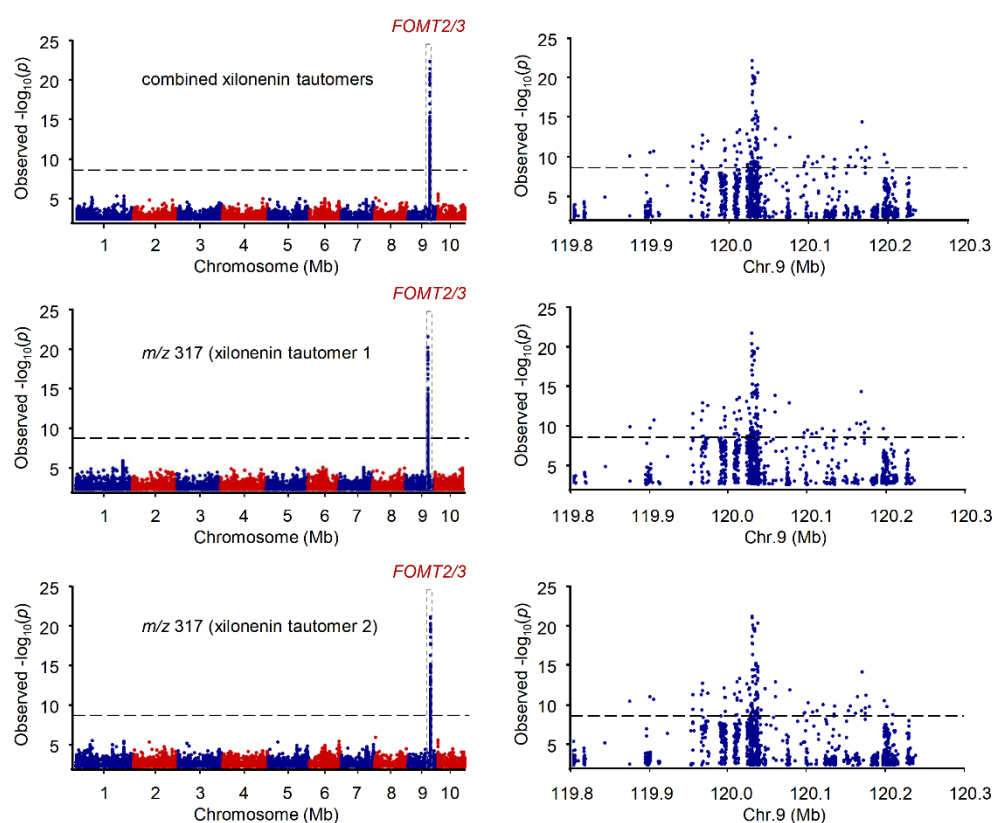
Transcript abundance of *BX10*, *BX11* and *BX14* derived from RNA-seq of damaged and either water treated (DAM) or *B. maydis*-infected (SLB) W22 leaves harvested after 4 days. Gene expression is given as reads per kilobase million (RPKM; Means \pm SE; $n = 4$). Stars indicate significant differences ($P < 0.05$) between treatments using a Bonferroni correction (for statistical values, see Supplemental Table S2).



Supplemental Figure S8. Regiospecific O-methylation and elution patterns of FOMT2 and FOMT4 products. The purified recombinant enzymes as well as the empty vector control (EV) were incubated with the substrate naringenin (**A**), apigenin (**B**) or hispidulin (**C**) in presence of the cosubstrate *S*-adenosyl-L-methionine. Reaction products were analysed by LC-MS/MS. Peak numbers in panel A: 1, 5-*O*-methylnaringenin; 2, 7-*O*-methylnaringenin (sakuranetin); 3, 5,7-*O*-dimethylnaringenin. Peak numbers in panel B: 1, 5-*O*-methylapigenin; 2, 7-*O*-methylapigenin (genkwanin); 3, 5,7-*O*-dimethylapigenin. Peak numbers in panel C: 1, 6,7-*O*-dimethylscutellarein (cirsimaritin). cps, counts per second. (**D**) Structure of cirsimaritin, the FOMT4 product in panel C. (**E**) The elution pattern of flavonoid substrates and their 5- and 7-*O*-methylated products, illustrated using the example of scutellarein. Peak numbers: 1, 5-*O*-methyl(scutellarein); 2, 5,7-*O*-dimethyl(scutellarein); 3, substrate (scutellarein); 4, 7-*O*-methyl(scutellarein). **Note:** For illustration, the peaks of different enzyme assays are combined in the chromatogram.

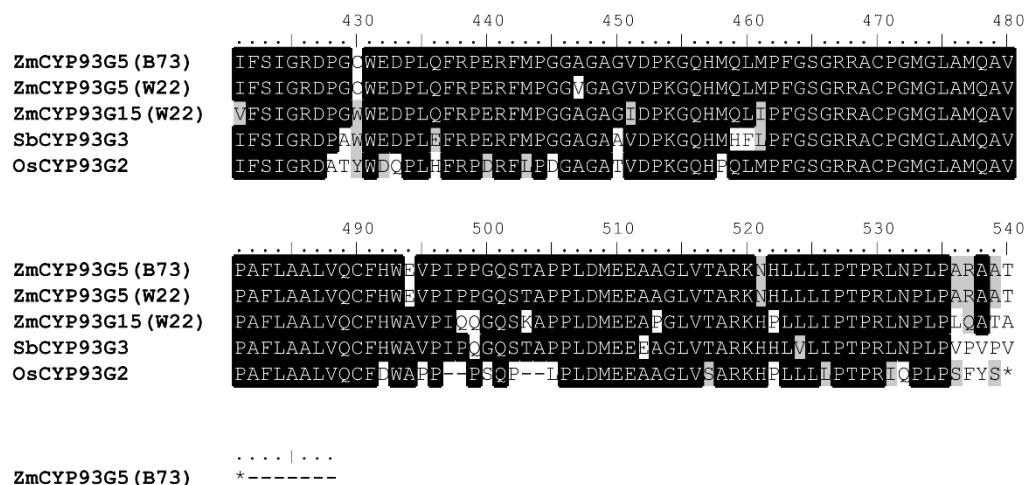


Supplemental Figure S9. Fragmentation patterns of 2-hydroxynaringenin and its O-methyl derivatives. Extracted ion chromatograms (A) and MS/MS spectra of 2-hydroxynaringenin (F) and different O-methyl derivatives (B-E), which were consistent with the fragmentation patterns of a mono- or di-O-methylated 2-hydroxynaringenin (G). The compounds were observed in *B. maydis*-infected W22 and/or B75 leaf tissue using untargeted LC-MS (full scan and auto MS/MS mode) as described in the methods section. 1, 2-hydroxynaringenin; 2.1 and 2.2, O-methyl-2-hydroxynaringenin; 3.1 and 3.2, O-dimethyl-2-hydroxynaringenin (xilonenin).

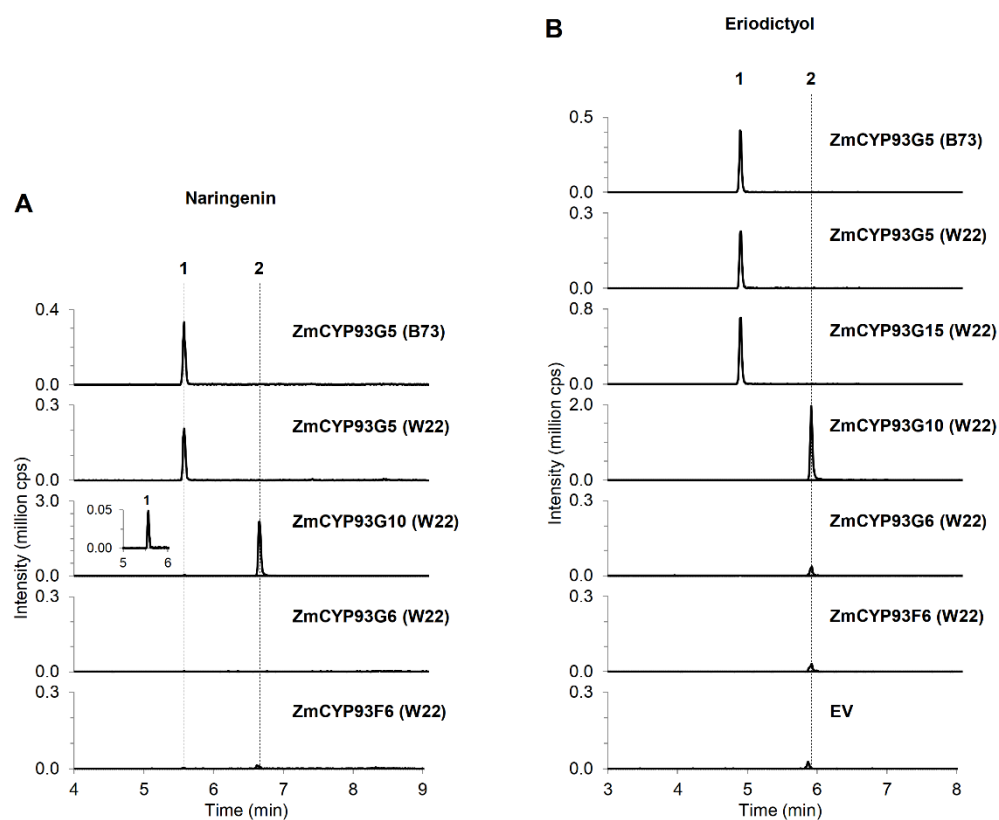


Supplemental Figure S10. GWAS mapping reveals association between the occurrence of xilonenin tautomers and *FOMT2/3*. Left panel: Manhattan plots of the association analysis (mixed linear model) of the indicated metabolites in the stems of maize plants from the Goodman diversity panel following 3 days of fungal elicitation. The black dashed line denotes the 5% Bonferroni corrected threshold for 25,457,708 SNP markers. The most statistically significant SNPs are located within the region of the maize *FOMT2/3* on chromosome 9 (*FOMT2*, Chr9: 120,033,582-120,035,107 bp; *FOMT3*, Chr9: 120,093,188-120,094,664 bp; B73 RefGen_v3). Right panel: Regional Manhattan plots representing a 'zoomed-in' view of the signals between 119.8 Mb and 120.3 Mb on chromosome 9, and each dot representing a single SNP.

	10	20	30	40	50	60
ZmCYP93G5 (B73)	MEAD	AAAA	SGG	LALL	PAVLLLV	ALSTLVFS
ZmCYP93G5 (W22)	MEAD	AAAA	SGG	LALL	PGVLLLV	ALSTLVFS
ZmCYP93G15 (W22)	ME	AAAA	VTP	LALL	LLLV	VTRWRNS
SbCYP93G3	MEAAE	AVTVGV	GSIGAPS	APGGVLL	LELLAL	STLIIIRWRNN
OsCYP93G2	MEE	GVVGGG		AAVL	VALLMTV	VLAVMRSAGSRSSKRGRLPPSPMA
	70	80	90	100	110	120
ZmCYP93G5 (B73)	LPLIGHLHLIRPPPHRA	FDRILARYGPLVYLRLGPSTH	CVVAGTADAARDLLKHEAS	IP		
ZmCYP93G5 (W22)	LPLIGHLHLIRPPPHRA	FDRILARYGPLVYLRLGPSTH	CVVAGTADAARDLLKHEAS	IP		
ZmCYP93G15 (W22)	LPLIGHLHLIRPPPHRA	FDRILARYGPLVYLRLGPSTH	CVVAGTADAARDLLKHEAS	IP		
SbCYP93G3	LPLIGHLHLIRPPPHRA	FDRILARYGPLVYLRLGPSTH	CVVAGTADAARDLLKHEAS	IP		
OsCYP93G2	LPLIGHLHLIRPPPHRA	FDRILARYGPLVYLRLGPSTH	CVVAGTADAARDLLKHEAS	IP		
	130	140	150	160	170	180
ZmCYP93G5 (B73)	RPLTAVTRHLAYDDAGFA	FAPYGFHWRFMKRLCMSELLGPRTVDQ	LRPVREAELAAVL	EA		
ZmCYP93G5 (W22)	RPLTAVTRHLAYDDAGFA	FAPYGAHWRFMKRLCMSELLGPRTVDQ	LRPVREAELAAVL	EA		
ZmCYP93G15 (W22)	RPLTAVTRHLAYDDAGFA	FAPYGAHWRFMKRLCMSELLGPRTVDQ	LRPVREAELAAVL	EA		
SbCYP93G3	RPLTAVTRHLAYDDAGFA	FAPYGAHWRFMKRLCMSELLGPRTVDQ	LRPVREAELAAVL	EA		
OsCYP93G2	RPLTAVTRHLAYDDAGFA	FAPYGAHWRFMKRLCMSELLGPRTVDQ	LRPVREAELAAVL	EA		
	190	200	210	220	230	240
ZmCYP93G5 (B73)	ARQAAAA	REPIDVSRHLISMSNNAIMRMVASALPGHMT	EAARDCAKHVAELVGAFN	VE		
ZmCYP93G5 (W22)	ARQAAAA	REPIDVSRHLISMSNNAIMRMVASALPGHMT	EAARDCAKHVAELVGAFN	VE		
ZmCYP93G15 (W22)	AASASAS	GEPIDVSRHLISMSNNAIMRMVASALPGHMT	EAARDCAKHVAELVGAFN	VE		
SbCYP93G3	ARQASAS	GERIDVSRHLISMSNNAIMRMVASALPGHMT	EAARDCAKHVAELVGAFN	VE		
OsCYP93G2	AQSAAER	GEGVDVSHELVMANNSIMRMVASALPGHMT	EAARDCAKHVAELVGAFN	VE		
	250	260	270	280	290	300
ZmCYP93G5 (B73)	DYVGLCRGWDLQGLTRRTREVRDKFDALLE	IMITCKEESRRRRHATTD	TGGG	TKDLLD	IL	
ZmCYP93G5 (W22)	DYVGLCRGWDLQGLTRRTREVRDKFDALLE	IMITCKEESRRRRHATTD	TGGG	TKDLLD	IL	
ZmCYP93G15 (W22)	DYVGLCRGWDLQGLTRRTREVRDKFDALLE	IMITAKEEKRRRRQ	---	QCQGDH	DKDLLD	IL
SbCYP93G3	DYVGLCRGWDLQGLTRRTREVRDKFDALLE	IMITAKEEKRRSQGDDGAETPT	DKDLLD	IL		
OsCYP93G2	DEVAVCRGWDLQGLTRRTREVRDKFDALLE	ITAKEEKARRSLRLGRRESS	SKDLLD	IL		
	310	320	330	340	350	360
ZmCYP93G5 (B73)	MDAAEDANA	EVRLTREN	IKAFVLDIFTAGSDTTATSV	EWMLAL	LINHPACMDK	LRAELDA
ZmCYP93G5 (W22)	MDAAEDANA	EVRLTREN	IKAFVLDIFTAGSDTTATSV	EWMLAL	LINHPACMDK	LRAELDA
ZmCYP93G15 (W22)	MDAAEDANA	EVRLTREN	IKAFVLDIFTAGSDTTATSV	EWMLAL	LINHPACMDK	LRAELDA
SbCYP93G3	MDAAEDANA	EVRLTREN	IKAFVLDIFTAGSDTTATSV	EWMLAL	LINHPACMDK	LRAELDA
OsCYP93G2	MDAAEDANA	EVRLTREN	IKAFVLDIFTAGSDTTATSV	EWMLAL	LINHPACMDK	LRAELDA
	370	380	390	400	410	420
ZmCYP93G5 (B73)	VVGASRLVGEQDVPR	LPYLQAVFKETLRLQPPAVFAQRET	IEPVHVRGYV	IP	PKTSVFFN	
ZmCYP93G5 (W22)	VVGASRLVGEQDVPR	LPYLQAVFKETLRLQPPAVFAQRET	IEPVHVRGYV	IP	PKTSVFFN	
ZmCYP93G15 (W22)	VVGASRLVGEQDVPR	LPYLQAVFKETLRLQPPAVFAQRET	VDIVSVR	GYV	IP	PKTSVFFN
SbCYP93G3	VVGASRLVGEQDVPR	LPYLQAVFKETLRLQPPAVFAQRET	IEPVHVRGYV	IP	PKTSVFFN	
OsCYP93G2	VVGASRLVGEQDVPR	LPYLQAVFKETLRLQPPAVFAQRET	IEPVHVRGYV	IP	PKTSVFFN	



Supplemental Figure S11. Amino acid sequence alignment of Poaceae F2Hs belonging to the CYP93G subfamily. The amino acid sequences encoded by GRMZM2G167336 (*ZmCYP93G5*; F2H1-B73), Zm00004b033614 (*ZmCYP93G5*; F2H1-W22), Zm00004b010826 (*ZmCYP93G15*; F2H2-W22), SbCYP93G3 (*Sorghum bicolor*; XM_002461241), and OsCYP93G2 (*Oryza sativa*; AK099468) were aligned using the MUSCLE codon algorithm implemented in the software MEGA7 and visualized with the program BioEdit. Identical amino acids are shaded in black and similar amino acids in grey. F2H2-W22 characterized in this study shares 85%, 84%, 80%, and 69% amino acid identity with F2H1-B73, F2H1-W22, SbCYP93G3, and OsCYP93G2, respectively.



Supplemental Figure S12. Enzymatic activity of CYP93G family members similar to F2H1 (CYP93G5) with naringenin or eriodictyol. The CYP93Gs were heterologously expressed in yeast and the microsomal fraction was incubated with the substrate naringenin (**A**) or eriodictyol (**B**) in presence of the cosubstrate NADPH. Enzyme products were analysed by LC-MS/MS. Numbers in panel A: 1, 2-hydroxynaringenin; 2, apigenin. Numbers in panel B: 1, 2-hydroxyeriodictyol; 2, luteolin. cps, counts per second; EV, empty vector control.

A

(2Z)-3-hydroxy-1-(4-hydroxy-2,6-dimethoxyphenyl)-3-(4-hydroxyphenyl)prop-2-en-1-one

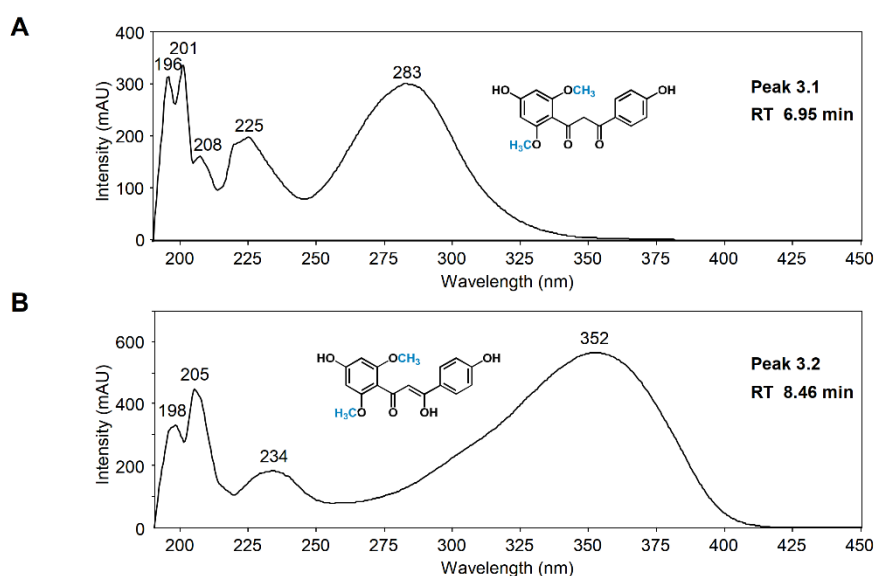
pos.	δ_H	mult., J_{HH} [Hz]	δ_C
1	-	-	189.5
2	6.33	s	100.5
3	-	-	183.2
1'	-	-	109.6
2'	-	-	160.3
3'	6.13	s	92.8
4'	-	-	162.2
5'	6.13	s	92.8
6'	-	-	160.3
1''	-	-	126.9
2''	7.79	d, 7.8	130.0
3''	6.84	m	116.3
4''	-	-	162.9
5''	6.84	m	116.3
6''	7.79	d, 7.8	130.0
-OCH ₃	3.75	s	56.0

B

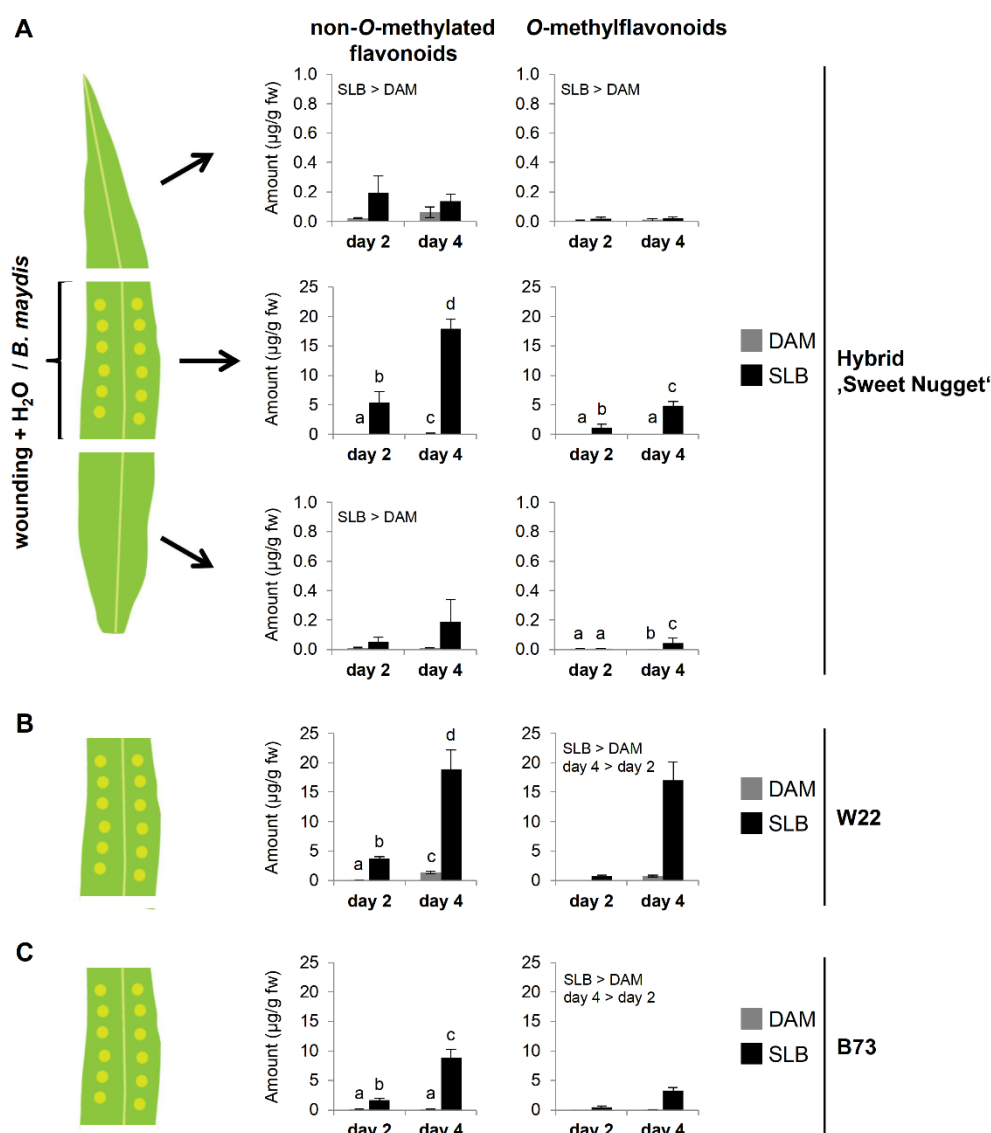
1-(4-hydroxy-2,6-dimethoxyphenyl)-3-(4-hydroxyphenyl)propane-1,3-dione

pos.	δ_H	mult., J_{HH} [Hz]	δ_C
1	-	-	198.4
2	4.34	s	56.0
3	-	-	194.8
1'	-	-	111.5
2'	-	-	160.3
3'	6.07	s	92.8
4'	-	-	162.9
5'	6.07	s	92.8
6'	-	-	160.3
1''	-	-	130.0
2''	7.84	d, 7.8	132.2
3''	6.84	m	116.3
4''	-	-	163.9
5''	6.84	m	116.3
6''	7.84	d, 7.8	132.2
-OCH ₃	3.68	s	56.0

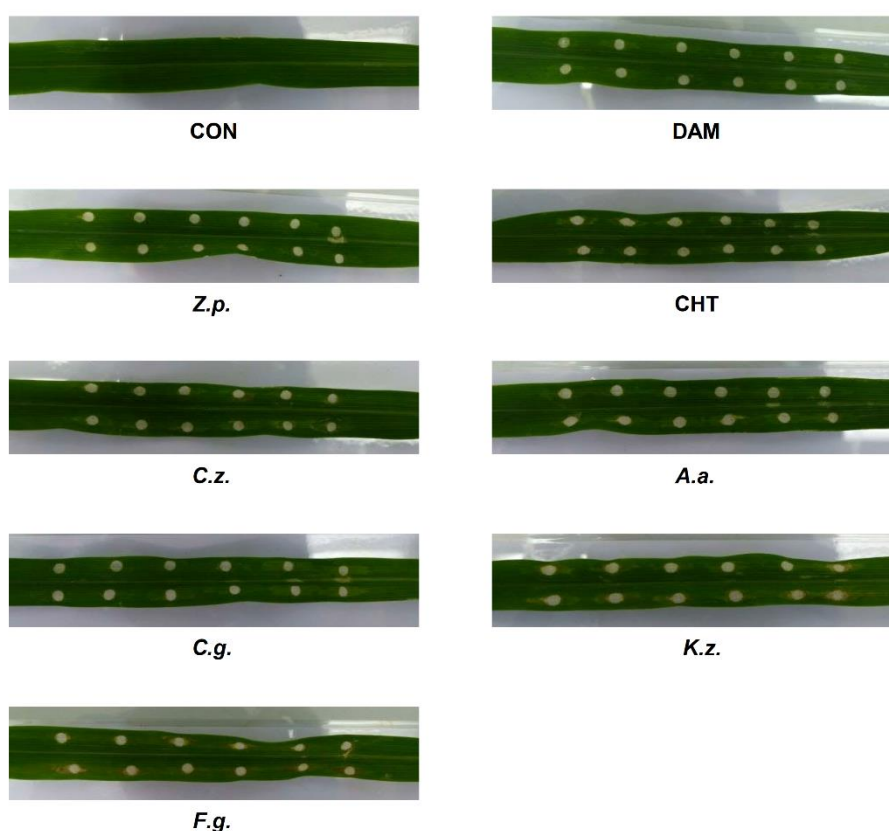
Supplemental Figure S13. NMR chemical shift data of xilonenin tautomers (in MeOH- d_3). The enol form (**A**) and keto form (**B**) occurred in a ratio of 2:1 at room temperature. In both tautomers the aromatic rings did not change into a quinoid conformation as is reflected in the chemical shifts; the tautomerism occurred only within the positions 2 and 3 of the propanoid moiety connecting the two aromatic rings. Another tautomeric structure could not be identified from the spectral data. The structures have been solved as follows: The methylene group in position 2 of tautomer B showed two long-range C-H correlations with keto functions at position 1 (δ_C 198.4) and position 2 (δ_C 194.8). The latter showed a long-range C-H correlation with positions 2''/6'' (d , d_H 7.84/ δ_C 132.2) of a 4-hydroxylated aromatic ring. The chemical shifts of positions 3''/5'' (d_H 6.84/ δ_C 116.3) were determined by COSY/HSQC correlations. Tautomer A showed a similar long-range C-H correlation 2''/6'' (d , d_H 7.79/ δ_C 130.0) \rightarrow 3 (δ_C 183.2). Position 2 in tautomer A was an unsaturated methine (s, d_H 6.33/ δ_C 100.5) showing long-range C-H correlations with a keto function at position 1 (δ_C 189.5) and the unsaturated hydroxyl function at position 3. For both tautomers A and B the connection of the second aromatic ring with the tautomeric 1,3-diketo propane moiety could be proven by a four-bond long-range C-H correlation (3'/5' \rightarrow 1). This second aromatic ring was symmetrically O-substituted as the signal for position 3'/5' appeared as singlet (B: d_H 6.07/ A: d_H 6.13). The position 2'/6' was shown to be methoxylated in both tautomers; a four-bond long-range C-H correlation (-OCH₃ \rightarrow 3'/5') determined the structure of the ring.



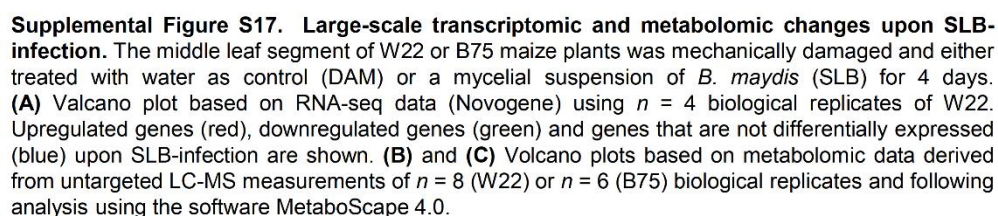
Supplemental Figure S14. The two xilonenin tautomers exhibit different UV absorption. UV spectra of the first (**A**) and second (**B**) peak of xilonenin (compare to Supplemental Figure S9A) were recorded using the purified compound and a LC-MS instrument additionally equipped with an UV detector as described in the methods section. The shift of the UV absorption maximum from 283 nm to 352 nm is indicative for the enol tautomer having a longer conjugated system than the keto tautomer.

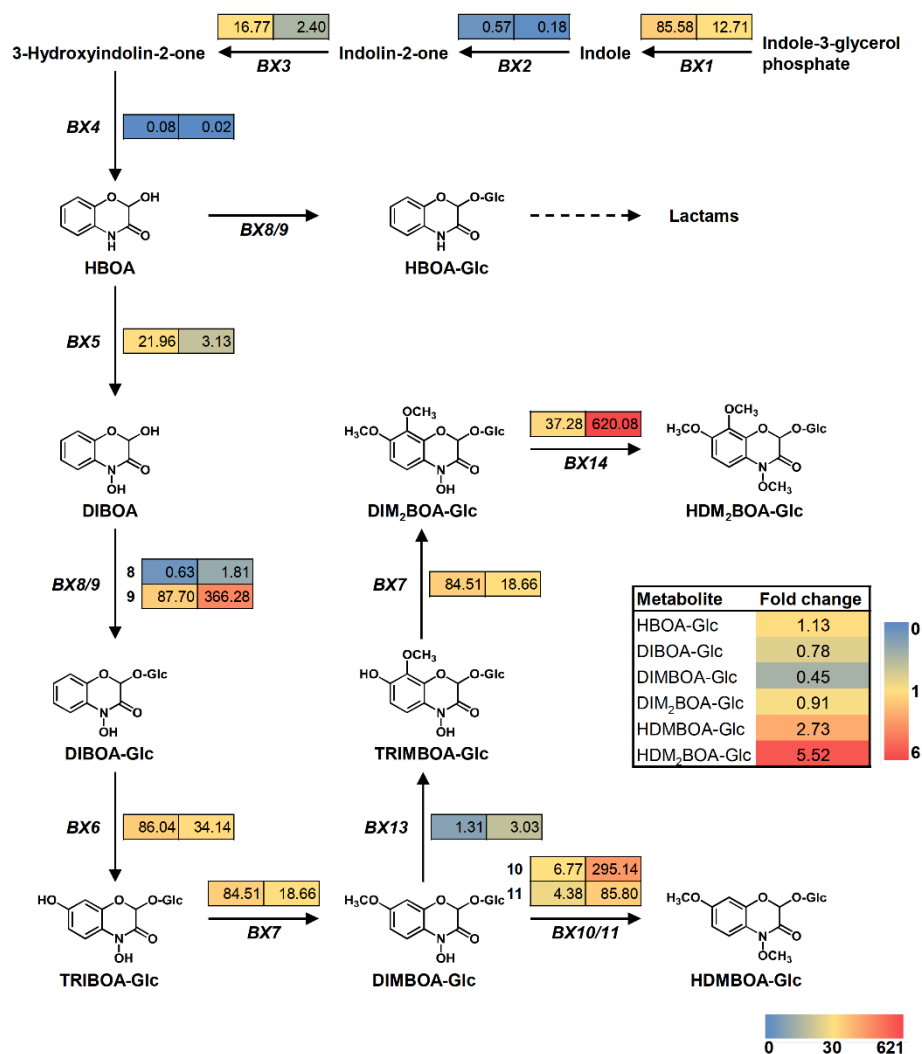


Supplemental Figure S15. De novo production of flavonoids in different maize lines after fungal infection. (A) Spatial distribution of non-O-methylated and O-methylated flavonoids in 'upper', 'middle' and 'lower' (top down) leaf segments of hybrid maize ('Sweet Nugget'). The middle leaf segment was damaged and either treated with water as control (DAM) or a mycelial suspension of *B. maydis* (SLB) for 2 or 4 days, and several different non-O-methylated and O-methylated flavonoids were quantified in the three leaf parts using LC-MS/MS. (B) and (C) The experiment was repeated with W22 and B73, respectively, with only the middle leaf segment harvested and analyzed. Shown are the total amounts of all analyzed non-O-methylated and O-methylated flavonoids (left and right panel, respectively; Means \pm SE; $n = 8$). Significant differences for the factors treatment or day are stated. Different letters indicate significant differences between treatments and days (for statistical values, see Supplemental Table S9). Results for individual analytes can be taken from Supplemental Tables S7 and S8.

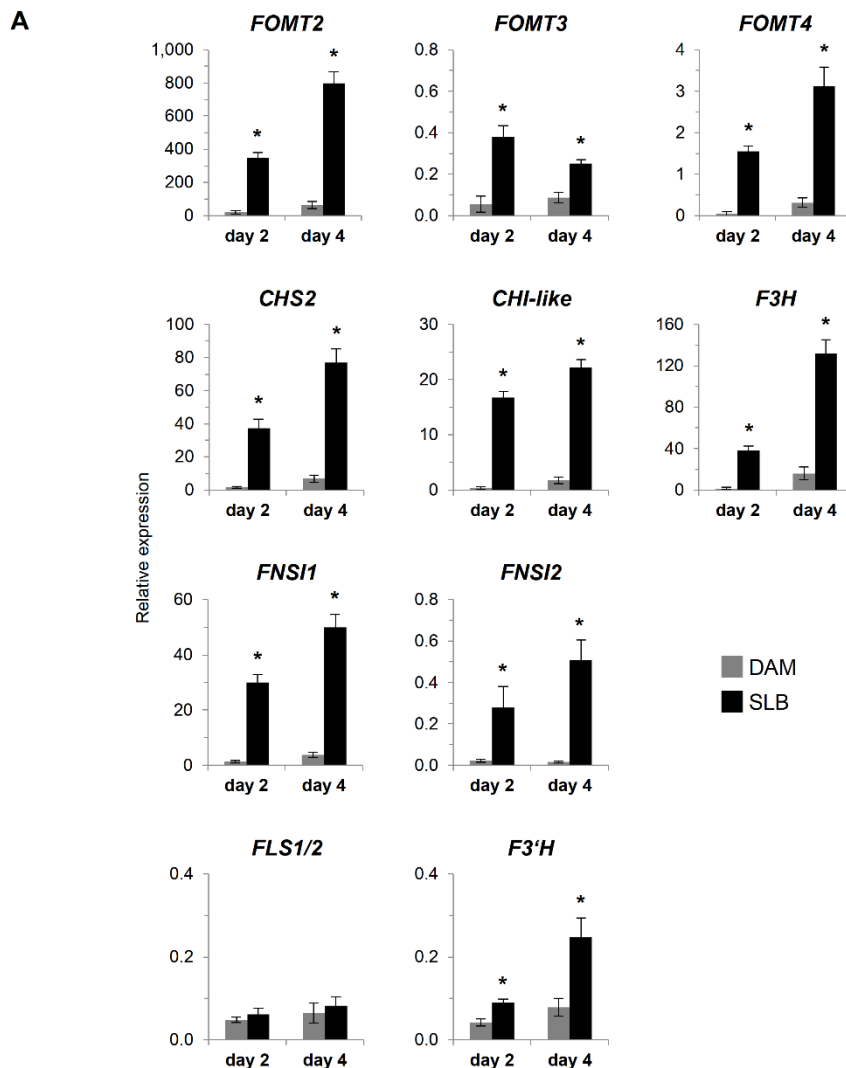


Supplemental Figure S16. Visible signs of infection on hybrid maize after inoculation with different pathogenic fungi. Shown are representative pictures of the following treatments: CON, undamaged; DAM, damaged and treated with water; Z.p., *Zymoseptoria pseudotritici*; CHT, chitosan; C.z., *Cercospora zeae-maydis*; A.a., *Alternaria alternata*; C.g., *Colletotrichum graminicola*; K.z., *Kabatiella zeae*; F.g., *Fusarium graminearum*.

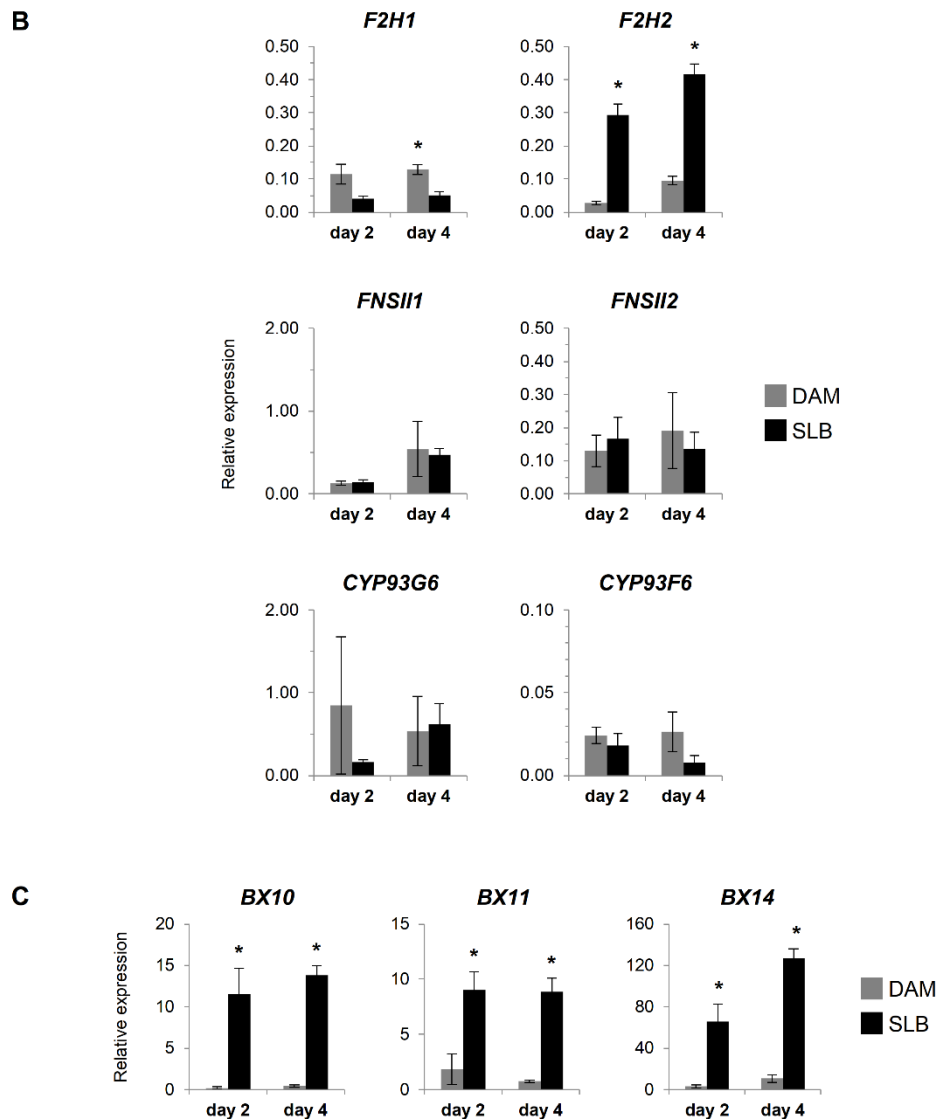




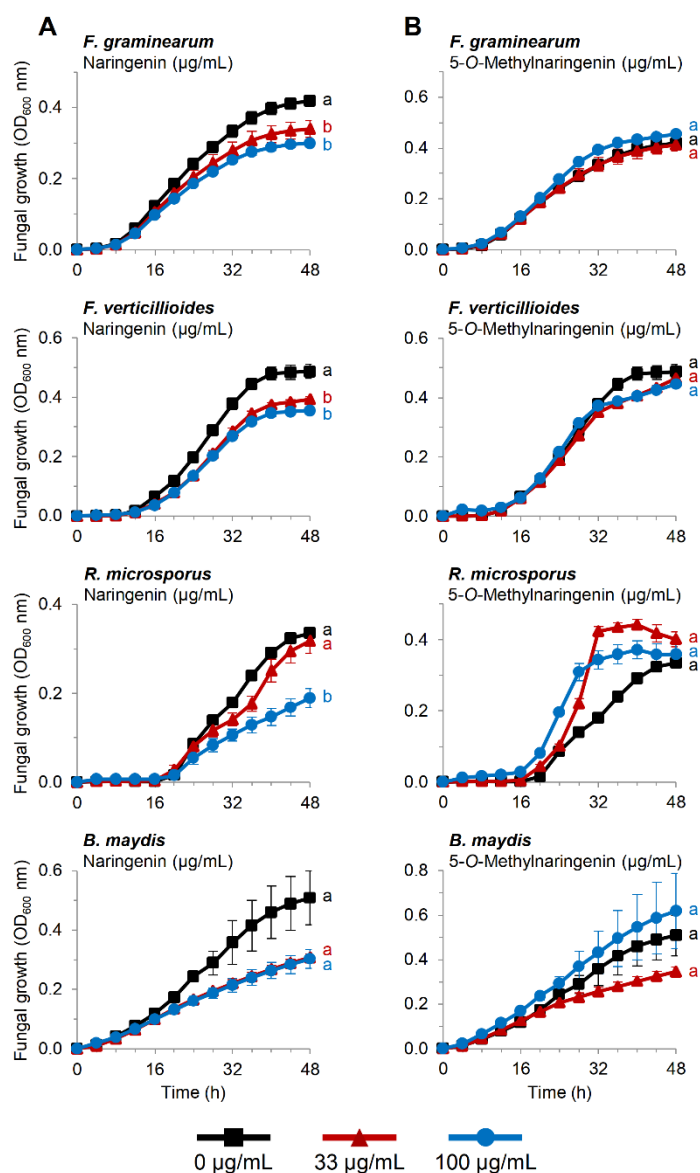
Supplemental Figure S18. Expression of the BX biosynthetic pathway during fungal infection. Expression of genes involved in the BX biosynthetic pathway in damaged and either water treated control (DAM) or *B. maydis*-infected (SLB) W22 leaves after 4 days of treatment. Transcriptomes were sequenced and mapped to the *Zea mays* W22 NRGene V2 genome. RPKM values for each gene are shown as a heat map next to the gene abbreviation (Means; $n = 4$): DAM (left column) and SLB (right column). For statistics see Supplemental Table S2. The inserted table gives fold changes of corresponding BX metabolites analysed by LC-MS/MS. Relative values can be taken from Supplemental Table S11). HBOA, 2-Hydroxy-3,4-dihydro-2*H*-1,4-benzoxazin-3-one; HBOA-Glc, 2-Hydroxy-3,4-dihydro-2*H*-1,4-benzoxazin-3-one glucoside;



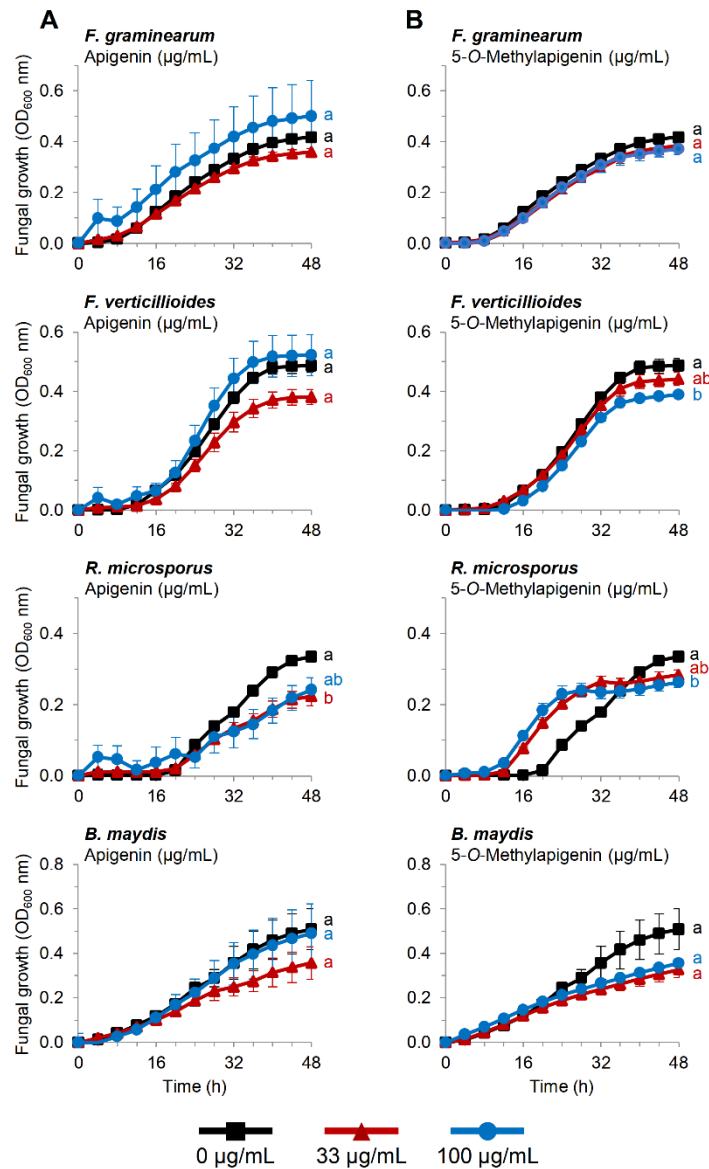
Supplemental Figure S19. RT-qPCR validation of flavonoid and BX pathway gene expression results in noninfected and fungus-infected W22 leaves. Expression of the indicated genes in damaged and either water treated (DAM) or *B. maydis*-infected (SLB) W22 leaves was measured by RT-qPCR relative to UBCP and MEP (Means \pm SE; $n = 4$). The relative expression is normalized in a way that values < 1 reflect cq values > 30 and hence rather low expression. Stars indicate statistically significant differences ($P < 0.05$) between treatments (Student's t -test or Mann-Whitney Rank Sum Test). All gene abbreviations and corresponding IDs are provided in Supplemental Table S2. **(A)** Relative expression of *FOMTs* investigated in this study and flavonoid core pathway genes. *FOMT2*, day 2 ($P = 0.029$, $T = 10$); *FOMT2*, day 4 ($P = 0.029$, $T = 10$); *FOMT3*, day 2 ($P = 0.003$, $t = -4.937$); *FOMT3*, day 4 ($P = 0.002$, $t = -5.267$); *FOMT4*, day 2 ($P = < 0.001$, $t = -10.804$); *FOMT4*, day 4 ($P = < 0.001$, $t = -6.086$); *CHS2*, day 2 ($P = 0.029$, $T = 10$); *CHS2*, day 4 ($P = < 0.001$, $t = -8.247$); *CHI-like*, day 2 ($P = 0.029$, $T = 10$); *CHI-like*, day 4 ($P = 0.029$, $T = 10$); *F3H*, day 2 ($P = 0.029$, $T = 10$); *F3H*, day 4 ($P = < 0.001$, $t = -7.997$); *FNSI1*, day 2 ($P = < 0.001$, $t = -9.460$); *FNSI1*, day 4 ($P = < 0.001$, $t = -9.520$); *FNSI2*, day 2 ($P = 0.044$, $t = -2.536$); *FNSI2*, day 4 ($P = 0.029$, $T = 10$); *FLS1/2*, day 2 ($P = 0.407$, $t = -0.892$); *FLS1/2*, day 4 ($P = 0.617$, $t = -0.528$); *F3'H*, day 2 ($P = 0.008$, $t = -3.951$); *F3'H*, day 4 ($P = 0.018$, $t = -3.246$).



Supplemental Figure S19 continued. (B) Relative expression of *CYP93s* investigated in this study. *F2H1*, day 2 ($P = 0.029$, $T = 10$); *F2H1*, day 4 ($P = 0.029$, $T = 10$); *F2H2*, day 2 ($P = 0.051$, $t = 2.430$); *F2H2* ($P = 0.007$, $t = 4.000$); *FNSII1*, day 2 ($P = 0.735$, $t = -0.354$); *FNSII1*, day 4 ($P = 0.486$, $T = 15$); *FNSII2*, day 2 ($P = 0.486$, $T = 15$); *FNSII2*, day 4 ($P = 0.686$, $T = 20$); *CYP93G6*, day 2 ($P = 0.343$, $T = 14$); *CYP93G6*, day 4 ($P = 0.343$, $T = 14$); *CYP93F6*, day 2 ($P = 0.517$, $t = 0.688$); *CYP93F6*, day 4 ($P = 0.400$, $T = 9$). **(C)** Relative expression of *BX OMTs*. *BX10*, day 2 ($P = 0.029$, $T = 10$); *BX10*, day 4 ($P = < 0.001$, $t = -11.636$); *BX11*, day 2 ($P = 0.014$, $t = -3.435$); *BX11*, day 4 ($P = < 0.001$, $t = -6.572$); *BX14*, day 2 ($P = 0.010$, $t = -3.718$); *BX14*, day 4 ($P = < 0.001$, $t = -12.104$).



Supplemental Figure S20. Antifungal activity of naringenin and 5-O-methylnaringenin. Growth (optical density at 600 nm) of *F. graminearum*, *F. verticillioides*, *R. microsporus* and *B. maydis* in the absence and presence of naringenin (A) and purified 5-O-methylnaringenin (B) measured over a 48-h time course in a defined minimal broth medium using a microtiter plate assay. Data are shown as means \pm SE ($n = 4$). Different letters indicate significant differences ($P < 0.05$) between treatments at 48 h (one-way ANOVA followed by Tukey-Kramer's post-hoc test or Student's t-test). *F. graminearum*: naringenin ($F = 12.948$, $P = 0.002$); 5-O-methylnaringenin ($F = 1.552$, $P = 0.264$); *F. verticillioides*: naringenin ($F = 20.144$, $P < 0.001$); 5-O-methylnaringenin ($F = 1.923$, $P = 0.202$); *R. microsporus*: naringenin ($F = 14.022$, $P = 0.002$); 5-O-methylnaringenin ($F = 1.901$, $P = 0.205$); *B. maydis*: naringenin ($F = 4.350$, $P = 0.048$); 5-O-methylnaringenin ($F = 1.531$, $P = 0.268$).



Supplemental Figure S21. Antifungal activity of apigenin and 5-O-methylapigenin. Growth (optical density at 600 nm) of *F. graminearum*, *F. verticillioides*, *R. microsporus* and *B. maydis* in the absence and presence of apigenin (A) and purified 5-O-methylapigenin (B) measured over a 48-h time course in a defined minimal broth medium using a microtiter plate assay. Data are shown as means \pm SE ($n = 4$). Different letters indicate significant differences ($P < 0.05$) between treatments at 48 h (one-way ANOVA followed by Tukey-Kramer's post-hoc test). *F. graminearum*: apigenin ($F = 0.775$, $P = 0.489$); 5-O-methylapigenin ($F = 1.634$, $P = 0.248$); *F. verticillioides*: apigenin ($F = 2.707$, $P = 0.120$); 5-O-methylapigenin ($F = 6.781$, $P = 0.016$); *R. microsporus*: apigenin ($F = 5.397$, $P = 0.029$); 5-O-methylapigenin ($F = 7.061$, $P = 0.014$); *B. maydis*: apigenin ($F = 0.660$, $P = 0.540$); 5-O-methylapigenin ($F = 2.914$, $P = 0.106$).

FOMT3-B73 codon optimized

ATGGCGTTTACGGAAGAGAGTTCCCAAGACCTCCTGCAAGCGCACGATGAATTATGGCACCAGAGTGTACGTACCTGAAATCGCTCGCCTTAAC
GGTGGCGTTGGATCTGCGCATCCAGATGCCATTCCACCACCATGGTGGCGGTGCCACACTCCTGCAGATTCTTGACAAAACCGCACTGCATCAGA
GCAAATTGCGTGCCTTACGTCGCCTCATGCGTGTCTTACGGTTAGCGGGACCTTCAGTGTGGTACAAACCTCCGTGTGGCGACGATGACTCA
ACCGTATATCGCTTAACCGCGGCGAGCCGGTTCTTAGTGAGCGAAGAAGTGTGCTGCGACACTGGCTCCTTTCATGTCCGTGGTACTTCACCC
GATTAGCCAGAGCTCCCATGCGCGTGGTATCTGCGCATGGTTTCGCCAAGAGCACCATGATCCGAGTGCATTGGTCTGGCGTTTGGACAGGCAC
CTACCATTTGGGAACATGCCGATGATACCAATGCCATTCTGAACAAAGGCCTGGCGGCTCAGTCTCGCTTCTGGTTCCGGTTTATGCTGCGCGAA
TGTGGTGAAGCCGTGTTTCGTGGAATTGACTCTCTTGTGCGACGTTGGTGGTGGCCATGGCGGAGCCGCAACTGCCATCGCGGCAGCCTTCCGCA
TCTGAAATGCTCAGTGTGGATCTGCCACATGTGGTTGCAGGGGCTCCCTCAGATGGGAATGTGCAGTTTGTCTGCTGGCGACATGTTTCAGTCGA
TTCCACCGGCAACTGCGGTGTTTCTGAAAACGGCTCTGCATGATTGGGGTGACGATGAATGCGTGAAAACTCTGAAGAACTGCCGCCAAGCCATT
TCGCCGTGTGATGAAGCGGCAAGTCATCATCATGGATATGGTTGTTGGCTATGATGAGTCCAACACCAAGCGCTTGGAGGTCCAGATTCTGTT
CGATCTGTTTCATCATGATGGTCAATGGTGCCGACGGGATGAACAGGAATGGAAGAAATCTTCATTACGGCTGGCTTCAAAGACTACAAAATC
TGCCGGTAGTAGGGAGCTTGCTGTGATTGAGGTCTATCCCTAA

FOMT5-B73 codon optimized

ATGGCCTTACTCGGGGAATACTCCAGCCAAGAGCTGTGCAAGGGCAACTGCAGCTGTGGCATCAGTCGCTGGGCTTCTTTAAGTCACTGGCCCT
GGCCGTGCGATGGATCTGCGCATTCAGATGCGATTACCGCTTGGGTGGCGAGCGACGCTTCCGCAGATTCTGGCGGAAGCGGGCATCAAAA
TTGACCCCTTGTAACAACAACTGCGGGACTTACGCCGTGTAATGCGCGCCCTGACCGTGAGCGGGATCTTACGGTCGTACAACGTCAGCGAGT
TCGTCCGATGGCGGTGGCCGTGCTGGTGTGAAGCGGAAGTCCGGTTTACAACTGACAGCGGCTCTCGCTTACTGGTAGTTGGCGAGAAAGA
GTGCTCTACTACCGCCACTACCGTCAATTGCCGCCGCCGCTTCTTAAACGGTGTATGTGCAGCTGTTGCTGGAACCTGTGCGGCGAGTGCCT
TTAGTCGTGCTGTTGCGGAGTGGTTCCAATTCCAACAGCCGCCACAGGACGATGGTTCAGCATCAGCAGCCAGCTGGCCGTCTTAGCAGTCCCTTT
GCCTTGGCATGTGGTGACAGACCATTTGGGAACGTGCAGAACGCGATGCGCACGCATTCCGTTTGACGATGCCATGGCGTCCGATACCGCGTT
TCTGATGCCGATTGTATTACGGGAATGCGCGATGAAGTTTTCGGTCTGGCCTTACCAGCTTGGTGGATGTTGCTGGTGGACTGGGAGGAGCGG
CCGCGACGATTCAGCTGCTTTTCCCGATCTTAGCTGCACAGTCTCGATCTGCCCCATGTGGTTGCGAAAGCAGCGGCCGGCACTACCGATAGC
AATGTCCAGTATGTGGCAGGCGACATGTTCCAGTGCATTCCGCTGCGAGATGCCGTCTTACTCAAATGGATTCTCCACGATTGGTCCGACGACGA
GTGTGTGCGTATTCTGAAGAACTGCAACAGGCTATTCGCCACGCGCTGCCGGTGGGAAAGTGATTATCATCGACATGGTGGTTCGGGTCTCTG
GCTCAGGGTCCGCAGATGATGAACCGAGCGAAAGCGATCTGCGCCATGTGCAAAACCCAGATCTTGTGATCTGCTGATGATGTGCGTGAATGGT
GTGGAACGCGACGAACAAGAGTGAAGAAAAATCTTCTCAGAGGCGGTTTCCAGGACTATCGCATCATGCCGTCTTGGCGTTTCGCTCTATCAT
CGAAGTGTACCCGAATTA

Supplemental Figure S22. Codon-optimized gene sequences of *FOMT3-B73* and *FOMT5-B73* synthesized for expression in *E. coli*. Synthetic genes were inserted in the pUC57 vector.

ATGGAAGCTGATGCTGCTGCTGCAGCTGCTTCTGGTGGTTTGGCTTTGTTGCCAAGGTGTTTGTGTTGGTGGCTTTGTCTACTTTGGTTTTCTCT
TACCTGGTCTACCAAGAAACTAGATTGGTCCACCATTCCAATTGGCTTTGGCATTGATGGTCACTTGGTACTTGCATTGGATAGACCACCACACATAGAG
CTTCCTGAGAAGAAATTTGGCTAGATATGGTCACTTTGGTCTACTTGAGATTGGGTGCATCACTAAGTGTGTTGCTGTGCACTCAGATGCTGCTG
AGAGATTGTTCTGAAACCATGAAGCTCTATTCAGGAAGAACATTGACTGCTGTTACTAGACATTGGCTTATGATGATGCTGGTTTGGTTTGGT
TCCATATTGGTGTCTATTGGAGGTTTATAGAAGATTTGTCATGCTCCGAATTTGGGTCTTGAAGACTTGTGATCAATTGAGGCCAGTTAGAAGA
CTGAATTTGGCTGCTGTTTTGGAAAGCTGCTAGACAAGCTGCTGCGCTAGAGAACCATTGATGTTTCAAGACATCTGATCTGCCATGTCCAACAAC
GCTATTTAGAAGATGGTGCTCTGCTGTTTGGCAGGTCAACATAGCTGAAGCTCAGAGAGATTGGCTGTAAGCTGGTGTGAATTTGGTGGCTT
TACGTTTGAAGATTACGTTGGTTTGTGTAGAGTTGGGACTTGAAGGTTTGAACAGAAGAACTGAGAAGTCAGATAAGTTTCATGCGCTTCT
TGGAAATTATGATCACCGGTAAGAAAGAGTCTAGAAGAAGAAGGCACGCTACTACTGATACAGTGGTGGTACAAAAGACTTGTGGATATATTG
ATGATGCTGCTCCGAAGAAATGCAATGCTCAAGTTAGTTAGACAGTGAAAACATCAAGCTTTCGTTTGGATATTTTCACTGCTGGTTCTGATAC
AAGTGCTACTTCTGTGTGAATGGATGTGGCTTGTGATTAAACCTCAACGCTTGTATGGTAAGTGTGAGAGCAGAAATGATAGCAATGTTTGTGGT
CATCTAGATTGGTGGTGAACAAGATGTTCCAAGATTGCCATACTTGAAGCCGTTTTCAAAGAACTTTGAGATTACAACCACCAGCTGTTTTC
CTCCAAAGAGAAAACAAATGCAACGATTCACGTTAGAGGTTACGTTATCCATCTAAGACCTCCGTTGTTCTTCAACATTTTCCATATGCTGGTAGAGA
TCCAGGTTTGTGGGAAGTTCAATTCGAATTCAGACAGGAAGAATTCATGCGAGGTGGTGTGGTGGCGGTTTGTATCCAAAGGTCAACATATGC
AATTGATGCCAATTGGTCTGTTAGAAGGGCTGTCCAGGATGGGTTTAGCTATCAAGACTGTTCAGCTTTTTTGGCTGCTTGTATGTTCAATGT
TTCCATTGGGAAGTTCCAATTCCACAGGCTCAATCTCACTGTTCCAGCATTTGGATATGGAAGAAGCTGCTGGTTTGGTTACTGCTAGAAGAACCA
CTGTGGTTGATTCCAACCAAGGATTGAATCCATTGCCAGTAGAGCTGCTACTTTAA

ATGGAAGCTGCTGCTGCAGTTACCCATTGGCTTTGTTGTTGTTGCTTTTGTGGTACTAGATGGCGTTGGTCCTCTCTAGAAGTTCTAAAT
GCCACCATCACCAATGGCCCTGCCATTGATTTGGTCACTTGCATTTGGATAGAAGATTGCCACACAGATCTGGATAGAATTTTGGCTAGATATG
GCTACCTGGTCTACTGATTGAGTTGGGTGCATCTACTCATTCATGATGCTGATGCTGATGCTGATAGATTTGTGAACATGAAGCCTCT
ATCCACAAAGACCATTGACAGTTGTTGCTAGACATTGGCTTATGATGATGCTGGTTTGGCTTTTGGCTCCATATGGTGCTCATTTGAGATTCAT
AAGAGATTTGTCATGCTCGCAATTATTTGGGTGCCATAGAACCTTGATGATGATTTGAGGCCAGTTAGAGAAGCTGAATTTGGCTGGTCTG
CTGCTCTGCTTCAGCATCTGGTGAAGTGAACTTATGATGTTTCCAGACATCTGATCTGATGCTTCCAAACATGCTATTTAGATGAGTTGGTGGCT
TCAGCTTTGCCAGGTCACATGCTCAAGCAGCATAGACAGTCTGCTAAACATGTTGCTCAATGATTTGGTGGCTCTCAACATCGCAAGATTCAGTTGG
TTTGTGTAGAGTTTGGGACTTGCAAGGTTTGACTAGAGAAGCATAGACAAGTCAGAGATAAGTCTCGATGCTTGTGGAAATGATGATTACCGCCCA
AAGAAGAAAAGCGTAGAAGAAGGCCAACAAAGGTCAGGTTGATCATGATGATTTGCTGGATATTTTGTATGGATGCTGCGAGCTGACGAAAATGCTGAA
GTAGATTGACTAGGGAAAACCATCAAGGCTTTGCTTTTGGATATCTTCACTGCTGGTCTTGATGCAACTGCTACTCTCTTGTGATGATGTTGGC
CTACTTGATTAAACCATTCAGTTCTGATGATAAGTGTAGAGACGAATGGATGGTGTGTTGTGGTGCATCTAGATTTGGTTGGTGAACAAAGTTGTT
CACATTTGCCATACTTGAAGCCGTTTTTCAAAGAACTTTGAGATTGCAACCACCAGCTGTTTTTGGCTCAAAGAGAAACAGTTGATACCGTTAGA
GTAGAGGTTGACGTTATCCCAACAAAACCTTCGTCATTTTCAAGCTGTTTTTCCATATGCTGGTAGAGATCCAGGTTTGGTGGGAATCCATTGCAATTT
CAGACAGAAAGATTCATGCGAGGTGGTGGTGGCAGGTTATGATGCAAAAGGTCACATATGCAATTTGATCCATTTGGTCTTGGTAGAAGGG
CTTGCCAGTATGGGTTTAGCTATGCAAGCTGTTCCAGCTTTTTTGGCTGCTTTGGTTCATGTTCCATTTGCTGGGCTGTTCAATTTCAACAAAGC
CAATCTAAAGCTCCACCATTTGGATATGGAAGAAGCTCCAGGTTTGGTTACTGCTAGAAAAACCTCTTGGCTGTGATTCCAATCCAAGATTGAA
TCCATTGCCATTTGCAAGCTCACGCTACTTGA

ATGAGGAAACAACACCTAGACCACACCATTCATTATGTTGCTTTTATCCTCTTTGGCTAAGAACAAACCCAGAAGCTCTTTTGGCTTTGATTGCTGTTGTTGTTGCTTTGGCCCTTGAGACACTTGATTTCATCTTGGAGAACAAAGCTCCATTGGCCACCATCTCCAACATCTTTGGCAGTTATTTGGTCATCTTCATTTGTTAAGACCAACGTCATCATAGAACCCTCCAAGAATTTGGCTCTAGAAATTTGCCATTGATGCATATCAGATTTGGGTTCTACTCATTCGGCTGTGTCGATCTCTCCAGAAGTTCGCTCTGAATTTGATAGGTCATCAGGGTTCATTCTTGAAAGACCATCTGACTGCTGTTGCTAGACATAATTTGTTTATGATTTCTGCTGGTTTCTTTCGCTCCATAACAATCACTTTGGAGATCTCAAGAAGGCTGTGCATGCTGAATTTGGGTCCTCAAGAACCCTTGAAACCACTAAGACCAATTAGACGTGCTGGTACTGTTTCTTTGTTGGGTGATTTGTTGGGTTCTTCTGCTAGAGGTGAAACTGTTGATTAGACACAGATTTTGATCAGGTTGTCCAAACACTCCATTATTAGAATGGTGTGCTCTTACTGTTCCAGGTTCTGTTTACTGATGAAGCTCAAAAGTGTGTTAAGGATTTGTTGCAATTTGGTTGGCTCTTAAAGCTTGATGATTACATGTCAGTTTGTAGAGGTTGGGACTTGCAGAGTTTAAAGCATAGAGCTGCTGATTCGCCATAAGAAGATTGATGCTTTGTTGGAGGACATCTTGAGGCCAAGAAGAAGCTAGACAGCATAGAAGATTGGAATCAAGATGATGGTCAAGGTATCTCTTCCAAGCAAGAATGAAGAAACAGCTACCACCTCTAAGGACTTGTGGATATTTGATGGATAAGGCTGAAGATCAAGCTGCGCAAGTTAAGTTGACTAGAGAAAACTTAAGGCCCTCATCATCGATGTTGTTACAGCTGGTTCGTACTCTGCTGCTATGTTGTAATGGATGTGTCGCAAAATTGATGAACCATCAAGAAAGCTTGAGAAAGGTCGTTGAGAANAATTGATCGCGTTGTTGGTGGTGAAGAANAATGCTAGTGAAGCATGATTCGCAAGATTTGCCATATTGATGGCTGCTTACAAAGAGACTTTGAGATTGCATCCAGCTGGCTCAATGCTCATAGACATCTTCAGAAGATTTGGTCTGAGAGGTTTACAGTTTCCAGCCAGCAAACTGCTGTTTCCATTAAAGCTTTGGGCTTGTGTGATGAATCCAGCTTATTTGGGAAGAACCACTTGGCATAGGACCAAGAAGATTCATGCCAGGTGTGGTCTGCTGAATCTTTGGAACCTTAGAGGTCAACATTTTCAGTACATGCCATTTGGTTCTGGTGAATGAGGATGTCAGGTTATGGGTTTAGCTTTACAATCTGTTCCAGCTGGTTTAGCGCTTTGGTCCAATGTTTCCATTTGGGCTACTGTTGATGGTGAATGGTGGTGAATGATGTCAGAAATCTGATATGTCAAGATCTGATGGTTTGGTTTTCGCTAGAAAAAGGCCTTTGCTATTAAAGACCACTCCAAGGTTGACTCTCTTTCCAGCAGTTGTTTAA

Zm00004b039147 codon optimized

ATGGAAGAACAACAATTGAGAGCCAGACCAAAATATGATGGTCTTATCTTCTTTGGCCAAGAACAATCCAGAAGCTGTTTTGGCTTTGATTGCTTT
CGTTACTGTTGTTGCCCTTGAGACACTTGATTTTCATCTTGGAGACAACATGGTAGATTGCCACCAGGTCCAAACATCTTTGCCAGTTATTGGTCACT
TGCATTTGTTAAGACCACCACTTCATAGAACCTTGCAAGAATTGGCTTCTAGAATTGGTCCATTGATGCATATCAGATTGGGTTCTACCAATTGC
GTTGTTGCATCTTCTCCAGAAGTTGCCTCTGAATTGATTAGAGGTCATGAAGGTTCAATTTCCGCTAGACCTTTTACTGCTGTTGCTAGAAAAGTT
CTCTTATGATTCTGCTGGTTTCGTGTTTTCGAACCATACAATACTCATTTGGAGATTTCATGAAGAGGTTGTGCATGTCTGAATTATTGGGTCCAAAGAA
CCGTTGAACAACCTAAGACCAGTTAGAAGGGCTGTACTGTTTCTTTGGTTTCTGATTTGTTGGCTTCTTCTGCTAGAGGTGAAACTGTTGATATT
ACCAGACATTTGATCAGGTTGACCAACACCTCCATTATTAGAATTGGTTGCTTCTACCGTTTCTGGTTCTGTTACTGATGAAGCTCATGAATTGGC
TAAGGCCGTTATTGAAGTTGTTGGTGCCTTTAACGTTGACGATTACATTGCTGTTGTTAGAGGTTGGGATTTTCAAGGTTTGGGTAGAAAAGCTG
CTGATGTCCATAGAAGATTGATGCCTTGTGGAGGATATCTTGAGGCACAAGAAGAAGCTAGAGCTGCTAGAAGATTGGACGATGGTCATGGT
AAACAAGCTACTCATTCTAAGGACTTGTGGACATCTTGATGGATAAGGCTGAAGATCCAGCTGCTGAAGTTAAGTTGACTAGAGAAAACATTAA
GGCCTTCGTTATCGATGTTGTTACCTCTGGTTCAGATACTTCTGCTGCTATGGCTGAATGGATGTTGGCAGAATTGATGAATCATCCAGAAACCT
TGAGAAAGGTCGTTGAAGAAATTGATGCTTGTAGGTGGTGGTAGAATTGCTTCTGAAGCTGATTTGCCACAATTGCCATATTGATGGCCGTT
TACAAAAGAGACTTTGAGATTGCATCCAGCTGGTCAATTGCTCATAGACAATCTACTGAAGAAATGGTTGTTTCAATGGTTTCACTGTTCCACCACA
ATCCACTGTTTTGATTCATGTTTGGGCTATTGGTAGAGATCCAGCATATTGGGAAGAACCTTTGTTGTTAGACCAGAAAAGATTTCATGCCAGGTG
GTGCTGCTGAATCTTTGGAGCCAAGAGGTAAACATTTTCAGTACATTCCATTGCGTTCTGGTAGAAGAGGATGCCAGGTATGGGTTTAGCTATG
CAATCTGTTCCAGCAGTTGTTGCTGCATTGGTTCAATGTTTTCATTGGTCTACTGTTGATGGTGGTATGGATAAGATCGACATGTCAGAACTCTGA
TGGTTTGGTTTGGCTAGAAAAAAGCCTTTGCTATTAAAGACCAACCTCCAGATTGACTCCATTTCACCTGTTGTTTGA

Zm00004b033036 codon optimized

ATGGAAGTTGTTACCGCTAGGGAATTGATTAAACCAACTGGTTTGCCAACTCTGTTGTTGGTTGCTGGTTTGACTGTTTTCTACGTTTTGCGTAG
AAGATCATCTGGTGGTTTGAGATTGCCACCATCTCCATTTGCTTTGCCAGTTTGGGTCACTTGCAATTTGTTGGCTCCATTGCCACATCAAGCCT
TGCTAGATTGGCTGCTAGACATGGTCCTTTGTTGATTGAGATTAGGTTCCATGCCAGCTATTGCTGCTGTTCTCCAGATGCTGCTAGAGAA
GTTTTGAAAACCTCATGAAGCTGCTTTCTTGGATAGACAAAACCTACTGCTGTTTCATAGATTGACTTATGGTGGTCAAGACTTCTCTTTTCTCC
ATATGGTCCTTATTGGAGTTTATGAAGAGGGCTTGTGTTTCATGAATTATTGGCTGGTAGAACCTTGGAAGATTGAGACATGTTAGAAGGGAAG
AAGCTCTAGATTGGTTGGTTCTTGTCTAGATCTGCTGGTGATGGTGCTGCTGTTGATGTTGATGCAGTTTGTATGGGTGTTACCGGTGATATT
ATCTCCAGAATGGTTATGCTAGAAAGATGGACTGGTGATGATTCTACTACCGAAGAAATGAGATCTTTGGTTGCAGAACTGCTGAATTGATGCTGG
TACTTTCAACTTGCAAGATTACATCGGTATGTTCAAGCACTGGGATGTTCAAGGTTTGGGTAAAAGAATTGATGCCGTTCCAGAAAAGTTCCGATG
CTATGATGGAAAAGATTTTGACCGCTAGAGATGCTGAAAGAAGGTGTAGAAGAAAAGGTGCTGCAGATGGTGCCGTTGAAGGTGATAAGAAAGAT
TTGTTGGATATGCTGTTTCGATATGCACGAAGATGAAGGTGCTGAAATGAGACTAAGTATAGAGATAACATTAAGGCCTTCATGCTGGATATTTTTCG
TGCTGGTACTGATACCCTACCATTACTTTGGAATGGGCTTTGCTGAGTTGATTAACAATCCAGCTGTTTTGAGAAGGGCTCAAGCTGAATTGG
ATGCAGCTGTTGTTGCTTCTAGATTAGCTGATGAATCTGATATCCACGTTTGCCATCTTGCAAGCTATTGCCAAAAGAACTTTAAGATTGCAT
CCAAACCGTCCATTGGTTGTTAGAAGATCTATGGCTCCATGTAACGTTTCTGGTTATGATGTTCCAGCTGGTGCTACTGTTTTTGTGTTAATGTTTG
GGCTATTGGTAGAGATCCAGCTTTGTTGGCTCCAGATCCATTGGCTTTTAGACCTGAAAGATTCTTGAAGAGGAAGGTGGCGGAGAATCAGCTG
GTTTGGATGTTAGAGGTCAACATTTTCATTTGTTGCCATTGCGTTCCGGTAGAAGAAATTTGTCAGGTGCTTCTTTGGCTATGTTGGTTGTTCAA
GCTGCATTAGCTGCTATGTTGCAATGTTTGAATGGACTCCAGTTGGTGGTGGCTCCAGTTGATATGGAAGAAGGTCCAGGTTTACTTTTGGCAAG
AAAAAGACCATTGGCTGTACTGTAAAGGTAGATTGCACCCATTGCCAGTTCCAGCCGCTGCTGCTGATAATGGTGTGAAGAAACCGCTGGTG
TTTGA

Supplemental Figure S23. Codon-optimized gene sequences of CYP93G candidates synthesized for expression in *S. cerevisiae*. Synthetic genes were inserted in the pMA-T vector.

Supplemental Table S1. *P*-values of *t*-test analysis to determine statistical significant differences of flavonoid content between treatments obtained by the LC-MS measurements shown in Supplemental Figure 1B. T-test was performed as implemented in the MetaboScape 4.0 software (Bruker Daltonics). na, not available.

Compound	RT (min)	<i>m/z</i> quan. ion	P-value (Rank) B75	P-value (Rank) W22
Apigenin*	8.25	271.06012 [M+H] ⁺	0.003948	0.000778
Naringenin chalcone*	8.12	273.07572 [M+H] ⁺	0.010406	0.000778
Naringenin*	8.31	273.07558 [M+H] ⁺	0.003948	0.000778
5-O-Methylapigenin**	6.24	285.07584 [M+H] ⁺	0.003948	0.000778
Genkwanin*	10.61	285.07580 [M+H] ⁺	0.003948	na
Luteolin*	7.35	287.05502 [M+H] ⁺	0.003948	0.000778
Flavonoid aglucone	4.83	287.09140 [M+H] ⁺	0.003948	0.000778
5-O-Methylnaringenin*	6.35	287.09156 [M+H] ⁺	0.003948	0.000778
Flavonoid aglucone	7.24	287.09141 [M+H] ⁺	0.003948	0.000778
Flavonoid aglucone	9.25	287.09153 [M+H] ⁺	0.003948	0.000778
Dihydrokaempferol*	6.53	287.05618 [M-H] ⁻	0.003948	0.000778
2-OH-Naringenin**	7.00	289.07083 [M+H] ⁺	0.003948	0.000778
5,7-O-Dimethylapigenin**	7.88	299.09161 [M+H] ⁺	0.003948	na
5-O-Methyluteolin***	5.65	301.07103 [M+H] ⁺	0.003948	0.000778
5-O-Methylscutellarein**	5.92	301.07112 [M+H] ⁺	0.003948	0.000778
7-O-Methylscutellarein**	7.51	301.07120 [M+H] ⁺	0.003948	0.001131
Flavonoid aglucone	8.42	301.07108 [M+H] ⁺	0.003948	0.000778
Flavonoid aglucone	4.18	303.08649 [M+H] ⁺	0.003948	0.002322
5-O-Methyldihydrokaempferol***	5.67	303.08633 [M+H] ⁺	0.003948	0.000778
O-Methyl-2-OH-naringenin***	8.03	303.08647 [M+H] ⁺	0.003948	0.000778
O-Methyl-2-OH-naringenin***	10.24	303.08649 [M+H] ⁺	0.003948	0.000778
Taxifolin*	5.69	303.05109 [M-H] ⁻	0.003948	0.000778
Flavonoid aglucone	6.15	315.08639 [M+H] ⁺	0.003948	na
Flavonoid aglucone	6.39	315.08656 [M+H] ⁺	0.003948	0.000778
5,7-O-Dimethylscutellarein**	6.64	315.08660 [M+H] ⁺	0.003948	na
O-Dimethyluteolin***	10.84	315.08618 [M+H] ⁺	0.003948	na
Xilonenin tautomer 1**	6.95	317.10205 [M+H] ⁺	0.003948	0.000778
Xilonenin tautomer 2**	8.46	317.10197 [M+H] ⁺	0.003948	0.000778
5-O-Methyltaxifolin***	4.96	319.08117 [M+H] ⁺	0.003948	0.001131
Flavonoid aglucone	6.12	331.08100 [M+H] ⁺	0.003948	na
Flavonoid aglucone	6.20	331.08124 [M+H] ⁺	na	0.001131
Flavonoid aglucone	7.58	329.06674 [M-H] ⁻	na	0.000778
5,7-O-Dimethylquercetin***	7.70	331.08139 [M+H] ⁺	0.003948	na
Flavonoid aglucone	7.46	333.09688 [M+H] ⁺	0.003948	na
Flavonoid aglucone	7.59	331.08207 [M-H] ⁻	na	0.000778
Flavonoid aglucone	4.39	337.05555 [M+H] ⁺	0.003948	0.000778
Flavonoid aglucone	6.80	345.09700 [M+H] ⁺	0.003948	0.000778
Flavonoid aglucone	10.67	345.09713 [M+H] ⁺	0.003948	na

Supplemental Table S2: see Supplemental Tables (Excel file)

Supplemental Table S3. MaizeGDB/GenBank accessions and references corresponding to Figure 2D and Supplemental Figure S6.

Name	Plant species	MaizeGDB/GenBank accession	Reference
<i>ZmBX10</i>	<i>Zea mays</i>	Zm00001d029359	
<i>ZmBX11</i>	<i>Zea mays</i>	Zm00001d029356	Meihls et al., 2013
<i>ZmBX12</i>	<i>Zea mays</i>	Zm00025ab019610	
<i>ZmBX14</i>	<i>Zea mays</i>	Zm00001d004921	
<i>ZmBX7</i>	<i>Zea mays</i>	Zm00001d049179	Jonczyk et al., 2008
<i>ZmOMT1</i> (<i>ZmFOMT1</i> , <i>ZmCOMT1</i>)	<i>Zea mays</i>	Zm00001d049541; EF586877 / M73235	Zhou et al., 2008; Collazo et al., 1992
<i>ZmFOMT2</i>	<i>Zea mays</i>	Zm00001d047192	this work
<i>ZmFOMT3</i>	<i>Zea mays</i>	Zm00001d047194	this work
<i>ZmFOMT4</i>	<i>Zea mays</i>	Zm00001d048087	this work
<i>ZmFOMT5</i>	<i>Zea mays</i>	Zm00001d051934	this work
<i>ZmAAMT1</i>	<i>Zea mays</i>	HM242244	Köllner et al., 2010
<i>ZmAAMT2</i>	<i>Zea mays</i>	HM242246	Köllner et al., 2010
<i>ZmAAMT3</i>	<i>Zea mays</i>	HM242247	Köllner et al., 2010
<i>ZmOMT8</i>	<i>Zea mays</i>	HM242248	Köllner et al., 2010
<i>ZmZRP4</i>	<i>Zea mays</i>	Zm00001d049020	/
<i>ZmCCoAOMT1</i>	<i>Zea mays</i>	Zm00001d036293	Li et al., 2013
<i>ZmCCoAOMT2</i>	<i>Zea mays</i>	Zm00001d045206	Wang et al., 2016
<i>HvF1-OMT</i>	<i>Hordeum vulgare</i>	X77467	Christensen et al., 1998
<i>HvOMT1</i>	<i>Hordeum vulgare</i>	EF586876	Zhou et al., 2008
<i>TaOMT2</i>	<i>Triticum aestivum</i>	DQ223971	Zhou et al., 2006 (2)
<i>OsNOMT</i>	<i>Oryza sativa</i>	AB692949	Shimizu et al., 2012
<i>OsROMT9</i>	<i>Oryza sativa</i>	DQ288259	Kim et al., 2006
<i>Ms7IOMT</i>	<i>Medicago sativa</i>	AF000976	He et al., 1998
<i>Msl2'OMT</i>	<i>Medicago sativa</i>	L10211	Maxwell et al., 1993
<i>MtIOMT2</i>	<i>Medicago truncatula</i>	DQ419910	Deavours et al., 2006
<i>MtIOMT7</i>	<i>Medicago truncatula</i>	DQ419914	Deavours et al., 2006
<i>GeD7OMT</i>	<i>Glycyrrhiza echinata</i>	AB091685	Akashi et al., 2003
<i>GeHI4'OMT</i>	<i>Glycyrrhiza echinata</i>	AB091684	Akashi et al., 2003
<i>LjHI4'OMT</i>	<i>Lotus japonicus</i>	AB091686	Akashi et al., 2003

Supplemental Table S3 continued.

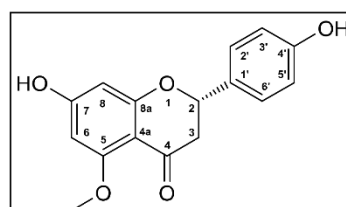
Name	Plant species	MaizeGDB/GenBank accession	Reference
<i>MxpOMT1A</i>	<i>Mentha x piperita</i>	AY337457	Willits et al., 2004
<i>MxpOMT2</i>	<i>Mentha x piperita</i>	AY337459	Willits et al., 2004
<i>MxpOMT3</i>	<i>Mentha x piperita</i>	AY337460	Willits et al., 2004
<i>MxpOMT4</i>	<i>Mentha x piperita</i>	AY337461	Willits et al., 2004
<i>ObOMT1</i>	<i>Ocimum basilicum</i>	JQ653275	Berim et al., 2012
<i>ObOMT5</i>	<i>Ocimum basilicum</i>	JQ653279	Berim et al., 2012
<i>ObOMT6</i>	<i>Ocimum basilicum</i>	JQ653280	Berim et al., 2012
<i>Pa4'OMT</i>	<i>Plagiochasma appendiculatum</i>	KY977687	Liu et al., 2017
<i>CroOMT6</i>	<i>Catharanthus roseus</i>	AY343490	Schröder et al., 2004
<i>CroOMT2</i>	<i>Catharanthus roseus</i>	AY127568	Cacace et al., 2003
<i>CaFOMT1</i>	<i>Chrysosplenium americanum</i>	U16794	Gauthier et al., 1996
<i>CaOMT2</i>	<i>Chrysosplenium americanum</i>	U16793	Gauthier et al., 1998
<i>AtOMT1</i>	<i>Arabidopsis thaliana</i>	U70424	Zhang et al., 1997
<i>CdFOMT5</i>	<i>Citrus depressa</i>	LC126059	Itoh et al., 2016
<i>CreOMT2</i>	<i>Citrus reticulata</i>	/	Liu et al., 2020
<i>VpOMT3</i>	<i>Vanilla planifolia</i>	DQ400400	Li et al., 2006
<i>ShMOMT1</i>	<i>Solanum habrochaites</i>	JF499656	Schmidt et al., 2011
<i>ShMOMT2</i>	<i>Solanum habrochaites</i>	JF499657	Schmidt et al., 2011
<i>SIMOMT4</i>	<i>Solanum lycopersicum</i>	KF740343	Kim et al., 2014

- Akashi, T., Sawada, Y., Shimada, N., Sakurai, N., Aoki, T., and Ayabe, S.** (2003). cDNA cloning and biochemical characterization of S-adenosyl-L-methionine: 2,7,4'-trihydroxyisoflavanone 4'-O-methyltransferase, a critical enzyme of the legume isoflavonoid phytoalexin pathway. *Plant Cell Physiol* **44**, 103-112.
- Berim, A., Hyatt, D.C., and Gang, D.R.** (2012). A Set of Regioselective O-Methyltransferases Gives Rise to the Complex Pattern of Methoxylated Flavones in Sweet Basil. *Plant Physiol* **160**, 1052-1069.
- Cacace, S., Schroder, G., Wehinger, E., Strack, D., Schmidt, J., and Schroder, J.** (2003). A flavonol O-methyltransferase from *Catharanthus roseus* performing two sequential methylations. *Phytochemistry* **62**, 127-137.
- Christensen, A.B., Gregersen, P.L., Olsen, C.E., and Collinge, D.B.** (1998). A flavonoid 7-O-methyltransferase is expressed in barley leaves in response to pathogen attack. *Plant Mol Biol* **36**, 219-227.
- Collazo, P., Montoliu, L., Puigdomenech, P., and Rigau, J.** (1992). Structure and Expression of the Lignin O-Methyltransferase Gene from *Zea Mays* L. *Plant Mol Biol* **20**, 857-867.
- Deavours, B.E., Liu, C.J., Naoumkina, M.A., Tang, Y.H., Farag, M.A., Sumner, L.W., Noel, J.P., and Dixon, R.A.** (2006). Functional analysis of members of the isoflavone and isoflavanone O-methyltransferase enzyme families from the model legume *Medicago truncatula*. *Plant Mol Biol* **62**, 715-733.
- Gauthier, A., Gulick, P.J., and Ibrahim, R.K.** (1996). cDNA cloning and characterization of a 3'/5'-O-methyltransferase for partially methylated flavonols from *Chrysosplenium americanum*. *Plant Mol Biol* **32**, 1163-1169.
- Gauthier, A., Gulick, P.J., and Ibrahim, R.K.** (1998). Characterization of two cDNA clones which encode O-methyltransferases for the methylation of both flavonoid and phenylpropanoid compounds. *Arch Biochem Biophys* **351**, 243-249.
- He, X.Z., Reddy, J.T., and Dixon, R.A.** (1998). Stress responses in alfalfa (*Medicago sativa* L). XXII. cDNA cloning and characterization of an elicitor-inducible isoflavone 7-O-methyltransferase. *Plant Mol Biol* **36**, 43-54.
- Itoh, N., Iwata, C., and Toda, H.** (2016). Molecular cloning and characterization of a flavonoid-O-methyltransferase with broad substrate specificity and regioselectivity from *Citrus depressa*. *Bmc Plant Biol* **16**.
- Jonczyk, R., Schmidt, H., Osterrieder, A., Fiesselmann, A., Schullehner, K., Haslbeck, M., Sicker, D., Hofmann, D., Yalpani, N., Simmons, C., Frey, M., and Gierl, A.** (2008). Elucidation of the final reactions of DIMBOA-glucoside biosynthesis in maize: Characterization of Bx6 and Bx7. *Plant Physiol* **146**, 1053-1063.
- Kim, B.G., Lee, Y., Hur, H.G., Lim, Y., and Ahn, J.H.** (2006). Flavonoid 3'-O-methyltransferase from rice: cDNA cloning, characterization and functional expression. *Phytochemistry* **67**, 387-394.
- Kim, J., Matsuba, Y., Ning, J., Schillmiller, A.L., Hammar, D., Jones, A.D., Pichersky, E., and Last, R.L.** (2014). Analysis of natural and induced variation in tomato glandular trichome flavonoids identifies a gene not present in the reference genome. *Plant Cell* **26**, 3272-3285.
- Kollner, T.G., Lenk, C., Zhao, N., Seidl-Adams, I., Gershenzon, J., Chen, F., and Degenhardt, J.** (2010). Herbivore-Induced SABATH Methyltransferases of Maize That Methylate Anthranilic Acid Using S-Adenosyl-L-Methionine. *Plant Physiol* **153**, 1795-1807.
- Li, H.M., Rotter, D., Hartman, T.G., Pak, F.E., Havkin-Frenkel, D., and Belanger, F.C.** (2006). Evolution of novel O-methyltransferases from the *Vanilla planifolia* caffeic acid O-methyltransferase. *Plant Mol Biol* **61**, 537-552.
- Li, X.Y., Chen, W.J., Zhao, Y., Xiang, Y., Jiang, H.Y., Zhu, S.W., and Cheng, B.J.** (2013). Downregulation of caffeoyl-CoA O-methyltransferase (CCoAOMT) by RNA interference leads to reduced lignin production in maize straw. *Genet Mol Biol* **36**, 540-U230.
- Liu, H., Xu, R.X., Gao, S., and Cheng, A.X.** (2017). The Functional Characterization of a Site-Specific Apigenin 4'-O-methyltransferase Synthesized by the Liverwort Species *Plagiochasma appendiculatum*. *Molecules* **22**.
- Liu, X., Wang, Y., Chen, Y., Xu, S., Gong, Q., Zhao, C., Cao, J., and Sun, C.** (2020). Characterization of a Flavonoid 3'/5'/7-O-Methyltransferase from *Citrus reticulata* and Evaluation of the In Vitro Cytotoxicity of Its Methylated Products. *Molecules* **25**.

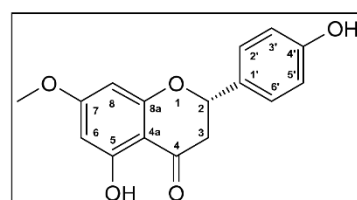
- Maxwell, C.A., Harrison, M.J., and Dixon, R.A.** (1993). Molecular Characterization and Expression of Alfalfa Isoliquiritigenin 2'-O-Methyltransferase, an Enzyme Specifically Involved in the Biosynthesis of an Inducer of *Rhizobium Meliloti* Nodulation Genes. *Plant J* **4**, 971-981.
- Meihls, L.N., Handrick, V., Glauser, G., Barbier, H., Kaur, H., Haribal, M.M., Lipka, A.E., Gershenzon, J., Buckler, E.S., Erb, M., Kollner, T.G., and Jander, G.** (2013). Natural Variation in Maize Aphid Resistance Is Associated with 2,4-Dihydroxy-7-Methoxy-1,4-Benzoxazin-3-One Glucoside Methyltransferase Activity. *Plant Cell* **25**, 2341-2355.
- Schmidt, A., Li, C., Shi, F., Jones, A.D., and Pichersky, E.** (2011). Polymethylated Myricetin in Trichomes of the Wild Tomato Species *Solanum habrochaites* and Characterization of Trichome-Specific 3'- and 7'-Myricetin O-Methyltransferases. *Plant Physiol* **155**, 1999-2009.
- Schroder, G., Wehinger, E., Lukacin, R., Wellmann, F., Seefelder, W., Schwab, W., and Schroder, J.** (2004). Flavonoid methylation: a novel 4'-O-methyltransferase from *Catharanthus roseus*, and evidence that partially methylated flavanones are substrates of four different flavonoid dioxygenases. *Phytochemistry* **65**, 1085-1094.
- Shimizu, T., Lin, F.Q., Hasegawa, M., Okada, K., Nojiri, H., and Yamane, H.** (2012). Purification and Identification of Naringenin 7-O-Methyltransferase, a Key Enzyme in Biosynthesis of Flavonoid Phytoalexin Sakuranetin in Rice. *J Biol Chem* **287**, 19315-19325.
- Wang, G.F., and Balint-Kurti, P.J.** (2016). Maize Homologs of CCoAOMT and HCT, Two Key Enzymes in Lignin Biosynthesis, Form Complexes with the NLR Rp1 Protein to Modulate the Defense Response. *Plant Physiol* **171**, 2166-2177.
- Willits, M.G., Giovanni, M., Prata, R.T.N., Kramer, C.M., De Luca, V., Steffens, J.C., and Graser, G.** (2004). Bio-fermentation of modified flavonoids: an example of in vivo diversification of secondary metabolites. *Phytochemistry* **65**, 31-41.
- Zhang, H., Wang, J., and Goodman, H.M.** (1997). An Arabidopsis gene encoding a putative 14-3-3-interacting protein, caffeic acid/5-hydroxyferulic acid O-methyltransferase. *Bba-Gen Struct Expr* **1353**, 199-202.
- Zhou, J.M., Fukushi, Y., Wollenweber, E., and Ibrahim, R.K.** (2008). Characterization of two O-methyltransferase-like genes in barley and maize. *Pharm Biol* **46**, 26-34.
- Zhou, J.M., Gold, N.D., Martin, V.J.J., Wollenweber, E., and Ibrahim, R.K.** (2006). Sequential O-methylation of tricetin by a single gene product in wheat. *Bba-Gen Subjects* **1760**, 1115-1124.

Supplemental Table S4. NMR structure elucidation of 5-/7-O-methyl- and 5,7-O-dimethyl-flavonoids.

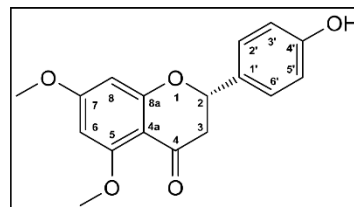
pos.	δ_{H}	<i>mult.</i> , J_{HH} [Hz]	δ_{C}
1	-	-	-
2	5.35	<i>dd</i> , 2.7/12.9	79.5
3a	2.95	<i>dd</i> , 12.9/16.3	46.1
3b	2.57	<i>dd</i> , 2.7/16.3	46.1
4	-	-	188.0
5	-	-	163.5
6	6.13	<i>d</i> , 2.0	93.8
7	-	-	165.7
8	6.05	<i>d</i> , 2.0	96.4
8a	-	-	164.4
4a	-	-	105.9
1'	-	-	131.0
2'	7.36	<i>d</i> , 8.5	128.6
3'	6.88	<i>d</i> , 8.5	115.9
4'	-	-	158.5
5'	6.88	<i>d</i> , 8.5	115.9
6'	7.36	<i>d</i> , 8.5	128.6
5-OCH ₃	3.79	<i>s</i>	55.8

5-O-methyl naringenin in acetone-*d*₆

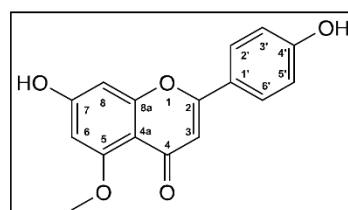
pos.	δ_{H}	<i>mult.</i> , J_{HH} [Hz]	δ_{C}
1	-	-	-
2	5.48	<i>dd</i> , 3.0/12.9	79.8
3a	3.21	<i>dd</i> , 12.9/17.2	43.3
3b	2.75	<i>dd</i> , 3.0/17.2	43.3
4	-	-	197.3
5	-	-	164.1
6	6.04	<i>d</i> , 2.2	94.3
7	-	-	168.5
8	6.03	<i>d</i> , 2.2	95.1
8a	-	-	n.d.
4a	-	-	103.8
1'	-	-	130.4
2'	7.39	<i>d</i> , 8.5	128.8
3'	6.89	<i>d</i> , 8.5	115.9
4'	-	-	158.5
5'	6.89	<i>d</i> , 8.5	115.9
6'	7.39	<i>d</i> , 8.5	128.8
7-OCH ₃	3.84	<i>s</i>	56.0
5-OH	12.13	<i>s</i>	-
4'-OH	8.55	<i>s</i>	-

7-O-methyl naringenin in acetone-*d*₆

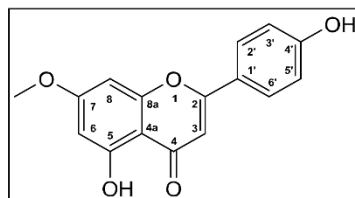
pos.	δ_{H}	mult., J_{HH} [Hz]	δ_{C}
1	-	-	-
2	5.37	<i>dd</i> , 2.8/12.9	79.6
3a	3.21	<i>dd</i> , 12.9/16.3	45.8
3b	2.75	<i>dd</i> , 2.8/16.3	45.8
4	-	-	187.8
5	-	-	162.9
6	6.17	<i>d</i> , 2.3	94.1
7	-	-	166.2
8	6.14	<i>d</i> , 2.3	94.1
8a	-	-	n.d.
4a	-	-	106.2
1'	-	-	130.9
2'	7.37	<i>d</i> , 8.5	128.8
3'	6.88	<i>d</i> , 8.5	115.9
4'	-	-	158.3
5'	6.88	<i>d</i> , 8.5	115.9
6'	7.37	<i>d</i> , 8.5	128.8
5-OCH ₃	3.81	<i>s</i>	55.8
7-OCH ₃	3.84	<i>s</i>	55.8
4'-OH	8.50	<i>s</i>	-

5,7-*O*-dimethyl naringenin in acetone-*d*₆

pos.	δ_{H}	mult., J_{HH} [Hz]	δ_{C}
1	-	-	-
2	-	-	161.2
3	6.46	<i>s</i>	106.5
4	-	-	177.5
5	-	-	161.9
6	6.42	<i>d</i> , 2.2	94.1
7	-	-	163.5
8	6.58	<i>d</i> , 2.2	95.9
8a	-	-	160.2
4a	-	-	107.8
1'	-	-	123.0
2'	7.83	<i>d</i> , 8.8	128.6
3'	6.97	<i>d</i> , 8.8	116.6
4'	-	-	161.9
5'	6.97	<i>d</i> , 8.8	116.6
6'	7.83	<i>d</i> , 8.8	128.6
5-OCH ₃	3.84	<i>s</i>	56.0

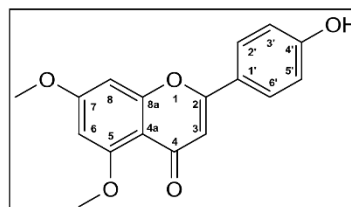
5-*O*-methyl apigenin in acetone-*d*₆

pos.	δ_{H}	mult., J_{HH} [Hz]
1	-	-
2	-	-
3	6.67	s
4	-	-
5	-	-
6	6.32	d, 2.2
7	-	-
8	6.69	d, 2.2
8a	-	-
4a	-	-
1'	-	-
2'	7.96	d, 8.9
3'	7.03	d, 8.9
4'	-	-
5'	7.03	d, 8.9
6'	7.96	d, 8.9
7-OCH ₃	3.92	s

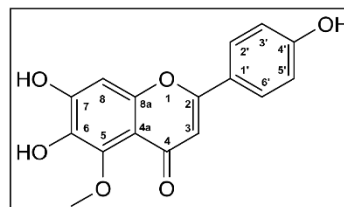
7-O-methyl apigenin in acetone- d_6

The identification was accomplished by comparison of the ^1H NMR data with that of an authentic reference standard.

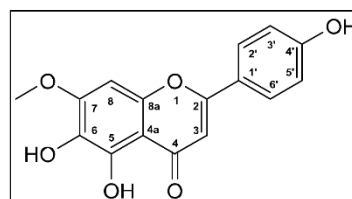
pos.	δ_{H}	mult., J_{HH} [Hz]	δ_{C}
1	-	-	-
2	-	-	161.2
3	6.45	s	107.3
4	-	-	176.5
5	-	-	161.7
6	6.47	d, 2.2	96.6
7	-	-	164.8
8	6.75	d, 2.2	93.8
8a	-	-	160.3
4a	-	-	110.0
1'	-	-	123.3
2'	7.87	d, 8.9	128.3
3'	7.00	d, 8.9	116.5
4'	-	-	161.3
5'	7.00	d, 8.9	116.5
6'	7.87	d, 8.9	128.3
5-OCH ₃	3.86	s	56.2
7-OCH ₃	3.94	s	55.1

5,7-O-dimethyl apigenin in acetone- d_6

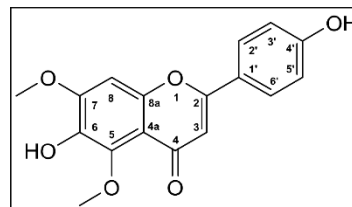
pos.	δ_{H}	<i>mult.</i> , J_{HH} [Hz]	δ_{C}
1	-	-	-
2	-	-	163.6
3	6.56	<i>s</i>	105.5
4	-	-	179.6
5	-	-	145.6
6	-	-	138.3
7	-	-	154.1
8	6.84	<i>s</i>	100.2
8a	-	-	153.2
4a	-	-	111.5
1'	-	-	123.2
2'	7.82	<i>d</i> , 8.8	128.7
3'	6.92	<i>d</i> , 8.8	116.6
4'	-	-	162.1
5'	6.92	<i>d</i> , 8.8	116.6
6'	7.82	<i>d</i> , 8.8	128.7
5-OCH ₃	3.85	<i>s</i>	62.6

5-*O*-methyl scutellarein in methanol-*d*₃

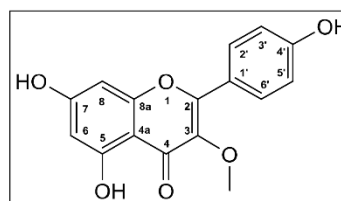
pos.	δ_{H}	<i>mult.</i> , J_{HH} [Hz]	δ_{C}
1	-	-	-
2	-	-	163.8
3	6.66	<i>s</i>	102.8
4	-	-	181.6
5	-	-	154.6
6	-	-	130.8
7	-	-	154.0
8	6.87	<i>s</i>	90.8
8a	-	-	150.6
4a	-	-	105.4
1'	-	-	122.7
2'	7.96	<i>d</i> , 8.8	128.3
3'	7.05	<i>d</i> , 8.8	116.2
4'	-	-	162.1
5'	7.05	<i>d</i> , 8.8	116.2
6'	7.96	<i>d</i> , 8.8	128.3
7-OCH ₃	3.99	<i>s</i>	55.9

7-*O*-methyl scutellarein in acetone-*d*₆

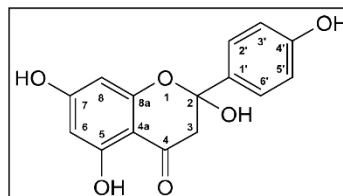
pos.	δ_{H}	mult., J_{HH} [Hz]	δ_{C}
1	-	-	-
2	-	-	161.2
3	6.50	s	105.9
4	-	-	176.1
5	-	-	144.5
6	-	-	137.5
7	-	-	153.0
8	7.09	s	96.6
8a	-	-	151.7
4a	-	-	112.5
1'	-	-	123.0
2'	7.90	d, 8.8	127.8
3'	7.01	d, 8.8	115.8
4'	-	-	160.0
5'	7.01	d, 8.8	115.8
6'	7.90	d, 8.8	127.8
5-OCH ₃	3.87	s	61.3
7-OCH ₃	4.00	s	55.9

5,7-O-dimethyl scutellarein in acetone- d_6

pos.	δ_{H}	mult., J_{HH} [Hz]	δ_{C}
1	-	-	-
2	-	-	155.6
3	-	-	138.3
4	-	-	n.d.
5	-	-	163.1
6	6.24	d, 2.1	98.9
7	-	-	165.3
8	6.47	d, 2.1	93.8
8a	-	-	157.3
4a	-	-	104.5
1'	-	-	121.7
2'	8.01	d, 8.9	127.8
3'	7.01	d, 8.9	115.9
4'	-	-	160.2
5'	7.01	d, 8.9	115.9
6'	8.01	d, 8.9	127.8
3-OCH ₃	3.86	s	59.5

3-O-methyl apigenin
(isokaempferide)
in acetone- d_6

pos.	δ_{H}	mult., J_{HH} [Hz]	δ_{C}
1	-	-	-
2	-	-	102.9
3a	2.83	<i>d</i> , 16.8	49.7
3b	3.20	<i>d</i> , 16.8	49.7
4	-	-	196.4
5	-	-	164.7
6	5.96	<i>d</i> , 2.0	96.6
7	-	-	167.2
8	5.99	<i>d</i> , 2.0	96.8
8a	-	-	161.8
4a	-	-	102.9
1'	-	-	134.6
2'	7.54	<i>d</i> , 8.7	127.7
3'	6.88	<i>d</i> , 8.7	115.6
4'	-	-	158.6
5'	6.88	<i>d</i> , 8.7	115.6
6'	7.54	<i>d</i> , 8.7	127.7
5-OH	12.10	<i>s</i>	-

2-hydroxy naringenin in methanol- d_3

Supplemental Table S5. Product formation of maize OMTs with different substrates. Data belong to the experiment shown in Figure 3. Enzyme assays were performed with substrate (A) naringenin.

Substrate	Analyte	Enzyme	Mean area	SE	Rate of product formation (%) relative to most active enzyme
naringenin	5-O-Me-naringenin	EV	nd	-	-
		FOMT2	45401370.0	1520553.3	100.000
		FOMT3	4308670.7	366608.5	9.490
		FOMT4	nd	-	-
		FOMT5	nd	-	-
		BX10	35527.7	2533.6	0.078
		BX11	19946.3	751.0	0.044
		BX12	38427.3	4261.4	0.085
		BX14	nd	-	-
	sakuranetin	EV	nd	-	-
		FOMT2	nd	-	-
		FOMT3	nd	-	-
		FOMT4	20238949.0	120674.6	100.000
		FOMT5	59594.0	2828.9	0.294
		BX10	68111.7	9895.7	0.337
		BX11	33719.7	5051.9	0.167
		BX12	73842.3	3920.3	0.365
		BX14	nd	-	-
	5,7-O-DiMe-naringenin	EV	nd	-	-
		FOMT2	nd	-	-
		FOMT3	nd	-	-
		FOMT4	nd	-	-
		FOMT5	nd	-	-
		FOMT2+4	1268022.0	37258.6	100.000
		FOMT4+2	631538.3	8818.4	49.805
		BX10	nd	-	-
		BX11	nd	-	-
		BX12	nd	-	-
		BX14	nd	-	-

Supplemental Table S5 continued. (B) apigenin.

Substrate	Analyte	Enzyme	Mean area	SE	Rate of product formation (%) relative to most active enzyme
apigenin	5-O-Me-apigenin	EV	nd	-	-
		FOMT2	33210895.0	1280700.4	100.000
		FOMT3	1225440.0	68099.8	3.690
		FOMT4	nd	-	-
		FOMT5	nd	-	-
		BX10	95205.0	2070.0	0.287
		BX11	96935.3	5771.2	0.292
		BX12	116276.0	11595.1	0.350
		BX14	70209.3	3049.2	0.211
	genkwanin	EV	nd	-	-
		FOMT2	nd	-	-
		FOMT3	nd	-	-
		FOMT4	31123877.7	652404.0	100.000
		FOMT5	nd	-	-
		BX10	nd	-	-
		BX11	nd	-	-
		BX12	nd	-	-
		BX14	nd	-	-
	5,7-O-DiMe-apigenin	EV	nd	-	-
		FOMT2	nd	-	-
		FOMT3	15968.3	1665.7	22.983
		FOMT4	nd	-	-
		FOMT5	nd	-	-
		FOMT2+4	69479.3	3485.8	100.000
		FOMT4+2	34356.0	1741.6	49.448
		BX10	33042.3	3200.0	47.557
		BX11	11115.7	1115.4	15.999
		BX12	41505.7	762.4	59.738
		BX14	nd	-	-

Supplemental Table S5 continued. (C) scutellarein

Substrate	Analyte	Enzyme	Mean area	SE	Rate of product formation (%) relative to most active enzyme
scutellarein	5-O-Me-scutellarein	EV	nd	-	-
		FOMT2	16750983.3	304101.2	100.000
		FOMT3	108764.7	8348.8	0.649
		FOMT4	nd	-	-
		FOMT5	nd	-	-
		BX10	15653.0	2434.7	0.093
		BX11	-	-	-
		BX12	-	-	-
		BX14	nd	-	-
	7-O-Me-scutellarein	EV	nd	-	-
		FOMT2	216538.7	12953.1	0.934
		FOMT3	176534.3	13467.1	0.761
		FOMT4	23189739.3	461690.8	100.000
		FOMT5	nd	-	-
		BX10	191362.3	5027.8	0.825
		BX11	-	-	-
		BX12	-	-	-
		BX14	6156.3	1172.1	0.027
	hispidulin	EV	nd	-	-
		FOMT2	26008.3	1882.4	0.113
		FOMT3	nd	-	-
		FOMT4	nd	-	-
		FOMT5	23059117.0	650611.1	100.000
		BX10	8545.0	970.9	0.037
		BX11	-	-	-
		BX12	-	-	-
		BX14	nd	-	-

Supplemental Table S5 continued. (D) DIMBOA-Glc

Substrate	Analyte	Enzyme	Mean area	SE	Rate of product formation (%) relative to most active enzyme
DIMBOA-Glc	HDMBOA-Glc	EV	nd	-	-
		FOMT2	nd	-	-
		FOMT3	nd	-	-
		FOMT4	nd	-	-
		FOMT5	nd	-	-
		BX10	37476.3	4382.2	66.949
		BX11	24555.7	2428.6	43.867
		BX12	55977.3	3493.1	100.000
		BX14	5553.3	810.8	9.921

Supplemental Table S6. GenBank accessions and references corresponding to Figure 4B.

Name	Plant species	MaizeGDB/GenBank accession	Reference
CYP93G5 (B73)	<i>Zea mays</i>	GRMZM2G167336	Morohashi et al., 2012
CYP93G5 (W22)	<i>Zea mays</i>	Zm00004b033614	this work
CYP93G15 (W22)	<i>Zea mays</i>	Zm00004b010826	this work
CYP93G7	<i>Zea mays</i>	GRMZM2G148441	Righini et al., 2019
CYP93G10 (W22)	<i>Zea mays</i>	Zm00004b008124	this work
CYP93G3	<i>Sorghum bicolor</i>	XM_002461241	Du et al., 2010b
CYP93G1	<i>Oryza sativa</i>	AK100972	Lam et al., 2014
CYP93G2	<i>Oryza sativa</i>	AK099468	Du et al., 2010a
CYP93B16	<i>Glycine max</i>	FJ767774	Fliegmann et al., 2010
CYP93B10	<i>Medicago truncatula</i>	AC146789	Zhang et al., 2007
CYP93B11	<i>Medicago truncatula</i>	DQ354373	Zhang et al., 2007
CYP93B1	<i>Glycyrrhiza echinata</i>	AB001380	Akashi et al., 1998
CYP93B2	<i>Gerbera hybrida</i>	AF156976	Martens and Forkmann, 1999
CYP93B13	<i>Gentiana triflora</i>	AB193314	Nakatsuka et al., 2005
CYP93B6	<i>Perilla frutescens</i>	AB045592	Kitada et al., 2001
CYP93B4	<i>Torenia hybrida</i>	AB028152	Akashi et al., 1999
CYP93B3	<i>Antirrhinum majus</i>	AB028151	Akashi et al., 1999
CYP93B23	<i>Ocimum basilicum</i>	JX162213	Berim et al., 2013
CYP93B80	<i>Scutellaria baicalensis</i>	KT963453	Zhao et al., 2016
CYP93B81	<i>Scutellaria baicalensis</i>	KT963454	Zhao et al., 2016
CYP93B82	<i>Lonicera japonica</i>	KU127576	Wu et al., 2016
CYP93B83	<i>Lonicera japonica</i>	KU127578	Wu et al., 2016
CYP93B84	<i>Lonicera macranthoides</i>	KU127580	Wu et al., 2016

- Akashi, T., Aoki, T., and Ayabe, S.** (1998). Identification of a cytochrome P450 cDNA encoding (2S)-flavanone 2-hydroxylase of licorice (*Glycyrrhiza echinata* L.; Fabaceae) which represents licodione synthase and flavone synthase II. *FEBS letters* **431**, 287-290.
- Akashi, T., Fukuchi-Mizutani, M., Aoki, T., Ueyama, Y., Yonekura-Sakakibara, K., Tanaka, Y., Kusumi, T., and Ayabe, S.** (1999). Molecular cloning and biochemical characterization of a novel cytochrome P450, flavone synthase II, that catalyzes direct conversion of flavanones to flavones. *Plant Cell Physiol* **40**, 1182-1186.
- Berim, A., and Gang, D.R.** (2013). The Roles of a Flavone-6-Hydroxylase and 7-O-Demethylation in the Flavone Biosynthetic Network of Sweet Basil. *J Biol Chem* **288**, 1795-1805.
- Du, Y.G., Chu, H., Chu, I.K., and Lo, C.** (2010). CYP93G2 Is a Flavanone 2-Hydroxylase Required for C-Glycosylflavone Biosynthesis in Rice. *Plant Physiol* **154**, 324-333.
- Du, Y.G., Chu, H., Wang, M.F., Chu, I.K., and Lo, C.** (2010). Identification of flavone phytoalexins and a pathogen-inducible flavone synthase II gene (SbFNSII) in sorghum. *J Exp Bot* **61**, 983-994.
- Fliegmann, J., Furtwangler, K., Malterer, G., Cantarello, C., Schuler, G., Ebel, J., and Mithofer, A.** (2010). Flavone synthase II (CYP93B16) from soybean (*Glycine max* L.). *Phytochemistry* **71**, 508-514.
- Kitada, C., Gong, Z.Z., Tanaka, Y., Yamazaki, M., and Saito, K.** (2001). Differential expression of two cytochrome P450s involved in the biosynthesis of flavones and anthocyanins in chemo-varietal forms of *Perilla frutescens*. *Plant Cell Physiol* **42**, 1338-1344.
- Lam, P.Y., Zhu, F.Y., Chan, W.L., Liu, H.J., and Lo, C.** (2014). Cytochrome P450 93G1 Is a Flavone Synthase II That Channels Flavanones to the Biosynthesis of Tricin O-Linked Conjugates in Rice. *Plant Physiol* **165**, 1315-1327.
- Martens, S., and Forkmann, G.** (1999). Cloning and expression of flavone synthase II from Gerbera hybrids. *Plant J* **20**, 611-618.
- Morohashi, K., Casas, M.I., Ferreyra, M.L.F., Mejia-Guerra, M.K., Pourcel, L., Yilmaz, A., Feller, A., Carvalho, B., Emiliani, J., Rodriguez, E., Pellegrinet, S., McMullen, M., Casati, P., and Grotewold, E.** (2016). A genome-wide regulatory framework identifies maize Pericarp color1 controlled genes (vol 24, pg 2745, 2012). *Plant Cell* **28**, 3058-3060.
- Nakatsuka, T., Nishihara, M., Mishiba, K., and Yamamura, S.** (2005). Temporal expression of flavonoid biosynthesis-related genes regulates flower pigmentation in gentian plants. *Plant Sci* **168**, 1309-1318.
- Righini, S., Rodriguez, E.J., Berosich, C., Grotewold, E., Casati, P., and Falcone Ferreyra, M.L.** (2019). Apigenin produced by maize flavone synthase I and II protects plants against UV-B-induced damage. *Plant Cell Environ* **42**, 495-508.
- Wu, J., Wang, X.C., Liu, Y., Du, H., Shu, Q.Y., Su, S., Wang, L.J., Li, S.S., and Wang, L.S.** (2016). Flavone synthases from *Lonicera japonica* and *L. macranthoides* reveal differential flavone accumulation. *Sci Rep-Uk* **6**.
- Zhang, J.A., Subramanian, S., Zhang, Y.S., and Yu, O.** (2007). Flavone synthases from *Medicago truncatula* are flavanone-2-hydroxylases and are important for nodulation. *Plant Physiol* **144**, 741-751.
- Zhao, Q., Zhang, Y., Wang, G., Hill, L., Weng, J.K., Chen, X.Y., Xue, H.W., and Martin, C.** (2016). A specialized flavone biosynthetic pathway has evolved in the medicinal plant, *Scutellaria baicalensis*. *Sci Adv* **2**.

Supplemental Table S7: see Supplemental Tables (Excel file)

Supplemental Table S8: see Supplemental Tables (Excel file)

Supplemental Table S9. Statistical values for the analysis of the amount of non-O-methylated- and O-methylated flavonoids in different maize lines according to treatment, duration of treatment (day), and the interaction between treatment and its duration corresponding to the experiments shown in Figure 5A and Supplemental Figure S15. Values in bold indicate significant differences ($P < 0.05$). Depending which statistical test was used F-values or Likelihood ratios are given. F-values are given in italics.

Maize line	Leaf segment	Flavonoid type	Statistical test used	Variance structure	Trans-formation	Factor	Likelihood ratio/ F-value	P-value
B75	upper	non-O-methylated	ANOVA	none	log	treatment	1.119	0.303
						day	0.889	0.357
						treatment:day	1.036	0.321
		O-methylated	gls*	day	log	treatment	0.183	0.669
						day	5.537	0.019
						treatment:day	6.380	0.012
B75	middle	non-O-methylated	ANOVA	log	log	treatment	213.755	< 0.001
						day	9.782	0.005
						treatment:day	0.273	0.607
		O-methylated	ANOVA	log	log	treatment	299.102	< 0.001
						day	103.501	< 0.001
						treatment:day	0.013	0.911
B75	lower	non-O-methylated	gls*	day	log	treatment	2.581	0.108
						day	5.014	0.025
						treatment:day	0.066	0.797
		O-methylated	gls*	day-treatment	log	treatment	0.234	0.629
						day	12.835	< 0.001
						treatment:day	13.147	< 0.001
Hybrid ,Sweet Nugget'	upper	non-O-methylated	ANOVA	log	log	treatment	18.120	< 0.001
						day	0.261	0.613
						treatment:day	0.635	0.432
		O-methylated	ANOVA	log	log	treatment	8.361	0.007
						day	0.461	0.502
						treatment:day	0.604	0.443
Hybrid ,Sweet Nugget'	middle	non-O-methylated	gls*	day-treatment	none	treatment	14.052	< 0.001
						day	4.855	0.028
						treatment:day	15.459	< 0.001
		O-methylated	gls*	day-treatment	log	treatment	56.102	< 0.001
						day	0.011	0.916
						treatment:day	9.091	0.003
Hybrid ,Sweet Nugget'	lower	non-O-methylated	gls*	treatment	log	treatment	6.836	0.009
						day	0.310	0.578
						treatment:day	1.277	0.259
		O-methylated	gls*	day-treatment	log	treatment	10.955	< 0.001
						day	3.805	0.051
						treatment:day	6.398	0.011
W22	middle	non-O-methylated	ANOVA	log	log	treatment	309.744	< 0.001
						day	118.761	< 0.001
						treatment:day	4.206	0.050
		O-methylated	ANOVA	log	log	treatment	251.700	< 0.001
						day	231.600	< 0.001
						treatment:day	2.237	0.146
B73	middle	non-O-methylated	ANOVA	log	log	treatment	299.930	< 0.001
						day	24.126	< 0.001
						treatment:day	8.544	0.007
		O-methylated	gls*	day-treatment	log	treatment	50.882	< 0.001
						day	12.482	< 0.001
						treatment:day	3.204	0.074

*gls, generalized least squares; The varident error structure for each day-treatment combination (day-treatment), or just for each treatment (treatment) was used.

Supplemental Table S10: see Supplemental Tables (Excel file)

Supplemental Table S11: see Supplemental Tables (Excel file)

Supplemental Table S12. MS settings used for the analysis on the timsTOF mass spectrometer.

ESI ion source settings				
Ionization mode:	positive	positive	negative	negative
Capillary voltage:	4500 V	4500 V	3500 V	3500 V
Drying gas (nitrogen):	8 L/min, 280°C	8 L/min, 280°C	8 L/min, 280°C	10 L/min, 230°C
Nebulizer gas (nitrogen):	2.8 bar	2.8 bar	2.8 bar	1.8 bar
Aquisition parameters				
Scan mode:	full	auto MS/MS	full	auto MS/MS
Collision energy:	-	alternating 20 eV/50 eV	-	alternating 20 eV/50 eV

Supplemental Table S13. MS settings used for the analysis on the QTRAP 6500+.

Turbospray ESI ion source settings			
Analytes	flavonoids	flavonoid glycosides	benzoxazinoids
Ionization mode:	positive	negative	negative
Ion spray voltage:	+5500 V	-4500 V	-4500 V
Turbo gas temperature:	650°C	650°C	650°C
Curtain gas:	40 psi	40 psi	40 psi
Collision gas:	medium level	medium level	medium level
Nebulizer gas:	60 psi	60 psi	70 psi
Heating gas:	60 psi	60 psi	70 psi

Supplemental Table S14. Mass analyzer settings used for the analysis of flavonoids and additional phenylpropanoids on the QTRAP 6500+. Retention time (RT) was used to distinguish between compounds with the same MRM transition. Compounds marked with (*) were verified by an authentic standard. Abbreviations: Me, methyl; DP, declustering potential; EP, entrance potential; CE, collision energy; CXP, collision cell exit potential; V, volts.

Flavonoid / phenylpropanoid	RT (min)	MRM transition m/z	DP (V)	EP (V)	CE (V)	CXP (V)
Caffeic acid*	3.01	181 [M+H] ⁺ → 163	6	5	13	24
O-Me-Caffeic acid-1	-	195 [M+H] ⁺ → 180	50	5	10	6
O-Me-Caffeic acid-2	-	195 [M+H] ⁺ → 162	50	5	20	6
Resveratrol*	5.45	229 [M+H] ⁺ → 107	51	5	27	14
O-Me-Resveratrol	7.23	243 [M+H] ⁺ → 107	50	5	30	6
Chrysin*	8.36	255 [M+H] ⁺ → 153	20	5	51	12
5-O-Me-Chrysin	6.40	269 [M+H] ⁺ → 254	50	5	35	6
Apigenin*	6.63	271 [M+H] ⁺ → 153	50	3.5	41	4
Genistein*	6.66	271 [M+H] ⁺ → 153	50	3.5	41	4
Naringenin chalcone*	6.51	273 [M+H] ⁺ → 153	46	3	29	4
Naringenin*	6.64	273 [M+H] ⁺ → 153	41	4.5	31	4
5-O-Me-Apigenin*	5.04	285 [M+H] ⁺ → 270	50	6	31	8
7-O-Me-Apigenin (Genkwanin)*	8.53	285 [M+H] ⁺ → 242	50	6	43	4
5-O-Me-Genistein	5.22	285 [M+H] ⁺ → 270	50	6	31	8
4'-O-Me-Apigenin (Acacetin)*	8.44	285 [M+H] ⁺ → 242	50	7	43	4
5-O-Me-Naringenin*	5.04	287 [M+H] ⁺ → 167	36	5	31	6
7-O-Me-Naringenin (Sakuranetin)*	8.43	287 [M+H] ⁺ → 167	36	5	31	6
Scutellarein*	5.32	287 [M+H] ⁺ → 123	50	3.5	47	4
Luteolin*	5.89	287 [M+H] ⁺ → 153	50	3	43	4
Kaempferol*	6.80	287 [M+H] ⁺ → 153	50	2	39	4
Dihydrokaempferol*	5.12	289 [M+H] ⁺ → 243	50	4	15	6
2-Hydroxynaringenin*	5.53	289 [M+H] ⁺ → 121	21	5	21	14
Eriodictyol*	5.83	289 [M+H] ⁺ → 153	46	7	33	4
5,7-O-DiMe-Apigenin*	6.38	299 [M+H] ⁺ → 284	50	4	37	6
5-O-Me-Luteolin	4.53	301 [M+H] ⁺ → 286	50	3	35	6
7-O-Me-Luteolin	7.57	301 [M+H] ⁺ → 286	50	3	35	6
5-O-Me-Scutellarein*	4.75	301 [M+H] ⁺ → 286	50	3	33	6
7-O-Me-Scutellarein*	6.01	301 [M+H] ⁺ → 286	50	3	33	6
6-O-Me-Scutellarein (Hispidulin)*	6.67	301 [M+H] ⁺ → 286	21	5	33	28
5-O-Me-Kaempferol	5.54	301 [M+H] ⁺ → 286	50	2	35	6
3-O-Me-Kaempferol (Isokaempferide)*	7.03	301 [M+H] ⁺ → 286	50	4	27	8
7-O-Me-Kaempferol	8.66	301 [M+H] ⁺ → 286	50	2	35	6
5,7-O-DiMe-Naringenin*	6.60	301 [M+H] ⁺ → 181	46	11	31	6
5-O-Me-Eriodictyol	4.42	303 [M+H] ⁺ → 124	50	7	55	4
7-O-Me-Eriodictyol	7.50	303 [M+H] ⁺ → 124	50	7	55	4
5-O-Me-Dihydrokaempferol	4.44	303 [M+H] ⁺ → 107	50	4	55	2
7-O-Me-Dihydrokaempferol	6.99	303 [M+H] ⁺ → 107	50	4	55	2
Quercetin*	5.96	303 [M+H] ⁺ → 153	50	7	45	4
O-Me-2-hydroxynaringenin (peak 1)	6.44	303 [M+H] ⁺ → 167	21	5	21	20
7-O-Me-2-hydroxynaringenin	7.07	303 [M+H] ⁺ → 167	21	5	21	20
O-Me-2-hydroxynaringenin (peak 2)	8.32	303 [M+H] ⁺ → 167	21	5	21	20
Dihydroquercetin (Taxifolin)*	4.41	305 [M+H] ⁺ → 153	50	7.5	25	6
2-Hydroxyeriodictyol	4.88	305 [M+H] ⁺ → 137	21	5	21	14
5,7-O-DiMe-Luteolin	5.15	315 [M+H] ⁺ → 300	50	3	35	6
O-DiMe-Luteolin (O-Methyl group likely on A + B ring)	8.70	315 [M+H] ⁺ → 300	50	3	35	6
5-O-Me-Isokaempferide	5.25	315 [M+H] ⁺ → 254	11	5	39	30
7-O-Me-Isokaempferide	8.96	315 [M+H] ⁺ → 254	11	5	39	30
5,7-O-DiMe-Scutellarein*	5.34	315 [M+H] ⁺ → 254	50	3	41	8
5,6-O-DiMe-Scutellarein	5.50	315 [M+H] ⁺ → 282	11	5	33	34
6,7-O-DiMe-Scutellarein (Cirsimaritin)*	7.68	315 [M+H] ⁺ → 282	11	5	33	34
5-O-Me-Quercetin	4.85	317 [M+H] ⁺ → 302	50	7	35	6
7-O-Me-Quercetin	7.63	317 [M+H] ⁺ → 302	50	7	35	6
O-DiMe-2-Hydroxynaringenin (Xilonenin; peak 1)*	5.51	317 [M+H] ⁺ → 181	1	5	21	20
O-DiMe-2-Hydroxynaringenin (Xilonenin; peak 2)*	6.81	317 [M+H] ⁺ → 181	1	5	21	20
5-O-Me-Dihydroquercetin	3.81	319 [M+H] ⁺ → 123	50	7.5	55	6
7-O-Me-Dihydroquercetin	6.18	319 [M+H] ⁺ → 123	50	7.5	55	6
Myricetin*	5.07	319 [M+H] ⁺ → 153	50	7	40	4
5-O-Me-Myricetin	4.12	333 [M+H] ⁺ → 318	50	7	35	6
7-O-Me-Myricetin	6.57	333 [M+H] ⁺ → 318	50	7	35	6

Supplemental Table S15. Mass analyzer settings used for the analysis of flavonoid glycosides on the QTRAP 6500+. Compounds marked with (*) were verified by an authentic standard. Abbreviations: Me, methyl; DP, declustering potential; EP, entrance potential; CE, collision energy; CXP, collision cell exit potential; V, volts.

flavonoid glycoside	MRM transition <i>m/z</i>	DP (V)	EP (V)	CE (V)	CXP (V)
Kaempferol-7-O-beta-D-glucopyranoside*	447 [M-H] ⁻ → 285	-50	-11	-38	-8
O-Me-Kaempferol-7-O-beta-D-glucopyranoside-1	461 [M-H] ⁻ → 299	-50	-6	-40	-4
O-Me-Kaempferol-7-O-beta-D-glucopyranoside-2	461 [M-H] ⁻ → 284	-50	-6	-50	-4
Kaempferol-3-O-beta-rutinoside*	593 [M-H] ⁻ → 285	-50	-6	-46	-8
O-Me-Kaempferol-3-O-beta-rutinoside-1	607 [M-H] ⁻ → 299	-50	-6	-40	-4
O-Me-Kaempferol-3-O-beta-rutinoside-2	607 [M-H] ⁻ → 284	-50	-6	-50	-4

Supplemental Table S16. Mass analyzer settings used for the analysis of BXs on the QTRAP 6500+. Compounds marked with (*) were verified by an authentic standard. Abbreviations: DP, declustering potential; EP, entrance potential; CE, collision energy; CXP, collision cell exit potential; V, volts.

benzoxazinoid	MRM transition <i>m/z</i>	DP (V)	EP (V)	CE (V)	CXP (V)
MBOA	164 [M-H] ⁻ → 149	-40	-4	-20	-2
HBOA-Glc	326 [M-H] ⁻ → 164	-40	-4	-20	-5
DIBOA-Glc	342 [M-H] ⁻ → 134	-40	-4	-24	-4
HMBOA-Glc	356 [M-H] ⁻ → 194	-40	-4	-15	-4
DIMBOA-Glc*	372 [M-H] ⁻ → 210	-40	-4	-15	-4
HM ₂ BOA-Glc	386 [M-H] ⁻ → 224	-40	-4	-15	-4
HDMBOA-Glc*	432 [M+FA-H] ⁻ → 356	-40	-4	-20	-3
DIM ₂ BOA-Glc	402 [M-H] ⁻ → 194	-40	-4	-18	-5
HDM ₂ BOA-Glc	462 [M+FA-H] ⁻ → 194	-40	-4	-25	-3

Supplemental Table S17. Authentic standards used for identification and quantification. Abbreviations: Me, methyl.

Compound	Supplier	self purified
Phenylpropanoids		
Caffeic acid	Merck; S23175, > 98 % (HPLC)	-
Resveratrol	Sigma, R-5010, approx. 99 %	-
Flavonoids		
Chrysin	Sigma, 95082, analyt. Standard	-
Apigenin	Sigma, 42251, analyt. standard	-
Genistein	Carl Roth, 0716.2, >= 98 %, für Biochemie	-
Naringenin	Sigma, W530098, 98 %	-
Naringenin-chalcone	PhytoLab, 83877, phyproof	-
Scutellarein	Sigma, S0327, >= 98 % (HPLC)	-
Luteolin	Enzo Life Sciences, ALX-385-007	-
Kaempferol	EMD Chemicals San Diego, 420345	-
Dihydrokaempferol	Sigma, 91216, >= 95 % (HPLC)	-
2-Hydroxynaringenin		✓
Eriodictyol	Sigma, 94258, >= 95 % (HPLC)	-
Quercetin hydrate	Acros organics, 95 %	-
Dihydroquercetin (Taxifolin) hydrate	Sigma, T4512, >= 90 % (HPLC)	-
Myricetin	Carl Roth, 6461.1, >= 95 %	-
Flavonoid glycosides		
Kaempferol-7-O-β-D-glucopyranoside	Sigma, 18854, >= 90 % (HPLC)	-
Kaempferol-3-O-β-rutinoside	Sigma, 90242, >= 98 % (HPLC)	-
O-methylflavonoids		
5-O-Me-Apigenin	-	✓
7-O-Me-Apigenin (Genkwanin)	TRC, G360000	✓
4'-O-Me-Apigenin (Acacetin)	Carl Roth, 5010.1	-
5-O-Me-Naringenin	Sigma, SMB00201, >= 95 %	✓
7-O-Me-Naringenin (Sakuranetin)	Sigma, 73422, analyt. Standard	✓
5,7-O-DiMe-Apigenin	-	✓
5-O-Me-Scutellarein	-	✓
7-O-Me-Scutellarein	-	✓
6-O-Me-Scutellarein (Hispidulin)	Sigma, SML0582, >= 98 % (HPLC)	-
3-O-Me-Kaempferol (Isokaempferide)	-	✓
5,7-O-DiMe-Naringenin	-	✓
5,7-O-DiMe-Scutellarein	-	✓
6,7-O-DiMe-Scutellarein (Cirsimaritin)	Sigma, SMB00174, ≥90% (LC/MS-ELSD)	-
O-DiMe-2-Hydroxynaringenin (Xilonenin)	-	✓

Supplemental Table S18: see Supplemental Tables (Excel file)

Supplemental Table S19. RT-qPCR primers.

Primer name	Target gene	Primer Sequence (5' → 3')
ZmFOMT2_qPCR_Fwd	<i>FOMT2</i>	GTCCCTGTGCTACGCCAAAT
ZmFOMT2_qPCR_Rev		GTGACGGTCAATCATCAC
ZmFOMT3_qPCR_Fwd_neu1	<i>FOMT3</i>	TGATGAGTCAAATACAAAACGTC
ZmFOMT3_qPCR_Rev_neu1		GGGAGCCAACAACGGGTAGA
GRMZM2G423331_Fwd3	<i>FOMT4</i>	CCCAGTACAAGCACCTGAGAG
GRMZM2G423331_Rev3		ACCACCTACATGTTCCACACC
GRMZM2G422750-Fwd2	<i>CHS2</i> (UTR)	CGTCCGCAAATAATGTGCTCTC
GRMZM2G422750-Rev2		TAGCTCTACCCTGGTCTTGC
GRMZM2G175076-Fwd1	<i>CHIL</i> (UTR)	TTCGTGAATGTCCGTCCTGT
GRMZM2G175076-Rev1		CCACAACGACAATCTGCACAA
GRMZM2G062396-Fwd1	<i>F3H</i> (UTR)	TATAGCTACGTGCGACCGTG
GRMZM2G062396-Rev1		CTGGAACCGCACGTTGAAAA
ZmFNSI_Fwd	<i>FNSI1</i>	AGGAGAAGGCCAAGCTCTACT
ZmFNSI_Rev		CCCATGGTCTCCTTGAAATC
FNSI2_qPCR_Fwd2	<i>FNSI2</i>	CCGGACAACCCACCATCCTT
FNSI2_qPCR_Rev2		CCCAGCGCCTCCTTGATGTA
ZmFLS1/2_qPCR_Fwd2	<i>FLS1/FLS2</i>	TACGAGGCCAAGTACGTGCC
ZmFLS1/2_qPCR_Rev2		TCCACGAACATCGGCCATGA
ZmF3-H_qPCR_Fwd1	<i>F3,H</i>	ATCCGGACGTGCTCAGGAAG
ZmF3-H_qPCR_Rev1		TCTCCTTGATCACCGCCGTG
Zm33614_qPCR_Fwd1	<i>F2H1</i>	CAATCCACTGCGCCGCCCT
Zm33614_qPCR_Rev1		TACGTAGCCGCTCTTGCCG
Zm10826_qPCR_Fwd3	<i>F2H2</i>	GGCAGCAGGGACAGGGAG
Zm10826_qPCR_Fwd3		GGCAGCAGGGACAGGGAG
FNSII_qPCR_Fwd1	<i>FNSII1</i>	GCGTACAAGGAGACGTTGCG
FNSII_qPCR_Rev1		CGATGGCCACACGTTGATG
Zm08124_qPCR_Fwd3	<i>FNSII2</i>	AAGACGATGGACAAGGAATAAG
Zm08124_qPCR_Rev3		CCGCCGCTGGTCCTCC
Zm39147_qPCR_Fwd2	<i>ZmCYP93G6</i>	AGTCGACGGTGCTTATCCAC
Zm39147_qPCR_Rev2		ATGTATTGGAAGTGCTTCCCG
Zm33036_qPCR_Fwd3	<i>ZmCYP93F6</i>	ACCTGCAGGACTACATCGGC
Zm33036_qPCR_Rev3		GCCGTCAAGTATCCGCTCCAT
ZmBx10/11_UTR_qFwd2	<i>BX10</i> (UTR)	GAAGGTGTTGATAGTATATTATG
ZmBx10_UTR_qRev2		ACTGGTACGCTTGTAACCTGA
ZmBx11_UTR_qFwd3	<i>BX11</i> (UTR)	TGTGTGTTGGTCAAGTAGTCGA
ZmBx11_UTR_qRev3		TCCTTGTTGCCATGACACAAC
BxD-2.1	<i>BX14</i>	GAAAGCCGCTTCTTGATGCC
BxD-2.2		GGAACATATTGCCCGCAACG
ZmUBCP_qPCR_Fwd1	<i>UBCP</i> (GRMZM2G102471)	TTGTCCCTGAGATTGCTCACA
ZmUBCP_qPCR_Rev1		CACCAGTTTGCCAGCTTTTA
ZmMEP_qPCR_Fwd	<i>MEP</i> (GRMZM2G018103)	TGTACTCGGCAATGCTCTTG
ZmMEP_qPCR_Rev		TTTGATGCTCCAGGCTTACC

Supplemental Table S20. PCR primers for the amplification of full-length open reading frames of investigated FOMTs and CYP93Gs.

Primer name	Target gene	Primer Sequence (5' → 3')	Restriction recognition site	Application
FOMT2-W22-fwd FOMT2-W22-rev	FOMT2	CACCATGGCACTCAGCACTCAGGA TCATGGATAGACCTCGATGAC		TOPO cloning
FOMT4-W22-IBA-F FOMT4-W22-IBA-R	FOMT4	ATGGTACGTCTCAGCGCATGGCCTGCACGACGGCAGC ATGGTACGTCTCATATCACTTGGTGAACCTCGAGCGCCCA	BsmBI	
Bx10g-synt_pASK-37.fwd Bx10g-synt_pASK-37.rev	FOMT3	ATGGTAGGTCTCAGCGCATGGCGTTTACGGAAGAGAGTTTC ATGGTAGGTCTCATATCAGGGATAGACCTCAATCACAGACA	Bsal	pASK-IBA37plus cloning
Bx10e-synt_pASK-37.fwd Bx10e-synt_pASK-37.rev	FOMT5	ATGGTAGGTCTCAGCGCATGGCCTTACTCGGGGAATACTC ATGGTAGGTCTCATATCAATTCCGGGTACAGTTTCGATGATAGA	Bsal	
SpeI-ZmG167336_Fwd ZmG167336-PacI_Rev	F2H1 (B73)	TCGTACTAGTATGGAAGCTGATGCTGCT ACACTTAATTAACCTACGTAGCCGCTCTTGC	SpeI PacI	
Zm33614_NotI_Fwd Zm33614_SacI_Rev	F2H1 (W22)	CGTGCGGCCGCAATGGAAGCTGATGCTGC AGGGAGCTCTTAAGTAGCAGCTCTAGCTG	NotI SacI	
Zm10826_NotI_Fwd Zm10826_SacI_Rev	F2H2	CGTGCGGCCGCAATGGAAGCTGCTGCTG AGGGAGCTCTCAAGTAGCTGTAGCTTGC	NotI SacI	
Zm08124_NotI_Fwd Zm08124_SacI_Rev	FNSII2	CGTGCGGCCGCAATGAAGGAACAACAACCTAGA AGGGAGCTCTTAAACAACCTGCTGGAATGGA	NotI SacI	subcloning into pESC-Leu2d
Zm39147_NotI_Fwd Zm39147_SacI_Rev	ZmCYP93G6	CGTGCGGCCGCAATGGAAGAACAACAATTGAGAG AGGGAGCTCTCAACAACAGGTGGAATG	NotI SacI	
Zm33036_NotI_Fwd Zm33036_SacI_Rev	ZmCYP93F6	CGTGCGGCCGCAATGGAAGTTGTTACCGCTA AGGGAGCTCTCAACACCAGCGGTTT	NotI SacI	

11.3 Manuscript III

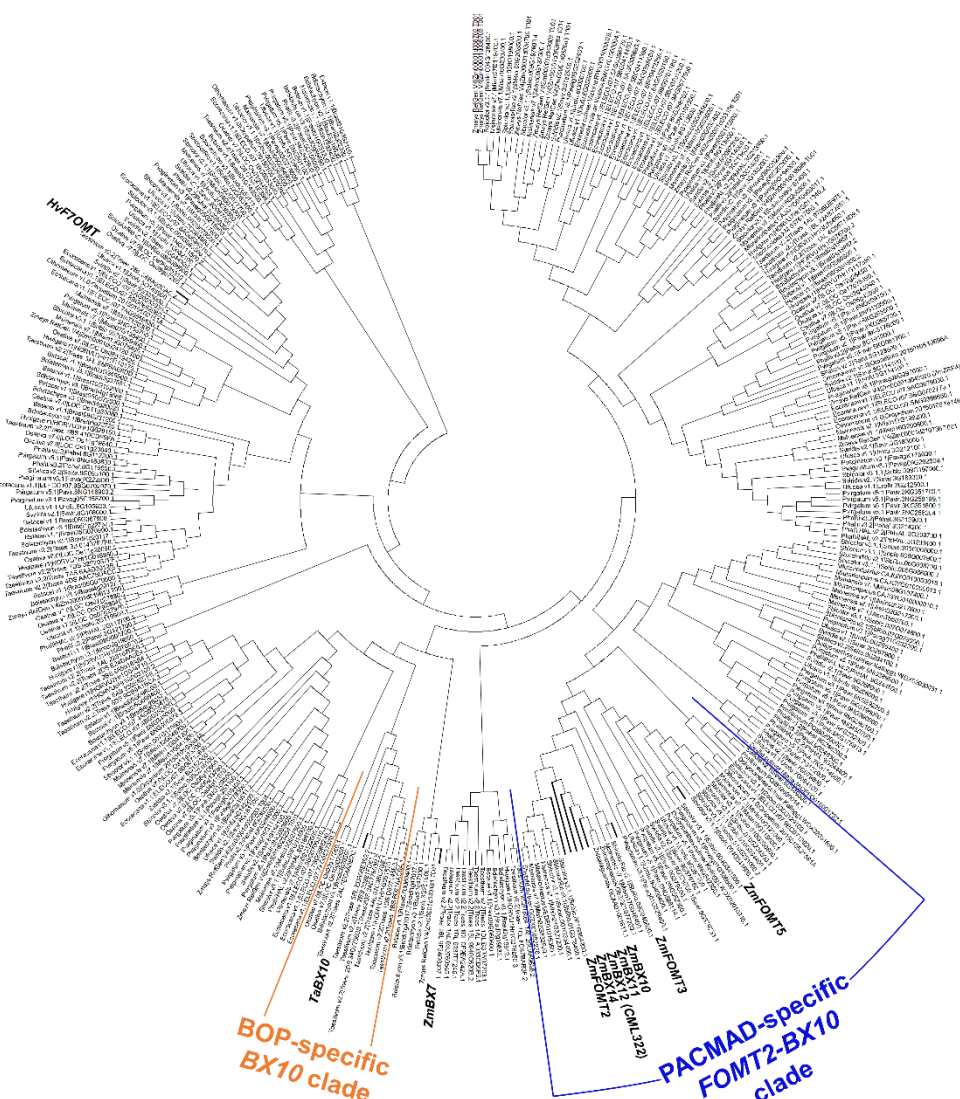


Figure S1. Phylogenetic tree of Poaceae OMT genes similar to *ZmFOMT2*. OMTs were identified by BLASTP analysis with *ZmFOMT2* as query and using Poaceae protein datasets available in the Phytozome 13 (<https://phytozome-next.jgi.doe.gov/>) and NCBI (<https://www.ncbi.nlm.nih.gov/>) databases. Additional sequences were obtained from the NCBI TSA database (<https://www.ncbi.nlm.nih.gov/genbank/tsa/>) by a local BLAST search using BioEdit followed by an NCBI search for full sequences. Only genes (ORFs) with $\geq 80\%$ query coverage and a corresponding amino acid identity of $\geq 40\%$ were included. The tree was inferred using the maximum likelihood method based on the General Time Reversible model, including gamma distributed rate variation among sites (+G, 1.8577). All positions with $< 90\%$ site coverage were eliminated. OMTs previously characterized in the literature are highlighted in black bold, and the "PACMAD-specific *FOMT2-BX10* clade" and "BOP-specific *BX10* clade" are marked in blue and orange, respectively. Sequences of the following species were included in the tree: *Brachypodium distachyon*; *Brachypodium stacei*; *Dichanthelium oligosanthes* Kellogg; *Digitaria exilis* Niatia; *Eleusine coracana*; *Eragrostis curvula* Victoria; *Hordeum vulgare* (Hv); *Miscanthus lutarioriparius*; *Miscanthus sinensis*; *Oropetium thomaeum*; *Oryza sativa*; *Panicum hallii*; *Panicum hallii* HAL; *Panicum miliaceum*; *Panicum virgatum*; *Paspalum vaginatum*; *Saccharum hybrid*; *Setaria italica*; *Setaria viridis*; *Sorghum bicolor*; *Sorghum bicolor* Rio; *Triticum aestivum* (Ta); *Triticum dicoccoides*; *Urochloa fusca*; *Zea mays* (Zm); *Zea nicaraguensis*.

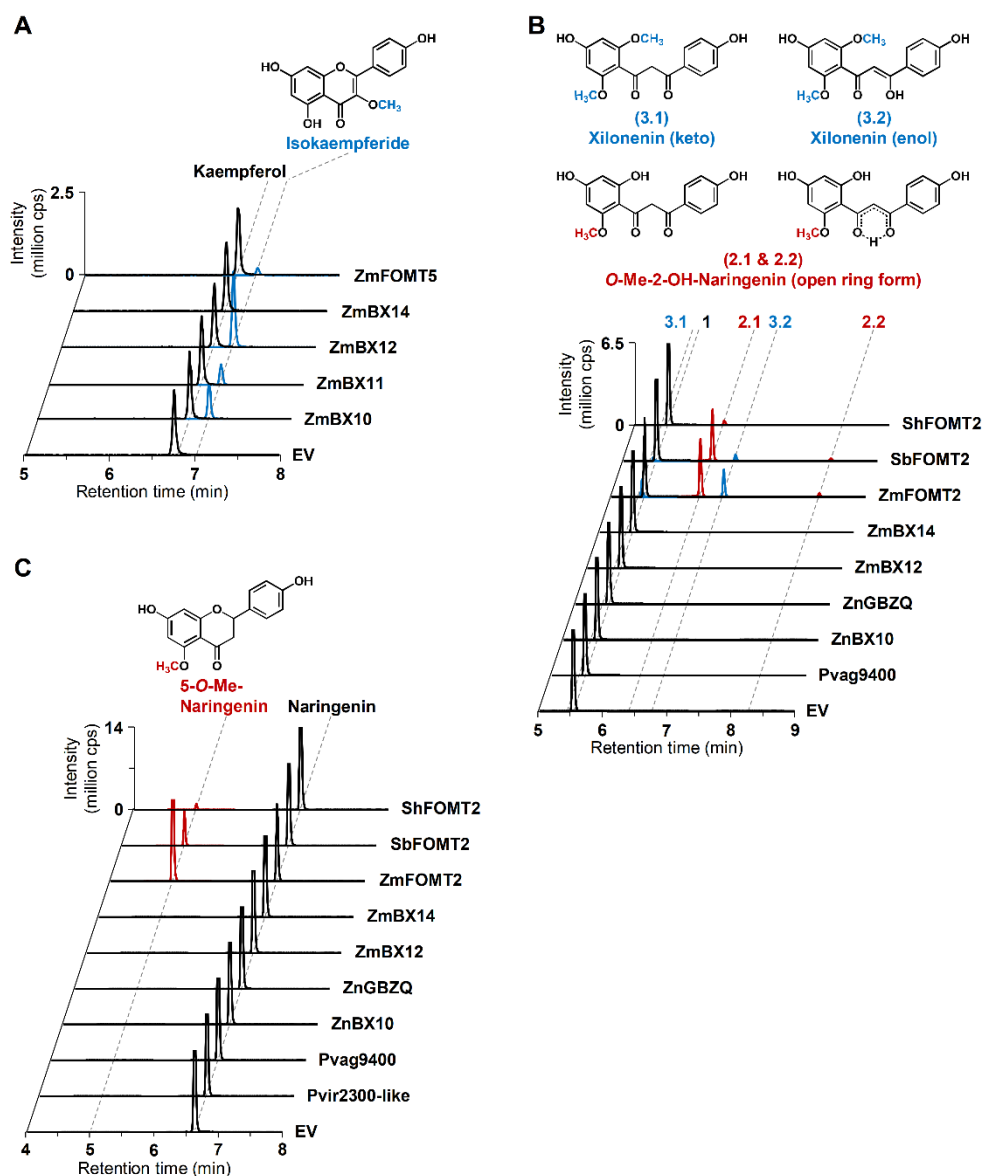


Figure S2. Enzymatic activity of *FOMT2*-like group members with different flavonoid substrates. The purified recombinant enzymes as well as an empty vector control (EV) were incubated with the potential substrates kaempferol (**A**), 2-hydroxynaringenin (**B**), and naringenin (**C**) in presence of the cosubstrate SAM. Reaction products were analyzed by LC-MS/MS. Chromatograms of specific MRM transitions (see methods section) are shown. The upper part of each panel shows the structures of the enzyme products, with the attached methyl groups highlighted in blue or red. All assays were performed in technical triplicates. Peak numbers in panel B: 1, 2-hydroxynaringenin; 2.1 and 2.2, O-methyl-2-hydroxynaringenin; 3.1, xilonenin (keto); 3.2, xilonenin (enol). Abbreviations: Me, methyl; cps, counts per second. **Note:** The data shown in panel A were collected independently from the experiments shown in Figure 2 and panel B and C.

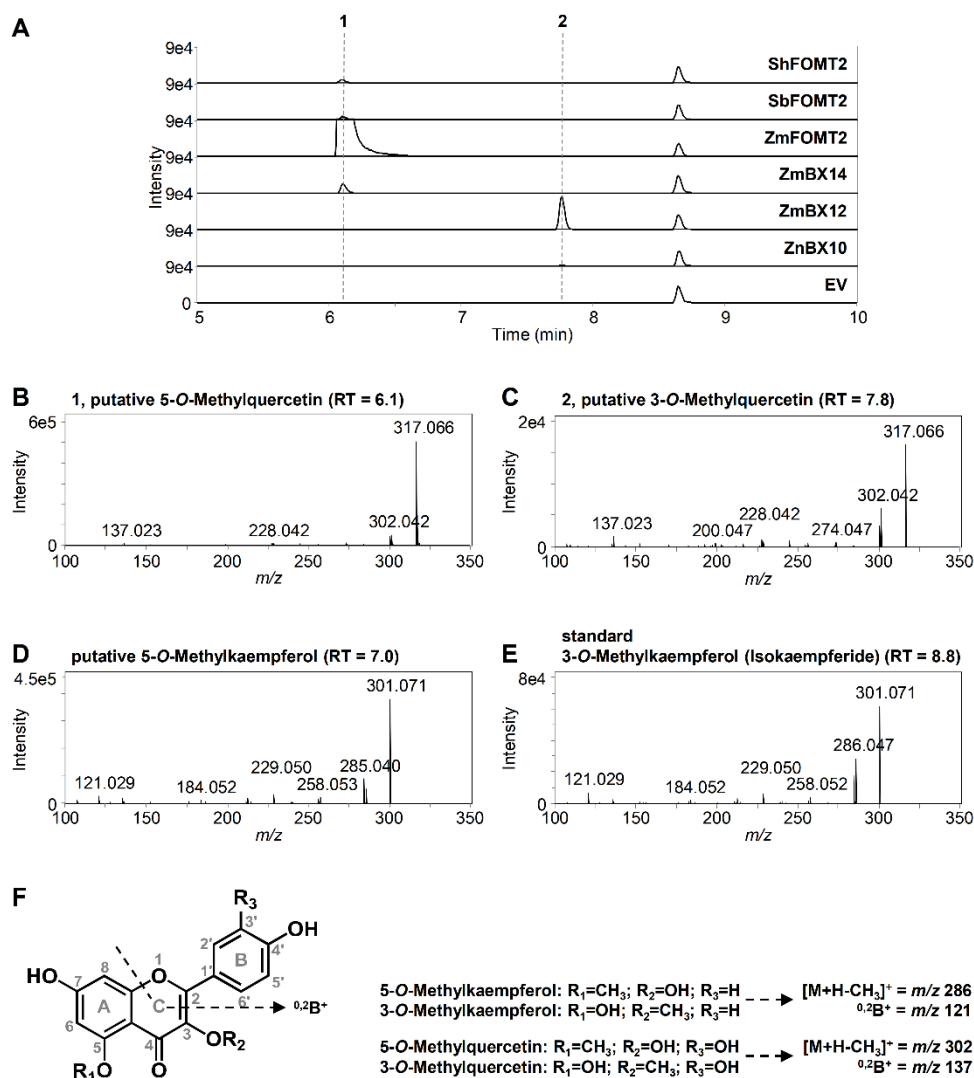


Figure S3. BX OMTs catalyze the 3-O-methylation of flavonols. Extracted ion chromatograms (m/z 317.066 $[M+H]^+$) (**A**) and MS/MS spectra (**B-C**) of quercetin products produced by *FOMT*-like FOMTs and BX OMTs. For comparison the MS/MS spectra of the corresponding kaempferol products putative 5-O-methylkaempferol and 3-O-methylkaempferol (isokaempferide) are shown (**D-E**). Fragmentation patterns are similar and consistent with mono-O-methylation on the flavonol A- or C-ring, as a typical B-ring fragment is observed (**F**). The position of O-methylation can be distinguished by retention time (RT). Enzyme assays using quercetin or kaempferol as substrate were analyzed using untargeted LC-MS (full scan and auto MS/MS mode) as described in the methods section. The MS/MS spectrum of isokaempferide was obtained using the purified compound. 1, putative 5-O-methylquercetin; 2, putative 3-O-methylquercetin.

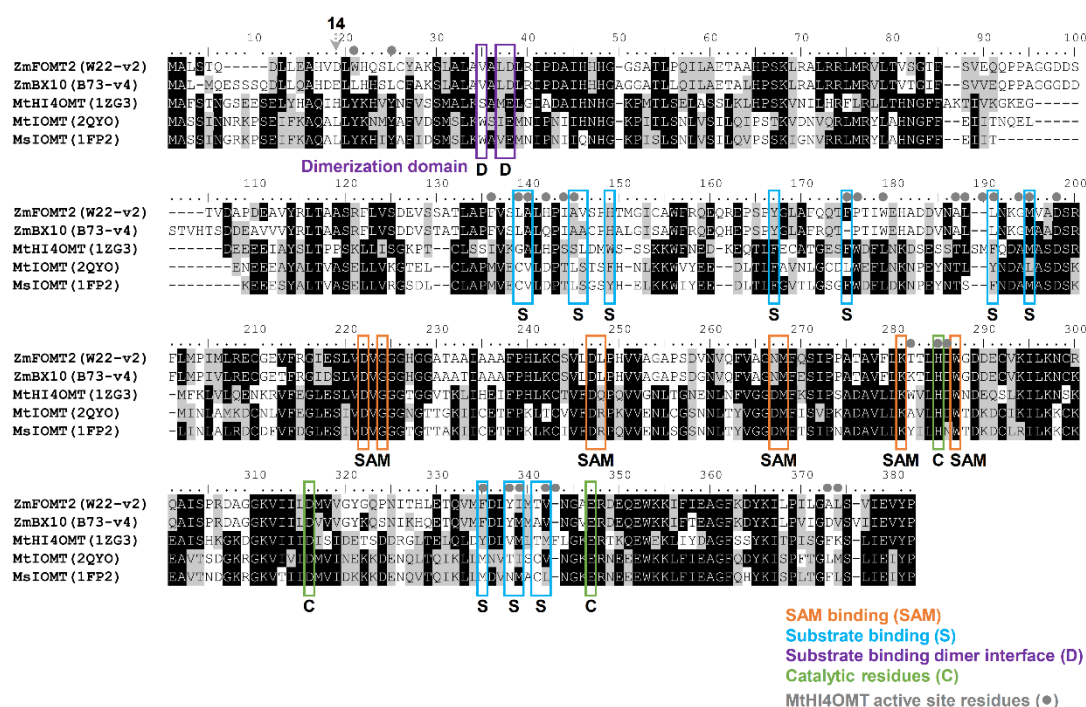
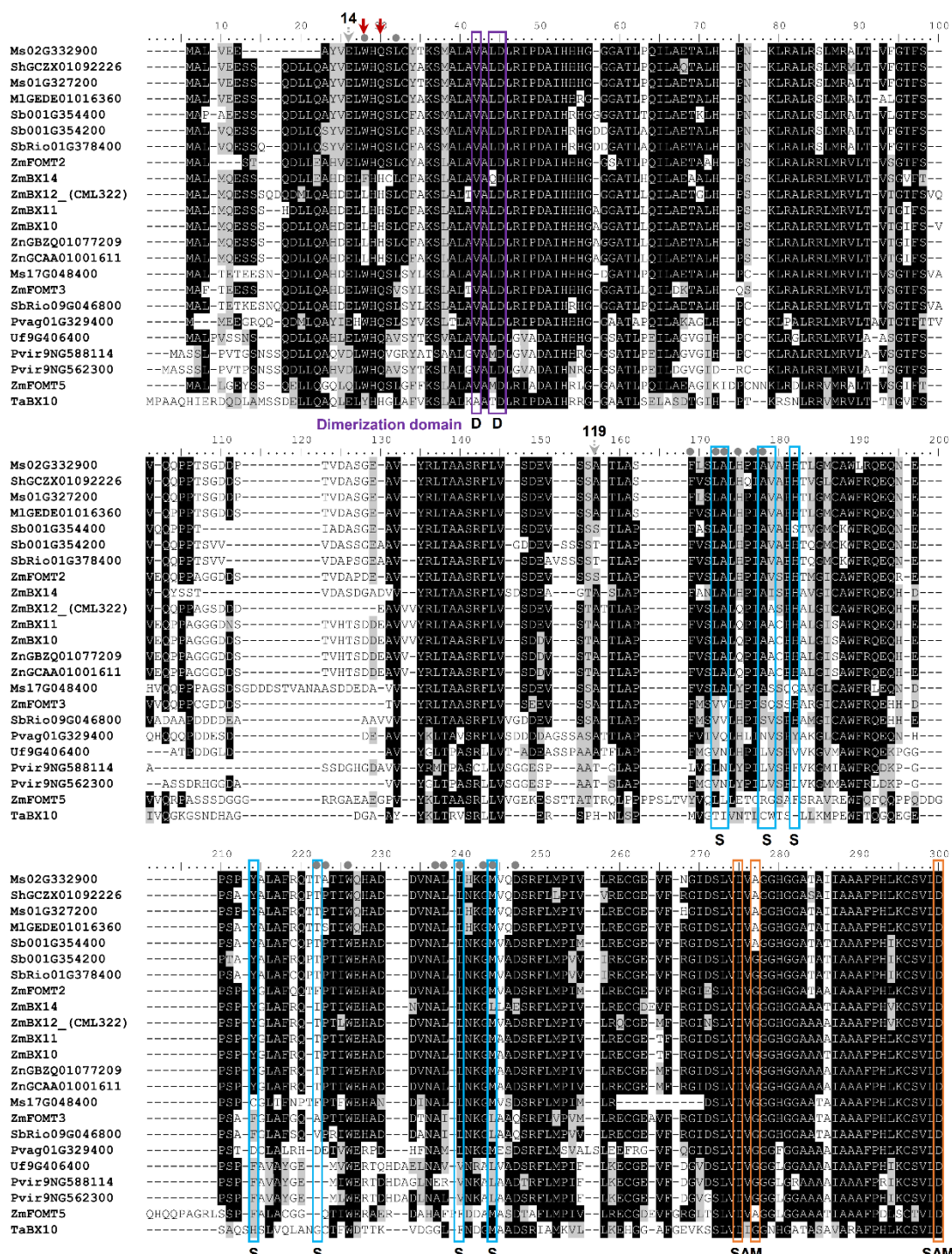


Figure S4. Amino acid sequence alignment of ZmFOMT2 and ZmBX10 with isoflavone OMTs. Isoflavone 4'-OMT from *Medicago truncatula* (MthI4OMT; PDB-ID: 1ZG3), Isoflavone-OMT from *M. truncatula* (MtiIOMT; PDB-ID: 2QYO), and Isoflavone-OMT from *Medicago sativa* (MsiIOMT; PDB-ID: 1FP2) were identified as the best templates for homology modelling with ZmFOMT2 (MZ484743) using the Swiss-Model server (<https://swissmodel.expasy.org/>). The sequences were aligned using MEGA7 and visualized with BioEdit. Identical amino acids are shaded in black and similar amino acids in grey. Amino acid residues involved in SAM binding (orange), substrate binding (blue), substrate binding from the second polypeptide chain of the homodimer (purple), catalysis (green) are highlighted (modified from Zubieta et al., 2001). MthI4OMT active site residues are marked with grey dots (modified from Liu et al., 2006). ZmFOMT2 shares 39%, 34%, 35%, and 84% amino acid identity with MthI4OMT, MtiIOMT, MsiIOMT, and ZmBX10, respectively. ZmBX10 is encoded by *Zm00001d029359*. **Note:** Unlike the MaizeGDB database sequence encoded by *Zm00004b033403/Zm00004b033399* (W22_v2), the cloned ZmFOMT2 (MZ484743) sequence displayed here contains a D instead of an E in position 14 (grey dashed arrow).



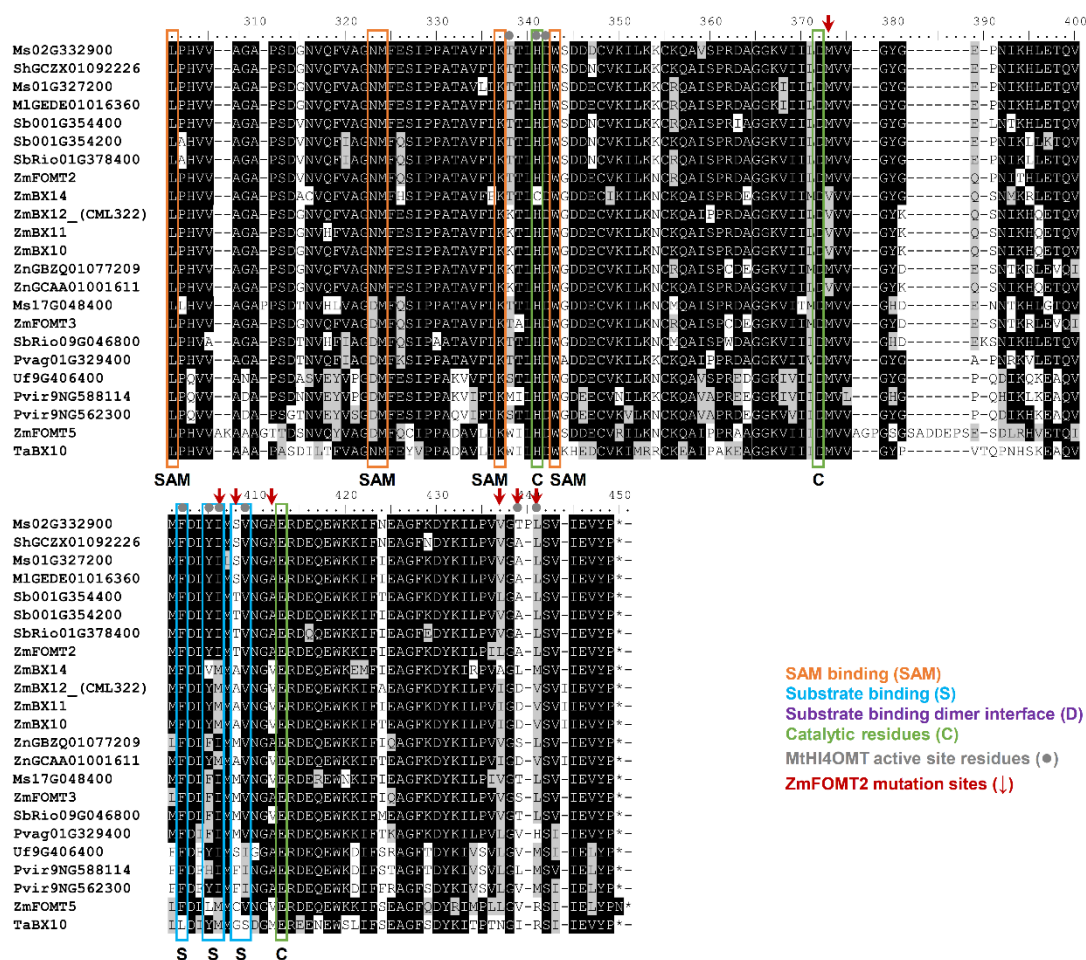


Figure S5. Amino acid sequence alignment of OMTs in the *FOMT2*-like group. The amino acid sequences were aligned using the MUSCLE codon algorithm implemented in MEGA7 and visualized with BioEdit. Identical amino acids are shaded in black and similar amino acids in grey. Amino acid residues involved in SAM binding (orange), substrate binding (blue), substrate binding from the second polypeptide chain of the homodimer (purple), catalysis (green) are highlighted (modified from Zubieta et al., 2001). MthI4OMT active site residues are marked with grey dots (modified from Liu et al., 2006). ZmFOMT2 mutation sites are marked with red arrows. The amino acid sequences are encoded by Zm00001d047192 (*ZmFOMT2*), Zm00001d004921 (*ZmBX12*), Zm00025ab019610 (*ZmBX12*), Zm00001d029356 (*ZmBX11*), Zm00001d029359 (*ZmBX10*), Zm00001d047194 (*ZmFOMT3*), Zm00001d051934 (*ZmFOMT5*), and 4AL_C467B516F (*TaBX10*). **Note:** Unlike the cloned W22 sequence displayed in Figure S4, ZmFOMT2 (B73) shown here contains an E instead of a D in position 14 and an A instead of an S in position 119 (grey dashed arrows).

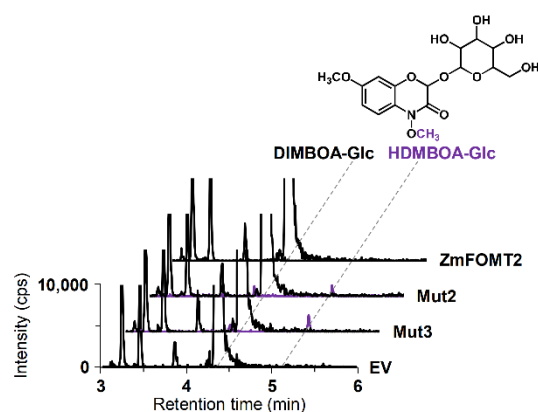


Figure S6. Enzymatic activity of ZmFOMT2 mutants with DIMBOA-Glc. The purified recombinant enzymes as well as an empty vector control (EV) were incubated with the substrate in presence of the cosubstrate SAM. In contrast to the assays shown in Figure 4, a 2.5-fold amount of purified recombinant enzyme ($\sim 2 \mu\text{g}/\text{assay}$), a 2.5-fold amount of substrate ($50 \mu\text{M}$), and a 5-fold amount of cosubstrate were used. Reaction products were analyzed by LC-MS/MS. Chromatograms of specific MRM transitions (see methods section) are shown. In the upper part, the structure of the enzymatic product HDMBOA-Glc is shown with the attached methyl group highlighted in purple. Abbreviations: cps, counts per second.

ShGCZX01092226 codon optimized

ATGGCACTGGTTGAAGAAAGCAGCCAGGATCTGCTGCAGGCATATGTTGAACGTGGCATCAGAGCCTGTGTTATGCAAAAAGCATGGCCCTGGC
AGTTGCACTGGATCTGCGTATTCCGGATGCAATTCATCATCATGGTGGTGGTGAACCCCTGCCCTCAGATTCTGGCACAGACCCGACTGCATCCGA
ATAAACGTGCGTGCACTGCGTAGCCTGATGCGTATGCTGACCGTTTTTGGCACCTTTAGCGTTCAGCAGCCTCCGACCAGCGGTGATGATAGCACC
GTGATGCAAGCGGTGAAGCAGTTTATCGTCTGACCCGAGCAAGCCGTTTTCTGGTTAGTGATGAAGTTAGCAGCGCAACCCCTGGCAAGCTTTGT
TAGCCTGGCGCTGCATCAGATTGCCGTTGCACCCGATACCGTTGGTCTGTGTGCATGGTTTCTCAAGAACAGAAATGAACCGAGCGCATATGCAC
TGGCATTTCTGCAGCCGACCCGACCATTTGGCAGCATGCAGATGATGTTAATGCACTGCTGAATAAAGGTATGGTTTCAAGTAGTCGTTTTCTG
CTGCCGATTTGTTCTCGTGAATGTTGGTGAAGTTTTTGGCGGTATTGATAGCCTGGTTGATGTTGCCGGTGGTCATGGTGGCGCAAGCGCAATTAT
TGCAGCAGCATTTCCGCATCTGAAATGTAGCGTTCTGGACCTGCCGCATGTTGTGCGGGTGACCCGAGTGATGGTAATGTTAGTTTGTTCAGTTTGTGCAG
GTAACATGTTTGAAGCATTCCGCCCTGCAACCGCAGTTTTTCTGAAAACCACTGCATGATGGTCCGATGATAACTGTGTGAAAATCCTGAAA
AAATGCAAGCAGCGAATTAGTCCGCGTATGCAGGCGGTAAAGTTATTATTCTGGATATGGTTGTGGTTATGGCGAGCCGAACATTAAACATCT
GGAAACCCAGGTTATGTTCCGACCTGTATATTATGAGCGTTAATGGTGCAGAACGTGATGAACAAGAGTGGAAAAAATCTTTAACGAGGCAGGCT
TCAACGACTACAAAATTTCTGCCGTTGTGGGTGCATGAGCGTTATTGAAGTTTATCCGTAA

ZnGBZQ01077209 codon optimized

ATGGCACTGATGCAAGAAAGCAGCAGCCAGGATCTGCTGCAGGCACATGATGAACGTGCTGCATCATAGCCTGTGTTTTGGCAAAAAGCCTGGCACT
GGCAGTTGCACTGGATCTGCGTATTCCGGATGCAATTCATCATCATGGTGGTGGTGGTGAACCCCTGCTGCAAAATCTGGCAGAAAACCGCACTGC
ATCCGAGCAAACTGCGTGCACTGCGTCTGCTGATGCGTGTCTGACCGTTACCGGTATTTTTAGCGTTGAACAGCCTCCGCGAGCGGTGGTGTAT
GATAGCACCCTTCATACCTCAGATGATGAAGCCGTTGTTTATCGTCTGACCCGAGCAAGCCGTTTTCTGGTTAGTGATGATGTTAGCAGCAAC
CCTGGCACCCTTTGTTAGCCTGGCGCTGCAGCCGATTGCAGCATGTCCGCATGCATGGGTATTAGCGCATGGTTTCTGCAAGAACAGCATGAAC
CGAGTCCGATATGTTGTCGATTTCTGTCAGACCCGACCATTTGGGAACATGCAGATGATGTAATGCATGCTGAATAAAGGTATGGCAGCAGAT
AGTCGTTTTCTGATGCCGATTGTTCTGCGTGAATGTGGTGAATGTTTCTGGTATTGATAGCCTGGTTGATGTTGGTGGTGGTTCATGGTGGTGC
AGCAGCAGCAATTCAGCAGCCTTTCCGCATCTGAAATGTAGCGTTCTGGACCTGCCGCATGTTGTTGCCGGTGCACCGAGTGATGGTAATGTTTC
AGTTTGTTCAGGCAACATGTTTGAAGCATTCCGCCCTGCAACCGCAGTTTTTCTGAAAAAACCCTGCATGATTTGGGTGATGATGAGTGTGTT
AAAAATCTGAAGAAATGGCGTCAGGCAATTAGCCCGTGTGATGAAGTGGTAAAGTGATTTATTATGGATATGGTGGTGGTTATGATGAGAGCAA
TACCAACGCTCTGGAAGTGCAGATTCTGTTGACCTGTTTATTATGATGGTGAATGGTGGCGAACGTGATGAACAAGAAATGGAAAAAATCTTTA
TCCAGGCAGGCTTCAAGGACTATAAAATCCTGCCGTTGTTGGTATGAGCGTTATTGAAGTTTATCCGTAA

ZnGCAA01001611 codon optimized

ATGGCACTGATGCAAGAAAGCAGCAGCCAGGATCTGCTGCAGGCACATGATGAACGTGCTGCATCATAGCCTGTGTTTTGGCAAAAAGCCTGGCACT
GGCAGTTGCACTGGATCTGCGTATTCCGGATGCAATTCATCATCATGGTGGTGGTGGTGAACCCCTGCTGCAAAATCTGGCAGAAAACCGCACTGC
ATCCGAGCAAACTGCGTGCACTGCGTCTGCTGATGCGTGTCTGACCGTTACCGGTATTTTTAGCGTTGAACAGCCTCCGCGAGCGGTGGTGTAT
GATAGCACCCTTCATACCTCAGATGATGAAGCCGTTGTTTATCGTCTGACCCGAGCAAGCCGTTTTCTGGTTAGTGATGATGTTAGCAGCAAC
CCTGGCACCCTTTGTTAGCCTGGCGCTGCAGCCGATTGCAGCATGTCCGCATGCATGGGTATTAGCGCATGGTTTCTGCAAGAACAGCATGAAC
CGAGTCCGATATGTTGTCGATTTCTGTCAGACCCGACCATTTGGGAACATGCAGATGATGTAATGCATGCTGAATAAAGGTATGGCAGCAGAT
AGTCGTTTTCTGATGCCGATTGTTCTGCGTGAATGTGGTGAATGTTTCTGGTATTGATAGCCTGGTTGATGTTGGTGGTGGTTCATGGTGGTGC
AGCAGCAGCAATTCAGCAGCCTTTCCGCATCTGAAATGTAGCGTTCTGGACCTGCCGCATGTTGTTGCCGGTGCACCGAGTGATGGTAATGTTTC
AGTTTGTTCAGGCAACATGTTTGAAGCATTCCGCCCTGCAACCCGAGTTTTTCTGAAAAAACCCTGCATGATTTGGGTGATGATGAGTGTGTT
AAAAATCTGAAGAAATGGCAGGCAATTAGTCCGCGTGTGATGAGGCGGTAAAGTTATTATTCTGGATGTTGTTGTGGGCTACAAACAGAGCAA
CATCAAACTCAAGAAACCCAGGTTATGTTGACCTGTATATGATGGCAGTTAATGGTGTGAACGTGATGAACAAGAGTGGAAAAAATCTTTA
CCGAGGCAGGCTTCAAGGACTATAAAATCCTGCCGTTTATTGGTATGAGCGTTATTATTGAAGTGTACCCGTAA

Pavag01G329400 codon optimized

ATGATGGAAGAAGGTGCTCAGCAGCAGGATATGCTGCAGGCCTATATTGAACATTTGGCATCAGAGCCTGAGCTATGTTAAAGTCTGACCCCTGGC
AGTTGCACTGGATCTGCGTATTCCGGATGCAATTCATCATCATGGTGGTGGTGGTGAACCCCTGCCCTCAGATTCTGGCAAAAAGCAGGTCTGCATCCGT
GTAAACTGCTGCACTGCGTCTGCTGATGCGTGTCTGACCCGAGTTACCGGCACCTTTACCACCGTTTACGACCCAGCAGCAGCCGGATGATGAA
AGCGACGATGAAGCAGTGTATAAATGACAGCAGTTAGCCGTTTTCTGGTGAGTGATGATGACGATGCAGGTAGCAGCGCAAGCGCAACCCACACT
GGCACCCTTTGTTACAGTTACGCTGCATCTGATTAAATGTTAGCCCGTATGCAAAAAGGTCTGTGTGCATGGTTTCTGCAAGAACAGAAATCATCCGA
GCACCGATTGTCTGGCCCTGCGTCTGATGAAACCGTTTGGGAACCTCCGGATCATTTTAATGCAATGCTGAATAAAGGATGGAAAGCGATAGT
CGTTTTCTGATGCTGTTGCACTGAGCCTGGAAGAATTTGTTGGTGTGTTTTTACGGGTATTGATAGCCTGGTTGATGTTGGTGGTGGTTTTGGTGG
TGCCGAGCAGCAATTCAGCAGCATTTCGCCATCTGAAATGTAGCGTTCTGGACCTGCCGCATGTTGTTGCCGGTGCACCGAGCGATACCAATG
TGCAGTTTATTGCCGGTGATATGTTTAAAGCATTCCGCCCTGCAACCCGAGTTTTTCTGAAAAAACCCTGCATGATTTGGGCGAGATGATGAGTGT
GTGAAAATTTCTGAAAAGTGCAAAACAGGCAATTCCGCCCTGCTGATGCAGGCGGTAAAGTTATTATTGTTGATATGGTGGTTGGTTATGGCCGACC
GAATCGTAAAGTTCTGAAAACCCAGGTTATGTTTCGATATCTTTATCATGATGGTGAATGGTGGCGAACGTGATGAACAAGAAATGGAAGAAAATCT
TTACCAAGGCAGGCTTCAAAGACTATAAAATCCTGCCGTTTCTGGGTGTCATAGCATTATTGAAGTTTATCCGTAA

Figure S7. Codon-optimized gene sequences of Poaceae OMTs synthesized for expression in *E. coli*.

Table S1. Enzymatic activity of Poaceae OMTs in the *FOMT2*-like group with different substrates. Data belong to the experiment shown in Figure 2 and Figure S2 (panel B and C). The purified recombinant enzymes as well as an empty vector control (EV) were incubated with the potential substrates listed in presence of the cosubstrate SAM. Reaction products were analyzed by LC-MS/MS. Product formation is given as mean area \pm SE ($n = 3$). Numbers in grey are considered as trace activities, because they represent product formation rates less than 1% relative to the most active enzyme, which is either ZnBX12 or ZnFOMT2. Abbreviations: Me, methyl; nd, not detected.

Substrate	Analyte	EV	ShFOMT2	SbFOMT2	ZnFOMT2	ZmBX14	ZmBX12	ZnGBZQ	ZnBX10	Pvag9400	Pv2300-like	
DIMBOA-Glc	HDMBOA-Glc	nd	nd	nd	nd	2.3E+04	1.8E+05	nd	4.1E+04	nd	nd	
		-	-	-	-	± 7.6E+02	± 8.7E+03	-	± 2.2E+03	-	-	
Naringenin	5-O-Me-Naringenin	nd	1.9E+06	1.1E+07	6.5E+07	5.5E+03	3.9E+04	8.3E+03	4.3E+03	3.4E+04	nd	
		-	± 5.6E+04	± 2.1E+05	± 1.0E+06	1.0E+03	± 2.7E+02	4.6E+02	4.6E+02	± 2.8E+03	-	
2-OH-Naringenin	O-Me-2-OH-Naringenin_P1	nd	7.9E+05	8.6E+06	1.1E+07	nd	nd	nd	nd	3.1E+03	-	
		-	± 1.5E+04	± 1.8E+05	± 2.8E+05	-	-	-	-	± 4.4E+02	-	
	O-Me-2-OH-Naringenin_P2	nd	3.9E+04	5.1E+05	6.5E+05	nd	nd	nd	nd	nd	-	
		-	± 1.2E+03	± 3.4E+04	± 3.6E+03	-	-	-	-	-	-	
	Xilonenin (keto)	nd	nd	4.3E+05	1.7E+06	nd	nd	nd	nd	nd	-	
		-	-	± 2.7E+04	± 1.1E+05	-	-	-	-	-	-	
	Xilonenin (enol)	nd	nd	1.1E+06	4.6E+06	nd	nd	nd	nd	nd	-	
		-	-	± 2.8E+04	± 1.3E+05	-	-	-	-	-	-	
	Apigenin	5-O-Me-Apigenin	nd	1.1E+06	4.2E+06	5.2E+07	nd	1.5E+05	nd	nd	1.5E+05	-
			-	± 1.5E+04	± 3.3E+05	± 3.8E+05	-	± 1.3E+02	-	-	± 2.6E+03	-
Scutellarein	5-O-Me-Scutellarein	nd	4.8E+05	3.2E+06	1.9E+07	1.3E+04	1.8E+04	nd	nd	8.7E+03	nd	
		-	± 8.3E+03	± 2.8E+04	± 6.2E+04	± 3.3E+03	± 2.0E+02	-	-	± 9.8E+02	-	
Dihydrokaempferol	5-O-Me-Dihydrokaempferol	nd	2.6E+04	3.2E+05	2.7E+06	nd	nd	nd	nd	nd	-	
		-	± 7.5E+02	± 8.5E+02	± 7.4E+04	-	-	-	-	-	-	
Kaempferol	5-O-Me-Kaempferol	nd	7.2E+05	4.1E+06	4.3E+07	6.0E+04	2.0E+04	nd	nd	2.1E+04	nd	
		-	± 3.8E+04	± 7.6E+04	± 5.9E+05	± 2.0E+04	± 3.0E+02	-	-	± 3.3E+03	-	
Quercetin	Isokaempferide	nd	nd	9.8E+04	1.7E+04	nd	5.8E+06	nd	3.9E+05	nd	nd	
		-	-	± 2.3E+03	± 2.5E+03	-	± 6.6E+04	-	± 1.1E+04	-	-	
Quercetin	5-O-Me-Quercetin	nd	3.9E+05	1.1E+05	3.6E+07	4.6E+04	nd	nd	nd	6.9E+03	-	
		-	± 2.3E+04	± 5.3E+03	± 9.2E+05	± 2.0E+04	-	-	-	± 7.1E+02	-	

Table S2. Resulting binding modes for docking of naringenin into the homology model of ZmFOMT2 using AutoDock Vina (<http://vina.scripps.edu/>; Trott and Olson, 2010) with the grid box (size x/y/z = 26 Å) centered on His271 (C-2) base of the catalytic triad and with the exhaustiveness set to 8. The binding mode displayed in Figures 3A and 3B is highlighted in grey.

Mode #	Binding affinity (kcal/mol)	Distance from best mode (RMSD lower bound)	Distance from best mode (RMSD upper bound)
1	-7.0	0.000	0.000
2	-6.5	6.297	9.188
3	-6.5	3.298	8.730
4	-6.5	1.240	2.743
5	-6.4	2.578	8.358
6	-6.3	3.695	6.598
7	-6.3	6.088	9.199
8	-6.2	2.337	3.544
9	-6.2	3.132	5.571

Table S3. PCR primers for the amplification of full-length ORFs of investigated OMTs and for site-directed mutagenesis.

Primer name	Target gene (GenBank accession)	Primer Sequence (5' → 3')	Restriction recognition site / mutation	Application
Sb-001G354400-F	Sb001G354400	CACCATGGCACCCGCGGAGGAGAG		TOPO cloning
Sb-001G354400-R		TCATGGATAGACCTCGATGAC		
Pv-9NG562300-IBA-F	Pv9NG562300	ATGTGAGGTCGACGGCATCGGCTATCATCGCTCCCTG	BsaI	pASK-IBA37plus cloning
Pv-9NG562300-IBA-R		ATGTGAGGTCATATCAAGGGTAGAGTCGATGATTGACAT		
Font2-Mut8+9-F2	ZnfFOMT2 (MZ484743)	CGACCTCTTGACCAATTCCTCTGTCTACGCCAAATCGCTC	W16L + Q18H	site-directed mutagenesis
Font2-Mut8+9-R2		CACAGGGAATGGTCAAGAGGTCGACGTGAGCTTCGAGC		
Font2-W22-Mut3-F		GGTAATACTTGGACGTGGTAGTTGGATATGG	M303V	
Font2-W22-Mut3-R		CCATATCCAACTACCAACGTCCTCAAGATTATTACC		
Font2-W22-Mut1+2-F2		GTTATGTTTGATTTGTATATGATGGCGGTTAATGGAGCTGAGCGC	I325M + T327A	
Font2-W22-Mut1+2-R2		CGGCTCAGCTCCATTAAACGCCCATATACAAATCAACATAAC		
Font2-W22-Mut4+5-F2		CAAAATCCTACCAATCCTTTGGTACGTATCAGTCATCGAGGTCTATCC	A358D + L359V	
Font2-W22-Mut4+5-R2		GGATAGACCTCGATGACTGATACGTACCAAGGATTGGTAGGATTTTG		
Font2-W22-Mut1+2+6-F		GTATATGATGGCGGTTAATGGAGTTGAGCGCGACGACGACGAGGTGG	I325M + T327A + A331V	
Font2-W22-Mut1+2+6-R		CCACTCTTGCTCGCGGCTCAACTCCATTAAACGCCCATCATAC		
Font2-W22-Mut4+5+7-F		GACTACAAAATCCTACCAATCATTTGGTGACGTATCAGTCATCG	A358D + L359V + L356I	
Font2-W22-Mut4+5+7-R		CGATGACTGATAGCTACCAATGATTGGTAGGATTTTGTAGTC		

Table S4. MS settings used for the analysis on the QTRAP 6500+.

Turbospray ESI ion source settings		
Analytes	flavonoids	benzoxazinoids
Ionization mode:	positive	negative
Ion spray voltage:	+5500 V	-4500 V
Turbo gas temperature:	650°C	650°C
Curtain gas:	40 psi	40 psi
Collision gas:	medium level	medium level
Nebulizer gas:	60 psi	70 psi
Heating gas:	60 psi	70 psi

Table S5. Mass analyzer settings used for the analysis of BXs and flavonoids on the QTRAP 6500+. Retention time (RT) was used to distinguish between compounds with the same MRM transition. Compounds marked with (*) were verified by an authentic standard, while the remaining O-methylflavonoids were inferred from the specific ZmFOMT2 enzymatic activity as described previously in Förster et al. (2021). Abbreviations: Me, methyl; DP, declustering potential; EP, entrance potential; CE, collision energy; CXP, collision cell exit potential; V, volts.

Compound	RT (min)	MRM transition <i>m/z</i>	DP (V)	EP (V)	CE (V)	CXP (V)
Benzoxazinoids (negative mode)						
DIMBOA-Glc*	4.35	372 [M-H] ⁻ → 210	-40	-4	-15	-4
HDMBOA-Glc*	5.16	432 [M+FA-H] ⁻ → 356	-40	-4	-20	-3
Flavonoids (positive mode)						
Apigenin*	6.59	271 [M+H] ⁺ → 153	50	3.5	41	4
Naringenin*	6.64	273 [M+H] ⁺ → 153	41	4.5	31	4
5-O-Me-Apigenin*	4.94	285 [M+H] ⁺ → 270	50	6	31	8
5-O-Me-Naringenin*	4.98	287 [M+H] ⁺ → 167	36	5	31	6
Scutellarein*	5.32	287 [M+H] ⁺ → 123	50	3.5	47	4
Kaempferol*	6.80	287 [M+H] ⁺ → 153	50	2	39	4
Dihydrokaempferol*	5.11	289 [M+H] ⁺ → 243	50	4	15	6
2-Hydroxynaringenin*	5.52	289 [M+H] ⁺ → 121	21	5	21	14
5-O-Me-Scutellarein*	4.67	301 [M+H] ⁺ → 286	50	3	33	6
5-O-Me-Kaempferol	5.50	301 [M+H] ⁺ → 286	50	2	35	6
3-O-Me-Kaempferol (Isokaempferide)*	7.03	301 [M+H] ⁺ → 286	50	4	27	8
5-O-Me-Dihydrokaempferol	4.40	303 [M+H] ⁺ → 107	50	4	55	2
Quercetin*	5.93	303 [M+H] ⁺ → 153	50	7	45	4
O-Me-2-Hydroxynaringenin (peak 1)	6.41	303 [M+H] ⁺ → 167	21	5	21	20
O-Me-2-Hydroxynaringenin (peak 2)	8.29	303 [M+H] ⁺ → 167	21	5	21	20
5-O-Me-Quercetin	4.78	317 [M+H] ⁺ → 302	50	7	35	6
O-DiMe-2-Hydroxynaringenin (Xilonenin; peak 1)*	5.48	317 [M+H] ⁺ → 181	1	5	21	20
O-DiMe-2-Hydroxynaringenin (Xilonenin; peak 2)*	6.78	317 [M+H] ⁺ → 181	1	5	21	20

Table S6. Phytozome 13 (<https://phytozome-next.jgi.doe.gov/>) data sets used and corresponding references for the phylogenetic analysis shown in Figure 1 and Figure S1.

Plant species	Data set version	Reference
<i>Brachipodium distachyon</i>	3.1	https://phytozome-next.jgi.doe.gov/info/Bdistachyon_v3_1
<i>Brachipodium stacei</i>	1.1	Gordon et al., 2020
<i>Eleusine coracana</i>	1.1	https://phytozome-next.jgi.doe.gov/info/Ecoracana_v1_1
<i>Hordeum vulgare</i>	v1	Beier et al., 2017
<i>Miscanthus sinensis</i>	7.1	Mitros et al., 2020
<i>Oropetium thomaeum</i>	1.0	VanBuren et al., 2015
<i>Oryza sativa</i>	7.0	Ouyang et al., 2007
<i>Panicum hallii</i>	3.2	Lovell et al., 2018
<i>Panicum hallii HAL</i>	2.2	Lovell et al., 2018
<i>Panicum virgatum</i>	5.1	Lovell et al., 2021
<i>Paspalum vaginatum</i>	3.1	DOE-JGI, https://phytozome-next.jgi.doe.gov/info/Pvaginatum_v3_1
<i>Setaria italica</i>	2.2	Bennetzen et al., 2012
<i>Setaria viridis</i>	2.1	Mamidi et al., 2020
<i>Sorghum bicolor</i>	3.1.1	McCormick et al., 2018
<i>Sorghum bicolor Rio</i>	2.1	Cooper et al., 2019
<i>Triticum aestivum</i>	2.2	International Wheat Genome Sequencing Consortium (IWGSC), 2014
<i>Urochloa fusca</i>	1.1	DOE-JGI, https://phytozome-next.jgi.doe.gov/info/Ufusca_v1_1
<i>Zea mays</i>	B73_v4	Jiao et al., 2017

- Beier, S., Himmelbach, A., Colmsee, C., Zhang, X.Q., Barrero, R.A., Zhang, Q., Li, L., Bayer, M., Bolser, D., Taudien, S., Groth, M., Felder, M., Hastie, A., Simkova, H., Stankova, H., Vrana, J., Chan, S., Munoz-Amatriain, M., Ounit, R., Wanamaker, S., Schmutz, T., Aliyeva-Schnorr, L., Grasso, S., Tanskanen, J., Sampath, D., Heavens, D., Cao, S., Chapman, B., Dai, F., Han, Y., Li, H., Li, X., Lin, C., McCooke, J.K., Tan, C., Wang, S., Yin, S., Zhou, G., Poland, J.A., Bellgard, M.I., Houben, A., Dolezel, J., Ayling, S., Lonardi, S., Langridge, P., Muehlbauer, G.J., Kersey, P., Clark, M.D., Caccamo, M., Schulman, A.H., Platzer, M., Close, T.J., Hansson, M., Zhang, G., Braumann, I., Li, C., Waugh, R., Scholz, U., Stein, N., and Mascher, M. (2017). Construction of a map-based reference genome sequence for barley, *Hordeum vulgare* L. *Sci Data* **4**, 170044.
- Bennetzen, J.L., Schmutz, J., Wang, H., Percifield, R., Hawkins, J., Pontaroli, A.C., Estep, M., Feng, L., Vaughn, J.N., Grimwood, J., Jenkins, J., Barry, K., Lindquist, E., Hellsten, U., Deshpande, S., Wang, X., Wu, X., Mitros, T., Triplett, J., Yang, X., Ye, C.Y., Mauro-Herrera, M., Wang, L., Li, P., Sharma, M., Sharma, R., Ronald, P.C., Panaud, O., Kellogg, E.A., Brutnell, T.P., Doust, A.N., Tuskan, G.A., Rokhsar, D., and Devos, K.M. (2012). Reference genome sequence of the model plant *Setaria*. *Nat Biotechnol* **30**, 555-561.
- Cooper, E.A., Brenton, Z.W., Flinn, B.S., Jenkins, J., Shu, S., Flowers, D., Luo, F., Wang, Y., Xia, P., Barry, K., Daum, C., Lipzen, A., Yoshinaga, Y., Schmutz, J., Saski, C., Vermerris, W., and Kresovich, S. (2019). A new reference genome for *Sorghum bicolor* reveals high levels of sequence similarity between sweet and grain genotypes: implications for the genetics of sugar metabolism. *Bmc Genomics* **20**, 420.
- Gordon, S.P., Contreras-Moreira, B., Levy, J.J., Djamei, A., Czedik-Eysenberg, A., Tartaglio, V.S., Session, A., Martin, J., Cartwright, A., Katz, A., Singan, V.R., Goltsman, E., Barry, K., Dinh-Thi, V.H., Chalhou, B., Diaz-Perez, A., Sancho, R., Lusinska, J., Wolny, E., Nibau, C., Doonan, J.H., Mur, L.A.J., Plott, C., Jenkins, J., Hazen, S.P., Lee, S.J., Shu, S., Goodstein, D., Rokhsar, D., Schmutz, J., Hasterok, R., Catalan, P., and Vogel, J.P. (2020). Gradual polyploid genome evolution revealed by pan-genomic analysis of *Brachypodium hybridum* and its diploid progenitors. *Nat Commun* **11**, 3670.
- IWGSC. (2014). A chromosome-based draft sequence of the hexaploid bread wheat (*Triticum aestivum*) genome. *Science* **345**, 1251788.
- Jiao, Y., Peluso, P., Shi, J., Liang, T., Stitzer, M.C., Wang, B., Campbell, M.S., Stein, J.C., Wei, X., Chin, C.S., Guill, K., Regulski, M., Kumari, S., Olson, A., Gent, J., Schneider, K.L., Wolfgruber, T.K., May, M.R., Springer, N.M., Antoniou, E., McCombie, W.R., Presting, G.G., McMullen, M., Ross-Ibarra, J., Dawe, R.K., Hastie, A., Rank, D.R., and Ware, D. (2017). Improved maize reference genome with single-molecule technologies. *Nature* **546**, 524-527.
- Lovell, J.T., Jenkins, J., Lowry, D.B., Mamidi, S., Sreedasyam, A., Weng, X., Barry, K., Bonnette, J., Campitelli, B., Daum, C., Gordon, S.P., Gould, B.A., Khasanova, A., Lipzen, A., MacQueen, A., Palacio-Mejia, J.D., Plott, C., Shakirov, E.V., Shu, S., Yoshinaga, Y., Zane, M., Kudrna, D., Talag, J.D., Rokhsar, D., Grimwood, J., Schmutz, J., and Juenger, T.E. (2018). The genomic landscape of molecular responses to natural drought stress in *Panicum hallii*. *Nat Commun* **9**, 5213.
- Lovell, J.T., MacQueen, A.H., Mamidi, S., Bonnette, J., Jenkins, J., Napier, J.D., Sreedasyam, A., Healey, A., Session, A., Shu, S., Barry, K., Bonos, S., Boston, L., Daum, C., Deshpande, S., Ewing, A., Grabowski, P.P., Haque, T., Harrison, M., Jiang, J., Kudrna, D., Lipzen, A., Pendergast, T.H.t., Plott, C., Qi, P., Saski, C.A., Shakirov, E.V., Sims, D., Sharma, M., Sharma, R., Stewart, A., Singan, V.R., Tang, Y., Thibivillier, S., Webber, J., Weng, X., Williams, M., Wu, G.A., Yoshinaga, Y., Zane, M., Zhang, L., Zhang, J., Behrman, K.D., Boe, A.R., Fay, P.A., Fritsch, F.B., Jastrow, J.D., Lloyd-Reilly, J., Martinez-Reyna, J.M., Matamala, R., Mitchell, R.B., Rouquette, F.M., Jr., Ronald, P., Saha, M., Tobias, C.M., Udvardi, M., Wing, R.A., Wu, Y., Bartley, L.E., Casler, M., Devos, K.M., Lowry, D.B., Rokhsar, D.S., Grimwood, J., Juenger, T.E., and Schmutz, J. (2021). Genomic mechanisms of climate adaptation in polyploid bioenergy switchgrass. *Nature* **590**, 438-444.

- Mamidi, S., Healey, A., Huang, P., Grimwood, J., Jenkins, J., Barry, K., Sreedasyam, A., Shu, S., Lovell, J.T., Feldman, M., Wu, J., Yu, Y., Chen, C., Johnson, J., Sakakibara, H., Kiba, T., Sakurai, T., Tavares, R., Nusinow, D.A., Baxter, I., Schmutz, J., Brutnell, T.P., and Kellogg, E.A. (2020). A genome resource for green millet *Setaria viridis* enables discovery of agronomically valuable loci. *Nat Biotechnol* **38**, 1203-1210.
- McCormick, R.F., Truong, S.K., Sreedasyam, A., Jenkins, J., Shu, S., Sims, D., Kennedy, M., Amirebrahimi, M., Weers, B.D., McKinley, B., Mattison, A., Morishige, D.T., Grimwood, J., Schmutz, J., and Mullet, J.E. (2018). The *Sorghum bicolor* reference genome: improved assembly, gene annotations, a transcriptome atlas, and signatures of genome organization. *Plant J* **93**, 338-354.
- Mitros, T., Session, A.M., James, B.T., Wu, G.A., Belaffif, M.B., Clark, L.V., Shu, S., Dong, H., Barling, A., Holmes, J.R., Mattick, J.E., Bredeson, J.V., Liu, S., Farrar, K., Glowacka, K., Jezowski, S., Barry, K., Chae, W.B., Juvik, J.A., Gifford, J., Oladeinde, A., Yamada, T., Grimwood, J., Putnam, N.H., De Vega, J., Barth, S., Klaas, M., Hodgkinson, T., Li, L., Jin, X., Peng, J., Yu, C.Y., Heo, K., Yoo, J.H., Ghimire, B.K., Donnison, I.S., Schmutz, J., Hudson, M.E., Sacks, E.J., Moose, S.P., Swaminathan, K., and Rokhsar, D.S. (2020). Genome biology of the paleotetraploid perennial biomass crop *Miscanthus*. *Nat Commun* **11**, 5442.
- Ouyang, S., Zhu, W., Hamilton, J., Lin, H., Campbell, M., Childs, K., Thibaud-Nissen, F., Malek, R.L., Lee, Y., Zheng, L., Orvis, J., Haas, B., Wortman, J., and Buell, C.R. (2007). The TIGR Rice Genome Annotation Resource: improvements and new features. *Nucleic Acids Res* **35**, D883-887.
- VanBuren, R., Bryant, D., Edger, P.P., Tang, H., Burgess, D., Challabathula, D., Spittle, K., Hall, R., Gu, J., Lyons, E., Freeling, M., Bartels, D., Ten Hallers, B., Hastie, A., Michael, T.P., and Mockler, T.C. (2015). Single-molecule sequencing of the desiccation-tolerant grass *Oropetium thomaeum*. *Nature* **527**, 508-511.

11.4 Detailed author contributions to Manuscript I

Convergent evolution of a metabolic switch between aphid and caterpillar resistance in cereals

Beibei Li, Christiane Förster, Christelle A. M. Robert, Tobias Züst, Lingfei Hu, Ricardo A. R. Machado, Jean-Daniel Berset, Vinzenz Handrick, Torsten Knauer, Götz Hensel, Wanxin Chen, Jochen Kumlehn, Ping Yang, Beat Keller, Jonathan Gershenzon, Georg Jander, Tobias G. Köllner, and Matthias Erb

Published in Science Advances (2018), 4, doi:10.1126/sciadv.aat6797

Author contributions:

Based on ideas of JG, GJ, TGK, ME

Designed experiments: BL, **CF (5%)**, CAMR, TZ, LH, RARM, J-DB, VH, TK, GH, WC, JK, PY, BK, GJ, TGK, and ME

Performed experiments: BL, **CF (25%)**, CAMR, TZ, LH, RARM, J-DB, VH, TK, GH, WC, JK, PY, BK, and TGK

Analyzed data: BL, **CF (25%)**, CAMR, TZ, LH, RARM, J-DB, GH, WC, JK, PY, BK, TGK, and ME

Wrote the manuscript: TGK and ME, with contributions from all other authors

The study was conceptualized based on the ideas of JG, GJ, TGK, and ME. CF performed the LC-MS/MS measurements of BX and amino acids in phloem sap and analyzed the data (Figure 1C; Figure S1E). The identification and characterization of DIMBOA-Glc *OMT* candidate genes was also performed by CF, and included screening of transcriptomic data, sequence analyses, phylogenetic tree constructions, qRT-PCRs, cloning, heterologous expression, and *in vitro* enzyme assays (Figure 5; Figures S7B, C; Figures S8, S9, S11, and S13). Transcriptome assembly and analysis (genome-based and *de novo*) and phylogenetic analysis of glucosinolate *OMT* genes were performed by TGK (Table S1; Figures S10 and S14). TK conducted the collection of phloem sap. The vector construct for generating *ZmBX12*-expressing transgenic wheat was prepared by VH and used by GH, WC, and JK to generate transgenic wheat plants. All other experiments were designed, performed and analyzed by BL, with contributions from CAMR, TZ, LH, RARM, J-DB, PY,

BK, and ME (Figures 1A, B, D-F; Figures 2, 3, and 4; Figures S1A-D; Figures S2, S3, S4, S5, S6, S7A, and S12).

11.5 Detailed author contributions to Manuscript II

Biosynthesis and antifungal activity of fungus-induced O-methylated flavonoids in maize

Christiane Förster, Vinzenz Handrick, Yezhang Ding, Yoko Nakamura, Christian Paetz, Bernd Schneider, Gabriel Castro-Falcón, Chambers C. Hughes, Katrin Luck, Sowmya Poosapati, Grit Kunert, Alisa Huffaker, Jonathan Gershenzon, Eric A. Schmelz, and Tobias. G. Köllner

Published in Plant Physiology (2021), doi:10.1093/plphys/kiab496

Author contributions:

Based on ideas of **CF (20%)**, VH, JG, EAS, TGK

Designed experiments: **CF (60%)**, VH, YD, YN, KL, SP, AH, EAS, TGK

Performed experiments: **CF (70%)**, VH, YD, YN, KL, SP

Performed NMR analyses and structure elucidation: YN, CP, BS, GCF, CCH

Analyzed data: **CF (75%)**, VH, YD, KL, SP, GK, AH, EAS, TGK

Visualized data: **CF (90%)**, YD, CP

Wrote the manuscript: **CF (70%)**, JG, EAS, TGK, with contributions from all other authors

The project was built on fundamental findings of VH and EAS. The study was conceptualized based on the ideas of CF, VH, JG, EAS, and TGK. CF planned and performed the following experiments; analyzed and visualized the corresponding data: in particular inoculations of maize plants (leaves) with fungi and chitosan, untargeted LC-MS and LC-UV-MS measurements, targeted LC-MS/MS measurements of flavonoids and BX, cloning and heterologous expression of *OMT* genes in *E. coli*, *in vitro* enzyme assays with OMTs and CYP93Gs, sequence analyses, and phylogenetic tree constructions (Figure 1; Figures 2D, E; Figure 3; Figures 4B, D, E; Figure 5; Figure 6B; Figures S1, S4, S5, S6, S8, S9, S11, S12, S14, S15, S16, S17, and S18; Tables S1, S3, S5, S6, S7, S8, S10, S11, and several tables with details about the methods). TGK in particular, but also JG and CP contributed with helpful discussions. The LC-MS/MS method for the analysis of flavonoids was further developed based on a method originally developed by VH. KL performed the cloning and heterologous expression of CYP93G genes in yeast. GK contributed statistical analyses of flavonoid amounts in maize leaves (Figure 5; Figure S15; Table S9) and gave

general advice on statistics. The purification of O-methylated flavonoids was largely performed by CF, with a contribution from YN (Table S17). 2-Hydroxynaringenin was synthesized and purified by YN. NMR analyses and structural elucidations were conducted by YN, CP, BS, GCF, and CCH (Figure S13; Table S4; Supplemental data set S2). Association mappings were performed by YD (Figures 2A, B; Figure 4A; Figures S2, S3, and S10). Transcriptome assembly was performed by TGK (Supplemental data set S1). CF screened the transcriptomic data for candidate genes and visualized the data (Figures 2C, 4C, 6A; Figures S7, S18; Table S2). Fungal bioassays were designed, performed, and analyzed by YD and SP, with contributions from AH and EAS (Figure 7; Figures S20 and S21). RT-qPCR validation of transcriptomic data was performed and analyzed by KL (Figure S19). The corresponding statistical analysis and visualization was conducted by CF. The draft of the manuscript was written by CF, with contributions from YD, CP, GK, and EAS. TGK, EAS and JG revised the manuscript; all other authors contributed, and the draft was written in the final form by CF and TGK.

11.6 Detailed author contributions to Manuscript III

Evolution of DIMBOA-Glc O-methyltransferases from flavonoid O-methyltransferases in the grasses

Christiane Förster, Jonathan Gershenzon, and Tobias G. Köllner

Submitted for publication to Molecules (MDPI)

Author contributions:

Based on ideas of **CF (50%)**, JG, and TGK

Designed experiments: **CF (90%)**

Performed experiments: **CF (100%)**

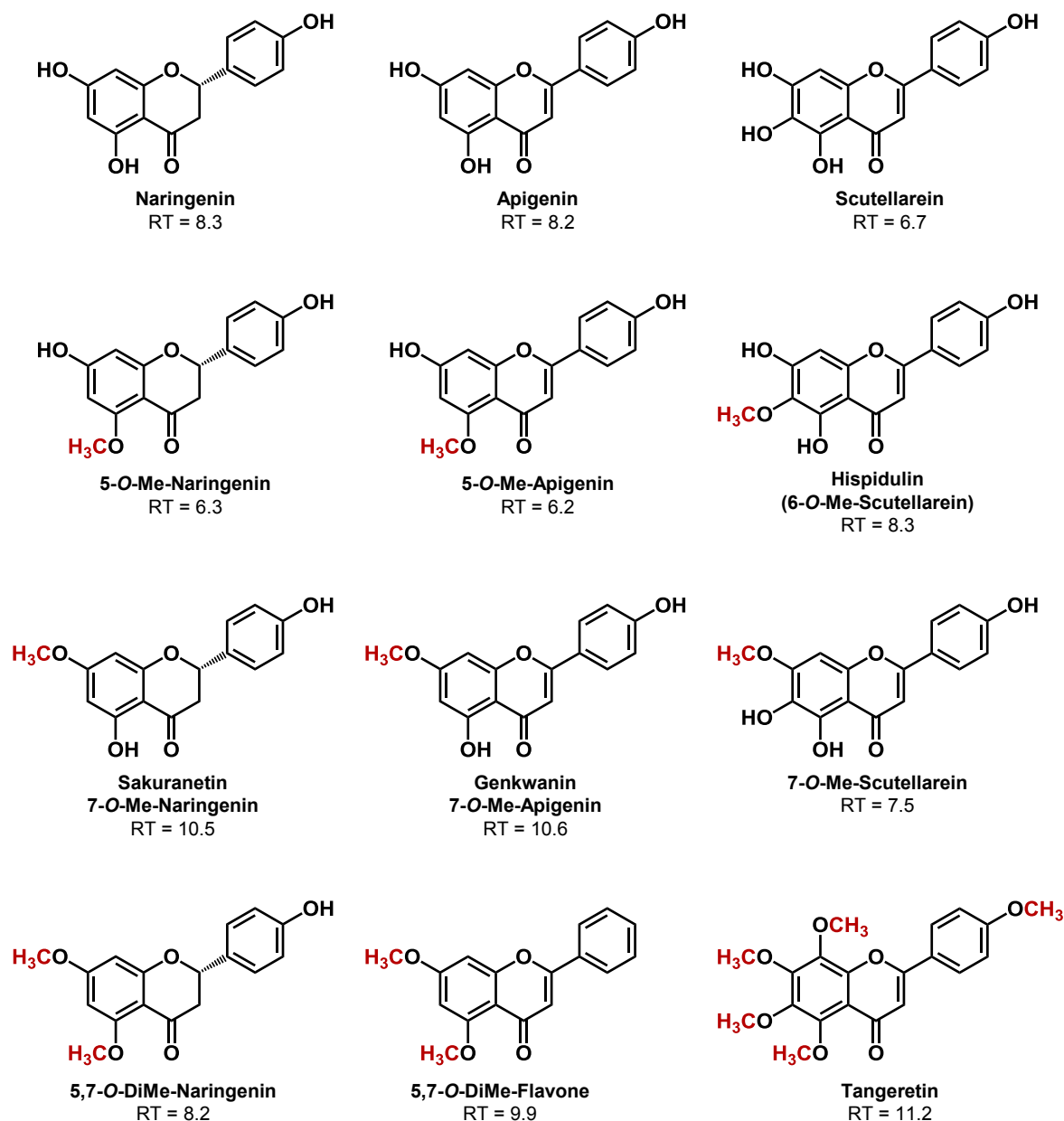
Analyzed data: **CF (100%)**

Visualized data: **CF (100%)**

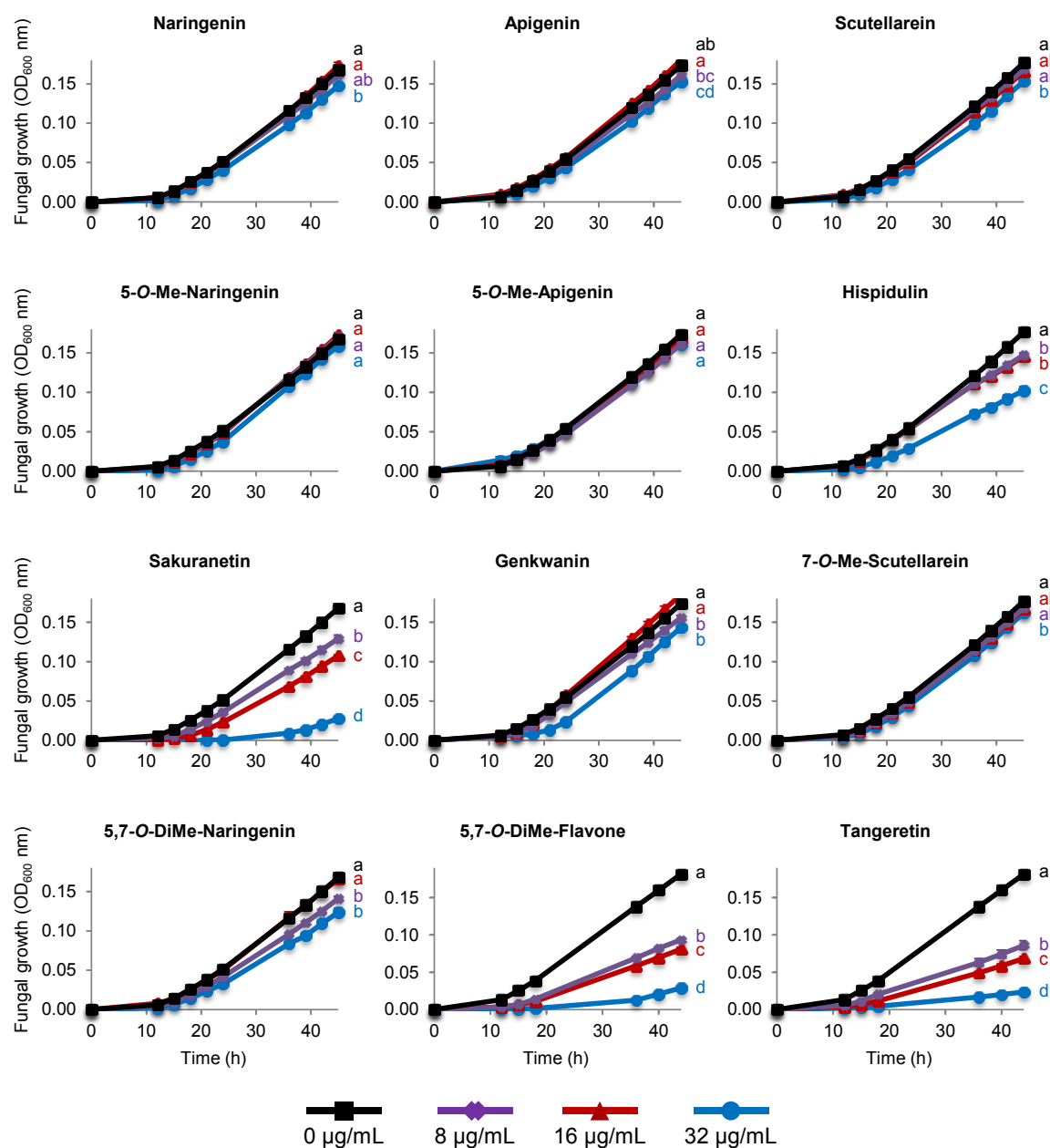
Wrote the manuscript: **CF (75%)**, JG, and TGK

The study was conceptualized based on the ideas of CF, JG and TGK. The experiments were designed by CF, with contributions from TGK. CF performed all experiments and analyzed and visualized the data (Figure 1-4, Figure S1-S6, and Table S1-S2). The draft of the manuscript was written by CF. TGK and JG revised the manuscript and the draft was written in the final form by CF.

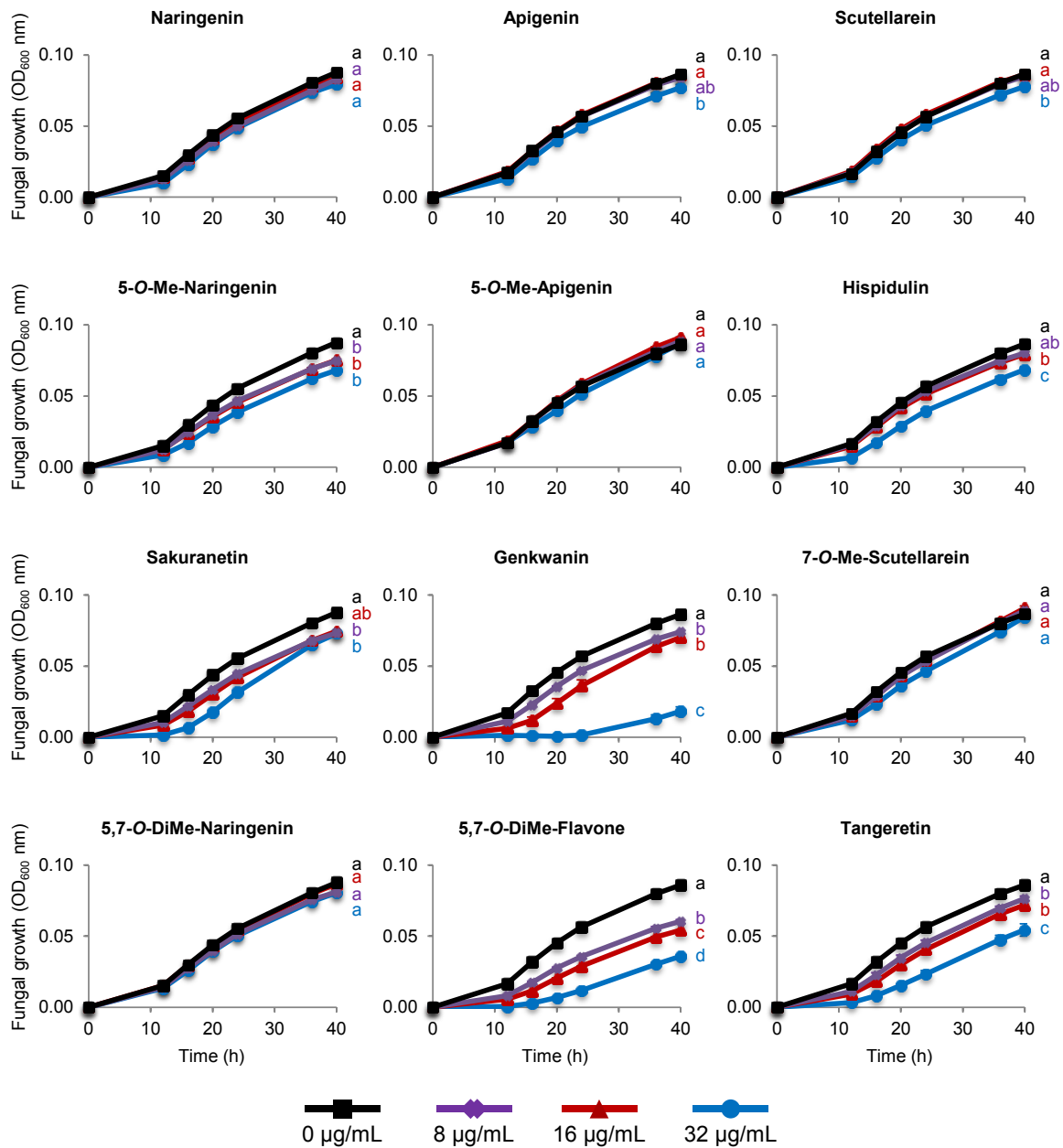
11.7 Supplemental Figures and Tables



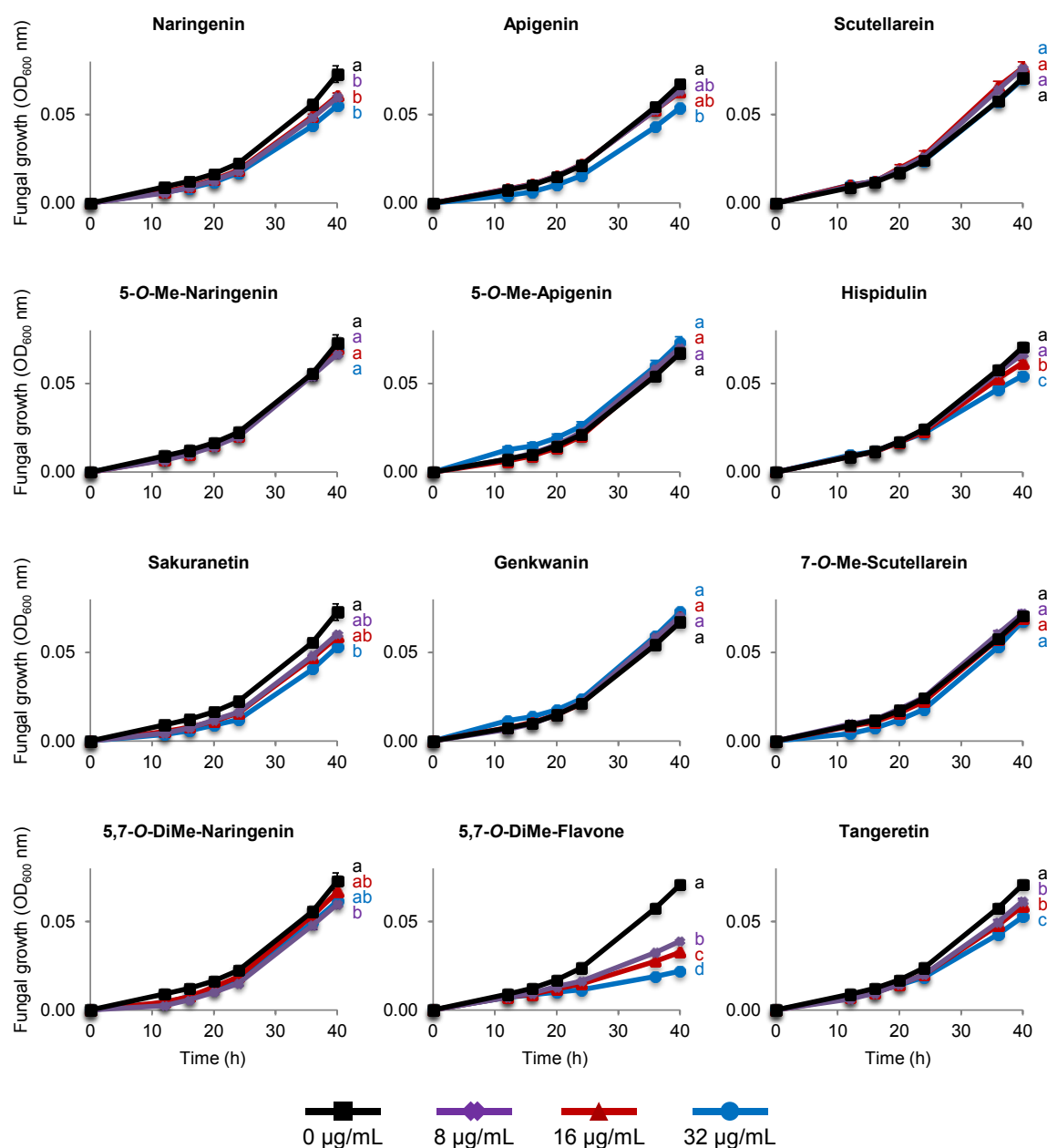
Supplemental Figure 1. Chemical structures of the O-methyl- and non-O-methylflavonoids used in the fungal bioassays shown in Supplemental Figures 2-5. Methyl groups are highlighted in red. The retention times (RTs) in minutes on the used C18 RP-LC column are given. Abbreviations: Me, methyl; DiMe, dimethyl.



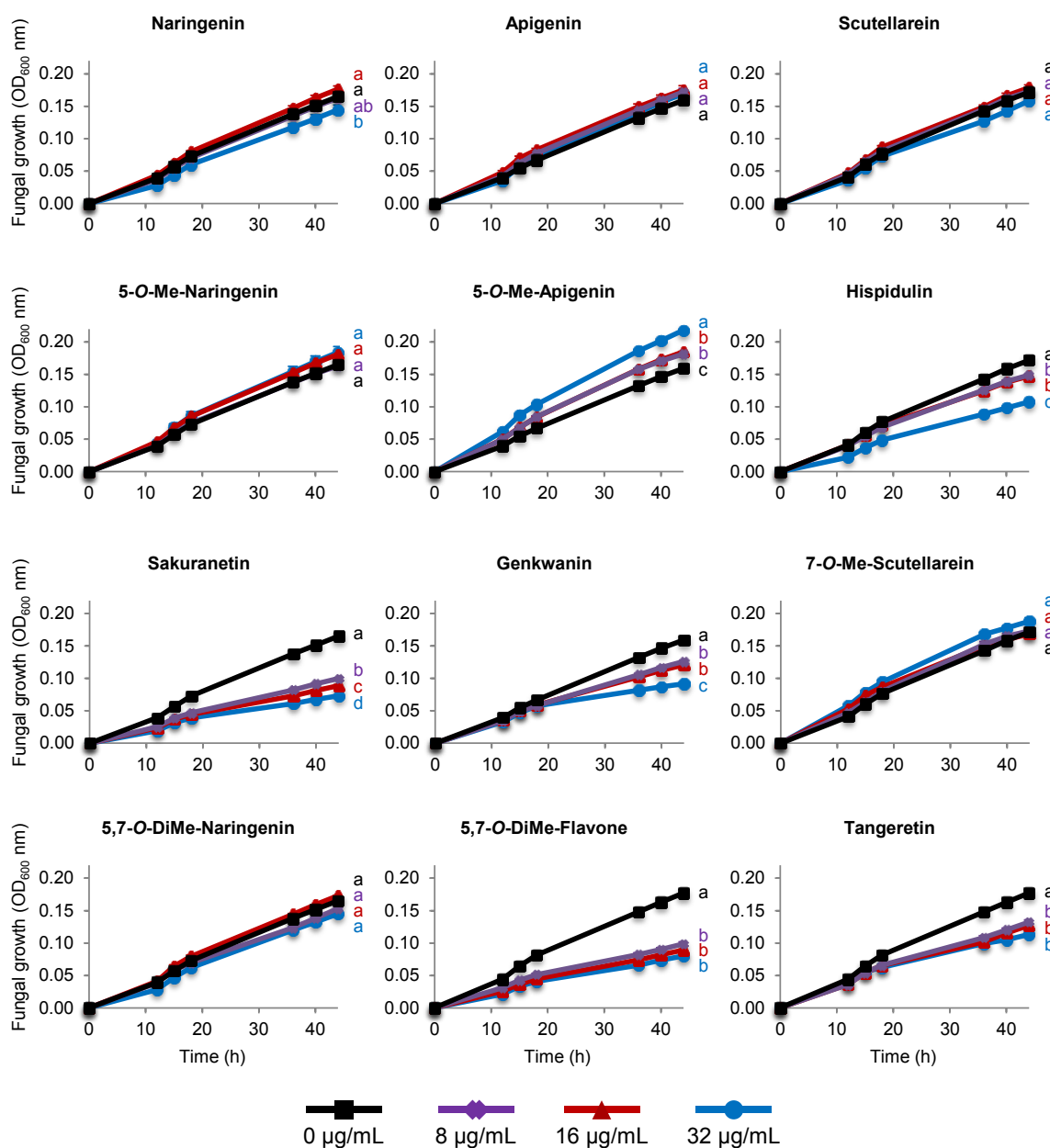
Supplemental Figure 2. Antifungal activity of O-methyl- and non-O-methylflavonoids against *Colletotrichum graminicola*. Growth (optical density at 600 nm) of *C. graminicola* in the absence and presence of self-purified or commercially available flavonoids measured over a 45-h time course in potato dextrose broth using a microtiter plate assay. Data are shown as means \pm SE ($n = 3$). Different letters indicate significant differences ($P < 0.05$) between treatments at 45 h (one-way ANOVA followed by Tukey's post-hoc test or one-way ANOVA on Ranks followed by Dunn's post-hoc test). naringenin ($F = 8.669$, $P = 0.003$); 5-O-Me-naringenin ($F = 2.717$, $P = 0.096$); sakuranetin ($F = 389.079$, $P < 0.001$); 5,7-O-DiMe-naringenin ($F = 27.860$, $P < 0.001$); apigenin ($F = 12.699$, $P < 0.001$); 5-O-Me-apigenin ($F = 3.187$, $P = 0.067$); genkwanin ($F = 21.537$, $P < 0.001$); 5,7-O-DiMe-flavone ($F = 806.943$, $P < 0.001$); scutellarein ($H = 8.158$, $P = 0.043$); hispidulin ($F = 89.479$, $P < 0.001$); 7-O-Me-scutellarein ($F = 5.107$, $P = 0.019$); tangeretin ($F = 480.234$, $P < 0.001$). Abbreviations: Me, methyl; DiMe, dimethyl.



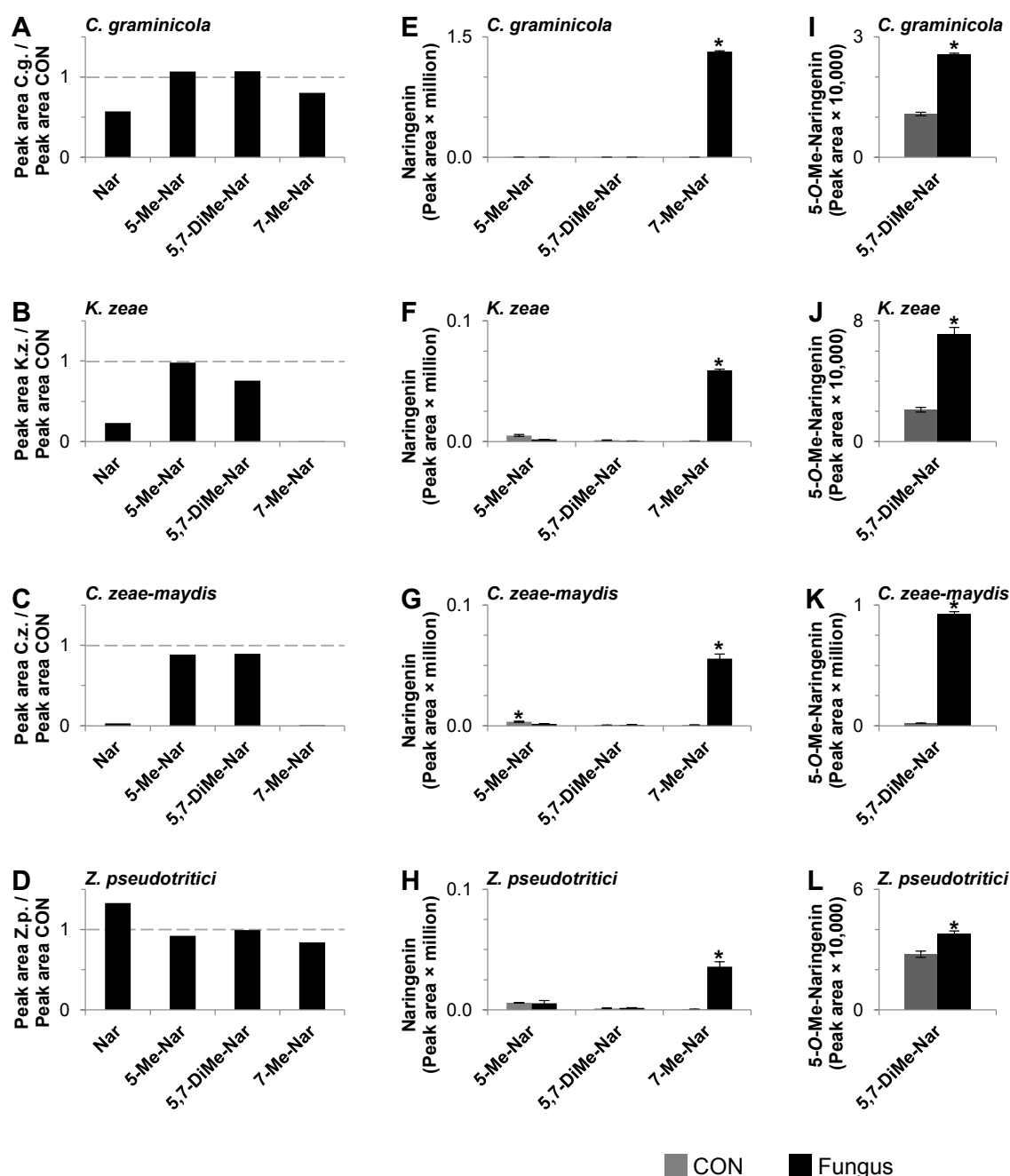
Supplemental Figure 3. Antifungal activity of O-methyl- and non-O-methylflavonoids against *Kabatiella zeae*. Growth (optical density at 600 nm) of *K. zeae* in the absence and presence of self-purified or commercially available flavonoids measured over a 40-h time course in potato dextrose broth using a microtiter plate assay. Data are shown as means \pm SE ($n = 3$). Different letters indicate significant differences ($P < 0.05$) between treatments at 40 h (one-way ANOVA followed by Tukey's post-hoc test or one-way ANOVA on Ranks followed by Dunn's post-hoc test). naringenin ($H = 4.433$, $P = 0.218$); 5-O-Me-naringenin ($H = 12.158$, $P = 0.007$); sakuranetin ($H = 11.758$, $P = 0.008$); 5,7-O-DiMe-naringenin ($F = 2.371$, $P = 0.126$); apigenin ($F = 6.081$, $P = 0.011$); 5-O-Me-apigenin ($F = 2.399$, $P = 0.123$); genkwanin ($F = 214.400$, $P < 0.001$); 5,7-O-DiMe-flavone ($F = 444.112$, $P < 0.001$); scutellarein ($F = 6.024$, $P = 0.011$); hispidulin ($F = 21.078$, $P < 0.001$); 7-O-Me-scutellarein ($F = 2.357$, $P = 0.128$); tangeretin ($F = 43.271$, $P < 0.001$). Abbreviations: Me, methyl; DiMe, dimethyl.



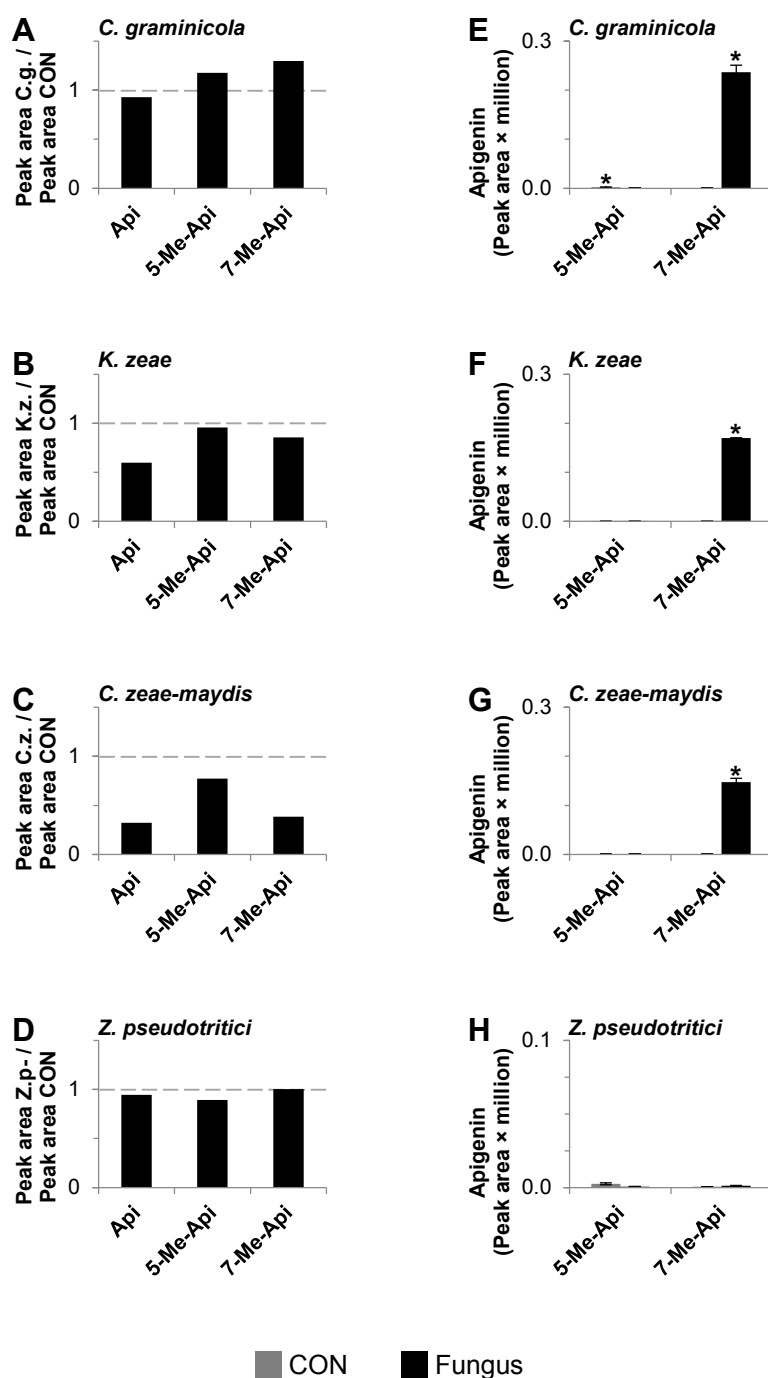
Supplemental Figure 4. Antifungal activity of O-methyl- and non-O-methylflavonoids against *Cercospora zeae-maydis*. Growth (optical density at 600 nm) of *C. zeae-maydis* in the absence and presence of self-purified or commercially available flavonoids measured over a 40-h time course in potato dextrose broth using a microtiter plate assay. Data are shown as means \pm SE ($n = 3$). Different letters indicate significant differences ($P < 0.05$) between treatments at 40 h (one-way ANOVA followed by Tukey's post-hoc test or one-way ANOVA on Ranks followed by Dunn's post-hoc test). naringenin ($H = 11.758$, $P = 0.008$); 5-O-Me-naringenin ($H = 1.725$, $P = 0.631$); sakuranetin ($H = 12.825$, $P = 0.005$); 5,7-O-DiMe-naringenin ($H = 10.600$, $P = 0.014$); apigenin ($H = 10.092$, $P = 0.018$); 5-O-Me-apigenin ($F = 2.000$, $P = 0.172$); genkwanin ($H = 7.358$, $P = 0.061$); 5,7-O-DiMe-flavone ($F = 414.245$, $P < 0.001$); scutellarein ($F = 2.443$, $P = 0.119$); hispidulin ($F = 12.311$, $P < 0.001$); 7-O-Me-scutellarein ($F = 0.719$, $P = 0.561$); tangeretin ($F = 37.124$, $P < 0.001$). Abbreviations: Me, methyl; DiMe, dimethyl.



Supplemental Figure 5. Antifungal activity of O-methyl- and non-O-methylflavonoids against *Zymoseptoria pseudotritici*. Growth (optical density at 600 nm) of *Z. pseudotritici* in the absence and presence of self-purified or commercially available flavonoids measured over a 44-h time course in yeast malt sucrose using a microtiter plate assay. Data are shown as means \pm SE ($n = 3$). Different letters indicate significant differences ($P < 0.05$) between treatments at 44 h (one-way ANOVA followed by Tukey's post-hoc test or one-way ANOVA on Ranks followed by Dunn's post-hoc test). naringenin ($F = 5.522$, $P = 0.015$); 5-O-Me-naringenin ($F = 4.333$, $P = 0.030$); sakuranetin ($F = 245.260$, $P < 0.001$); 5,7-O-DiMe-naringenin ($H = 7.892$, $P = 0.048$); apigenin ($F = 2.057$, $P = 0.185$); 5-O-Me-apigenin ($F = 201.513$, $P < 0.001$); genkwanin ($F = 203.880$, $P < 0.001$); 5,7-O-DiMe-flavone ($F = 117.019$, $P < 0.001$); scutellarein ($F = 3.097$, $P = 0.071$); hispidulin ($F = 44.041$, $P < 0.001$); 7-O-Me-scutellarein ($F = 2.777$, $P = 0.091$); tangeretin ($F = 44.222$, $P < 0.001$). Abbreviations: Me, methyl; DiMe, dimethyl.



Supplemental Figure 6. Detoxification of naringenin and its O-methyl derivatives by plant pathogenic fungi. The flavonoids were extracted after completion of the *in vitro* fungal bioassays from wells of the 96-well plate with and without (CON) fungus and an initially applied flavonoid concentration of 32 $\mu\text{g/mL}$ and analyzed by LC-MS/MS. **Left panel (A-D):** ratio of different test flavonoids in wells with or without (CON) the indicated fungus. Values < 1 (grey dashed line) indicate a decrease in the corresponding flavonoid in wells with fungus compared to control wells without fungus. **Middle panel (E-H) and right panel (I-L):** Relative amount of the demethylation product naringenin (E-H) and 5-methoxynaringenin (I-L), respectively, in wells with and without (CON) the indicated fungus and different O-methyl derivatives of naringenin as initially applied test compounds. Relative flavonoid amounts are shown as means \pm SE ($n = 3$). Stars indicate statistically significant differences ($P < 0.05$) between treatments (for statistical values, see Supplemental Table 1). Abbreviations: Nar, naringenin; 5-Me-Nar, 5-methoxynaringenin; 5,7-DiMe-Nar, 5,7-dimethoxynaringenin; 7-Me-Nar, 7-methoxynaringenin (sakuranetin).



Supplemental Figure 7. Detoxification of apigenin and its O-methyl derivatives by plant pathogenic fungi. The flavonoids were extracted after completion of the *in vitro* fungal bioassays from wells of the 96-well plate with and without (CON) fungus and an initially applied flavonoid concentration of 32 µg/mL and analyzed by LC-MS/MS. **Left panel (A-D):** ratio of different test flavonoids in wells with or without (CON) the indicated fungus. Values < 1 (grey dashed line) indicate a decrease in the corresponding flavonoid in wells with fungus compared to control wells without fungus. **Right panel (E-H):** Relative amount of the demethylation product apigenin in wells with and without (CON) the indicated fungus and different O-methyl derivatives of apigenin as initially applied test compounds. Relative flavonoid amounts are shown as means ± SE ($n = 3$). Stars indicate statistically significant differences ($P < 0.05$) between treatments (for statistical values, see Supplemental Table 1). Abbreviations: Api, apigenin; 5-Me-Api, 5-methoxyapigenin; 7-Me-Api, 7-methoxyapigenin (genkwanin).

Supplemental Table 1. Statistical values for the analysis of demethylation products of different O-methylflavonoids in fungal bioassays corresponding to the results shown in Supplemental Figures 6 and 7. Values in bold indicate significant differences ($P < 0.05$) between treatments. MWRST, Mann-Whitney Rank Sum Test.

Fungus	Flavonoid tested	Flavonoid analyzed	Statistical test used	<i>t</i> / <i>T</i> -value	P-value
<i>C. graminicola</i>	5-Me-Nar			-1.660	0.172
	5,7-DiMe-Nar	Nar	<i>t</i> -test	-1.164	0.309
	7-Me-Nar			-105.336	< 0.001
	5,7-DiMe-Nar	5-Me-Nar		-29.248	< 0.001
<i>K. zeae</i>	5-Me-Nar		MWRST	15.000	0.100
	5,7-DiMe-Nar	Nar		1.966	0.121
	7-Me-Nar		<i>t</i> -test	69.769	< 0.001
	5,7-DiMe-Nar	5-Me-Nar		-10.910	< 0.001
<i>C. zeae-maydis</i>	5-Me-Nar			4.175	0.014
	5,7-DiMe-Nar	Nar	<i>t</i> -test	-1.798	0.147
	7-Me-Nar			-14.020	< 0.001
	5,7-DiMe-Nar	5-Me-Nar		-37.230	< 0.001
<i>Z. pseudotritici</i>	5-Me-Nar		MWRST	12.000	0.700
	5,7-DiMe-Nar	Nar		-0.710	0.517
	7-Me-Nar		<i>t</i> -test	-8.467	< 0.001
	5,7-DiMe-Nar	5-Me-Nar		-4.758	< 0.009
<i>C. graminicola</i>	5-Me-Api			4.729	0.009
	7-Me-Api	Api	<i>t</i> -test	-16.397	< 0.001
<i>K. zeae</i>	5-Me-Api		MWRST	10.500	1.000
	7-Me-Api	Api	<i>t</i> -test	-160.727	< 0.001
<i>C. zeae-maydis</i>	5-Me-Api			-0.278	0.795
	7-Me-Api	Api	<i>t</i> -test	-20.199	< 0.001
<i>Z. pseudotritici</i>	5-Me-Api			2.649	0.057
	7-Me-Api	Api	<i>t</i> -test	-1.908	0.129

11.8 Supplemental Methods

11.8.1 *In vitro* fungal bioassays with O-methyl- and non-O-methylflavonoids

Fungal cultures of *Colletotrichum graminicola* (Leibniz-Institut, Deutsche Sammlung von Mikroorganismen und Zellkulturen GmbH (DSMZ), strain (DSM) no. 63127), *Kabatiella zeae* (DSM 62737), and *Cercospora zeae-maydis* (Westerdijk Fungal Biodiversity Institute (CBS), strain no. 117755) were grown on potato dextrose agar (PDA, Sigma-Aldrich) at 25°C in the dark for seven, four, and 14 days, respectively, before subculturing (see below) to enhance sporulation. *C. graminicola* was subcultured on oatmeal agar (OMA, Sigma-Aldrich) at 25°C in the dark for six days. Sporulation of *K. zeae* was enhanced using liquid *K. zeae* medium (KZM; Reifschneider and Arny, 1979). Briefly, 50 mL KZM were inoculated with a colony plug and incubated at 25°C and 150 rpm for four days. Afterwards, 400 µL of the liquid culture were plated on corn meal agar (CMA, Sigma-Aldrich) and grown for another four days. To promote sporulation of *C. zeae-maydis*, the mycelium of 3 plates (each approx. 2 cm²) was cut in little pieces, suspended in 25 mL sterile water, mixed vigorously and then the suspension was pipetted (2 mL/plate) on modified V8 agar (V8 replaced by tomato juice, pH 6.5). After 15 min, remaining liquid was decanted and the plate was incubated at room temperature and 12 h daylight for five days. Spores of *C. graminicola*, *K. zeae*, and *C. zeae-maydis* were harvested directly in refrigerated broth medium (potato dextrose broth (PDB) buffered with 40 mM HEPES pH 7). Before use, all broth media were filtered under sterile conditions using a vacuum filter (Filtropur V25, 0.45 µm, Sarstedt). Spore suspensions of *C. graminicola* and *K. zeae* were filtered through a 40 µm cell strainer and quantified for use. Because spores of *C. zeae-maydis* were difficult to separate from the mycelial fragments, the suspension was gently homogenized using a tissue homogenizer (Potter-Elvehjem, Carl Roth, Karlsruhe, Germany), before successive filtration through first a 100 µm and then a 40 µm cell strainer. Final spore concentrations used in the bioassays were 5×10^4 /mL, 2×10^5 /mL, and 1.25×10^4 /mL for *C. graminicola*, *K. zeae*, and *C. zeae-maydis*, respectively.

Zymoseptoria pseudotritici (STIR04 2.2.1) was kindly provided by Eva Stukenbrock (Stukenbrock et al., 2011; Stukenbrock et al., 2012) and grown on yeast-malt agar (YMA; 4 g/L yeast extract, 4 g/L malt extract, 4 g/L sucrose, 15 g/L agar) at 18°C in the dark for seven days. Then, colonies were picked, used to inoculate liquid yeast-malt sucrose (YMS; 4 g/L yeast extract, 4 g/L malt extract, 4 g/L sucrose), and incubated at 25°C and 150 rpm

for five days. Spores of *Z. pseudotritici* were harvested by centrifugation, resuspended in filtered and refrigerated YMS buffered with 40 mM HEPES (pH 7), and quantified for use as 4×10^5 spores/mL.

The *in vitro* bioassays were performed using 96-well microtiter plates (Greiner 655090), each well containing 150 μ L of broth medium (buffered PDB/YMS pH7) containing the fungal inoculum and flavonoids at concentrations of 32, 16, and 8 μ g/mL (for all compounds used, see Supplemental Figure 1). All flavonoids were diluted from stock solutions containing 3.2 mg/mL in 100% dimethylsulfoxide (DMSO) shortly before use. For this, the stocks were first diluted in 100% methanol and subsequently in buffered broth medium; final concentration of DMSO and methanol in all wells were 1% and 3%, respectively. The 2-fold dilution series was pipetted directly on the plate using a multichannel pipette. Control samples included wells with medium only (blanks), 32 μ g/mL flavonoid without fungal inoculum, and no flavonoid containing growth controls. The bioassays were incubated at 25°C in the dark for 40-45 h and fungal growth was monitored through periodic measurements of the optical density (OD) at 600 nm using a Tecan infinite 200 microplate reader (Tecan) and Magellan software (Tecan) for instrument control and data analysis. All samples were measured in technical triplicates.

After the last measurement, the samples were transferred to a 96-well deep well plate (Ritter Riplate, 1 mL) for flavonoid extraction. The wells of the bioassay plate were subsequently washed out with each 125 μ L pure methanol, and the wash fraction was combined with the corresponding assay mixture in the 96-well deep well plate. Then, another 125 μ L of 100% methanol was added to obtain a final concentration of 60% methanol, and the deep well plate was incubated for 10 min at 25°C and 1600 rpm using a ThermoMixer C (Eppendorf). Afterwards, the plate was centrifuged at 4000 g and 4°C for 10 min to remove mycelial fragments and 180 μ L of the supernatant was carefully transferred to a new 96-well deep well plate. All samples were stored at -20°C before analysis of flavonoids using targeted LC-MS/MS as described in manuscript II (Förster et al., 2021).

11.8.2 Statistical analysis

Statistical analyses were performed using SigmaPlot 11.0 for Windows (Systat Software). The statistical test applied is indicated in the respective figure legends. Whenever necessary, the data were log-transformed to meet statistical assumptions such as normality and homogeneity of variances.